

Dissertation zur Erlangung des Doktorgrades
der Fakultät für Chemie und Pharmazie
der Ludwig-Maximilians-Universität München

**The role of Kindlin-3
in cells of the haematopoietic system**

Sarah Marianne Schmidt

aus

Lauingen a.d. Donau

2011

Erklärung

Diese Dissertation wurde im Sinne von § 13 Abs. 3 bzw. 4 der Promotionsordnung vom 29. Januar 1998 (in der Fassung der vierten Änderungssatzung vom 26. November 2004) von Herrn Prof. Dr. Reinhard Fässler betreut.

Ehrenwörtliche Versicherung

Diese Dissertation wurde selbstständig, ohne unerlaubte Hilfe erarbeitet.

München, am 17.03.2011

Sarah Schmidt

Dissertation eingereicht am 22.03.2011

- | | |
|--------------|---------------------------------|
| 1. Gutachter | Prof. Dr. Reinhard Fässler |
| 2. Gutachter | Prof. Dr. Christian Wahl-Schott |

Mündliche Prüfung am 27.04.2011

Für meine Eltern

To my parents

1. Table of contents

1. Table of contents	I
2. List of publications	III
3. Abbreviations	V
4. Summary	IX
5. Introduction	1
5.1. Kindlins	1
5.1.1. <i>The family of kindlin proteins</i>	1
5.1.2. <i>Domain structure of kindlin proteins</i>	1
5.1.3. <i>Role of Unc-112 in C. elegans</i>	3
5.1.4. <i>Role of fermitin 1 and 2 in Drosophila</i>	4
5.1.5. <i>Kindlin-1</i>	4
5.1.6. <i>Kindlin-2</i>	5
5.1.7. <i>Kindlin-3</i>	6
5.2. Integrins	8
5.2.1. <i>The integrin family</i>	8
5.2.2. <i>Structure of integrins</i>	10
5.2.3. <i>Integrins and their ligands</i>	13
5.2.4. <i>Integrins as bidirectional signaling molecules</i>	14
5.2.4.1. <i>Inside-out signaling</i>	15
5.2.4.2. <i>Outside-in signaling</i>	19
5.2.5. <i>Integrin crosstalk with growth factor and cytokine signaling</i>	22
5.2.6. <i>Integrins in mouse development</i>	25
5.3. Integrins and cells of the haematopoietic system	26
5.3.1. <i>The haematopoietic system</i>	26
5.3.2. <i>Erythrocytes</i>	28
5.3.3. <i>Platelets</i>	29
5.3.4. <i>Neutrophils</i>	31
5.3.4.1. <i>The leukocyte extravasation cascade</i>	32
5.3.4.2. <i>Leukocyte adhesion deficiency syndromes</i>	34
5.3.5. <i>Monocytes and macrophages</i>	35
5.3.6. <i>Osteoclasts</i>	36
5.3.6.1. <i>Adhesion structures of osteoclasts</i>	38
5.3.6.2. <i>Osteoclasts and integrins</i>	41
5.4. Osteopetrosis	42
5.4.1. <i>Bone homeostasis and osteopetrosis</i>	42
5.4.2. <i>Mouse models</i>	42
6. Aim of the thesis	47

7. Brief summaries of the publications.....	49
7.1. Paper I	49
7.2. Paper II	50
7.3. Paper III	51
8. References.....	53
9. Acknowledgements.....	73
10. Curriculum Vitae	75
11. Supplements.....	77

2. List of publications

This thesis is based on the following publications, which are referred to in the text by their Roman numerals (**I-III**):

- I Krüger M*, Moser M*, Ussar S, Thievensen I, Luber CA, Forner F, **Schmidt S**, Zanivan S, Fässler R, Mann M (2008): SILAC mouse for quantitative proteomics uncovers Kindlin-3 as an essential factor for red blood cell function. *Cell* 134:353-364.
* equal contribution
- II Moser M, Bauer M, Schmid S, Ruppert R, **Schmidt S**, Sixt M, Wang H, Sperandio M, Fässler R (2009): Kindlin-3 is required for b2 integrin-mediated leukocyte adhesion to endothelial cells. *Nat Med* 15:300-305.
- III **Schmidt S**, Nakchbandi I, Ruppert R, Kawelke N, Hess MW, Pfaller K, Jurdic P, Fässler R, Moser M (2011): Kindlin-3 mediated signaling from multiple integrin classes is required for osteoclast-mediated bone resorption. *J Cell Biol* 192:883-897.

3. Abbreviations

+/+	wild-type
-/-	knockout
ADAM	a disintegrin and metalloproteinase
AdMIDAS	adjacent to metal ion dependent adhesion site
ADP	adenosine diphosphate
AE	anion exchanger
AGM	aorta-gonad-mesonephros region
Akt	RAC-alpha serine/threonine protein kinase
Arp2/3	actin-related protein 2/3 complex
ATP	adenosine triphosphate
bp	base pair
CAII	carbonic anhydrase II
CD	cluster of differentiation
<i>C. elegans</i>	<i>Caenorhabditis elegans</i>
CIC-7	chloride channel 7
Cre	cyclization recombinase
D	aspartate
DAP12	DNAX-activating protein of 12 kDa
DC	dendritic cell
DOCK180	dedicator of cytokinesis 1
E	glutamate
EGF	epidermal growth factor
EGFR	epidermal growth factor receptor
ECM	extracellular matrix
<i>E.coli</i>	<i>Escherichia coli</i>
Epo	erythropoietin
ERK	extracellular signal-regulated kinase
ESAM	endothelial cell-selective adhesion molecule
EX	embryonic day X
F	phenylalanine
F1-3	FERM subdomain 1-3
FA	focal adhesion
FAK	focal adhesion kinase
FcR γ	fragment (crystallisable) receptor γ
FERM	four-point-one/ezrin/radixin/moesin
G	glycine
GAP	GTPase-activating protein
G-CSF	granulocyte colony stimulating factor
GDI	guanine nucleotide dissociation inhibitor
GDP	guanosine diphosphate
GEF	guanine nucleotide exchange factors
GFP	green fluorescent protein
GIT	G-coupled receptor kinase-interacting protein
GM-CSF	granulocyte macrophage colony stimulating factor
GP	glycoprotein
GPCR	G-protein coupled receptor
GPI	glycosylphosphatidyl inositol
GTP	guanosine triphosphate
GTPase	guanosine triphosphatase
H	histidine
HGFR	hepatocyte growth factor receptor
HSC	haematopoietic stem cell
ICAM	intercellular adhesion molecule

ABBREVIATIONS

Ig	immunoglobulin
ILK	Integrin linked kinase
IPP	ILK/pinch/parvin
ITAM	immunoreceptor tyrosine-based activation motif
JAM-A	junctional adhesion molecule A
JNK	c-Jun N-terminal kinase
K	lysine
L	leucine
LAD	leukocyte adhesion deficiency
LAP	latency-associated peptide
LDV	lysine/aspartate/valine
LFA	lymphocyte function associated protein
LPS	lipopolysaccharide
MadCAM	mucosal vascular addressin cell adhesion molecule
M-CSF	macrophage colony stimulating factor
MFGE8	milk fat globule-EGF factor 8
MHC	major histocompatibility complex
MIDAS	metal ion dependent adhesion site
Mig-2	mitogen inducible gene 2
MLC	myosin light chain
MMP	matrix metalloproteinase
mRNA	messenger RNA
N	asparagine
neo	neomycin resistance gene
NFATc1	nuclear factor of activated T cells, cytoplasmic, calcineurin-dependent 1
NF- κ B	nuclear factor- κ B
NK	natural killer cells
ODF	osteoclast differentiation factor
OPG	osteoprotegerin
OPGL	osteoprotegerin ligand
P	proline
p130Cas	p130 Crk-associated substrate
PAT	paralysed, arrested elongation at twofold stage
PDGFR	platelet-derived growth factor receptor
PECAM-1	platelet/endothelial cell adhesion molecule 1
PH	pleckstrin homology
PI3K	phosphatidylinositol 3-kinase
PINCH	particularly interesting new cysteine-histidine-rich protein
PIP2	phosphatidylinositol-4,5-bisphosphate
PIP3	phosphatidylinositol-3,4,5-trisphosphate
PIPKI γ	phosphatidylinositol 4-phosphate 5-kinase γ
PIX	PAK interactive exchange factor
PLC	phospholipase C
PGI2	prostacyclin
PML/PMN	polymorphonuclear leukocytes
PSGL-1	P-selectin glycoprotein ligand 1
PSI	plexin/semaphorin/integrin domain
PTB	phosphotyrosine binding domain
PtdIns	phosphatidylinositol
PTEN	phosphatase and tensin homolog
PTH	parathyroid hormone
pY	phosphotyrosine
Pyk2	proline-rich tyrosine kinase 2
Q	glutamine
R	arginine
RANKL	receptor activator of nuclear factor κ B ligand

ABBREVIATIONS

RGD	arginine/glycine/aspartate
RGDfV	arginine/glycine/aspartate/D-phenylalanine/valine
RIAM	Rap1-GTP-interacting adaptor molecule
ROCK	Rho-associated protein kinase
ROS	reactive oxygen species
RTK	receptor tyrosine kinase
S	serine
SH2	Src homology 2
SILAC	stable isotope labelling by amino acids in cell culture
STAT	signal transducer and activator of transcription
SyMBS	synergistic metal ion binding site
T	threonine
β TD	β tail domain
TGF β	transforming growth factor β
TNF	tumour necrosis factor
TRAF-6	tumour necrosis factor receptor-associated factor-6
TRANCE	tumour necrosis factor-related activation-induced cytokine
TRAP	tartrate resistant acid phosphatase
Unc-112	uncoordinated protein 112
URP	Unc-112 related protein
VCAM	vascular cell adhesion molecule
VE-cadherin	vascular endothelial cadherin
VLA	very late antigen
VEGFR	vascular endothelial growth factor receptor
vWF	von Willebrand factor
W	tryptophan
WASp	Wiskott-Aldrich syndrome protein
WIP	WASp interacting protein
Y	tyrosine

4. Summary

Integrins are ubiquitously expressed cell surface receptors consisting of an α and a β subunit. They represent the major class of cell-extracellular matrix receptors and some of them also mediate cell-cell adhesion. A hallmark of integrins is their ability to shift between different conformational states. The shift from an inactive integrin with a low affinity for the ligand towards an active integrin with high ligand affinity is regulated by intracellular signals. Recently it has been shown that the final step in integrin activation is triggered by talin and kindlins, which are cytoplasmic proteins. The family of kindlin proteins consists of three members: kindlin-1, -2 and -3. Kindlin-1 is mainly expressed in epithelia, kindlin-2 is almost ubiquitously expressed and the expression of kindlin-3 is restricted to haematopoietic cells. Kindlins are characterized by a FERM (four-point-one/ezrin/radixin/moesin) domain with an inserted PH (pleckstrin homology) domain. These domains suggest that kindlins predominantly associate with cell membranes. All kindlins localize to integrin-mediated adhesion sites by binding to the cytoplasmic domain of integrins.

Kindlin-3 deficient mice die within one week after birth due to bleedings and severe anemia, caused by impaired platelet integrin activation and aggregation. It was already shown that kindlin-3 is essential for activation of β 1 and β 3 integrins on platelets but the role of kindlin-3 in other haematopoietic cells was not yet examined.

In order to quantitatively analyse the proteome of various cell types and tissues, we applied the SILAC (stable isotope labelling by amino acids in cell culture) method to the whole mouse organism by using a diet, which contained a $^{13}\text{C}_6$ -substituted version of lysine. This technique was used to compare the proteomes of control and kindlin-3 deficient erythrocytes. In examinations of kindlin-3^{-/-} erythrocytes we found a profound defect in the composition of structural proteins of the membrane skeleton leading to less stable erythrocytes. This partly contributes to the anemia of kindlin-3 null mice (Paper I).

In a further study we analysed the role of kindlin-3 in leukocytes (Paper II) and could show that kindlin-3 is also required for the activation of β 2 integrins on leukocytes. In humans impaired activation of β 1, β 2 and β 3 integrins on platelets and leukocytes leads to the rare autosomal recessive leukocyte adhesion deficiency syndrome type III (LAD-III), which is characterized by severe bleeding and impaired adhesion of leukocytes to the endothelium of inflamed tissues. Based on the analyses of kindlin-3 null mice mutations in the human kindlin-3 gene were identified in LAD-III patients.

Since kindlin-3 deficient mice reveal the same symptoms as LAD-III patients, this mouse mutant can serve as a valuable model to characterize the molecular basis of this disease.

A number of LAD-III patients additionally suffer from osteopetrosis. Kindlin-3 deficient mice also develop severe osteopetrosis, which is already apparent at birth. We examined the role of kindlin-3 in bone homeostasis (Paper III). Kindlin-3 deficient osteoclasts show a profound adhesion and spreading defect owing to impaired activation of $\beta 1$, $\beta 2$ and $\beta 3$ integrins. However, integrin independent functions of kindlin-3 in osteoclasts can not be fully excluded. The defect of kindlin-3^{-/-} osteoclasts was compared to osteoclasts lacking one, two or all three integrin classes. We found that loss of a single integrin class already affects osteoclast function and that the loss of all integrins indeed mimics kindlin-3 deficiency.

Altogether our findings show that kindlin-3 is an essential regulator of blood cell integrins required for bidirectional integrin signaling. A number of open questions still remain. The mode of kindlin-3 regulation and its crosstalk with talin at the integrin cytoplasmic domain are two major issues that have to be addressed in near future.

5. Introduction

5.1. Kindlins

5.1.1. *The family of kindlin proteins*

The kindlins are a new family of intracellular cell adhesion proteins consisting of three members in mice and humans, kindlin-1, -2 and -3. In *C. elegans* one kindlin orthologue exists, which is named Unc-112 (uncoordinated protein 112) and the *Drosophila* genome encodes for two kindlin-related proteins (fermitin-1 and -2). The kindlin family is named after the gene mutated in kindler syndrome, which is an autosomal recessive inherited genodermatosis in humans [1].

Kindlin-2, previously described as Mig-2 (mitogen inducible gene 2), was discovered in a cDNA screen for mitogen inducible genes [1]. Kindlin-1 and kindlin-3 were initially named Unc-112 related protein 1 (URP-1) and URP-2, respectively [2]. Siegel et al. [3] proposed to name the three different genes kindlin-1 (URP-1), kindlin-2 (Mig-2) and kindlin-3 (URP-2).

The kindlin proteins share an evolutionary conserved gene structure. Both human and murine kindlin genes consist of 15 exons. The ATG start codon is located in exon 2 of all three genes. Translation of the murine cDNAs gives rise to proteins with 677 amino acids (kindlin-1), 680 amino acids (kindlin-2) and 655 amino acids (kindlin-3). Sequence alignments revealed a high similarity of the kindlin proteins to each other. Kindlin-1 and kindlin-2 are most closely related with an identity of 60% and a similarity of 74%. Kindlin-3 has less homology to its relatives with 53% identity and 69% similarity to kindlin-1 and 49% identity and 67% similarity to kindlin-2, respectively [4].

5.1.2. *Domain structure of kindlin proteins*

All kindlin proteins exhibit the same and unique protein domain structure. Kindlins harbour a FERM domain (Band four-point-one/ezrin/radixin/moesin), which consists of three subdomains: F1-F3 (Figure 1). The subdomain F1 is folded in an ubiquitin-like manner, subdomain F2 has an α -helix bundle structure and subdomain F3 reveals a phosphotyrosine binding (PTB) domain, which belongs to the pleckstrin homology (PH) domain folding superfamily [5-7]. A hallmark of kindlin proteins is a PH domain, which is inserted in the F2 subdomain [8].

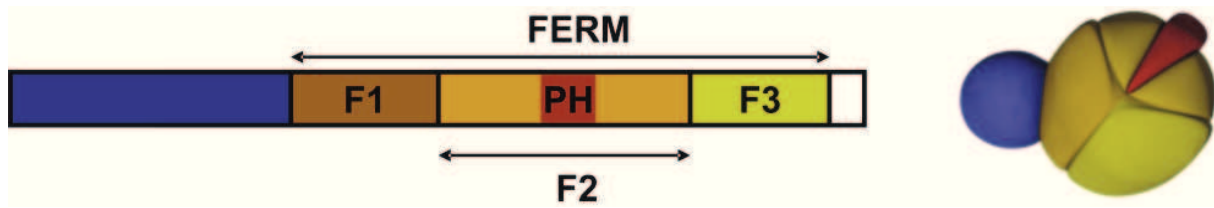


Figure 1: Common domain structure of kindlin proteins. F1-F3 represent the FERM subdomains. Subdomain F2 is inserted by a PH domain.

More than 80 FERM domain containing proteins are known in mouse and man. The common feature of this heterogeneous group of proteins is their ability to link intracellular proteins to the cytoplasmic domains of transmembrane proteins. They furthermore can link filamentous actin within the cell cortex to cell surface proteins such as integrins, CD44, CD43, intercellular adhesion molecule-2 (ICAM-2) and ICAM-3 [9]. FERM domains consist of 200-300 amino acids. The conformation and activity of FERM proteins is regulated by a combination of phospholipid binding and phosphorylation [10].

Different members of the PH/PTB superfamily show only little sequence homology. PH/PTB domains consist of approximately 120 amino acids and are characterized by a common folding structure, in which two nearly orthogonal anti-parallel β sheets form a β sandwich flanked by an α -helix that holds this structure together [7, 11; 12]. Approximately 50 proteins in mice and men contain a PTB domain. This domain was initially identified in the Src homology 2 domain adaptor protein Shc, where it mediates the binding of Shc to an NPXpY motif in activated receptor tyrosine kinases [13]. Interestingly, this recognition motif differs fundamentally from those of SH2 (Src homology 2) domains, which also bind to phosphorylated tyrosine residues. PTB domain containing proteins including talin [14] can also bind with the same or higher affinity to a non-phosphorylated NPxY motif.

Proteins harbouring a PH domain fulfil a very broad range of tasks [11]. PH domains are found in approximately 250 human and murine proteins, such as protein kinases, guanine nucleotide exchange factors (GEFs), phospholipases and cytoskeletal proteins [15]. The main function of PH domains is to bind phosphatidylinositol lipids within cell membranes [16-18].

Phosphatidylinositol (PtdIns) can be phosphorylated at three hydroxyl groups of the inositol, at the positions 3, 4 and 5. These phosphorylation sites are phosphorylated and dephosphorylated by different kinases such as phosphatidylinositol 3-kinase (PI3K) and lipid phosphatases like phosphatase and tensin homolog (PTEN) [12].

This results in all kinds of combinations of mono-, bi- and triphosphorylated PtdIns. All PtdIns have a very distinct spatial and temporal distribution pattern within the various membranes of the cell. PtdIns(4,5)P₂ (PtdIns 4,5-bisphosphate) for instance is predominantly found in the plasma membrane and the Golgi apparatus at steady state levels. PtdIns(3,4,5)P₃ and PtdIns(3,4)P₂ instead accumulate transiently at the plasma membrane only upon receptor stimulation. Different PH domains vary in their affinities to PtdIns depending on their phosphorylation status. Therefore, PH domains play an important role in targeting proteins to the membranes of various cellular compartments.

Taken together, the kindlins are typical adaptor proteins containing two domains known to mediate membrane association.

5.1.3. Role of *Unc-112* in *C. elegans*

First functional data on kindlin proteins were reported from *Unc-112*, the kindlin orthologue of *C. elegans*. *Unc-112* was identified as a novel membrane-associated, cytoplasmic protein that colocalizes with integrins at cell-extracellular matrix (ECM) adhesion sites. Animals homozygous for the r367 allele of the *unc-112* gene show a phenotype with a disorganized body wall muscle leading to paralysis in adult worms and uncoordinated movement [19]. Null mutants of the *unc-112* gene show a much more severe phenotype. They display a paralyzed, arrested elongation at twofold stage (PAT) phenotype.

PAT phenotypes occur after loss of proteins that are essential for the formation of functional embryonic body wall muscles [20]. Null mutants of *unc-52*, a homologue of perlecan, *pat-2* (α integrin subunit) and *pat-3* (β integrin subunit) reveal a PAT phenotype variant, which is very similar to the phenotype of *Unc-112* null mutants [21]. In the body wall muscle cells of these mutants, myosin and actin are not organized into sarcomeres, and dense body and M-line components fail to assemble. Experiments with GFP-tagged *Unc-112* showed that *Unc-112* colocalizes with *PAT-3* at dense bodies and M-lines as well as at the basal plasma membrane of muscle cells where they contact neighbouring cells [20]. Upon loss of *Unc-112* *PAT-3* loses its specific targeting to dense bodies and M-lines. *Unc-112* is not required for the initial polarized localisation of integrins in the muscle cells and their clustering into nascent adhesions, instead *Unc-112* is necessary for the subsequent organization of these nascent adhesion sites into an ordered array within the muscle cell membrane.

Furthermore, PAT-4, the *C. elegans* orthologue of integrin linked kinase (ILK), recruits Unc-112 to the plasma membrane. But proper localisation of PAT-4 also depends on Unc-112. This process might be due to direct protein-protein interaction, since a direct interaction between Unc-112 and PAT-4 was suggested in a yeast two-hybrid screen [22].

Depletion of Unc-112 in later, post-embryonic stages by RNAi results in sterility due to defective ovulation and impaired migration of the distal tip cells that form the gonads [23]. Failure in ovulation is a consequence of defective contraction and dilation of somatic gonad structures, as Unc-112 acts as an important regulator of actin mediated cell contractility.

In summary, these data describe roles of Unc-112 in integrin mediated cell adhesion structures and in the linkage of integrins to the actin cytoskeleton.

5.1.4. Role of *fermitin 1* and *2* in *Drosophila*

Little is known about the role of the kindlin orthologues *fermitin 1* and *2* in *Drosophila*. *fermitin 1* and *fermitin 2* are both expressed in the musculature of the fly. *In vitro* studies on cultured cells and *in vivo* studies showed that *fermitin 1* and *2* act in a partially redundant manner to maintain muscle integrity. siRNA knock-downs of *fermitin 1* and *fermitin 2* individually by injecting their corresponding dsRNAs into embryos result only in partial rounded-up muscle phenotypes caused by detachment of the muscles from the tendon cells. However, knock-down of both genes together leads to a complete rounded-up muscle phenotype, suggesting a partial redundancy in their function [24].

5.1.5. *Kindlin-1*

Kindlin-1 mRNA is predominantly transcribed in epithelial cells. The highest mRNA levels can be found in bladder and colon, less transcription is detected in kidney, stomach, small intestine and skin. The expression level in the epidermis is much higher than in the dermis. *Kindlin-1* is transcribed in two splice variants. The main isoform has a length of 4.6 kb. The other splice variant includes intron 7 into the coding sequence and results in a 5.2 kb transcript that encodes for a short 352 amino acid protein, which is expressed in kidney, colon and small intestine [3]. The larger

isoform exists in a non-phosphorylated and phosphorylated form with molecular masses of 74 kDa and 78 kDa, respectively [25].

Loss of function mutations within the human kindlin-1 gene cause Kindler syndrome. Mutations can occur within the entire gene and result in different truncated kindlin-1 proteins [26]. Patients suffering from this disease show several skin pathologies. The severity of the symptoms varies among different patients [27]. The syndrome is characterized by skin atrophy and trauma induced skin blistering in very young patients. The blistering becomes less severe with age but photosensitivity and progressive poikiloderma arise. Additionally there are hints that Kindler syndrome patients are more prone to squamous cell carcinoma [28]. Some patients also develop ulcerative colitis [26; 29; 30], which together with Crohn's disease belongs to idiopathic inflammatory bowel diseases. Kindlin-1 deficient mice also develop skin atrophy and an ulcerative colitis, which results in early postnatal lethality [31].

The Kindler syndrome is the first known skin blistering disease, which results from defective anchorage of the actin cytoskeleton to cell matrix adhesion sites [3; 32]. However, this cannot fully explain the phenotype and the mechanism how loss of kindlin-1 causes photosensitivity and poikiloderma still needs to be investigated.

In vivo kindlin-1 shows a polar distribution within basal epidermal keratinocytes and is localized along the dermal-epidermal junction zone in areas between the hemidesmosomes. In kindlin-1-deficient skin, basal keratinocytes lose their polarity, their proliferation is strongly reduced and apoptotic cell death is increased [25; 31].

In vitro studies have shown that kindlin-1 plays an essential role in cell adhesion and spreading, as loss of kindlin-1 leads to reduced adhesion and delayed cell spreading in different cell lines. Kindlin-1 can interact with the cytoplasmic domains of the integrin subunits $\beta 1$ and $\beta 3$ [31]. In cultured cells it localizes to integrin-mediated cell adhesion sites, so called focal adhesions (FA). Kindlin-1 deficiency also impairs the motility of keratinocytes. These cells migrate slower and undirected due to a defect in integrin-mediated adhesion, loss of polarity and defects in organization of the actin cytoskeleton [8; 25; 31; 33].

5.1.6. Kindlin-2

Kindlin-2 is the best characterized member of the kindlin protein family. Expression of kindlin-2 can be detected in all organs and cell types except for haematopoietic cells. The highest levels are found in striated and smooth muscle cells. Expression of

kindlin-2 can already be detected in embryonic stem cells [34]. Interestingly, kindlin-2 is inversely expressed in the skin compared to kindlin-1, with higher expression in the dermis and lower levels in the epidermis [4]. This distinct expression pattern could provide an explanation for the fact that the presence of kindlin-2 cannot compensate for the loss of kindlin-1 in Kindler syndrome patients and kindlin-1 knockout mice.

While kindlin-2, like kindlin-1, binds to the cytoplasmic tails of $\beta 1$ and $\beta 3$ integrins and localizes to focal adhesions in cultured keratinocytes, only kindlin-2 colocalizes with E-cadherin to cell-cell contacts in differentiated keratinocytes [4; 34; 35]. This differential subcellular localization could also explain why expression of kindlin-2 fails to rescue kindlin-1 deficiency in mice and men. In addition to the integrin-mediated adhesion sites, kindlin-2 localizes to actin stress fibers [4]. In cardiomyocytes, kindlin-2 colocalizes with α -actinin in Z-disks.

Equivalent to loss of kindlin-1, kindlin-2 deficiency also leads to impaired cell spreading and defective adhesion [33]. Additionally to its binding to integrins, kindlin-2 also interacts with migfilin and ILK, which both are involved in the linkage of integrins to the actin cytoskeleton [33; 34].

Kindlin-2 contains a nuclear localization sequence within its N-terminus, which is absent in both other kindlin family members. This nuclear localisation signal suggests additional, so far unknown functions. This is of particular interest as the kindlin-2 interacting protein migfilin can localize to the nucleus as well. Nuclear localization of kindlin-2 has been reported in leiomyosarcomas and leiomyomas [36].

Deficiency of kindlin-2 in mice results in peri-implantation lethality caused by a severe detachment of the endoderm and epiblast from the basement membrane [34].

Altogether, kindlin-1 and kindlin-2 play a role in various cellular processes, including adhesion, polarization, proliferation and migration. They are involved in connecting the actin cytoskeleton to integrin-associated adhesion sites.

5.1.7. Kindlin-3

The expression of kindlin-3 is restricted to cells of the haematopoietic system [4]. It can be detected in macrophages, monocytes, dendritic cells, neutrophils, erythrocytes, B-cells, T-cells, platelets, bone marrow cells, osteoclasts and megakaryocytes (Figure 2).

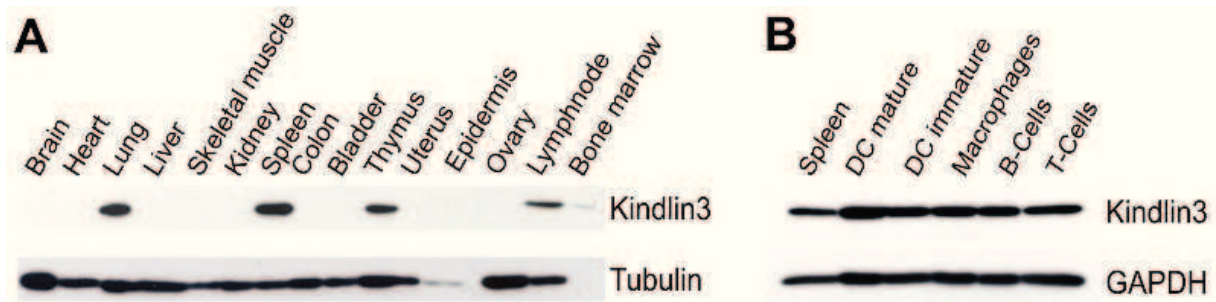


Figure 2: Expression profile of kindlin-3. (A) Western blotting of different mouse tissues from adult C57Bl/6 mice probed with kindlin-3 antibody shows haematopoietic expression of kindlin-3; tubulin serves as loading control. **(B)** Western blotting reveals expression of kindlin-3 in various cell types of haematopoietic origin; GAPDH is used as loading control [4].

Like kindlin-1 and -2, kindlin-3 also localizes to integrin-mediated adhesion structures and interacts with the cytoplasmic domain of β integrin subunits [4; 37]. But in contrast to fibroblasts or keratinocytes, haematopoietic cells do not form focal adhesions. Instead, they adhere via so called podosomes, which consist of a central actin core surrounded by a ring of plaque proteins such as talin, vinculin and paxillin [38; 39]. Kindlin-3 colocalizes with vinculin in the ring structure of podosomes (Figure 3) [4].

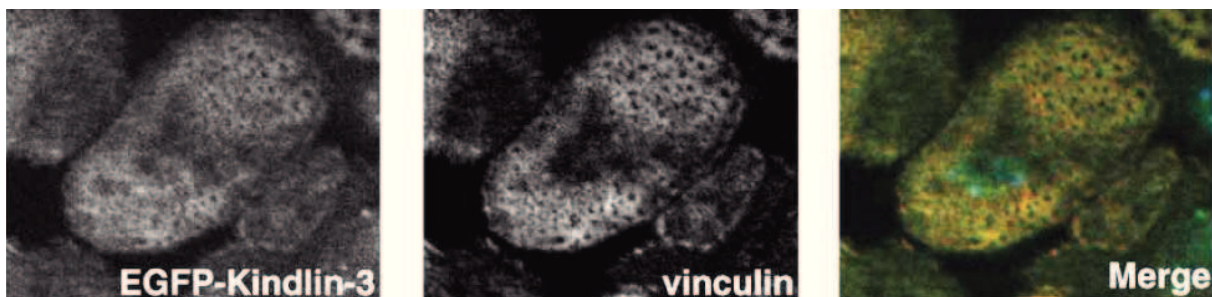


Figure 3: EGFP-kindlin-3 (left) colocalizes (merge, yellow, right) with Vinculin (middle) in the ring structure of podosomes of a dendritic cell [4].

Mice lacking kindlin-3 (*kindlin-3*^{-/-}; Figure 4) show a lethal phenotype [37]. They die within one week after birth due to a number of defects. Kindlin-3 heterozygous animals are normal and show no overt phenotype. Kindlin-3 knockout pups are pale due to a pronounced anaemia (Figure 4A) and reveal severe haemorrhages in the gastrointestinal tract (Figure 4B), skin, brain and bladder. Severe bleedings can be already detected during development, mainly between embryonic days E13-17 (Figure 4C). These severe bleedings are reminiscent of Glanzmann's thrombasthenia, a disorder arising from defects in either integrin α IIb or β 3.

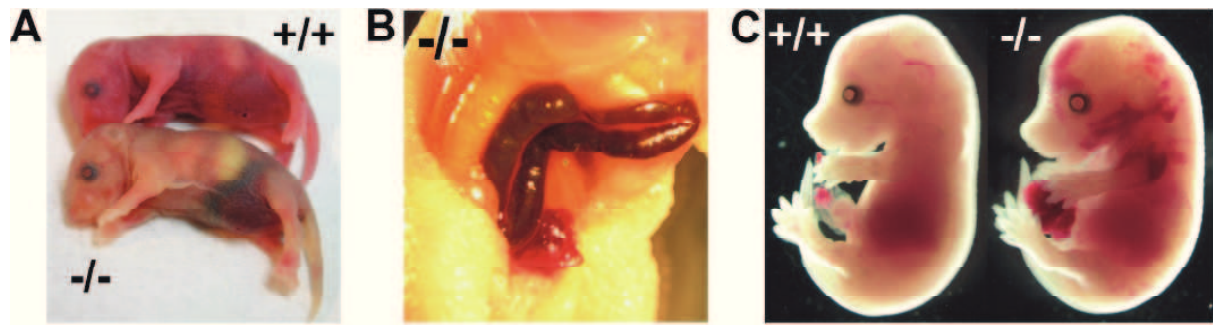


Figure 4: Kindlin-3^{-/-} mice suffer from severe bleeding. (A) P2 wild-type (+/+) and kindlin-3 knockout (-/-) pups show severe bleedings, (B) especially in the gastrointestinal tract and bladder of a newborn kindlin-3^{-/-} mouse. (C) E 14.5 wild-type (+/+) and kindlin-3 knockout (-/-) embryos. Modified from [37].

The severe bleeding of kindlin-3 deficient mice is due to impaired platelet function [37]. The mice suffer from a pronounced haemostatic defect. Platelet count is unchanged in these mice and platelet production seems to be unaffected. This was tested in fetal liver cell chimeras, which were produced by transferring kindlin-3^{-/-} fetal liver cells into lethally irradiated wild-type recipient mice [37]. However, *in vitro* and *in vivo* assays revealed that kindlin-3 deficient platelets fail to aggregate and show a defect in platelet adhesion and spreading.

In summary, all members of the kindlin gene family are important for adhesion and spreading of various cell types. They can interact with the cytoplasmic domain of β integrin subunits and localize to integrin mediated cell adhesion structures.

5.2. Integrins

5.2.1. *The integrin family*

Integrins are a family of heterodimeric cell adhesion receptors. They consist of two non-covalently associated glycoproteins, an α and a β chain. Integrins mediate both the attachment of cells to extracellular matrix and to other cells.

The family of integrin receptors is highly conserved throughout evolution from sponges to mammals. The number of integrins expressed by an organism increases with its complexity. In *C. elegans* two different integrins can be found, which result from the combination of two α integrin subunits (PAT-2 and INA-1 [40]) with one β integrin subunit (PAT-3). In *Drosophila melanogaster* the integrin family consists of five integrin heterodimers generated by five α subunits associated with one β subunit [41; 42].

The genomes of mice and men encode for 18 α and 8 β subunits. Various combinations give rise to at least 24 different integrin heterodimers. Only certain subunits are able to form functional heterodimers with each other (Figure 5) [43]. Integrins can be grouped by their ligand binding abilities and by their β subunit. While some subunits appear exclusively in one heterodimer, others are part of several integrins. For example, integrin $\beta 1$ can interact with twelve different α integrin subunits and five integrin heterodimers contain integrin αV . Within the integrin family overlapping binding abilities can be observed. Certain extracellular matrix proteins can be bound by many different integrins and several integrin heterodimers are capable of recognizing more than one ECM molecule [44].

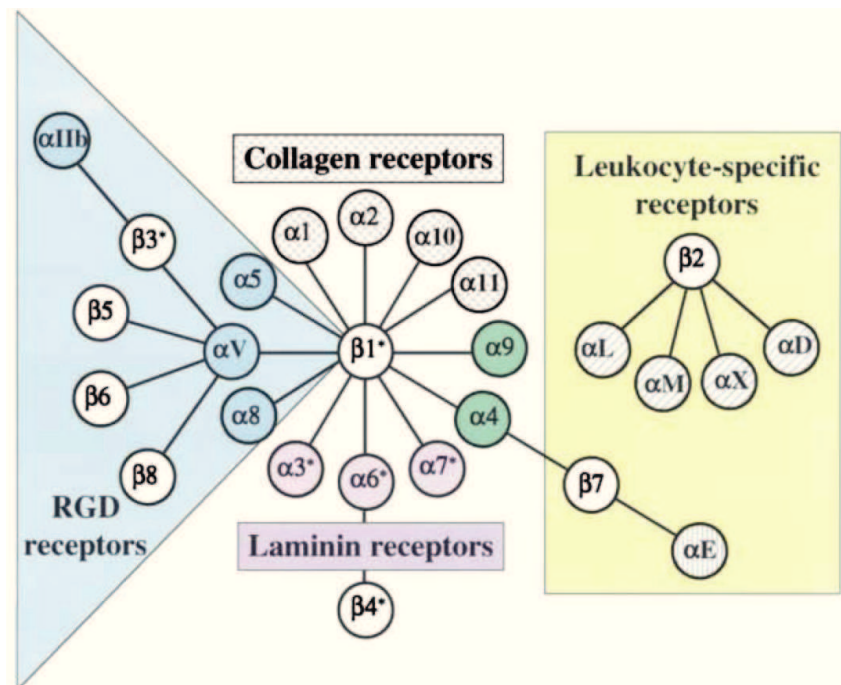


Figure 5: Family of integrin heterodimers sorted by their expression and their ability to bind certain extracellular matrix proteins. Shown are all known combinations of integrin subunits in mammals and their main ligands. Asterisks stand for alternatively spliced cytoplasmic domains [43].

The existence of different splice isoforms leads to a further diversity of the integrin family. Splice variants of the extracellular domain as well as of the cytoplasmic domain have been reported. Specific isoforms can be found in certain tissues and in some cases tissues can also switch between the expression of different isoforms during development. While for example the A isoform of the integrin $\beta 1$ ($\beta 1A$) is expressed in all tissues except for muscle and heart, these tissues only express the isoform $\beta 1D$ [45].

The integrins were named after their important role in the maintenance of the integrity of the cytoskeletal-ECM linkage [46; 47]. They provide a bidirectional connection between the interior of the cell and the extracellular environment across the cell membrane. The integrins link the extracellular matrix to the actin cytoskeleton, except for the integrin $\alpha 6\beta 4$, which connects the ECM to intermediate filaments.

Integrin ligand binding and integrin activation result in a large variety of signal transduction events within the cell that can influence different cell behaviours such as adhesion, proliferation, survival, apoptosis, cell shape, polarity, motility, gene expression and differentiation. The majority of these events depends on the modulation of the cell cytoskeleton [42].

5.2.2. Structure of integrins

Integrin function is closely connected to its structure. Each integrin subunit is a type I transmembrane protein composed of an extracellular domain consisting of approximately 700-900 amino acids, a single transmembrane helix and a cytoplasmic domain with a length of 10-70 amino acids except for integrin $\beta 4$ (1.072 amino acids) [48].

The cytoplasmic domains of β integrin subunits reveal a striking sequence homology among each other, while different α integrin subunits show highly divergent sequences except for a common $K\pi GFFKR$ sequence close to the plasma membrane with π standing for a conserved apolar amino acid [49; 50]. This sequence is essential for the association with the HDR(R/K)E motif in β integrin subunits via hydrophobic and electrostatic interactions. For some integrin heterodimers, the arginine residue in the α subunits and the aspartate residue in the β subunits are thought to form a salt bridge [51; 52].

Integrin cytoplasmic domains lack enzymatic activity and actin binding motifs. Therefore they depend on the binding of cytoskeletal and signaling proteins that mediate processes like signal transduction and coupling to the cytoskeleton. The cytoplasmic domains of most β integrin subunits reveal two recognition sites for PTB domains, a membrane proximal NPxY motif and a more distal NxxY motif. These motifs can be bound by FERM domain containing proteins like talin and kindlin, which play an important role in integrin activation [53].

The transmembrane domains of the integrins are merely characterized. Only the structures of the integrin subunits $\beta 3$ and $\alpha 11b$ are fully solved [54-56]. The

transmembrane domain of the integrin $\beta 3$ consists of 30 amino acids arranged in a linear α helix. This helix is longer than a common lipid bilayer suggesting that the helix is tilted within the membrane. The $\alpha 11b$ transmembrane domain forms an α helix of only 24 amino acids with an adjacent backbone reversal. This rare motif is conserved in all α integrin subunits pointing to a crucial role within the activation process.

The extracellular domains of the two integrin subunits arrange as a head sitting on two legs (Figure 6), revealed by electron microscopy and biophysical data [57; 58]. The head domain represents the ligand binding part of the heterodimer with the extracellular domain of the α subunit determining the ligand specificity of the integrin. The extracellular domain of the β subunit shows a more complex domain structure than the one of the α -subunit. It is composed of a βA (also called βI) domain, which is inserted into an immunoglobulin (Ig)-like “hybrid” domain, a N-terminal PSI (plexin, semaphorins, and integrins) domain, four tandem cysteine-rich epidermal growth factor (EGF)-like repeats and a β -tail domain (β -TD) (Figure 6). A disulfide bond connects the PSI domain to the distal EGF domain [43; 48].

The extracellular domains of the α integrins contain an N-terminal seven-bladed β -propeller domain followed by an Ig-like (thigh) and two β sandwich domains (calf1 and calf2) (Figure 6). The last three or four blades of the β -propeller contain EF hand domains that bind Ca^{2+} -ions and thereby allosterically affect ligand binding [49; 59].

The head region of the integrins is composed of the βA and the “hybrid” domains of the β subunit together with the β propeller domain of the α subunit. The ligand binding pocket lies at the interface between the β propeller and the βA domain. Tight interactions between integrins and their ligands are dependent on divalent cations. The βA domain of the β integrin subunit contains three metal ion binding sites, which are essential for ligand binding. A central Mg^{2+} binding site called MIDAS (metal ion dependent adhesion site) is flanked by two Ca^{2+} binding sites, which are referred to as SyMBS (synergistic metal ion binding site) and AdMIDAS (adjacent to MIDAS), respectively [58].

The collagen-binding and leukocyte-specific α integrin subunits contain an additional αA domain, which is inserted into the large β propeller domain and which is analogous to the βA domain of the β subunit. If present, its MIDAS motif is in most cases the ligand binding site [43; 60; 61].

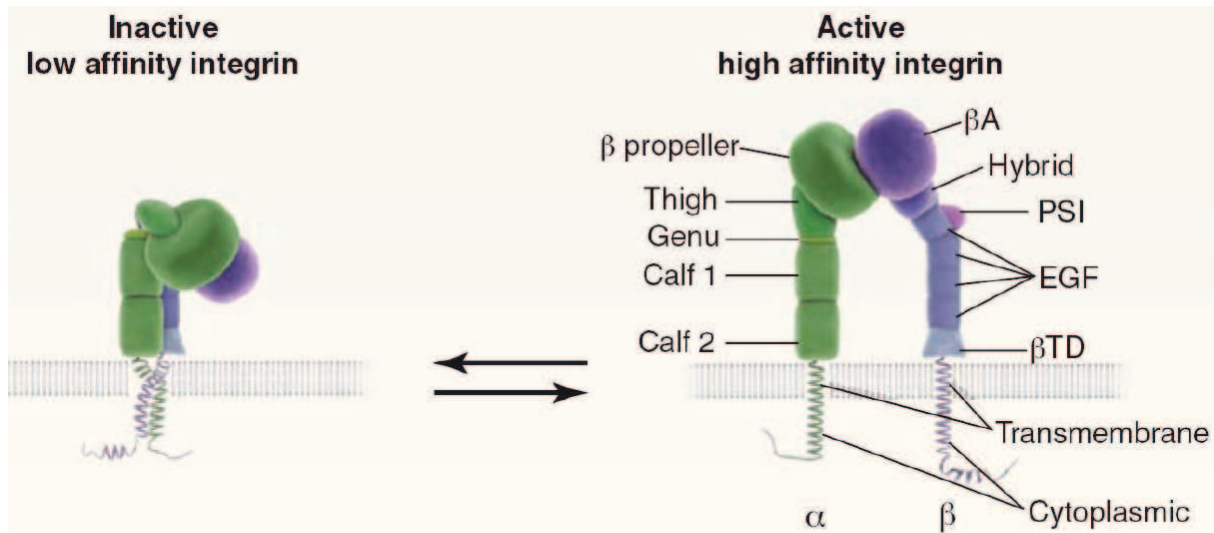


Figure 6: Schematic presentation of the integrin structure and integrin activation. The bent, inactive conformation (left) is characterized by certain contacts between the extracellular, the transmembrane and the cytoplasmic domains. Integrin activation leads to separation of the cytoplasmic and transmembrane domains and to an extended conformation (right). β TD: β tail domain; EGF: epidermal growth factor domain; PSI: plexin/semaphorin/integrin domain [60].

Dependent on their activation state integrins exist in different conformations. They can be observed in a low, an intermediate and a high affinity state. Structural studies and electron microscopy gave insights into the different conformational states of integrins. It is believed that integrins in a low affinity, inactive state show a bent conformation, while the extracellular domains are extended in active, high-affinity integrins (Figure 6 and 7) [60].

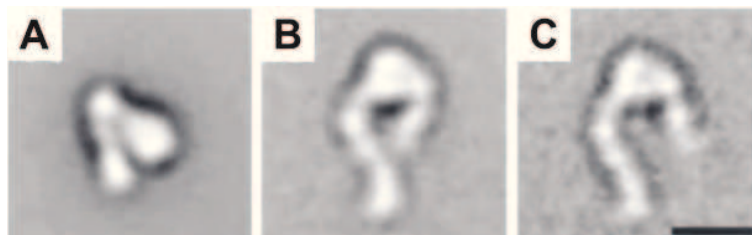


Figure 7: Representative 2D projection averages of negatively stained $\alpha v \beta 3$ integrin electron micrographs. (A) $\alpha v \beta 3$ integrin in the presence of Ca^{2+} showing a bent inactive conformation (B) and (C) show extended $\alpha v \beta 3$ integrins with an open headpiece purified in the presence of (B) Mn^{2+} or (C) Ca^{2+} and cyclo-RGDfV (arginine/glycine/aspartate/D-phenylalanine/valine). Size bar indicates 100 \AA . Modified from [62].

The mechanism, by which the conformational changes occur, is not yet fully elucidated. Two major models have been proposed for this process. Both models suggest that the integrin head faces the membrane in its bent, inactive conformation. The switchblade model on one hand claims that integrins can only bind ligands in their extended conformation. The conformational changes within the inactive, bent

integrin start with the dissociation of the cytoplasmic and transmembrane domains. In those integrins that form a salt bridge between both cytoplasmic domains, this connection ruptures. Currently it is believed that the separation of the integrin tails is triggered by the binding of proteins, among which talin and kindlins seem to be the most important ones. While the transmembrane domains of an inactive integrin heterodimer interact with each other in a coiled-coil conformation via canonical GxxxG dimerization motifs in each transmembrane sequence, they separate during integrin activation [60]. These changes lead to dislocation of an EGF-like repeat in the β integrin stalk, outwards extension of the head region in a switchblade-like movement and the opening of the ligand binding pocket [48].

The deadbolt model on the other hand does not require an unbending process before ligand binding. This model states a conformational change within the head domain to unmask the ligand binding site upon a change in the tilt of the transmembrane domains. The extension occurs after ligand binding [48; 58; 63].

Crystal structure analyses of the integrin $\alpha V\beta 3$ support the switchblade model. These experiments proved that the head region of an inactive integrin with low affinity to the ligand shows a bent conformation and that activated integrins show an extended conformation with a high affinity to ligands [42]. However, it has been shown that integrins in a bent conformation can also bind to ligands, especially in the case of small ligands indicating that bent integrins are not necessarily inactive [63].

5.2.3. Integrins and their ligands

Integrins connect the ECM to the actin cytoskeleton providing the architectural framework to determine cell shape and to react to changes in the microenvironment [64; 65]. Integrins influence the type and the organization of the ECM surrounding the cell. The spatial distribution of the ECM affects directional cell migration. Integrin-ligand interactions can also control the cell division axis during mitosis and therefore influence the arrangement of cells within multicellular tissues [66; 67].

According to their ligand-binding abilities, integrins can be divided into subclasses: the collagen-, the laminin- and the RGD (arginine/glycine/aspartate)-binding integrins [44]. The leukocyte-specific integrins represent the fourth main class of integrins (Figure 5). They mediate cell-cell interactions with endothelial cells by binding to cellular counter-receptors such as ICAMs and vascular cell adhesion molecules (VCAMs) [68].

The RGD sequence is the minimal integrin recognition site in various integrin ligands such as fibronectin, vitronectin, tenascin, osteopontin and fibrinogen. The family of RGD binding integrins is a very promiscuous group. This motif is recognized by all α V integrins and by the integrins $\alpha 5\beta 1$, $\alpha 8\beta 1$ and $\alpha 11\beta 3$. Especially the $\beta 3$ integrin family recognizes a large number of matrix proteins and soluble vascular ligands [44].

The LDV (lysine/aspartate/valine) sequence, recognized by the integrins $\alpha 4\beta 1$, $\alpha 4\beta 7$, $\alpha 9\beta 1$, the four members of the $\beta 2$ subfamily and $\alpha E\beta 7$, is functionally related to the RGD motif. The type III connecting segment region of fibronectin contains the prototype LDV ligand and integrin ligands such as VCAM-1 and MadCAM-1 reveal related sequences [44].

The combination of the integrin $\beta 1$ and the α A-domain containing integrins $\alpha 1$, $\alpha 2$, $\alpha 10$ or $\alpha 11$ forms the group of collagen binding integrins. The integrins $\alpha 3\beta 1$, $\alpha 6\beta 1$ and $\alpha 7\beta 1$ and the integrin $\alpha 6\beta 4$ interact selectively with laminins [44].

Additional integrin ligands are endostatin, endorepellin and tumstatin, which are derived by proteolysis from collagen XVIII, perlecan and collagen $\alpha 3$, respectively [69; 70]. Furthermore, $\alpha M\beta 2$ and $\alpha X\beta 2$ are able to interact with heparin as well as with negative charges in denatured proteins [44].

The family of integrin ligands includes further proteins, like milk fat globule-EGF factor 8 (MFGE8) and complement factor iC3b. The binding of integrins to complement factor is important for the phagocytosis of apoptotic cells as well as pathogens. Another ligand is the latency-associated peptide (LAP) of transforming growth factor β (TGF β), which regulates the activation of TGF β . Some proteins of the ADAM family (a disintegrin and metalloproteinase) and the matrix metalloproteinase-2 (MMP-2), which participate in ECM remodelling during cell adhesion and migration also belong to integrin ligands [53].

Furthermore, integrins can also bind to non-physiological ligands, such as snake toxins, several viruses and bacteria. Some of these ligands do not interact with the usual ligand-binding site of the integrin and reveal differences in their binding abilities compared to ECM molecules [59].

5.2.4. Integrins as bidirectional signaling molecules

In contrast to most transmembrane proteins integrins have the ability to transmit signals bidirectionally: from the environment into the cell as well as from the interior of the cell to its surface. Ligand engagement results in the recruitment of cytoplasmic

proteins to the integrin cytoplasmic domains. These proteins either link the integrin with the actin cytoskeleton or signal via diverse signaling pathways. This process is known as integrin outside-in signaling and controls different cellular functions such as cell spreading, migration, proliferation and apoptosis. On the contrary the process of integrin activation is called integrin inside-out signaling. Here, intracellular signaling cascades induce changes in the integrin conformation resulting in an integrin with increased ligand binding affinity [43; 71; 72].

Integrins expressed on blood cells had been extensively studied. Their activation and signaling needs to be tightly controlled. Integrin activation is for instance necessary for platelet adhesion and aggregation, which are essential for sealing injured blood vessels in order to prevent blood loss. But it is crucial to prevent excessive, pathological platelet aggregation as it can initiate arterial thrombosis, causing heart attacks and stroke [73]. Similarly, leukocytes require integrin activation in case of inflammation in order to extravasate from blood vessels and migrate to inflamed tissue. Impaired integrin activation can result in leukocyte adhesion deficiency. Therefore regulation of integrin affinity is fundamental in these processes.

5.2.4.1. Inside-out signaling

Integrins on resting cells are usually found in an inactive conformation with low affinity to extracellular ligands until they get activated by intracellular signaling events in the process of integrin inside-out signaling. This is accompanied by binding of a number of cytoplasmic proteins to the cytoplasmic domain of the β integrin subunit, yet only talin and kindlins are known to regulate integrin affinity [71; 74].

The cytoskeletal protein talin, an antiparallel homodimer of two approximately 270 kDa proteins, plays a crucial role during integrin activation. In mouse and man, talin exists in two isoforms, talin-1 and talin-2 [75]. The protein consists of a globular head at the N-terminus and a C-terminal rod domain. The rod domain consists of several helical bundles harbouring multiple vinculin binding sites. Both talin and vinculin can directly bind to actin filaments [75].

The FERM domain of the talin head binds to the cytoplasmic domain of the β integrin subunit via its PTB motif in the F3 subdomain. This event is essential for integrin activation. Talin binds at two distinct sites along the β integrin cytoplasmic domain. The talin head first interacts with the membrane proximal NPxY motif of β integrins and subsequently binds to its second, additional binding site, which is membrane

proximal where the integrin tails interact with each other. Binding of talin to both sites allows electrostatic interaction between a positively charged region in the F3 domain and the polar head groups of the plasma membrane (Figure 8, Figure 9A and B). Mutational studies of the β integrin tail showed that binding of talin to both regions is necessary to facilitate the separation of the integrin tails [51; 52; 76]. The amino acids R358 and W359 in the talin F3 domain are crucial for its function and mutations of these amino acids to alanine abolish the binding of talin to integrins and therefore its ability to mediate integrin activation [35].

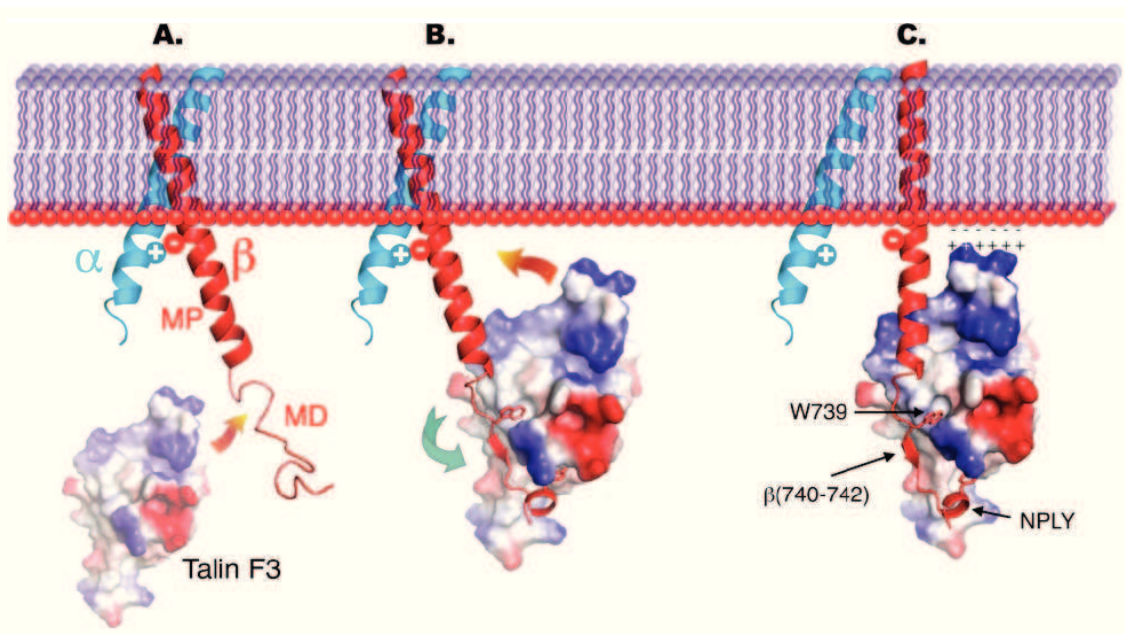


Figure 8: Schematic overview of talin mediated integrin activation of β_3 integrins. (A) The talin F3 domain (stained by charge) and the cytoplasmic domains of the integrin heterodimer connected by a salt bridge are shown. **(B)** The F3 domain binds to the membrane distal (MD) part of the β integrin tail (red) that includes the NPLY motif. This results in a higher order structure of the integrin tail but keeps the interaction between the subunits. **(C)** In the next step talin extends its interaction with the β integrin tail by binding to the membrane proximal (MP) part inducing the separation of the integrin subunits. Additionally a positively charged region in the F3 domain of talin forms electrostatic interactions with polar head groups of the plasma membrane. Together this leads to changes in the register of the transmembrane helices, which finally lead to integrin activation [76].

While binding of the talin head domain can increase integrin affinity, full-length talin is needed for connecting integrins with the cytoskeleton and for integrin clustering [77]. Talin reveals two binding sites for the β integrin subunit, one within the FERM domain and one in the rod domain. The presence of multiple integrin binding sites within a talin homodimer provides a possibility for integrin clustering [78].

Talin is necessary but not sufficient to activate integrins. A number of in vitro and in vivo studies have shown that in addition to talin the family of kindlin proteins is also

required for integrin activation [31; 34; 35; 37; 78]. Kindlins, like talin, also interact directly with the cytoplasmic tails of the β integrin subunits via their FERM domains [8; 35]. The FERM domains of kindlin proteins and talin reveal high similarities [8] but instead of the arginine 358 in the talin F3 domain, which is crucial for its interaction with the integrin tail, the kindlins reveal a glutamate [35].

All kindlins bind to the distal NxxY motif within the cytoplasmic domain of β integrins and have therefore a binding site, which is distinct from the talin binding site. Additionally, they interact with a serine/threonine motif, which is located between the two NxxY sequences (Figure 9A and 9C). Mutations within these sites abolish kindlin/integrin interaction. Furthermore, the integrin interaction site within the F3 subdomain of the FERM domain has been mapped since mutations of certain glutamate and tryptophan residues into alanine prevent integrin binding and activation [35; 37].

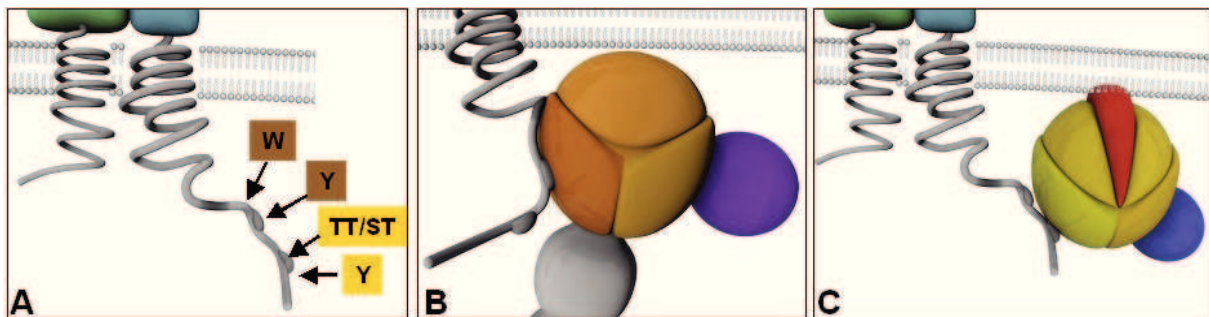


Figure 9: Scheme of integrin tail binding by talin and kindlin. (A) The tryptophan (W) and the tyrosine (Y) from the membrane proximal NPxY motif of the cytoplasmic domain of the β integrin subunit are bound by talin (B). The threonine/threonine (TT) or serine/threonine (ST) sequence and the tyrosine part of the membrane distal NxxY motif interact with kindlin (C). Modified from [60].

As integrin activation needs to be tightly regulated, the interaction of talin and probably also kindlin with the integrin underlies strict regulation. Non-activated talin exists in an autoinhibitory state, in which the C-terminal rod domain masks the integrin binding site of the FERM domain [80]. The mechanism, by which talin is activated, is not yet fully elucidated. Probably binding of the lipid second messenger phosphatidylinositol-4,5-bisphosphate (PIP₂) is involved in this process by inducing a conformational change that weakens the autoinhibition [80; 81]. Talin interacts with phosphatidylinositol 4-phosphate 5-kinase γ (PIP₅K γ) and directs it to focal adhesions [82; 83]. This may provide a feed-forward loop for the recruitment of talin to newly formed adhesion sites, as PIP₅K γ locally produces PIP₂, which can be bound by

additional talin molecules. Calpain cleavage and phosphorylation may be further mechanisms controlling talin activity.

In haematopoietic cells it could be shown that Rap1, a guanosine triphosphatase (GTPase) plays a role in talin recruitment to integrins [84; 85]. It associates with the Rap1 effector Rap1-GTP-interacting adaptor molecule (RIAM) and forms a ternary complex together with talin at the integrin cytoplasmic domain [86; 87]. A similar mechanism could take place in non-haematopoietic cells, in which the role of RIAM could be taken over by the RIAM-homolog lamellipodin [88].

A further possibility to regulate talin-integrin association is phosphorylation of the integrin's cytoplasmic domain. The tyrosine residue in the NPxY motifs of the integrins $\beta 1$ and $\beta 3$ can be phosphorylated by the non-receptor tyrosine kinase Src [89]. This phosphorylation probably inhibits the interaction between talin and the integrin tail or it maintains an inhibitory complex between Dok1 and the cytoplasmic domain of the β integrin subunit that keeps the integrin in an inactive state [90].

Since both talin and kindlins are essential for integrin regulation it is very likely that kindlins are also tightly regulated, however the mechanism is still elusive. As kindlins contain a PH domain, they may also be regulated by certain phosphoinositides. A further possibility might be phosphorylation. In case of kindlin-1 phosphorylation could already be shown [25] but so far prove of a correlation between kindlin phosphorylation and activity is missing.

Both talin and kindlins are crucial for integrin activation but neither of them is sufficient. They have to cooperate during the integrin activation process due to their distinct binding sites at the integrin tail [34; 91]. It was shown that overexpression of kindlins in cells with low talin levels has no or only little impact on integrin affinity [86], while coexpression of talin head together with kindlin results in an increase in integrin affinity.

Many question on how exactly integrins are activated are still open. Involvement of further proteins that regulate integrin affinity can not yet be excluded and the precise mechanism of how talin und kindlins cooperate to control integrin activity remains to be elucidated. Several scenarios are conceivable. One model proposes a sequential binding of talin and kindlin to the cytoplasmic domain of the β integrin subunit, but so far it is completely unclear, which of the two proteins binds first. Another possibility could be a simultaneous binding of both proteins due to the distinct binding regions.

It also needs to be further investigated whether integrins on certain blood cells, which have to be activated very rapidly, and integrins expressed on cells of solid tissues or epithelia, where fast activation is less crucial, are activated via the same mechanism.

5.2.4.2. Outside-in signaling

Activation of integrins, binding to extracellular ligands and integrin clustering allow outside-in signaling. The transduction of a variety of signaling events influences a whole set of different cellular behaviours. The signaling downstream of integrins is not only dependent on the integrin heterodimer itself and the bound ECM molecule but is also influenced by the mechanical properties of the ECM. Integrins can transmit and modulate intracellular forces [92].

Integrin activation positively influences the affinity of a single integrin to ligands. To establish a very strong attachment site to the ECM, the binding avidity needs to be increased. This requires the organization of integrins into clusters, in which many weak integrin-ECM interactions together form a tight adhesion. Newly formed, small clusters are known as nascent adhesions [93]. Some of them mature into focal complexes, further into focal adhesions and finally into fibrillar adhesions [94]. A huge number of proteins are recruited to these adhesion sites. They are assembled in dynamic, multimolecular complexes with many functions: they organize the cytoskeleton, mechanically link the ECM to the actin cytoskeleton and serve as biochemical signaling hubs to concentrate various signaling processes.

So far, more than 150 proteins are known that participate in integrin mediated adhesion sites as signaling, structural and adaptor proteins [95]. These proteins include enzymes, Rho family GTPases, protein and lipid kinases and phosphatases [96]. Proteins bound to the cytoplasmic domain of the integrin heavily influence the downstream effects and the formation of adhesion site itself as they bind additional proteins. Phosphorylation can provide further diversity. Modification of the integrin's cytoplasmic domain, for instance phosphorylation of the NxxY motifs by Src, can also contribute to the determination, which proteins can bind [53].

Activation of various signaling pathways upon integrin ligand interactions is not only controlled by the assembly of the integrin-mediated adhesion complex but in addition through organization of the plasma membrane in lipid rafts and endocytosis [77].

The first, immediate consequences following integrin activation and ligand engagement are an increase in phosphorylation of certain proteins, e. g. Src, focal

adhesion kinase (FAK), p130Cas (p130 Crk-associated substrate) and paxillin, and elevated levels of lipid second messengers, such as PIP2 and PIP3 (phosphatidylinositol-3,4,5-trisphosphate). Subsequently, cytoskeletal reorganization occurs and actin fibers get connected to integrins facilitating the cell to change shape or to start migration [77]. Adhesion to matrix over a longer period of time can lead to alterations in signaling pathways and finally to changes in gene expression.

The immediate effects upon integrin ligation include the autophosphorylation of Src and FAK on tyrosine 418 and tyrosine 397, respectively, by which both proteins become activated. This enables FAK to interact with Src stabilizing its active form and increasing its catalytic activity. The formation of the Src/FAK complex, which further activates ERK (extracellular signal-regulated kinase) and JNK (c-Jun N-terminal kinase), is central in the integrin signaling process [97]. Downstream of ERK cyclin D is activated and regulates cell cycle progression. Furthermore activated FAK recruits PI-3-kinase resulting in elevated PIP3 levels and activation of Akt (RAC-alpha serine/threonine protein kinase).

The Src/FAK complex can also act on RhoGTPases via Crk/Dock180 (dedicator of cytokinesis1) or the PIX/GIT (PAK interactive exchange factor/G-coupled receptor kinase-interacting protein) pathway (Figure 10 and 11A). RhoGTPases are important regulators of the downstream signals following integrin activation and regulate many aspects of actin dynamics. They are active in their GTP-bound form and inactive when harbouring GDP. They are controlled by GEFs, GTPase-activating proteins (GAPs) and guanine nucleotide dissociation inhibitors (GDIs). The major GTPases involved in integrin signaling are Rac, Cdc42 and RhoA [98]. Cdc42 and Rac1 activate Arp2/3 via the Wiskott-Aldrich Syndrome protein (WASp) and the Scar/WAVE proteins, respectively. Activated Arp2/3 can initiate actin polymerisation and branching of actin filaments [99]. RhoA is important for the regulation of cell contractility. It activates formins and ROCK (Rho-associated protein kinase), which phosphorylates myosin light chain (MLC) thus inducing actin-myosin contraction (Figure 10A) [77].

Beside the activation of signaling pathways, the organization of the cytoskeleton is a consequence of integrin binding to ECM. The linkage of integrins to actin fibers is established by a number of proteins (Figure 10). The recruitment of talin plays a central role in this process. The binding of talin to the integrin tails is followed by the recruitment of vinculin, which is important for the maturation of focal adhesions. Talin

deficient cells and cells expressing the talin head domain lack focal adhesions [100], while vinculin deficient cells make few but small and unstable adhesion sites that do not mature [101]. Talin can provide some direct connections to actin, enough for establishing nascent adhesions, but vinculin is required to strengthen the linkage [75]. The actin-binding protein α -actinin can directly bind to β integrins and interacts with talin as well as vinculin (Figure 10A) [102]. Its most important function seems to be the strengthening of the integrin-actin connection. α -actinin and also myosin-II are actin crosslinking proteins, important for FA growth and maturation [93].

Kindlins provide a link between adhesion sites and the cytoskeleton, too. Kindlin-1 and -2 interact with migfilin, which in turn binds to filamin, and ILK. Both interactions provide indirect connections to the actin cytoskeleton (Figure 10B) [33; 103].

The adaptor protein ILK is another integrin tail binding protein. It associates with pinch (particularly interesting new cysteine-histidine-rich protein) and parvin in the ILK-pinch-parvin (IPP) complex (Figure 10B). It forms connections to the actin cytoskeleton via parvin and paxillin, which in turn can interact with parvin and vinculin [53]. ILK contributes to adhesion strengthening by providing integrin-actin connections and supporting integrin clustering [104]. In addition ILK crosslinks integrin and growth factor signaling as pinch can interact with Nck-2, which in turn binds to receptor tyrosine kinases (RTK) (Figure 10) [105].

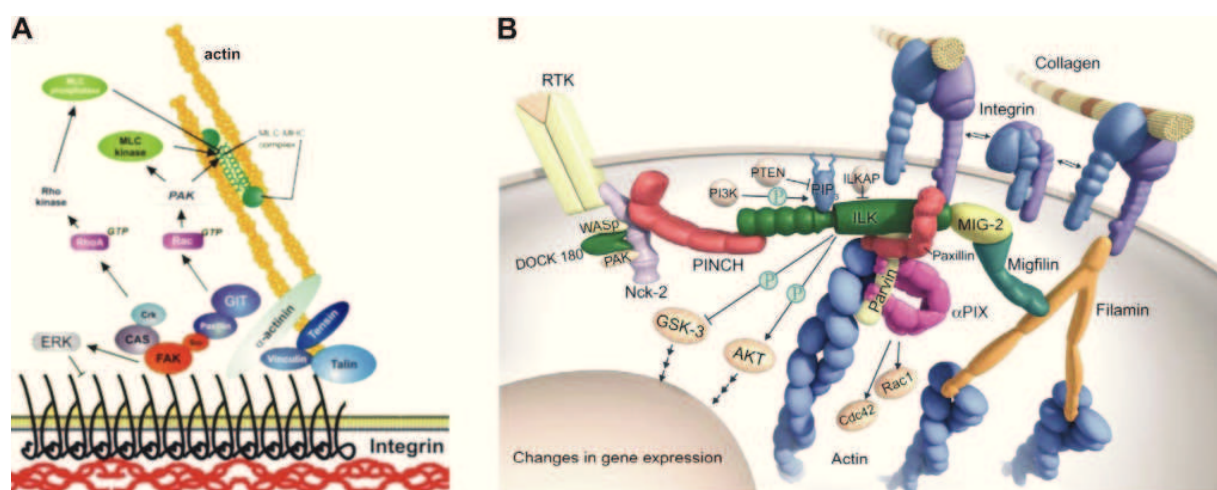


Figure 10: Schemes of a focal adhesion showing proteins involved in signal transduction and integrin-actin connection. (A) Integrin-actin linkage includes talin, vinculin and α -actinin. Other signaling adaptors like FAK and paxillin are also recruited. The adhesions generate signals like activated Rac and RhoA, leading to actin polymerisation and bundling. Modified from [106]. **(B)** ILK associates with Pinch and parvin in a ternary complex and binds to the cytoplasmic domain of the activated β integrin subunit. It can also interact with kindlin (Mig-2), providing a further linkage to the ECM via migfilin and filamin. ILK also links integrin signaling to receptor tyrosine kinase signaling via pinch and Nck-2. Modified from [107].

5.2.5. Integrin crosstalk with growth factor and cytokine signaling

The composition of proteins recruited to the cytoplasmic domains of the integrins is influenced by the integrin heterodimer, the ECM and the cell type. In addition, the growth factor environment plays an important role. Integrins and growth factor or cytokine receptors can cooperate to provide specificity in signaling processes. They can act independently of each other, but the ECM and soluble factors, such as growth factors, hormones or cytokines, can also simultaneously activate integrins and receptors, signal synergistically and lead to the regulation of complex events. Adhesion to matrix molecules can influence growth factor receptors and vice versa. A precise spatial and temporal organization of the signals is very important for the resulting downstream effects. The interaction between integrins and the ECM is rather stable and therefore the signals from the microenvironment are sustained over a period of time. In contrast the diffusible growth factors and cytokines signal in a more temporal manner [108].

Impaired crosstalk between integrin and growth factor signaling results in diseases, for instance cancer. Cancer is characterized by missregulation of growth factor signaling and tumour cells can be independent from integrins leading to increased proliferation and/or migration [109; 110]. Loss of integrin mediated adhesion is one step in the development of metastases. On the contrary, cells can also upregulate integrins during tumour progression to enhance downstream signals [111].

There are several ways, in which growth factors can influence integrin function. Growth factor signaling can for instance change the expression level of certain integrins or integrin-binding proteins. TGF β 1 uses this mechanism to increase the expression of the integrins β 1 and α 5 in endothelial cells [112]. A further possibility how growth factor signaling interferes with integrin signaling is by influencing integrin conformation and by this the ligand affinity. They control the activation status of integrin associated signaling proteins like FAK, Src and PI3K and/or regulate downstream signaling effectors such as ERK, Akt, JNK and RhoGTPases (Figure 11A). For example, ERK activation resulting from cooperative integrin and growth factor signaling is increased in intensity and duration [77].

Chemokine-activated G-protein coupled receptors (GPCR) signal via PI3-kinase and phospholipase C (PLC) to increase integrin affinity. This represents a form of integrin inside-out signaling and is especially important for immune cells. Activation of the T cell antigen receptor upon antigen binding increases integrin activation in a PLC γ 1-

and Rap1-dependent manner (Figure 11B) [113; 114]. Similar processes can activate integrins on platelets in the clotting cascade [115].

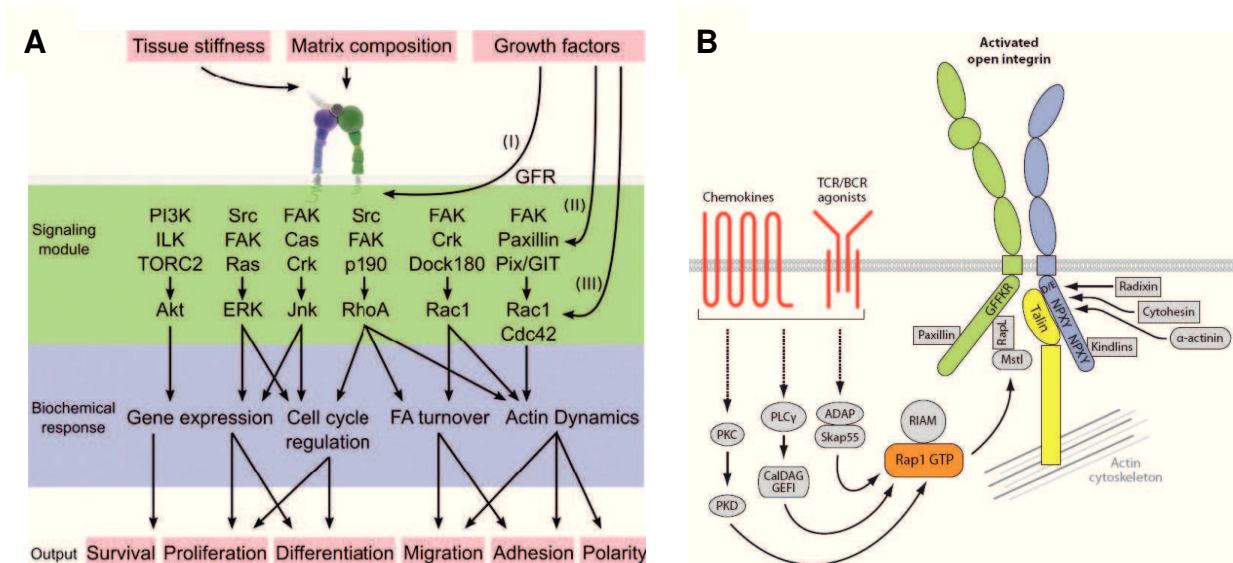


Figure 11: Signaling pathways resulting from crosstalk of integrins and growth factors. (A) Growth factor signaling influences integrin signaling in concert with the composition and the mechanical properties of the ECM [77]. (B) Signaling pathways leading to integrin activation in lymphocytes. Activation of a variety of receptors such as chemokine-activated G-protein coupled receptors or T cell receptors leads to recruitment of GTP-bound Rap1 and talin binding to the integrin tails, which results in activation of the integrins [114].

Conversely, integrins also have an impact on growth factor signaling. They can affect the cellular localization, posttranslational modification, expression of the receptors or the growth factors themselves. Integrins can also regulate receptor activation prior to ligand binding. Some integrins control for instance TGF β signaling via binding to latency-associated peptide [116]. Several receptor tyrosine kinases, such as PDGFR (platelet-derived growth factor receptor), EGFR (epidermal growth factor receptor), VEGFR (vascular endothelial growth factor receptor) and HGFR (hepatocyte growth factor receptor), can be activated simply by integrin mediated cell adhesion [117]. Most of these interactions are likely to be indirect.

An example for the crosstalk between integrins and RTKs is the cooperation of integrin β 1 and EGFR in several cell types. Both activate ERK and Akt pathways in order to regulate diverse cellular aspects, including cell cycle progression [118]. Integrins regulate proliferation via Src signaling and also in this process growth factor receptors contribute to the downstream effects. After ligand binding a fraction of EGFR is associated with integrin β 1 in a complex with Src and p130Cas. This complex is required for phosphorylation and activation of the EGF receptor [119].

Remarkably, this complex results in a distinct EGFR phosphorylation pattern, which is different from the phosphorylation pattern induced by EGF binding. This suggests additional functions of EGFR apart from the ones downstream of the growth factor.

Integrin-mediated adhesion also controls interferon responses in a protein kinase C ϵ dependent manner. For instance, STAT1 (signal transducer and activator of transcription) signaling in response to interferon γ is much stronger in adherent cells than in cells in suspension [120].

Another example, in which integrins and growth factors collaborate, is the crosstalk between the integrin α V β 3 and the M-CSF (macrophage colony stimulating factor) receptor c-Fms in osteoclasts and their precursors. Signals from both receptors are required to regulate the osteoclast cytoskeleton, osteoclast differentiation as well as the proliferation of osteoclast precursors. Ligand binding by the integrin and M-CSF exposure simultaneously lead to a prolonged ERK signal [121]. The short-term effect of ERK activation is stimulation of precursor proliferation. Long duration of the signal induces for instance the expression of the transcription factor c-Fos and its nuclear translocation. This in turn promotes the expression of nuclear factors for activation of T cells (NFATs) that are central in osteoclast differentiation by upregulation of certain genes (Figure 12) [122]. The activation of c-Fms also leads to signaling through PI3K, which further activates Akt. Both proteins are also downstream targets of integrin signaling and therefore represent a further intersection of integrin-growth factor crosstalk [123]. Furthermore, integrin α V β 3 and c-Fms act via the non-receptor tyrosine kinase Syk. Activation of the α V β 3 heterodimer is followed by the activation of Src, probably by autophosphorylation. Src phosphorylates DAP12 (DNAX-activating protein of 12 kDa) and FcR γ (fragment (crystallisable) receptor γ), which are adaptor molecules containing an immunoreceptor tyrosine-based activation motif (ITAM). The phosphorylation of ITAM provides a binding site for Syk and results in the recruitment of Syk to the cytoplasmic domain of the β integrin subunit. Syk subsequently interacts with Src and becomes activated. Downstream of Syk the Rac GEF Vav3 is activated. The GTP-bound form of Rac finally initiates cytoskeleton reorganization [123; 124]. Binding of M-CSF to its receptor on the other hand leads to autophosphorylation of the receptor generating a binding site for Src at tyrosine 559. This interaction also results in Src autophosphorylation and the phosphorylation of DAP12. The subsequent recruitment and activation of Syk again lead to cytoskeletal rearrangement via Vav3 and Rac (Figure 12) [123; 125].

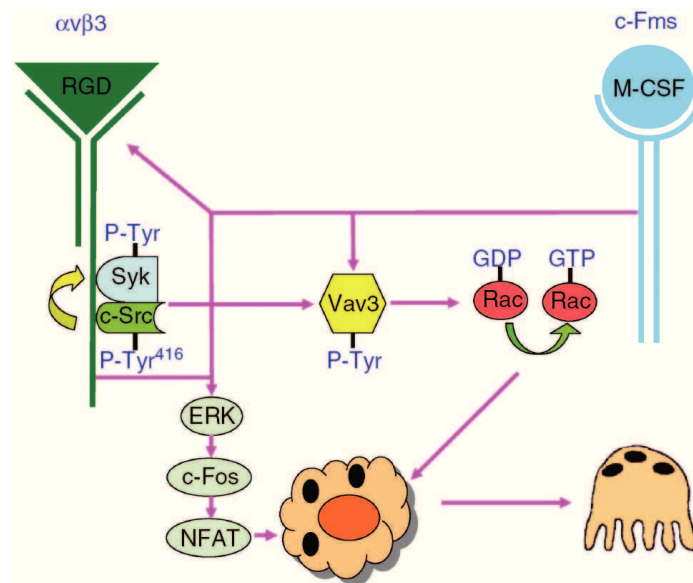


Figure 12: Scheme of the crosstalk between integrin $\alpha v\beta 3$ and the M-CSF receptor c-Fms. ECM binding and M-CSF exposure together lead to the activation of a signaling pathway including ERK, which leads to differentiation via the nuclear proteins c-Fos and NFAT. Ligand bound integrin $\alpha v\beta 3$ and activated c-Fms also result in activation of the RhoGTPase Rac via Src, Syk and Vav3 [123].

5.2.6. Integrins in mouse development

The 24 different integrins show specific ligand binding properties and different expression patterns. All of them have distinct non redundant functions. This fact becomes apparent by the phenotypes of individual integrin mouse mutants. In most cases these mice show diverse and specific phenotypes that vary significantly between the different subunits. The most important integrin is the $\beta 1$ subunit, which is ubiquitously expressed and which forms heterodimers with 12 different α subunits. None of these integrins is expressed in $\beta 1$ integrin mouse mutants. Consequently, these mice die already during early mouse development at the peri-implantation stage [126; 127].

Loss of $\alpha 4$, $\alpha 5$ and αV integrins in mice results in embryonic lethality, too. While $\alpha 5$ deficient mice die at embryonic days 9.5 and 10 (E9.5/10) due to embryonic and extra embryonic vascular defects [128], integrin $\alpha 4$ knockout mice die later during embryonic development between E11 and E14 from defective choriallantois fusion and abnormal cardiac development [129]. In case of αV deficiency, 80% of the mice die between E10 and E12 due to placental defects, while 20% survive embryonic development but die at birth because of a cleft palate and severe haemorrhages [130].

Genetic deletions of $\alpha 3$ [131-133], $\alpha 6$ [134; 135], $\alpha 8$ [136; 137], $\beta 4$ [138; 139] or $\beta 8$ [140] integrins cause perinatal lethality because of various defects. Integrin $\alpha 3$ deficient mice reveal abnormalities in several organs. They suffer from skin blistering, kidney, lung and brain defects. $\alpha 8$ deficient mice have small or no kidneys and inner ear defects.

Depending on their expression pattern deficiency of other integrin subunits has organ specific abnormalities but the knockout mice are viable and fertile. Absence of the integrins αL , αM , αE and $\beta 7$ lead to leukocyte malfunctions and other defects in the haematopoietic system [141-145]. Lack of $\beta 6$ results in inflammations of skin and airways [146; 147]. $\beta 2$ integrin deficiency causes leukocytosis, impaired inflammatory response, skin infections and T-cell defects [148].

$\beta 3$ and αIIb knockout mice reveal defects in platelet function. They suffer from bleedings due to impaired platelet aggregation [149-151]. $\beta 3$ deficient mice additionally suffer from osteopetrosis and defects in angiogenesis [152; 153].

The generation of tissue-specific integrin knockout mice is especially useful in cases of embryonic lethality and very severe phenotypes in multiple organs. In this way certain defects can be mapped to certain organs or cell types and less severe phenotypes and specific roles of integrins in later developmental stages become apparent in cases where a constitutive knockout is embryonic lethal. A skin specific knockout of integrin $\beta 1$ for example leads to skin blistering, defects in basement membrane arrangement and abnormal hair follicle morphogenesis [154]. Mice lacking the $\beta 1$ integrins in pericytes of blood vessels die perinatally because of blood vessel aneurysms and bleedings. This shows the essential role of integrin $\beta 1$ in vessel wall integrity [155].

5.3. Integrins and cells of the haematopoietic system

5.3.1. *The haematopoietic system*

The haematopoietic system consists of all organs and tissues that contribute to the production of blood. In mouse and man, these are primarily bone marrow, spleen, thymus and lymph nodes.

The process of blood cell formation is called haematopoiesis. All cellular components of the blood and the immune system are generated from haematopoietic stem cells (HSC), which are common pluripotent stem cells. The haematopoietic stem cells

reside in the bone marrow. These cells are not only multipotent, they also possess the ability to self-renew. Already a small number of HSCs can repopulate the haematopoietic system of an organism by proliferation, a phenomenon utilized in bone marrow transplantations [156].

Depending on the control of specific cytokines and granulocyte/monocyte stimulating factors haematopoietic stem cells give rise to myeloid and lymphoid precursor cells with progressively limited multipotency (Figure 13) [156]. Mature blood cells are divided into the two haematopoietic lineages: the myeloid lineage including neutrophils, monocytes, macrophages, erythrocytes, mast cells and megakaryocytes, and the lymphoid lineage made from B-cells, T-cells and natural killer (NK) cells [157]. Dendritic cells have a unique differentiation program, as they can derive from myeloid or lymphoid progenitors [158].

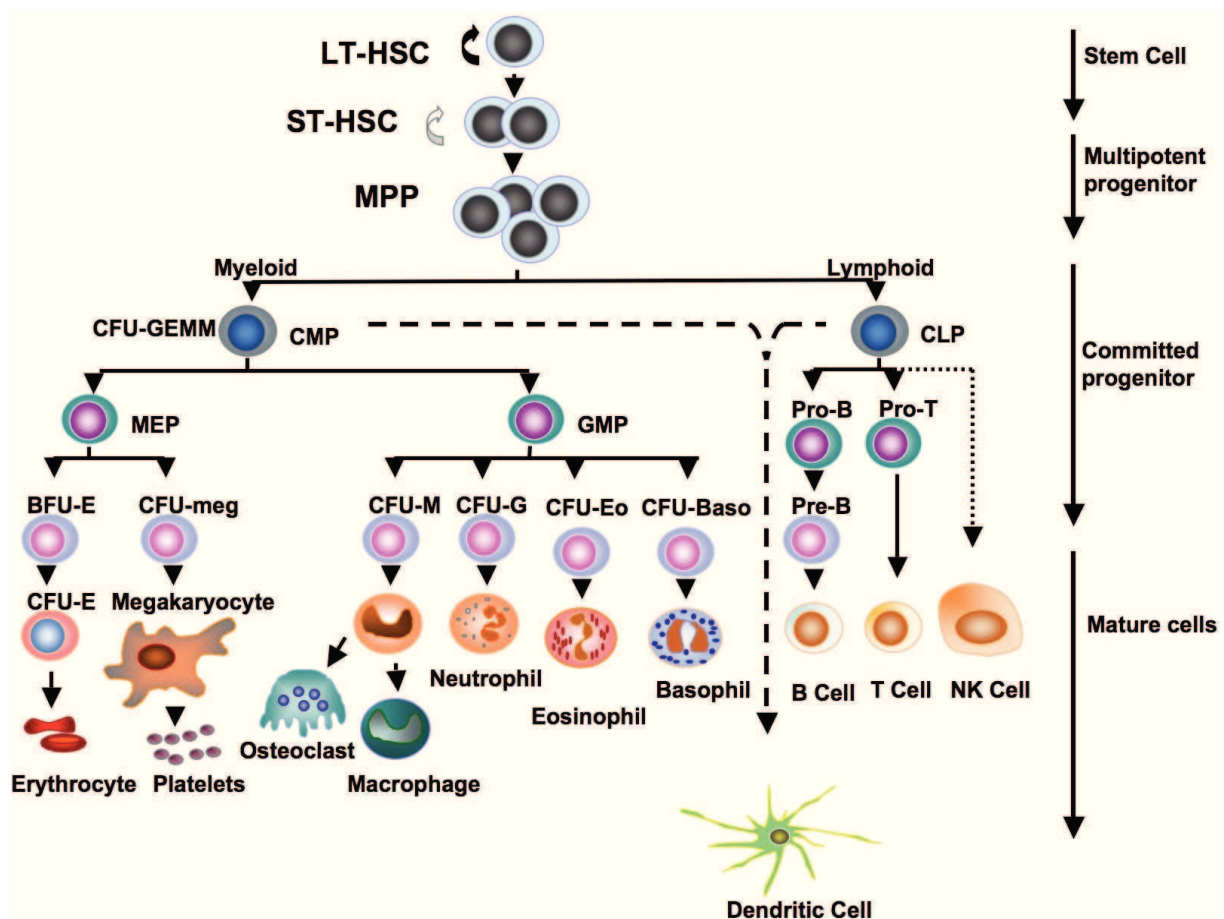


Figure 13: Diagram of the differentiation of the various mature blood cells from haematopoietic stem cells. LT-HSC: long term haematopoietic stem cells; ST-HSC: short term haematopoietic stem cells; MPP: multipotent progenitor; CMP: common myeloid progenitor; CLP: common lymphoid progenitor; CFU: colony forming unit; MEP: macrophage-erythrocyte progenitor; GMP: granulocyte-macrophage progenitor; BFU: burst forming unit. Modified from [159].

HSCs express high levels of integrin $\beta 1$. $\beta 1$ deficient HSCs are unable to colonize fetal liver, bone marrow, spleen and thymus due to impaired adhesion and migration [160]. The integrin $\alpha 4\beta 1$ is of special importance in this process by interacting with VCAM-1 [161; 162]. $\alpha 4\beta 1$ is critical to HSCs homing, retention and lodgement. Lack of the integrin $\alpha 4$ subunit instead does not prevent bone marrow colonization, indicating that several heterodimers are responsible for proper HSC migration [163]. The integrins $\alpha 5\beta 1$, $\alpha 4\beta 7$ and $\alpha 9\beta 1$ also contribute to HSC adhesion and migration by binding to fibronectin, MadCAM and osteopontin, respectively [164-167].

During embryonic development two different haematopoietic systems arise. The first, primitive haematopoietic system is built from aggregates of blood cells within the yolk sac called blood islands. They consist mainly of nucleated erythroid cells that deliver oxygen to the embryonic tissues [168]. With proceeding development and increasing size of the embryo this system is replaced by the definitive haematopoietic system. In the second wave of haematopoietic generation haematopoietic stem cells emerge from within the embryo in the aorta-gonad-mesonephros (AGM) region, which surrounds the dorsal aorta [169]. Subsequently, it is thought that some of these cells distribute via the circulation and/or interstitial migration to the fetal liver [170]. Blood cell formation then occurs mainly in the fetal liver, which is the most important haematopoietic organ, until the bone marrow develops and takes over the task of generating most of the blood cells for the whole organism. Under certain circumstances, liver, thymus and spleen can resume their ability to function as haematopoietic organs in a process called extramedullary haematopoiesis. This usually leads to an increase in the size of these organs.

5.3.2. Erythrocytes

Erythrocytes or red blood cells are the most abundant type of blood cells. They are the exclusive transporters of oxygen from the lung to the body tissues. In mammals mature erythrocytes are non-nucleated. Erythroblasts, the precursors of erythrocytes, do not yet express haemoglobin and still reveal nuclei during early erythropoiesis. After several cell divisions and during maturation, haemoglobin appears in the cell and the nucleus becomes progressively smaller. The cells finally extrude their nucleus to provide more space for haemoglobin. They also lose most of their intracellular organs, such as the Golgi apparatus, the endoplasmic reticulum and the mitochondria. Due to the lack of mitochondria erythrocytes do not consume

the oxygen they deliver. Instead they use fermentation of glucose to lactic acid to generate adenosine triphosphate (ATP) [171].

Erythrocyte generation occurs throughout life. The most important regulators of erythrocyte differentiation are the cytokine erythropoietin (Epo), produced in the kidneys, and its receptor, EpoR, expressed by erythroid progenitors. Furthermore the integrin $\alpha 4\beta 1$ is essential for erythropoiesis and lack of the $\alpha 4$ subunit in mice leads to decreased numbers of differentiated erythroid cells [172; 173]. Erythropoiesis is a two step process: the early phase depends on Epo and is followed by Epo-independent step that requires interaction of integrin $\alpha 4\beta 1$ with fibronectin [174].

Mature erythrocytes are deficient of integrins. Integrin-associated protein, also known as CD47, mediates cell-cell interaction with splenic macrophages, interacts with soluble thrombospondin and participates in linking the red blood cell membrane with the cytoskeleton [174-176].

Mammalian erythrocytes show a characteristic shape of a biconcave disk, optimal for the flow in large blood vessels and small capillaries. The red blood cells obtain their mechanical properties through the membrane skeleton laminating the lipid bilayer, which is interspersed by numerous transmembrane proteins. The filamentous network of the skeleton has an essential role in control of the erythrocyte shape and its structural integrity. The erythrocyte skeletal proteins include the multifunctional proteins spectrin α and β , which form dimers and tetramers. They build connections to actin and protein 4.1. β -spectrin is also linked to ankyrin, which in turn binds to the anion exchanger AE1, also called protein band 3, and is by this connected to transmembrane proteins. Additional important cytoskeletal proteins within the membrane skeleton are adducin and demantin. On the surface of the erythrocyte a number of proteins are presented, such as glycosylphosphatidyl inositol (GPI) anchored proteins [177; 178].

Lack of any of these important structural skeleton proteins or molecular defects lead to clinical manifestation due to loss of stability of the erythrocyte [177].

5.3.3. Platelets

Platelets, also known as thrombocytes, are small cell fragments. They are formed within the bone marrow from megakaryocytes by fragmentation of cytoplasmic extensions. Like erythrocytes they lack a nucleus and are incapable of mitosis. Each megakaryocyte gives rise to 5.000 to 10.000 platelets. Megakaryocytes reveal

polyploidy achieved by endomitosis, which is necessary for the production of enough templates for the high protein requirements. Platelet production is regulated by the hormone thrombopoietin produced in liver and kidneys. It promotes megakaryocyte proliferation and differentiation [179].

A prerequisite for thrombopoiesis is the production of secretory granules, like α - and dense granules. They are generated from the Golgi apparatus and contain for example ADP (adenosine diphosphate), ATP, PDGF, TGF β 1, coagulation factors, fibrinogen, P-selectin, α IIb β 3 integrin, van Willebrand Factor (vWF) and granulophysin, which are essential for platelet function. The granules are filled by protein synthesis and endocytosis [180].

The main function of platelets is to maintain haemostasis. In case of blood vessel injury, platelets immediately attach to the wounded surface and to each other forming a thrombus. Platelets also contribute to the resistance of capillaries. They fill up weak spots in vessel walls. Lack of platelets leads to more fragile capillaries increasing the probability of spontaneous blood loss [181].

Platelet function underlies tight control as abnormalities can cause pathological thrombus formation leading to myocardial infarction or stroke. Endothelial cells, covering the inner surface of blood vessels, help to keep platelets in an inactive state by secreting nitric oxide, endothelial ADPase and prostacyclin (PGI₂) [182]. The ADPase removes ADP, which is a platelet activator. Additionally, endothelial cells produce von Willebrand factor (vWF), which promotes their adhesion to the collagen of the basement membrane. In intact vessels collagen is not exposed to the bloodstream. In case of injury, collagen, vWF and further factors get accessible for platelets, which get activated by interaction of the platelet receptor glycoprotein GPIb and vWF (Figure 14A) [183]. Subsequently, GPVI, the main collagen adhesion molecule of platelets, binds to collagen in a low affinity interaction, initiating signaling pathways that activate integrins via inside-out signaling. This leads to the establishment of tight integrin-ligand interactions, required to mediate shear resistant attachment (Figure 14B). GPVI engagement also leads to the secretion of granule content, such as the secondary mediators ADP and thromboxane A₂ (Figure 14C). These factors mediate together with thrombin the activation of G protein coupled receptors and therefore full platelet activation. Activated platelets undergo shape changes. While resting platelets are spherical, they spread upon activation, form pseudopods and adopt a stellate shape (Figure 14C) [184; 185].

Platelet activation and adhesion is followed by aggregation. Integrin $\alpha\text{IIb}\beta_3$, also known as GPIIa/IIIb is the most abundant platelet aggregation receptor. This heterodimer binds to the RGD motifs present in fibrinogen, its cleavage product fibrin, vWF and fibronectin [186; 187]. Fibrinogen is of special importance as this dimer provides two binding sites for $\alpha\text{IIb}\beta_3$ integrin and can serve as a bridge between two platelets leading to crosslinking and finally to platelet aggregation (Figure 14D) [185; 188]. Adhesion and aggregation cooperate to form a platelet plug. Reinforcing of this plug is achieved by actin-myosin contraction of the activated platelets.

Beside $\alpha\text{IIb}\beta_3$, platelets express at least four other integrin heterodimers but their roles are less well characterized. The three β_1 integrins $\alpha_2\beta_1$, also described as GPIa/IIb, $\alpha_5\beta_1$ and $\alpha_6\beta_1$ mediate platelet adhesion to collagen, fibronectin and laminin, respectively [185; 186]. Additionally little amounts of $\alpha\nu\beta_3$ integrins are exposed on the platelet [183].

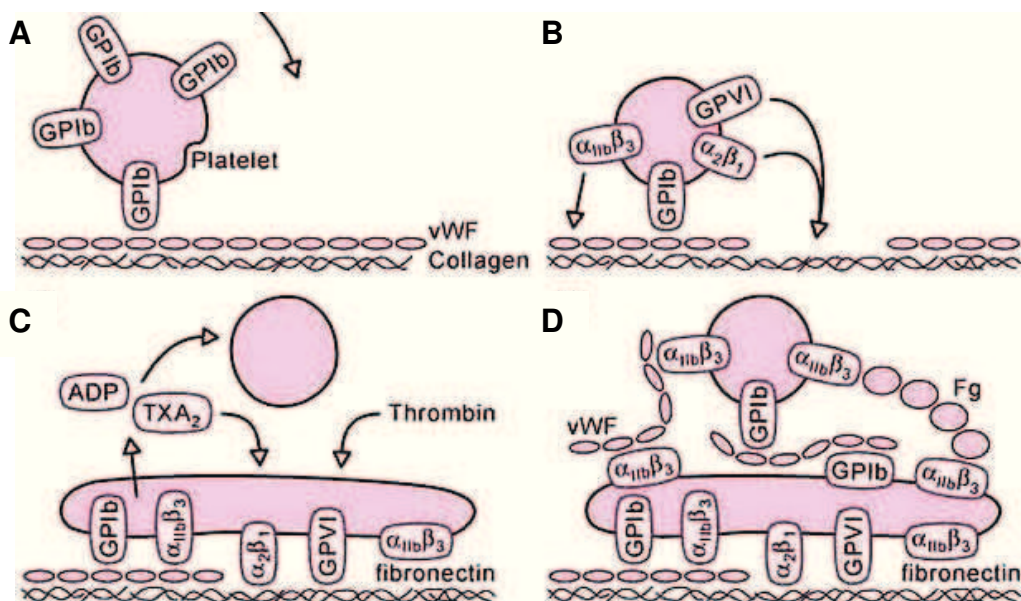


Figure 14: Scheme of platelet adhesion and aggregation under flow conditions. (A) Platelets adhere to collagen-bound von Willebrand factor (vWF) by glycoprotein Ib (GPIb). (B) Binding of GPIIb/IIIa to collagen leads to integrin activation and interaction of integrin $\alpha_2\beta_1$ and $\alpha\text{IIb}\beta_3$ with collagen and vWF, respectively. These contacts mediate firm adhesion. (C) Activated platelets spread and secrete ADP, thromboxane A2 (TXA₂) and other factors to activate additional platelets. (D) Aggregates form by crosslinking platelets via Fibrinogen (Fg) and vWF [189].

5.3.4. Neutrophils

Neutrophils represent the biggest group of white blood cells with 50-80%. Together with eosinophiles and basophiles, which constitute only 3% of white blood cells, they belong to the class of granulocytes. Granulocytes, also called polymorphonuclear

leukocytes (PMN or PML), are characterized by their multilobed nucleus and a large number of cytoplasmic granules [190].

Neutrophils are important mediators of the inflammatory response. Circulating cells are recruited to sites of injury, infection and inflammation by chemotaxis. Resident macrophages in the affected tissue secrete cytokines, such as interleukin-1, TNF α (tumour necrosis factor α) and attracting chemokines, upon recognition of and activation by pathogens. Further sources of cytokines are mast cells and activated endothelium [191]. Activated neutrophils release cytokines themselves, which in turn amplify inflammatory reactions by recruiting and activating several other cell types. Neutrophils play an important role in defending invading pathogens. They secrete soluble anti-microbials and belong to the group of phagocytes. They engulf bacteria and other microorganisms, which are digested and destroyed by enzymes and reactive oxygen species stored in the granules [192].

Neutrophil differentiation occurs within the bone marrow under the influence of G-CSF (granulocyte colony stimulating factor) and GM-CSF (granulocyte macrophage colony stimulating factor), beginning with the differentiation of a haematopoietic stem cell first into a myeloblast and then into a promyelocyte. The production of storage granules, which contain enzymes such as myeloperoxidase and elastase, starts already during the promyelocytic stage. Terminally differentiated neutrophils do not proliferate anymore. Once released into the blood stream, they have a half life of only a few hours and live slightly longer after migration into tissue. Most of the neutrophils never leave the bone marrow, which keeps a large number of them that can be released in case of inflammation or infection [193].

5.3.4.1. The leukocyte extravasation cascade

Neutrophils and other leukocytes have to leave the blood stream and migrate through the blood vessel endothelium in order to reach inflamed tissue. This extravasation is a multistep process with a general concept (Figure 15) [68; 194]. In the first step, selectins, which are exposed on the blood vessel endothelium upon induction by interleukin-1 and TNF α , interact with carbohydrate ligands on leukocytes. These transient contacts slow down the velocity of the leukocyte and lead to selectin-mediated rolling. The rolling process can also be mediated by binding of the integrins $\alpha 4\beta 1$, also called VLA4 (very late antigen 4), and $\alpha 4\beta 7$ to VCAM or MadCAM, respectively [195]. Reduction of speed allows the activation of G-protein coupled

chemokine receptors on leukocytes by chemokines presented on endothelial cells and released by macrophages. This induces integrin inside-out signaling and integrin activation via receptor crosstalk mechanisms. Activated integrins can firmly adhere to counter receptors on the endothelium, followed by arrest, reorganization of the cytoskeleton, cell spreading and transmigration [68].

Different leukocyte subtypes and tissues employ different selectins, chemoattractants and integrins in the process of extravasation. Lymphocytes for instance use predominantly the ICAM/ α L β 2 (LFA-1) interaction for arrest and α 4 β 1 seems to facilitate rolling and adhesion [196]. For monocyte extravasation the integrin α 4 β 1 is the most important integrin [197]. Neutrophils and monocytes additionally express integrin α M β 2 (Mac-1), which interacts with ICAM and fibrinogen. Neutrophil rolling and adhesion occurs via LFA-1, while Mac-1 allows the cell to crawl over the endothelium and search for the optimal spot for transmigration (Figure 15) [198; 199]. The cells protrude via podosomes into the endothelial cell layer to find a site to penetrate [200].

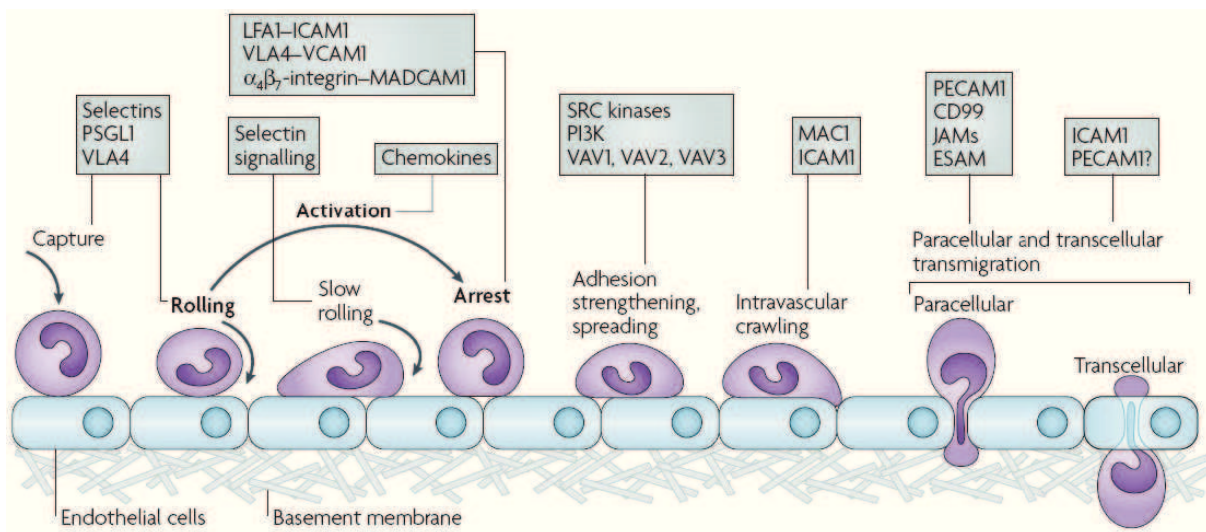


Figure 15: Scheme of the leukocyte extravasation cascade as a multistep process. Transient interactions initiate leukocyte capturing and start of rolling on the endothelium (step 1). In the second step, chemokine receptor signaling induces integrin activation and firm arrest (step 3). After adhesion strengthening and spreading the cells migrate on the vessel wall looking for an appropriate area for transmigration, which can occur paracellular or transcellular (step 4). The most important proteins involved in each step are shown in blue boxes. [68]

Transendothelial migration of the leukocytes occurs either by paracellular or transcellular migration [200; 201]. Proteins such as PECAM-1 (platelet/endothelial cell adhesion molecule 1), CD99, JAM-A (junctional adhesion molecule A) and VE-cadherin (vascular endothelial cadherin) are located in the junctions between

endothelial cells and collaborate in the opening of the endothelial junction. Integrin ligands such as ICAM and VCAM are expressed on the apical side of the endothelium and laterally in the junctions but the role of integrins in this process is unclear [202]. The laminin receptor $\alpha 6\beta 1$ is important for overcoming the basement membrane, underlying the endothelium [203]. The leukocytes secrete proteases like matrix metalloproteinases to degrade the basement membrane and to form wholes in order to escape the blood vessel. The process of proteinase release and activation also depends on signals downstream of integrins [204; 205]. Within the interstitial fluid, the cells follow a chemotactic gradient.

5.3.4.2. Leukocyte adhesion deficiency syndromes

Defects in the process of leukocyte extravasation lead to leukocyte adhesion deficiency (LAD). LAD is a rare autosomal recessive disorder of neutrophil function, which is characterized by immunodeficiency leading to recurrent infections. A defect in neutrophil adhesion results in poor or no extravasation and impaired phagocytosis. LAD is currently divided into three subtypes, LAD-I, -II and -III.

The most common type is LAD-I with an estimated prevalence of 1 in 100.000 births. It results from mutations in the $\beta 2$ integrin subunit [206]. Leukocytes of these patients either lack the integrin heterodimers such as $\alpha M\beta 2$ and $\alpha L\beta 2$ or express only very low levels. Consequently, leukocyte extravasation is heavily impaired and the cells do not reach infected tissues. This leads to leukocytosis, meaning strongly elevated levels of neutrophils in the peripheral blood. Also phagocytosis and chemotaxis are affected, which are secondary effects due to abnormal cell adhesion [207]. LAD-I is treated by bone marrow transplantation.

The course of disease is less severe in LAD-II, which is caused by a defect in the processing of glycans. Granulocytes and monocytes derived from LAD-II patients lack CD15, also named sialyl-Lewis^X, a ligand for selectins. Sialyl-Lewis^X is a fucose-containing carbohydrate structure on cell surface glycoproteins and glycolipids [208]. The mutant cells bind minimally or not at all to E- and P-selectins but reveal normal P-selectin and $\beta 2$ levels [209]. They show impaired rolling and decreased motility but normal phagocytosis. These cells adhere and migrate normally only in case of Mac-1 activation [209]. Beside leukocytosis and leukocyte defects, LAD-II patients suffer from moderate to severe psychomotor retardation and mild dysmorphism, which are also due to primary defects in fucose metabolism [210]. Additionally, the patients

manifest the Bombay blood type. Their erythrocytes lack the H antigen, a fucose-containing carbohydrate sequence and the precursor of the A, B and O blood types. The patients have deficiencies in many fucosylated carbohydrates [211]. This basic defect in fucose metabolism is due to low GDP-fucose import activity to the Golgi apparatus resulting from mutations in the GDP-L-fucose transporter [212; 213]. Some LAD-II patients can be treated by oral application of fucose, which induces expression of fucosylated selectin ligands [212].

The third subtype LAD-III is also known as LAD-I variant and is characterized by LAD-I like immunodeficiency and additional Glanzmann's thrombasthenia like bleedings. In a number of patients also an osteopetrosis was found [214]. Mutations within the kindlin-3 gene are responsible for LAD-III [215; 216]. As kindlin-3 is expressed in all haematopoietic cells, lack of the protein affects leukocytes, platelets and lymphocytes [217]. Neutrophil activation, adhesion, motility and spreading are defective despite normal integrin expression and hemorrhages occur regardless of regular platelet counts [218]. The leukocyte defects as well as the bleeding phenotype result from impaired activation of $\beta 1$, $\beta 2$ and $\beta 3$ integrins [219]. Like LAD-I, LAD-III can be cured by bone marrow transplantation.

5.3.5. Monocytes and macrophages

Monocytes and macrophages are critical for the non-specific innate immune response and help to initiate adaptive immunity. They are important for the regulation of inflammation, for example by producing inflammatory cytokines. They arrive at inflamed tissues later than granulocytes and are important in chronic infections. Monocytes and macrophages contain large numbers of small granules and, like granulocytes, belong to the phagocytes. They are able to ingest infectious agents as well as erythrocytes. Monocytes make up approximately 7% of the leukocytes.

Monocytes differentiate from common myeloid progenitors under the influence of M-CSF, GM-CSF and other cytokines. They leave the bone marrow, circulate in the blood and differentiate into macrophages or inflammatory dendritic cells after entering the tissue [220]. Monocytes and macrophages belong to the antigen presenting cells. They internalize antigens by phagocytosis or receptor-mediated endocytosis and present fragments of the antigen bound to a class II MHC (major histocompatibility complex) molecule on the surface. This complex is then recognized by T-cells,

leading to their activation. Macrophages are also important for tissue homeostasis as they phagocytose apoptotic cells and secrete various growth factors [221].

Characteristic for macrophages are their very high expression level of Mac-1 and the presence of $\alpha3\beta1$. Both are upregulated during differentiation of monocytes into macrophages. Macrophages can bind bacteria and LPS (lipopolysaccharide) by their $\beta2$ integrins. The phagocytosis of complement-opsonized particles and the interaction of T-cells with antigen presenting MHCs are also mediated by integrins containing the $\beta2$ subunit [222; 223]. These integrins are activated by receptor crosstalk mechanisms and inside-out signaling under pro-inflammatory conditions, for example under the influence of tumour necrosis factors and platelet-activating factor, in presence of bacterial products and after T-cell receptor crosslinking [224]. Macrophage integrins also interact heavily with Fc receptors. Fc receptors bind the Fc region of antibodies, which are attached to infected cells or pathogens. Integrins and Fc receptors can modify each other's response, achieved either by direct physical interactions within the cell membrane or by modifying the respective signaling pathways. Fc receptors modulate integrin adhesion by inside-out signaling. The integrin/Fc receptor crosstalk is bidirectional, as integrins also influence Fc receptor responses, such as adhesion to immune complexes and cell mediated antibody dependent cytotoxicity [225].

5.3.6. Osteoclasts

Osteoclasts are the exclusive bone resorbing cells. Bone resorption is important for several processes, including bone growth, bone remodelling, tooth eruption and fracture healing but also for maintenance of blood calcium levels.

Osteoclasts are huge acidophil cells with 25-30 nuclei and a size of up to 100 μm [226]. They are characterized by the expression of tartrate resistant acid phosphatase (TRAP) and cathepsin K [227].

Osteoclasts differentiate from monocyte/macrophage precursor cells by fusion into polykaryons [221]. Differentiation occurs under the influence of the cytokines M-CSF and RANKL (receptor activator of nuclear factor κB ligand, also called tumour necrosis factor-related activation-induced cytokine (TRANCE), osteoprotegerin ligand (OPGL) and osteoclast differentiation factor (ODF) [228]), which are necessary and sufficient for osteoclastogenesis [229-232]. Both molecules are produced by mesenchymal cells of the bone marrow environment, predominantly by osteoblasts,

as soluble and membrane bound proteins (Figure 16A). These cells need to be in direct contact with osteoclast precursors, which is mediated by cadherin-6 [227; 233]. By binding to its receptor c-Fms, M-CSF is responsible for cell survival and proliferation of precursors but also contributes to osteoclast differentiation and induces cytoskeletal reorganization important for bone resorption. RANKL activates NF- κ B (nuclear factor- κ B) and NFATc1 via its receptor RANK [234]. Osteoclast differentiation can be inhibited by osteoprotegerin (OPG), which binds RANKL and therefore prevents its interaction with RANK [231].

Osteoclasts can be found in small cavities called Howship's lacunae, which are formed by resorption of the underlying matrix. They undergo a resorptive cycle [235]. When they are not attached to bone, osteoclasts are non-polarized and contain diffusely distributed fibrillar actin. A prerequisite of matrix degradation is tight attachment of the osteoclast to the bone surface via integrins. This is achieved by the formation of sealing zones, which are ring-like structures that delineate the site of bone resorption (see below). Vesicles enriched with protons localize to the plasma membrane within sealing zones and eject their content. These processes generate the ruffled border, which is the functional organelle for resorption (Figure 16B). The now fully polarized osteoclast is capable of resorbing bone matrix. As the ruffled border and the underlying resorption lacunae are tightly isolated from the external space by the sealing zone, a microenvironment is provided that can further be acidified to a pH of approximately 4.5. This is achieved by secretion of hydrochloric acid through an electrogenic proton pump and a chloride channel [236]. The protons are produced by carbonic anhydrase II (CAII). At this acidic conditions the mineralized components of the bone matrix are dissolved into Ca^{2+} , H_3PO_4 , H_2CO_3 and H_2O and the organic parts consisting mainly of type I collagen are uncovered. The organic components are digested by proteases secreted by lysosomal vesicles that also contain additional protons. The most prominent protease is cathepsin K but MMPs, mainly MMP9, and other cathepsin family members support their function (Figure 16B) [228]. When a resorption depth of approximately 50 μm is reached, the cell detaches and migrates further to initiate another resorption cycle [237].

Osteoclasts undergo extensive vesicular trafficking. Beside the vesicles forming the ruffled border and delivering proteases and protons to the resorption lacunae, there are vesicles, which are transferred from the resorption lacunae through the ruffled border to the apical surface of the osteoclast, where they are unloaded (Figure 16B).

These vesicles contain cathepsin K, calcium- and phosphate-ions, as well as resorption products, which are further degraded by cathepsin K and reactive oxygen species (ROS) formed by TRAP (Figure 16B) [238].

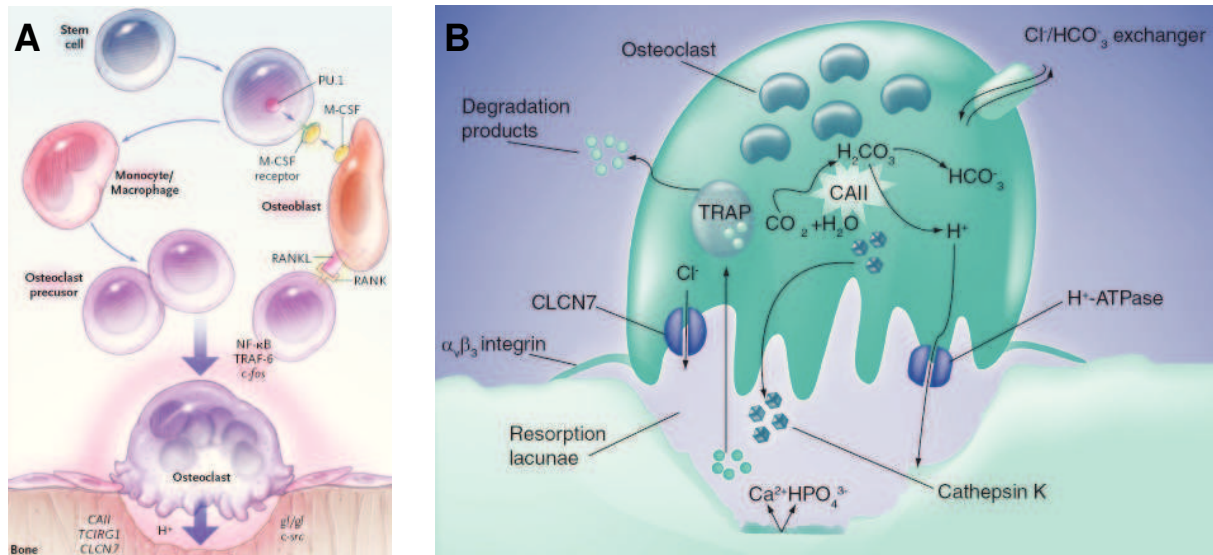


Figure 16: Schematic views of the differentiation and the resorption process of mature osteoclasts. (A) Osteoclasts differentiate from monocyte/macrophage precursors under the influence of RANKL and MCSF [233]. (B) Bone resorbing osteoclasts adhere via sealing zones, which contain integrins. Carbonic anhydrase II (CAII) generates H⁺ and HCO₃⁻. H⁺ and Cl⁻ are transported across the ruffled border into the resorption lacunae, a Cl⁻/HCO₃⁻ ion exchanger allows ionic charge balance within the cell. Cathepsin K and other proteases are secreted into the resorption lacunae, resorption products are uptaken, transported through the cell in TRAP-containing vesicles and exocytosed [239].

5.3.6.1. Adhesion structures of osteoclasts

Depending on the substrate, upon which osteoclasts are spread, they adhere either via podosomes or via sealing zones. Cells cultured on ECM coated glass form podosomes, which are special integrin-mediated adhesion structures of cells from the monocytic lineage. Podosomes are highly dynamic, actin rich structures with a half-life of 2-12 min [240]. They are also found in transformed fibroblasts, carcinoma cell lines and smooth muscle cells [39; 241]. Beside their function in adhesion, podosomes play a role in migration. They form at the leading edge and anchor the cell during translocation [242]. Furthermore, they are important for matrix remodelling and tissue invasion and accordingly, matrix metalloproteases such as MT1-MMP and MMP-9 localize to podosomes [39]. They have many molecular components in common with focal adhesions but differ from them in function and structure. They arrange already one hour after cell-substrate contact and are not dependent on *de novo* protein synthesis in contrast to focal adhesions [39].

Podosomes have a diameter of approximately 0.5-1 μm . They are composed of a central actin core surrounded by a ring of plaque proteins (Figure 17). Podosomes contain cytoskeletal components and regulators, protein kinases and RhoGTPases. Podosome assembly is controlled by several RhoGTPases, among them Cdc42, controls. The podosome core consists primarily of F-actin and actin associated molecules, such as WASp, WASp interacting protein (WIP) and Arp2/3 complex. These proteins regulate actin assembly and reorganization within the core and are activated downstream of Cdc42. The cell surface receptor CD44 plays a major role in nucleating podosome cores by binding to WASp. CD44 is a widely expressed receptor for hyaluronic acid but it can also bind to osteopontin, collagen and laminin. Ligand bound CD44 triggers signaling pathways, which are sufficient to initiate podosome core formation [243]. Lack of functional CD44, WASp, WIP or Arp2/3 lead to impaired podosome formation [39; 244; 245]. Cytochalasin or latrunculin treatment leads to disassembly of podosomes, suggesting that the F-actin core is essential for their stability [240; 246]. The actin core is surrounded by a cloud of G-actin and actin oligomers, which is a source for actin turnover. While the actin core depends on CD44, the actin cloud is organized by integrins but both actin subdomains are interconnected by actin branching and crosslinking proteins such as cortactin and fimbrin [240; 243].

Integrins, predominantly integrin $\alpha\text{V}\beta\text{3}$, and integrin associated proteins are mainly located in the ring structure. Integrin/ligand interactions lead to autophosphorylation of Pyk2 (proline-rich tyrosine kinase 2), necessary for complex formation with Src [247], and activation of Src and PI3K inducing the phosphorylation of p130Cas and Pyk2 at distinct sites by Src [248-250]. Also paxillin is phosphorylated upon integrin engagement. It binds to cytoplasmic domains of β integrin subunits and can provide a link to actin by interaction with vinculin, which in turn binds to talin and α -actinin [39]. Dephosphorylation events are involved in podosome turnover.

Podosomes are closely associated with microtubules and are influenced by them but the exact mechanism is still unclear [246]. Microtubules are not required for de novo assembly of podosomes, while reorganization, fission and fusion of podosomes are based on microtubule dynamics [251]. Podosomes also crosstalk with intermediate filaments and vimentin localizes to them.

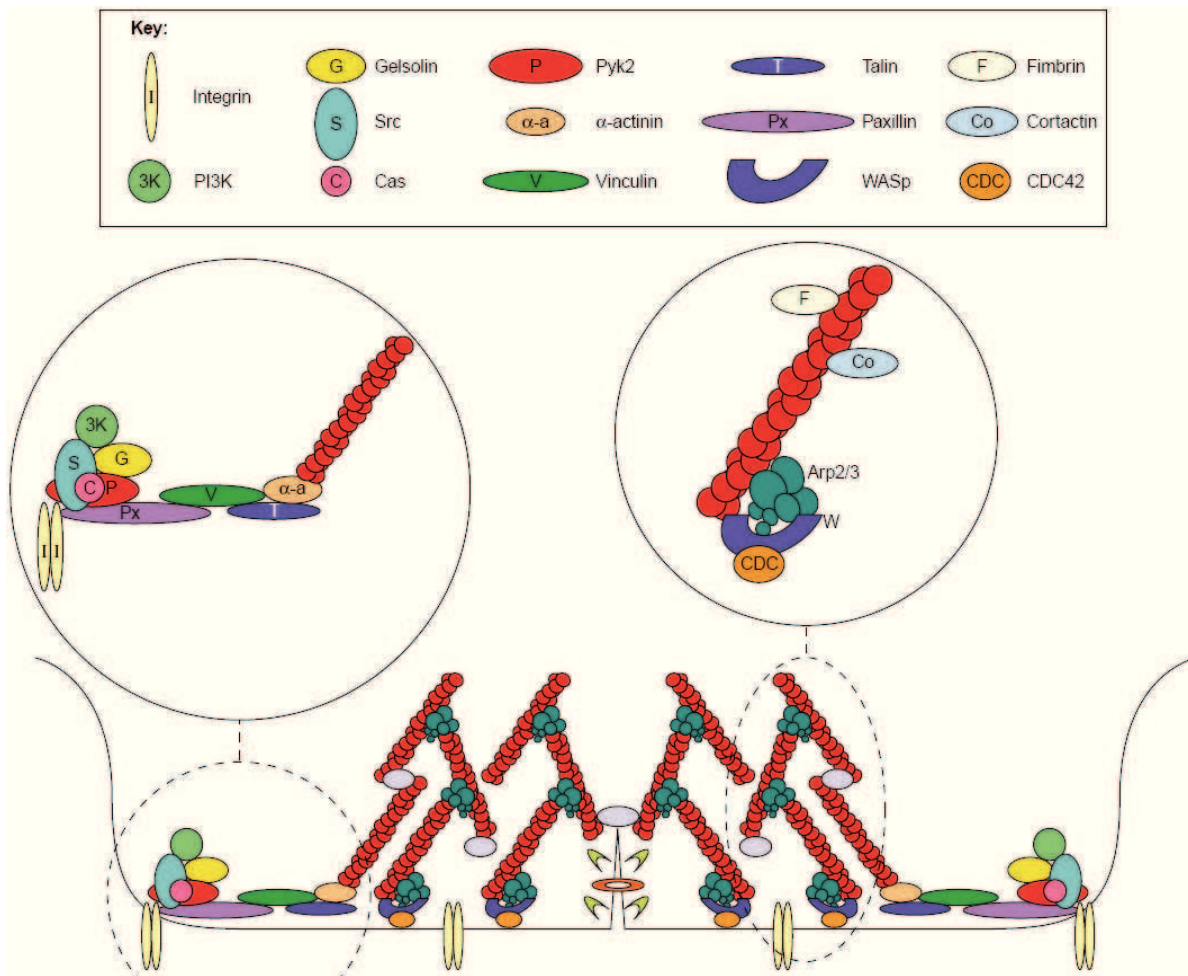


Figure 17: Podosome model, cross section perpendicular to the substrate. The membrane is delineated by a black line. Membrane invaginations can provide space for matrix metalloproteinase secretion. The upper left panel shows the podosomal ring structure. Integrins mediate the connection to the ECM. A complex consisting of paxillin, Src, Pyk2, gelsolin, PI3K and p130Cas is recruited to the adhesion site, vinculin, talin and α -actinin link the complex to actin. The upper right panel represents the podosomal core structure. WASp is activated by Cdc42 at the plasma membrane leading to the activation of the Arp2/3 complex. Cortactin and fimbrin crosslink the actin filaments [39].

Podosomes arrange into higher ordered structures. The actin cores of neighbouring podosomes are connected by radial actin filaments. In osteoclast precursors and immature osteoclasts, podosomes are usually organized in clusters that are embedded in an actin cloud composed of monomeric and polymerized actin [240]. The clusters can rearrange into short-lived rings. In fully differentiated osteoclasts these rings expand to a stable belt at the cell periphery by a treadmilling-like mechanism (Figure 18). Podosomes are newly formed at the periphery and disassembled in the centre. The centrifugal movement is reminiscent of Src activity waves [252]. Furthermore, this transition is dependent on microtubules, which are acetylated during the rearrangement process. Nocodazole treatment results in disorganisation of podosome belts and reappearance of clusters and rings [253].

When mature osteoclasts adhere to mineralized matrix, calcium apatite crystals induce the formation of sealing zones in a microtubule dependent process (Figure 18) [265]. Sealing zones consist of an actin ring with a width and height of approximately 4 μm and an inner and outer ring of vinculin and other plaque proteins. Sealing zones are composed of structural units that are closely related to individual podosomes but they are packed at very high density and are more heavily interconnected by a network of actin filaments than clustered podosomes [254].

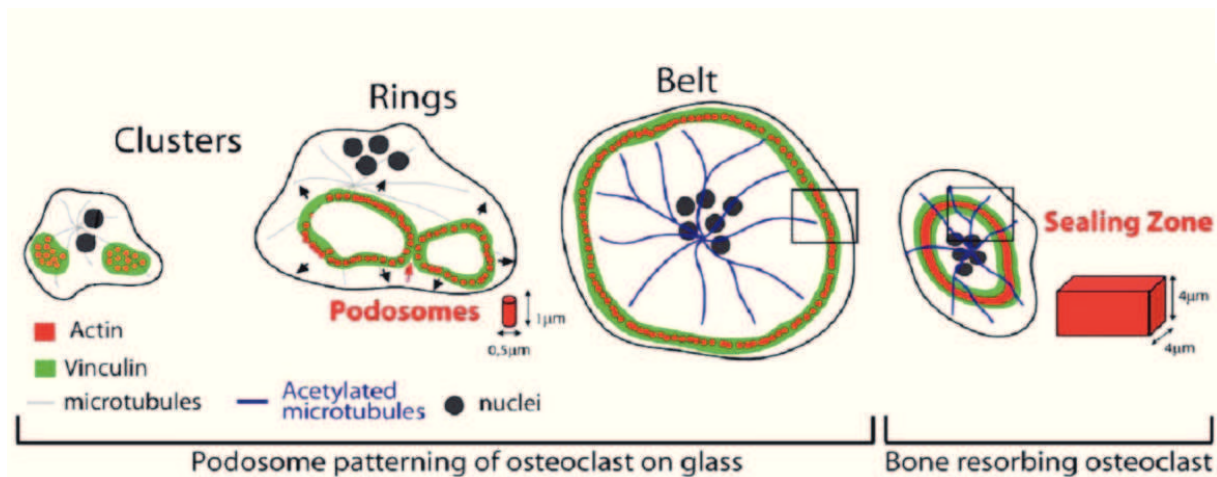


Figure 18: Scheme of podosome organizations along osteoclast differentiation. Preosteoclasts arrange their podosomes in clusters that evolve into dynamic rings. These rings expand to a belt at the cell periphery in mature osteoclast stabilized by acetylated microtubules. Osteoclasts adherent on mineralized matrix form sealing zones [253].

5.3.6.2. Osteoclasts and integrins

Integrin $\alpha\text{V}\beta\text{3}$ is the main osteoclast integrin. It recognizes the RGD motif, present in a number of non-collagenous bone-residing proteins, such as osteopontin and bone sialoprotein [123]. Osteoclast precursors express $\alpha\text{V}\beta\text{5}$, which also binds the RGD motif. $\alpha\text{V}\beta\text{5}$ is downregulated during osteoclast differentiation and genetic loss of $\alpha\text{V}\beta\text{5}$ results in enhanced osteoclast formation suggesting an inhibitory effect on differentiation [255].

Furthermore, β1 integrins are expressed on osteoclasts, such as $\alpha\text{2}\beta\text{1}$, $\alpha\text{5}\beta\text{1}$, $\alpha\text{9}\beta\text{1}$ and $\alpha\text{V}\beta\text{1}$ but the function of these integrins is not well characterized [256; 257]. Recognition of native collagen is mediated by integrin $\alpha\text{2}\beta\text{1}$, whereas denatured collagen is predominantly bound by $\alpha\text{V}\beta\text{3}$ in a RGD-dependent manner. The RGD sites in native collagen are inaccessible to $\alpha\text{V}\beta\text{3}$ but are exposed in the denatured form [256]. Integrin $\alpha\text{9}\beta\text{1}$ binds ADAM8, a disintegrin domain containing protein and MMP-like metalloproteinase. ADAM8 is an autocrine factor expressed on osteoclasts and $\alpha\text{9}\beta\text{1}/\text{ADAM8}$ interaction is involved in osteoclast differentiation [258].

5.4. Osteopetrosis

5.4.1. *Bone homeostasis and osteopetrosis*

Bone homeostasis is under the control of two cell types, osteoblasts and osteoclasts. Osteoblasts differentiate from mesenchymal stem cells and produce bone matrix. Osteoclasts are the exclusive bone resorbing cell type and derive from haematopoietic precursors by fusion into multinuclear cells. An intensive crosstalk between osteoblasts and osteoclasts exists in order to regulate bone mass. Osteoclast differentiation is dependent on the growth factors RANKL and M-CSF that are secreted by osteoblasts. RANKL and M-CSF production is triggered by parathyroid hormone (PTH) released from the parathyroid glands upon low serum calcium levels [259]. The balance between matrix production and matrix degradation needs to be maintained to achieve normal bone growth. This is essential to prevent both osteoporosis with a decreased amount of bone matrix and osteopetrosis, characterized by increased bone density. Osteopetrosis is a heterogeneous group of rare inheritable diseases, which is usually caused by a defect in bone resorption by osteoclasts [233; 260]. Defects in osteoclast function also affect shape and structure of bone due to impaired bone remodelling leading to brittle bone. In severe cases the medullary cavity is filled with endochondral bone. The consequence of an insufficient bone marrow cavity can be impaired haematopoiesis resulting in extramedullary haematopoiesis and hepatosplenomegaly.

The abnormalities of osteoclasts leading to osteopetrosis are divided into defects that are either of intrinsic or extrinsic nature. This is of particular importance for the treatment of patients, as bone marrow transplantations are able to cure intrinsic osteoclast defects, while extrinsic malfunctions will not respond [233].

5.4.2. *Mouse models*

A number of mouse models are available that reveal osteoclast abnormalities and therefore osteopetrosis. The defects can roughly be divided in early differentiation defects, defects caused by RANKL or related proteins, defects in acidification and functional defects. The osteopetrotic op/op mice have a mutation within the m-csf gene resulting in absence of circulating monocytes, macrophages and osteoclasts [230; 261]. This defect is extrinsic to the osteoclast, as stromal cells and osteoblasts are the main source of M-CSF. Osteopetrosis can also be caused by lack of the

M-CSF receptor c-Fms [262] or the transcription factor PU.1, which is functionally associated with the M-CSF pathway by binding to the promoter region of the M-CSF receptor gene and therefore regulates its synthesis [263].

Bone density is determined by the relative concentration of RANKL and OPG. OPG inhibits osteoclast differentiation by interacting with RANKL [232]. Overexpression of OPG results in osteopetrosis [264], while absence of OPG in mice leads to osteoporosis because of unregulated osteoclast differentiation and production [265]. Mice lacking RANK or RANKL develop osteopetrosis due to a lack of osteoclasts [266; 267]. Similarly, loss of proteins involved in RANK signaling, such as c-fos, NF κ B and TRAF-6 (tumour necrosis factor receptor-associated factor-6) also results in increased bone mass [268-270].

Osteopetrosis cannot only be caused by defective osteoclast differentiation, but can also result from dysfunctional osteoclasts. The generation of an acidic environment is crucial for dissolving mineralized matrix. Acidification of lysosomes and endosomes is achieved by proton pumps. Genetic ablation of *Atp6i*, which encodes for a subunit of an osteoclast specific ATP-dependent vacuolar proton pump results in osteopetrosis [271]. The same gene is mutated in naturally occurring osteosclerotic *oc/oc* mice [272]. Absence of the chloride channel ClC-7, which is necessary to achieve intracellular electroneutrality and is therefore charge coupled to the proton pump, also leads to osteopetrosis [273].

As tight adhesion is critical for osteoclast functionality, loss of the main osteoclast integrin α V β 3 results in osteopetrosis, which develops during adulthood, even if the osteoclast number in long bones from β 3^{-/-} mice is 3.5-times increased [152]. Their osteoclasts have a spreading defect and form abnormal ruffled borders, maybe due to loss of specific adhesive interactions between the resorption cavity and the ruffled border [121]. Actin organization is also affected leading to impaired podosome belt and sealing zone formation [152]. While retroviral expression of wild-type β 3 rescues the defect of β 3-deficient osteoclasts, the S752P mutant, which is incapable of kindlin-3 binding and is found in some patients with Glanzmann's thrombasthenia, cannot restore osteoclast function [37; 274].

Beside integrin α V β 3, β 1 integrins are also involved in osteoclast functionality. Blocking of the integrin subunits β 1 or α 2 by specific antibodies leads to reduced resorption [256], and lack of the subunit α 9 in mice results in osteopetrosis due to impaired polarization, actin reorganization and mobility, too [275]. Furthermore,

osteoclast specific gene ablation of ILK, which is a component of the multiprotein complex that transduces signals downstream of integrins, results in increased bone volume despite increased osteoclastogenesis. ILK^{-/-} osteoclasts are impaired in function and display decreased resorption activity [276].

Several transgenic mice lacking proteins that are involved in osteoclast integrin and M-CSF signaling are also osteopetrotic. For instance, mice deficient of Src, which is activated upon integrin ligation, also suffer from osteopetrosis despite slightly increased osteoclast numbers. Osteoclasts lacking Src show abnormal ruffled borders [277; 278] and the formation of podosomes and sealing zones is impaired [247; 279]. While kinase-dead Src can at least partially rescue the osteoclast defect by acting as an adaptor protein, Src's kinase activity is additionally required for full rescue [280; 281]. As Pyk2 associates with Src in a complex upon integrin engagement during podosome assembly, it is not surprising that Pyk2-deficient mice also develop osteopetrosis. Pyk2 deficient osteoclasts are dysfunctional, as their sealing zone formation is impaired. Additionally they are unable to rearrange podosome clusters into belts due to altered microtubule stability and organization. Surprisingly, expression of activated Src cannot rescue the defect of Pyk2^{-/-} osteoclasts, suggesting that Pyk2 mediates two separate signaling pathways, one regulating microtubule dependent podosome organization and one Src-dependent pathway involved in actin dynamics, adhesion and ruffled border formation [282].

Furthermore, Syk-deficient mice develop severe osteopetrosis and their osteoclasts are dysfunctional because they fail to properly organize their actin cytoskeleton [124]. As ITAM-containing adaptor proteins such as DAP12 and FcRγ couple the downstream signals of integrins and c-Fms to Syk, DAP12 deficient mice develop osteopetrosis, which becomes even more severe in DAP12/FcRγ double knockout mice [283; 284]. Furthermore, osteoclasts from these mice fail to form actin belts and sealing zones and osteoclasts deficient of DAP12 and FcRγ are additionally impaired in differentiation due to lack of NFATc1 expression. As Syk has no impact on this transcription factor, this finding indicates that ITAM molecules additionally play a role in a Syk-independent, RANKL-mediated signaling pathway [285]. Since the RhoGEF Vav3 is a downstream target of Syk, loss of Vav3 also affects osteoclast cytoskeleton organization resulting in increased bone mass [286].

Moreover, deficiencies of cathepsin K or TRAP, which both are involved in bone matrix resorption, lead to osteopetrosis due to non-functional osteoclasts [287; 288].

Understanding of the mechanisms involved in osteoclast differentiation and resorption provides opportunities to engineer new therapeutics to treat human bone diseases, predominantly osteoporosis. Orally active, non-peptide RGD mimetic $\alpha V\beta 3$ antagonists have been generated and for some of them it was shown that they can increase bone mineral density in women with postmenopausal osteoporosis [289-292]. Also other proteins can serve as potential targets for an anti-osteoporotic therapy, such as the chloride channel ClC-7, Src and Vav3.



6. Aim of the thesis

Kindlin-3 is restrictively expressed in haematopoietic cells and represents the solely kindlin expressed in blood cells. First *in vitro* studies on cultured cells showed that kindlins play an important role in integrin-mediated cell adhesion but *in vivo* functions were only partly examined.

The general aim of this thesis was to analyse the consequences of kindlin-3 deficiency on different haematopoietic cells. Genetic ablation of kindlin-3 in mice results in a lethal phenotype. These mice die within one week after birth and suffer from severe haemorrhages in the gastrointestinal tract, skin, brain and bladder, which are already apparent during development. Furthermore, kindlin-3 knockout mice develop anaemia, neutrophilia and a pronounced osteopetrosis.

Within this thesis, the major goal was to examine the role of kindlin-3 in bone homeostasis and osteoclast biology and to elucidate the cause of the osteopetrotic phenotype of kindlin-3 deficient mice. Previous studies showed a progressive osteopetrosis in mice lacking integrin $\beta 3$ expression and suggested an important role of integrin $\alpha V\beta 3$ in osteoclast function. Due to the far less pronounced osteopetrosis in integrin $\beta 3^{-/-}$ mice compared to kindlin-3 $^{-/-}$ mice we hypothesized that also other integrin classes play a role in osteoclast-mediated bone resorption and are controlled by kindlin-3. In order to test this hypothesis we investigated osteoclasts lacking $\beta 1$, $\beta 2$, $\beta 3$ and/or αV integrins and compared them with kindlin3 $^{-/-}$ osteoclasts.

Additional aims were to address also other phenotypes of the kindlin-3 deficient mice. It was already shown that kindlin-3 deficiency results in impaired platelet aggregation and therefore in bleedings and anaemia. To see if an erythrocyte defect contributes to the anaemia, we studied the effect of kindlin-3 loss on erythrocytes. In order to analyse the role of kindlin-3 in erythrocytes we used quantitative proteomics.

Another phenotype we wanted to investigate was the pronounced neutrophilia. Based on the studies that kindlin-3 is essential for the activation of $\beta 1$ and $\beta 3$ integrins on platelets, we wanted to analyse if the $\beta 1$, $\beta 2$ and $\beta 3$ integrins expressed on neutrophils are also dependent on kindlin-3. Therefore we performed *in vitro* as well as *in vivo* experiments on kindlin-3 $^{-/-}$ neutrophils.

A further task was to answer the question how much kindlin-3 is needed to maintain its functions. For this purpose we used hypomorphic kindlin-3 mice and analysed their constitution as well as the effect of low kindlin-3 expression on various cell types with different kindlin-3 levels.



7. Brief summaries of the publications

7.1. Paper I

SILAC-mouse for quantitative proteomics uncovers Kindlin-3 as an essential factor for red blood cell function

Krüger M.*, Moser M.*, Ussar S., Thievensen I., Luber C. A., Forner F., **Schmidt S.**, Zanivan S., Fässler R., Mann M.

*equal contribution

This publication describes the application of the stable isotope labelling by amino acids in cell culture (SILAC) method to the whole mouse organism. Mice were fed with a special diet, in which the common $^{12}\text{C}_6$ -lysine, referred to as “light”, was replaced by “heavy” lysine labelled with $^{13}\text{C}_6$ carbon. We were able to breed mice that were fully labelled with the heavy amino acid. This approach allows a quantitative analysis of whole proteomes by mass spectrometry. By applying this method to different genetically modified mice, it is possible to investigate the consequences of mutant genes on the proteome of distinct cell types within the whole mouse organism. By this method cell types can be analysed, which cannot be labelled in culture.

First we show that wild-type and $\beta 1$ integrin deficient platelets have comparable proteomes with the exception that the integrin $\beta 1$ and its dimerizing α subunits $\alpha 2$ and $\alpha 6$ are absent. Studies of hearts lacking β -parvin expression elucidate that upregulation of α -parvin expression compensates for the loss of β -parvin. Furthermore, analyses of kindlin-3 deficient erythrocytes reveal severe structural membrane defects. The mutant erythrocytes have an altered composition of membrane and cytoskeletal proteins and we found an almost complete absence of the proteins ankyrin-1, band 4.1, adducin-2, and dematin in membrane fractions of erythrocytes.

Altogether this publication describes how the whole mouse organism can be labelled with $^{13}\text{C}_6$ -lysine allowing the analyses of various cell types and organs by quantitative proteomics. We used this method to analyse kindlin-3 deficient erythrocytes and found that changes in protein composition of the erythrocyte membrane skeleton affect erythrocyte shape and stability, which contribute to the severe anaemia of kindlin-3 deficient mice.

7.2. Paper II

Kindlin-3 is required for β 2 integrin-mediated leukocyte adhesion to endothelial cells

Moser M., Bauer M., Schmid S., Ruppert R., **Schmidt S.**, Sixt M., Wang H., Sperandio M., Fässler R.

Impaired activation of β 1, β 2 and β 3 integrins on platelets and leukocytes is characteristic for LAD-III, a rare leukocyte adhesion deficiency syndrome in humans. The main symptoms of this disease are severe bleedings and impaired adhesion of leukocytes to inflamed endothelia. The main findings of this study are that kindlin-3 is not only required for activation of β 1 and β 3 integrins on platelets but also for activation of β 2 integrins on leukocytes and that loss of kindlin-3 results in a LAD-III like phenotype in mice.

We describe that kindlin-3 directly associates with the cytoplasmic domain of the β 2 integrin at the membrane distal NxxF motif and regulates binding of leukocytes to β 2 integrin ligands, such as ICAM and fibrinogen. Neutrophil adhesion is heavily impaired in the absence of kindlin-3. Kindlin-3 deficient neutrophils can slightly bind to immune complexes via their Fc receptors but spreading, which is dependent on Fc receptor triggered inside-out signaling of integrin α M β 2, is severely impaired.

We also show defects of kindlin-3 lacking neutrophils in *in vivo* experiments. Therefore we generated fetal liver cell chimeras by transferring wild-type and kindlin-3^{-/-} fetal liver cells into lethally irradiated wild-type recipient mice. Phorbol ester treatment of ears from kindlin3^{+/+} and kindlin3^{-/-} chimeric mice reveal an inability of kindlin-3 deficient neutrophils to extravasate into the perivascular tissue. A pronounced extravasation defect can also be found in TNF- α -stimulated cremaster muscle venules from kindlin3^{-/-} chimeric mice. A more detailed investigation by intravital microscopy shows a strongly reduced adhesion of kindlin-3^{-/-} neutrophils to the inflamed endothelium compared to control cells. Leukocyte rolling, which depends on P-selectin and E-selectin, is not affected in kindlin-3^{-/-} chimeras. Furthermore, it is shown that chemokines fail to trigger neutrophil adhesion in kindlin-3^{-/-} chimeras.

In summary, we conclude from *in vitro* and *in vivo* experiments that loss of kindlin-3 function is sufficient to cause a LAD-III-like phenotype in mice due to its essential role in activation of integrin β 1, β 2 and β 3 classes.

7.3. Paper III

Kindlin-3 mediated signaling from multiple integrin classes is required for osteoclast-mediated bone resorption

Schmidt S., Nakchbandi I., Ruppert R., Kawelke N., Hess M. W., Pfaller K., Jurdic P., Fässler R., Moser M.

The leukocyte adhesion deficiency syndrome LAD-III is caused by mutations in the *KINDLIN-3* gene. Beside severe bleedings and immunodeficiency several patients suffering from this disease show osteopetrosis as an additional symptom. In this publication we describe that kindlin-3 deficient mice also develop an osteopetrotic phenotype due to a profound defect in osteoclast-mediated bone resorption.

To test the influence of kindlin-3 on bone homeostasis, we analysed long bones of kindlin-3^{-/-} mice and found a severe, early onset osteopetrosis. Surprisingly, the number of TRAP-positive, bone resorbing osteoclasts is even increased in kindlin-3 null mice. Sera of mutant animals contain decreased Calcium and increased PTH and RANKL levels compared to control animals. As RANKL stimulates the formation of osteoclasts, this might explain the high number of osteoclasts in mutants.

In vitro investigations show that lack of kindlin-3 has only a mild impact on osteoclast differentiation, which can be overcome by the treatment with high M-CSF concentrations. Kindlin-3 deficient osteoclasts reveal normal marker gene expression and protease activity. However, they are functionally impaired due to defective cell adhesion and spreading. They are not able to form proper podosomes and sealing zones, which are essential adhesion structures required for bone resorption. These defects are due to failure in the activation of $\beta 1$, $\beta 2$ and $\beta 3$ integrins. Comparison of kindlin-3^{-/-} osteoclasts with osteoclasts lacking integrin $\beta 1$, $\beta 2$, $\beta 3$ or αv or lacking combinations of $\beta 1$, $\beta 2$ and αv integrins reveals that kindlin-3 loss mimics genetic ablation of $\beta 1$, $\beta 2$ and αv integrins, but that deficiency of a single or two integrin classes already leads to defects in osteoclast function.

Although we can not fully exclude integrin independent function of kindlin-3 in osteoclasts, our findings suggest that integrin $\alpha v \beta 3$, which was considered to be the most important integrin heterodimer of osteoclasts, is only one integrin involved in osteoclast mediated bone resorption and that the whole integrin repertoire expressed on osteoclasts is required for proper osteoclast function. Kindlin-3 regulates all these integrin classes and is important for adhesion to the ECM, the formation and rearrangement of podosomes, and adhesion-mediated signaling in osteoclasts.



8. References

1. Weinstein EJ, Bournier M, Head R, Zakeri H, Bauer C, Mazzearella R (2003): URP1: a member of a novel family of PH and FERM domain-containing membrane-associated proteins is significantly over-expressed in lung and colon carcinomas. *Biochim Biophys Acta* 1637:207-216.
2. Jobard F, Bouadjar B, Caux F, Hadj-Rabia S, Has C, Matsuda F, Weissenbach J, Lathrop M, Prud'homme JF, Fischer J (2003): Identification of mutations in a new gene encoding a FERM family protein with a pleckstrin homology domain in Kindler syndrome. *Hum Mol Genet* 12:925-935.
3. Siegel DH, Ashton GH, Penagos HG, Lee JV, Feiler HS, Wilhelmsen KC, South AP, Smith FJ, Prescott AR, Wessagowit V, Oyama N, Akiyama M, Al Aboud D, Al Aboud K, Al Githami A, Al Hawsawi K, Al Ismaily A, Al-Suwaid R, Atherton DJ, Caputo R, Fine JD, Frieden IJ, Fuchs E, Haber RM, Harada T, Kitajima Y, Mallory SB, Ogawa H, Sahin S, Shimizu H, Suga Y, Tadini G, Tsuchiya K, Wiebe CB, Wojnarowska F, Zaghloul AB, Hamada T, Mallipeddi R, Eady RA, McLean WH, McGrath JA, Epstein EH (2003): Loss of kindlin-1, a human homolog of the *Caenorhabditis elegans* actin-extracellular-matrix linker protein UNC-112, causes Kindler syndrome. *Am J Hum Genet* 73:174-187.
4. Ussar S, Wang HV, Linder S, Fassler R, Moser M (2006): The Kindlins: subcellular localization and expression during murine development. *Exp Cell Res* 312:3142-3151.
5. Hamada K, Shimizu T, Matsui T, Tsukita S, Hakoshima T (2000): Structural basis of the membrane-targeting and unmasking mechanisms of the radixin FERM domain. *Embo J* 19:4449-4462.
6. Hamada K, Shimizu T, Yonemura S, Tsukita S, Tsukita S, Hakoshima T (2003): Structural basis of adhesion-molecule recognition by ERM proteins revealed by the crystal structure of the radixin-ICAM-2 complex. *Embo J* 22:502-514.
7. Schlessinger J, Lemmon MA (2003): SH2 and PTB domains in tyrosine kinase signaling. *Sci STKE* 2003:RE12.
8. Kloeker S, Major MB, Calderwood DA, Ginsberg MH, Jones DA, Beckerle MC (2004): The Kindler syndrome protein is regulated by transforming growth factor-beta and involved in integrin-mediated adhesion. *J Biol Chem* 279:6824-6833.
9. Chishti AH, Kim AC, Marfatia SM, Lutchman M, Hanspal M, Jindal H, Liu SC, Low PS, Rouleau GA, Mohandas N, Chasis JA, Conboy JG, Gascard P, Takakuwa Y, Huang SC, Benz EJ, Jr., Bretscher A, Fehon RG, Gusella JF, Ramesh V, Solomon F, Marchesi VT, Tsukita S, Tsukita S, Hoover KB, et al. (1998): The FERM domain: a unique module involved in the linkage of cytoplasmic proteins to the membrane. *Trends Biochem Sci* 23:281-302.
10. Bretscher A, Edwards K, Fehon RG (2002): ERM proteins and merlin: integrators at the cell cortex. *Nat Rev Mol Cell Biol* 3:586-599.
11. Balla T (2005): Inositol-lipid binding motifs: signal integrators through protein-lipid and protein-protein interactions. *J Cell Sci* 118:2093-2104.
12. DiNitto JP, Lambright DG (2006): Membrane and juxtamembrane targeting by PH and PTB domains. *Biochim Biophys Acta* 1761:850-867.
13. Blaikie P, Immanuel D, Wu J, Li N, Yajnik V, Margolis B (1994): A region in Shc distinct from the SH2 domain can bind tyrosine-phosphorylated growth factor receptors. *J Biol Chem* 269:32031-32034.

14. Garcia-Alvarez B, de Pereda JM, Calderwood DA, Ulmer TS, Critchley D, Campbell ID, Ginsberg MH, Liddington RC (2003): Structural determinants of integrin recognition by talin. *Mol Cell* 11:49-58.
15. Lemmon MA (2004): Pleckstrin homology domains: not just for phosphoinositides. *Biochem Soc Trans* 32:707-711.
16. Lemmon MA (2005): Pleckstrin homology domains: two halves make a hole? *Cell* 120:574-576.
17. Lemmon MA, Ferguson KM (2000): Signal-dependent membrane targeting by pleckstrin homology (PH) domains. *Biochem J* 350 Pt 1:1-18.
18. Lemmon MA, Ferguson KM (2001): Molecular determinants in pleckstrin homology domains that allow specific recognition of phosphoinositides. *Biochem Soc Trans* 29:377-384.
19. Bejsovec A, Eide D, Anderson P (1984) Genetic techniques for analysis of nematode muscle. *Molecular Biology of the Cytoskeleton*: 267-273.
20. Rogalski TM, Mullen GP, Gilbert MM, Williams BD, Moerman DG (2000): The UNC-112 gene in *Caenorhabditis elegans* encodes a novel component of cell-matrix adhesion structures required for integrin localization in the muscle cell membrane. *J Cell Biol* 150:253-264.
21. Williams BD, Waterston RH (1994): Genes critical for muscle development and function in *Caenorhabditis elegans* identified through lethal mutations. *J Cell Biol* 124:475-490.
22. Mackinnon AC, Qadota H, Norman KR, Moerman DG, Williams BD (2002): *C. elegans* PAT-4/ILK functions as an adaptor protein within integrin adhesion complexes. *Curr Biol* 12:787-797.
23. Xu X, Rongali SC, Miles JP, Lee KD, Lee M (2006): pat-4/ILK and unc-112/Mig-2 are required for gonad function in *Caenorhabditis elegans*. *Exp Cell Res* 312:1475-1483.
24. Bai J, Binari R, Ni JQ, Vijayakanthan M, Li HS, Perrimon N (2008): RNA interference screening in *Drosophila* primary cells for genes involved in muscle assembly and maintenance. *Development* 135:1439-1449.
25. Herz C, Aumailley M, Schulte C, Schlotzer-Schrehardt U, Bruckner-Tuderman L, Has C (2006): Kindlin-1 is a phosphoprotein involved in regulation of polarity, proliferation, and motility of epidermal keratinocytes. *J Biol Chem* 281:36082-36090.
26. Kern JS, Herz C, Haan E, Moore D, Nottelmann S, von Lilien T, Greiner P, Schmitt-Graeff A, Opitz OG, Bruckner-Tuderman L, Has C (2007): Chronic colitis due to an epithelial barrier defect: the role of kindlin-1 isoforms. *J Pathol* 213:462-470.
27. Lai-Cheong JE, Liu L, Sethuraman G, Kumar R, Sharma VK, Reddy SR, Vahlquist A, Pather S, Arita K, Wessagowit V, McGrath JA (2007): Five new homozygous mutations in the KIND1 gene in Kindler syndrome. *J Invest Dermatol* 127:2268-2270.
28. Lotem M, Raben M, Zeltser R, Landau M, Sela M, Wygoda M, Tochner ZA (2001): Kindler syndrome complicated by squamous cell carcinoma of the hard palate: successful treatment with high-dose radiation therapy and granulocyte-macrophage colony-stimulating factor. *Br J Dermatol* 144:1284-1286.
29. Sadler E, Klausegger A, Muss W, Deinsberger U, Pohla-Gubo G, Laimer M, Lanschuetzer C, Bauer JW, Hintner H (2006): Novel KIND1 gene mutation in Kindler syndrome with severe gastrointestinal tract involvement. *Arch Dermatol* 142:1619-1624.

30. Freeman EB, Kogelmeier J, Martinez AE, Mellerio JE, Haynes L, Sebire NJ, Lindley KJ, Shah N (2008): Gastrointestinal complications of epidermolysis bullosa in children. *Br J Dermatol* 158:1308-1314.
31. Ussar S, Moser M, Widmaier M, Rognoni E, Harrer C, Genzel-Boroviczeny O, Fassler R (2008): Loss of Kindlin-1 causes skin atrophy and lethal neonatal intestinal epithelial dysfunction. *PLoS Genet* 4:e1000289.
32. Ashton GH, McLean WH, South AP, Oyama N, Smith FJ, Al-Suwaid R, Al-Ismaily A, Atherton DJ, Harwood CA, Leigh IM, Moss C, Didona B, Zambruno G, Patrizi A, Eady RA, McGrath JA (2004): Recurrent mutations in kindlin-1, a novel keratinocyte focal contact protein, in the autosomal recessive skin fragility and photosensitivity disorder, Kindler syndrome. *J Invest Dermatol* 122:78-83.
33. Tu Y, Wu S, Shi X, Chen K, Wu C (2003): Migfilin and Mig-2 link focal adhesions to filamin and the actin cytoskeleton and function in cell shape modulation. *Cell* 113:37-47.
34. Montanez E, Ussar S, Schifferer M, Bosl M, Zent R, Moser M, Fassler R (2008): Kindlin-2 controls bidirectional signaling of integrins. *Genes Dev* 22:1325-1330.
35. Shi X, Ma YQ, Tu Y, Chen K, Wu S, Fukuda K, Qin J, Plow EF, Wu C (2007): The MIG-2/integrin interaction strengthens cell-matrix adhesion and modulates cell motility. *J Biol Chem* 282:20455-20466.
36. Kato K, Shiozawa T, Mitsushita J, Toda A, Horiuchi A, Nikaido T, Fujii S, Konishi I (2004): Expression of the mitogen-inducible gene-2 (mig-2) is elevated in human uterine leiomyomas but not in leiomyosarcomas. *Hum Pathol* 35:55-60.
37. Moser M, Nieswandt B, Ussar S, Pozgajova M, Fassler R (2008): Kindlin-3 is essential for integrin activation and platelet aggregation. *Nat Med* 14:325-330.
38. Linder S, Kopp P (2005): Podosomes at a glance. *J Cell Sci* 118:2079-2082.
39. Linder S, Aepfelbacher M (2003): Podosomes: adhesion hot-spots of invasive cells. *Trends Cell Biol* 13:376-385.
40. Baum PD, Garriga G (1997): Neuronal migrations and axon fasciculation are disrupted in *ina-1* integrin mutants. *Neuron* 19:51-62.
41. Johnson MS, Lu N, Denessiouk K, Heino J, Gullberg D (2009): Integrins during evolution: evolutionary trees and model organisms. *Biochim Biophys Acta* 1788:779-789.
42. Takada Y, Ye X, Simon S (2007): The integrins. *Genome Biol* 8:215.
43. Hynes RO (2002): Integrins: bidirectional, allosteric signaling machines. *Cell* 110:673-687.
44. Humphries JD, Byron A, Humphries MJ (2006): Integrin ligands at a glance. *J Cell Sci* 119:3901-3903.
45. van der Flier A, Sonnenberg A (2001): Function and interactions of integrins. *Cell Tissue Res* 305:285-298.
46. Hynes RO (2004): The emergence of integrins: a personal and historical perspective. *Matrix Biol* 23:333-340.
47. Tamkun JW, DeSimone DW, Fonda D, Patel RS, Buck C, Horwitz AF, Hynes RO (1986): Structure of integrin, a glycoprotein involved in the transmembrane linkage between fibronectin and actin. *Cell* 46:271-282.

48. Arnaout MA, Mahalingam B, Xiong JP (2005): Integrin structure, allostery, and bidirectional signaling. *Annu Rev Cell Dev Biol* 21:381-410.
49. Humphries MJ, Symonds EJ, Mould AP (2003): Mapping functional residues onto integrin crystal structures. *Curr Opin Struct Biol* 13:236-243.
50. Hughes PE, Diaz-Gonzalez F, Leong L, Wu C, McDonald JA, Shattil SJ, Ginsberg MH (1996): Breaking the integrin hinge. A defined structural constraint regulates integrin signaling. *J Biol Chem* 271:6571-6574.
51. Vinogradova O, Haas T, Plow EF, Qin J (2000): A structural basis for integrin activation by the cytoplasmic tail of the alpha IIb-subunit. *Proc Natl Acad Sci U S A* 97:1450-1455.
52. Vinogradova O, Velyvis A, Velyviene A, Hu B, Haas T, Plow E, Qin J (2002): A structural mechanism of integrin alpha(IIb)beta(3) "inside-out" activation as regulated by its cytoplasmic face. *Cell* 110:587-597.
53. Legate KR, Fassler R (2009): Mechanisms that regulate adaptor binding to beta-integrin cytoplasmic tails. *J Cell Sci* 122:187-198.
54. Adair BD, Yeager M (2002): Three-dimensional model of the human platelet integrin alpha IIbbeta 3 based on electron cryomicroscopy and x-ray crystallography. *Proc Natl Acad Sci U S A* 99:14059-14064.
55. Lau TL, Dua V, Ulmer TS (2008): Structure of the integrin alphaIIb transmembrane segment. *J Biol Chem* 283:16162-16168.
56. Lau TL, Partridge AW, Ginsberg MH, Ulmer TS (2008): Structure of the integrin beta3 transmembrane segment in phospholipid bicelles and detergent micelles. *Biochemistry* 47:4008-4016.
57. Xiong JP, Stehle T, Diefenbach B, Zhang R, Dunker R, Scott DL, Joachimiak A, Goodman SL, Arnaout MA (2001): Crystal structure of the extracellular segment of integrin alpha Vbeta3. *Science* 294:339-345.
58. Zhu J, Luo BH, Xiao T, Zhang C, Nishida N, Springer TA (2008): Structure of a complete integrin ectodomain in a physiologic resting state and activation and deactivation by applied forces. *Mol Cell* 32:849-861.
59. Barczyk M, Carracedo S, Gullberg D (2010) Integrins. *Cell Tissue Res* 339:269-280.
60. Moser M, Legate KR, Zent R, Fassler R (2009): The tail of integrins, talin, and kindlins. *Science* 324:895-899.
61. Springer TA, Zhu J, Xiao T (2008): Structural basis for distinctive recognition of fibrinogen gammaC peptide by the platelet integrin alphaIIbbeta3. *J Cell Biol* 182:791-800.
62. Takagi J, Petre BM, Walz T, Springer TA (2002): Global conformational rearrangements in integrin extracellular domains in outside-in and inside-out signaling. *Cell* 110:599-611.
63. Askari JA, Buckley PA, Mould AP, Humphries MJ (2009): Linking integrin conformation to function. *J Cell Sci* 122:165-170.
64. Larsen M, Artym VV, Green JA, Yamada KM (2006): The matrix reorganized: extracellular matrix remodeling and integrin signaling. *Curr Opin Cell Biol* 18:463-471.
65. Discher DE, Janmey P, Wang YL (2005): Tissue cells feel and respond to the stiffness of their substrate. *Science* 310:1139-1143.

66. Ridley AJ, Schwartz MA, Burridge K, Firtel RA, Ginsberg MH, Borisy G, Parsons JT, Horwitz AR (2003): Cell migration: integrating signals from front to back. *Science* 302:1704-1709.
67. Streuli CH (2009): Integrins and cell-fate determination. *J Cell Sci* 122:171-177.
68. Ley K, Laudanna C, Cybulsky MI, Nourshargh S (2007): Getting to the site of inflammation: the leukocyte adhesion cascade updated. *Nat Rev Immunol* 7:678-689.
69. Bix G, Iozzo RV (2005): Matrix revolutions: "tails" of basement-membrane components with angiostatic functions. *Trends Cell Biol* 15:52-60.
70. Wickstrom SA, Alitalo K, Keski-Oja J (2005): Endostatin signaling and regulation of endothelial cell-matrix interactions. *Adv Cancer Res* 94:197-229.
71. Calderwood DA (2004): Integrin activation. *J Cell Sci* 117:657-666.
72. Travis MA, Humphries JD, Humphries MJ (2003): An unraveling tale of how integrins are activated from within. *Trends Pharmacol Sci* 24:192-197.
73. Ruggeri ZM (2002): Platelets in atherothrombosis. *Nat Med* 8:1227-1234.
74. Wegener KL, Campbell ID (2008): Transmembrane and cytoplasmic domains in integrin activation and protein-protein interactions (review). *Mol Membr Biol* 25:376-387.
75. Critchley DR, Gingras AR (2008): Talin at a glance. *J Cell Sci* 121:1345-1347.
76. Wegener KL, Partridge AW, Han J, Pickford AR, Liddington RC, Ginsberg MH, Campbell ID (2007): Structural basis of integrin activation by talin. *Cell* 128:171-182.
77. Legate KR, Wickstrom SA, Fassler R (2009): Genetic and cell biological analysis of integrin outside-in signaling. *Genes Dev* 23:397-418.
78. Franco SJ, Rodgers MA, Perrin BJ, Han J, Bennin DA, Critchley DR, Huttenlocher A (2004): Calpain-mediated proteolysis of talin regulates adhesion dynamics. *Nat Cell Biol* 6:977-983.
79. Ma YQ, Yang J, Pesho MM, Vinogradova O, Qin J, Plow EF (2006): Regulation of integrin α IIb β 3 activation by distinct regions of its cytoplasmic tails. *Biochemistry* 45:6656-6662.
80. Goksoy E, Ma YQ, Wang X, Kong X, Perera D, Plow EF, Qin J (2008): Structural basis for the autoinhibition of talin in regulating integrin activation. *Mol Cell* 31:124-133.
81. Martel V, Racaud-Sultan C, Dupe S, Marie C, Paulhe F, Galmiche A, Block MR, Albiges-Rizo C (2001): Conformation, localization, and integrin binding of talin depend on its interaction with phosphoinositides. *J Biol Chem* 276:21217-21227.
82. Di Paolo G, Pellegrini L, Letinic K, Cestra G, Zoncu R, Voronov S, Chang S, Guo J, Wenk MR, De Camilli P (2002): Recruitment and regulation of phosphatidylinositol phosphate kinase type 1 gamma by the FERM domain of talin. *Nature* 420:85-89.
83. Ling K, Doughman RL, Firestone AJ, Bunce MW, Anderson RA (2002): Type I gamma phosphatidylinositol phosphate kinase targets and regulates focal adhesions. *Nature* 420:89-93.
84. Sebзда E, Bracke M, Tugal T, Hogg N, Cantrell DA (2002): Rap1A positively regulates T cells via integrin activation rather than inhibiting lymphocyte signaling. *Nat Immunol* 3:251-258.

85. Chrzanowska-Wodnicka M, Smyth SS, Schoenwaelder SM, Fischer TH, White GC, 2nd (2005): Rap1b is required for normal platelet function and hemostasis in mice. *J Clin Invest* 115:680-687.
86. Han J, Lim CJ, Watanabe N, Soriani A, Ratnikov B, Calderwood DA, Puzon-McLaughlin W, Lafuente EM, Boussiotis VA, Shattil SJ, Ginsberg MH (2006): Reconstructing and deconstructing agonist-induced activation of integrin α IIb β 3. *Curr Biol* 16:1796-1806.
87. Watanabe N, Bodin L, Pandey M, Krause M, Coughlin S, Boussiotis VA, Ginsberg MH, Shattil SJ (2008): Mechanisms and consequences of agonist-induced talin recruitment to platelet integrin α IIb β 3. *J Cell Biol* 181:1211-1222.
88. Lee HS, Lim CJ, Puzon-McLaughlin W, Shattil SJ, Ginsberg MH (2009): RIAM activates integrins by linking talin to ras GTPase membrane-targeting sequences. *J Biol Chem* 284:5119-5127.
89. Sakai T, Jove R, Fassler R, Mosher DF (2001): Role of the cytoplasmic tyrosines of beta 1A integrins in transformation by v-src. *Proc Natl Acad Sci U S A* 98:3808-3813.
90. Oxley CL, Anthis NJ, Lowe ED, Vakonakis I, Campbell ID, Wegener KL (2008): An integrin phosphorylation switch: the effect of beta3 integrin tail phosphorylation on Dok1 and talin binding. *J Biol Chem* 283:5420-5426.
91. Calderwood DA, Yan B, de Pereda JM, Alvarez BG, Fujioka Y, Liddington RC, Ginsberg MH (2002): The phosphotyrosine binding-like domain of talin activates integrins. *J Biol Chem* 277:21749-21758.
92. Ingber DE (2006): Mechanical control of tissue morphogenesis during embryological development. *Int J Dev Biol* 50:255-266.
93. Choi CK, Vicente-Manzanares M, Zareno J, Whitmore LA, Mogilner A, Horwitz AR (2008): Actin and alpha-actinin orchestrate the assembly and maturation of nascent adhesions in a myosin II motor-independent manner. *Nat Cell Biol* 10:1039-1050.
94. Geiger B, Bershadsky A, Pankov R, Yamada KM (2001): Transmembrane crosstalk between the extracellular matrix--cytoskeleton crosstalk. *Nat Rev Mol Cell Biol* 2:793-805.
95. Zaidel-Bar R, Itzkovitz S, Ma'ayan A, Iyengar R, Geiger B (2007): Functional atlas of the integrin adhesome. *Nat Cell Biol* 9:858-867.
96. Burridge K, Wennerberg K (2004): Rho and Rac take center stage. *Cell* 116:167-179.
97. Martin KH, Slack JK, Boerner SA, Martin CC, Parsons JT (2002): Integrin connections map: to infinity and beyond. *Science* 296:1652-1653.
98. Hall A (1998): Rho GTPases and the actin cytoskeleton. *Science* 279:509-514.
99. Pollard TD (2007): Regulation of actin filament assembly by Arp2/3 complex and formins. *Annu Rev Biophys Biomol Struct* 36:451-477.
100. Zhang X, Jiang G, Cai Y, Monkley SJ, Critchley DR, Sheetz MP (2008): Talin depletion reveals independence of initial cell spreading from integrin activation and traction. *Nat Cell Biol* 10:1062-1068.
101. Saunders RM, Holt MR, Jennings L, Sutton DH, Barsukov IL, Bobkov A, Liddington RC, Adamson EA, Dunn GA, Critchley DR (2006): Role of vinculin in regulating focal adhesion turnover. *Eur J Cell Biol* 85:487-500.

102. Otey CA, Pavalko FM, Burridge K (1990): An interaction between alpha-actinin and the beta 1 integrin subunit in vitro. *J Cell Biol* 111:721-729.
103. Lai-Cheong JE, Ussar S, Arita K, Hart IR, McGrath JA (2008): Colocalization of kindlin-1, kindlin-2, and migfilin at keratinocyte focal adhesion and relevance to the pathophysiology of Kindler syndrome. *J Invest Dermatol* 128:2156-2165.
104. Wang HV, Chang LW, Brixius K, Wickstrom SA, Montanez E, Thievessen I, Schwander M, Muller U, Bloch W, Mayer U, Fassler R (2008): Integrin-linked kinase stabilizes myotendinous junctions and protects muscle from stress-induced damage. *J Cell Biol* 180:1037-1049.
105. Velyvis A, Vaynberg J, Yang Y, Vinogradova O, Zhang Y, Wu C, Qin J (2003): Structural and functional insights into PINCH LIM4 domain-mediated integrin signaling. *Nat Struct Biol* 10:558-564.
106. Vicente-Manzanares M, Webb DJ, Horwitz AR (2005): Cell migration at a glance. *J Cell Sci* 118:4917-4919.
107. Grashoff C, Thievessen I, Lorenz K, Ussar S, Fassler R (2004): Integrin-linked kinase: integrin's mysterious partner. *Curr Opin Cell Biol* 16:565-571.
108. Streuli CH, Akhtar N (2009): Signal co-operation between integrins and other receptor systems. *Biochem J* 418:491-506.
109. Hanahan D, Weinberg RA (2000): The hallmarks of cancer. *Cell* 100:57-70.
110. Streuli CH (2006): Cell adhesion and cancer. In *The Molecular Biology of Cancer* (Pelengaris S; Kahn M; eds), pp. 356-387, Blackwell Publishing, Malden, MA, U.S.A.
111. Lu S, Simin K, Khan A, Mercurio AM (2008): Analysis of integrin beta4 expression in human breast cancer: association with basal-like tumors and prognostic significance. *Clin Cancer Res* 14:1050-1058.
112. Collo G, Pepper MS (1999): Endothelial cell integrin alpha5beta1 expression is modulated by cytokines and during migration in vitro. *J Cell Sci* 112 (Pt 4):569-578.
113. Constantin G (2008): Chemokine signaling and integrin activation in lymphocyte migration into the inflamed brain. *J Neuroimmunol* 198:20-26.
114. Abram CL, Lowell CA (2009): The ins and outs of leukocyte integrin signaling. *Annu Rev Immunol* 27:339-362.
115. Ma YQ, Qin J, Plow EF (2007): Platelet integrin alpha(IIb)beta(3): activation mechanisms. *J Thromb Haemost* 5:1345-1352.
116. Tabata T, Kawakatsu H, Maidji E, Sakai T, Sakai K, Fang-Hoover J, Aiba M, Sheppard D, Pereira L (2008): Induction of an epithelial integrin alphavbeta6 in human cytomegalovirus-infected endothelial cells leads to activation of transforming growth factor-beta1 and increased collagen production. *Am J Pathol* 172:1127-1140.
117. Giancotti FG, Tarone G (2003): Positional control of cell fate through joint integrin/receptor protein kinase signaling. *Annu Rev Cell Dev Biol* 19:173-206.
118. Pu QQ, Streuli CH (2002): Integrin control of cell cycle: a new role for ubiquitin ligase. *Bioessays* 24:17-21.
119. Moro L, Dolce L, Cabodi S, Bergatto E, Boeri Erba E, Smeriglio M, Turco E, Retta SF, Giuffrida MG, Venturino M, Godovac-Zimmermann J, Conti A, Schaefer E, Beguinot L, Tacchetti C, Gaggini P, Silengo L, Tarone G, Defilippi P (2002): Integrin-induced epi-

- dermal growth factor (EGF) receptor activation requires c-Src and p130Cas and leads to phosphorylation of specific EGF receptor tyrosines. *J Biol Chem* 277:9405-9414.
120. Ivaska J, Bosca L, Parker PJ (2003): PKCepsilon is a permissive link in integrin-dependent IFN-gamma signalling that facilitates JAK phosphorylation of STAT1. *Nat Cell Biol* 5:363-369.
 121. Faccio R, Takeshita S, Zallone A, Ross FP, Teitelbaum SL (2003): c-Fms and the alphavbeta3 integrin collaborate during osteoclast differentiation. *J Clin Invest* 111:749-758.
 122. Wagner EF, Matsuo K (2003): Signalling in osteoclasts and the role of Fos/AP1 proteins. *Ann Rheum Dis* 62 Suppl 2:ii83-85.
 123. Ross FP, Teitelbaum SL (2005): alphavbeta3 and macrophage colony-stimulating factor: partners in osteoclast biology. *Immunol Rev* 208:88-105.
 124. Zou W, Kitaura H, Reeve J, Long F, Tybulewicz VL, Shattil SJ, Ginsberg MH, Ross FP, Teitelbaum SL (2007): Syk, c-Src, the alphavbeta3 integrin, and ITAM immunoreceptors, in concert, regulate osteoclastic bone resorption. *J Cell Biol* 176:877-888.
 125. Zou W, Reeve JL, Liu Y, Teitelbaum SL, Ross FP (2008): DAP12 couples c-Fms activation to the osteoclast cytoskeleton by recruitment of Syk. *Mol Cell* 31:422-431.
 126. Fassler R, Pfaff M, Murphy J, Noegel AA, Johansson S, Timpl R, Albrecht R (1995): Lack of beta 1 integrin gene in embryonic stem cells affects morphology, adhesion, and migration but not integration into the inner cell mass of blastocysts. *J Cell Biol* 128:979-988.
 127. Stephens LE, Sutherland AE, Klimanskaya IV, Andrieux A, Meneses J, Pedersen RA, Damsky CH (1995): Deletion of beta 1 integrins in mice results in inner cell mass failure and peri-implantation lethality. *Genes Dev* 9:1883-1895.
 128. Yang JT, Rayburn H, Hynes RO (1993): Embryonic mesodermal defects in alpha 5 integrin-deficient mice. *Development* 119:1093-1105.
 129. Yang JT, Rayburn H, Hynes RO (1995): Cell adhesion events mediated by alpha 4 integrins are essential in placental and cardiac development. *Development* 121:549-560.
 130. Bader BL, Rayburn H, Crowley D, Hynes RO (1998): Extensive vasculogenesis, angiogenesis, and organogenesis precede lethality in mice lacking all alpha v integrins. *Cell* 95:507-519.
 131. Kreidberg JA, Donovan MJ, Goldstein SL, Rennke H, Shepherd K, Jones RC, Jaenisch R (1996): Alpha 3 beta 1 integrin has a crucial role in kidney and lung organogenesis. *Development* 122:3537-3547.
 132. DiPersio CM, Hodivala-Dilke KM, Jaenisch R, Kreidberg JA, Hynes RO (1997): alpha3beta1 Integrin is required for normal development of the epidermal basement membrane. *J Cell Biol* 137:729-742.
 133. Anton ES, Kreidberg JA, Rakic P (1999): Distinct functions of alpha3 and alpha(v) integrin receptors in neuronal migration and laminar organization of the cerebral cortex. *Neuron* 22:277-289.
 134. Georges-Labouesse E, Messaddeq N, Yehia G, Cadalbert L, Dierich A, Le Meur M (1996): Absence of integrin alpha 6 leads to epidermolysis bullosa and neonatal death in mice. *Nat Genet* 13:370-373.
 135. Georges-Labouesse E, Mark M, Messaddeq N, Gansmuller A (1998): Essential role of alpha 6 integrins in cortical and retinal lamination. *Curr Biol* 8:983-986.

136. Muller U, Wang D, Denda S, Meneses JJ, Pedersen RA, Reichardt LF (1997): Integrin alpha8beta1 is critically important for epithelial-mesenchymal interactions during kidney morphogenesis. *Cell* 88:603-613.
137. Littlewood Evans A, Muller U (2000): Stereocilia defects in the sensory hair cells of the inner ear in mice deficient in integrin alpha8beta1. *Nat Genet* 24:424-248.
138. van der Neut R, Krimpenfort P, Calafat J, Niessen CM, Sonnenberg A (1996): Epithelial detachment due to absence of hemidesmosomes in integrin beta 4 null mice. *Nat Genet* 13:366-369.
139. Dowling J, Yu QC, Fuchs E (1996): Beta4 integrin is required for hemidesmosome formation, cell adhesion and cell survival. *J Cell Biol* 134:559-572.
140. Zhu J, Motejlek K, Wang D, Zang K, Schmidt A, Reichardt LF (2002): beta8 integrins are required for vascular morphogenesis in mouse embryos. *Development* 129:2891-2903.
141. Schmits R, Kundig TM, Baker DM, Shumaker G, Simard JJ, Duncan G, Wakeham A, Shahinian A, van der Heiden A, Bachmann MF, Ohashi PS, Mak TW, Hickstein DD (1996): LFA-1-deficient mice show normal CTL responses to virus but fail to reject immunogenic tumor. *J Exp Med* 183:1415-1426.
142. Coxon A, Rieu P, Barkalow FJ, Askari S, Sharpe AH, von Andrian UH, Arnaout MA, Mayadas TN (1996): A novel role for the beta 2 integrin CD11b/CD18 in neutrophil apoptosis: a homeostatic mechanism in inflammation. *Immunity* 5:653-666.
143. Tang T, Rosenkranz A, Assmann KJ, Goodman MJ, Gutierrez-Ramos JC, Carroll MC, Cotran RS, Mayadas TN (1997): A role for Mac-1 (CD11b/CD18) in immune complex-stimulated neutrophil function in vivo: Mac-1 deficiency abrogates sustained Fcgamma receptor-dependent neutrophil adhesion and complement-dependent proteinuria in acute glomerulonephritis. *J Exp Med* 186:1853-1863.
144. Schon MP, Arya A, Murphy EA, Adams CM, Strauch UG, Agace WW, Marsal J, Donohue JP, Her H, Beier DR, Olson S, Lefrancois L, Brenner MB, Grusby MJ, Parker CM (1999): Mucosal T lymphocyte numbers are selectively reduced in integrin alpha E (CD103)-deficient mice. *J Immunol* 162:6641-6649.
145. Wagner N, Lohler J, Kunkel EJ, Ley K, Leung E, Krissansen G, Rajewsky K, Muller W (1996): Critical role for beta7 integrins in formation of the gut-associated lymphoid tissue. *Nature* 382:366-370.
146. Huang XZ, Wu JF, Cass D, Erle DJ, Corry D, Young SG, Farese RV, Jr., Sheppard D (1996): Inactivation of the integrin beta 6 subunit gene reveals a role of epithelial integrins in regulating inflammation in the lung and skin. *J Cell Biol* 133:921-928.
147. Munger JS, Huang X, Kawakatsu H, Griffiths MJ, Dalton SL, Wu J, Pittet JF, Kaminski N, Garat C, Matthay MA, Rifkin DB, Sheppard D (1999): The integrin alpha v beta 6 binds and activates latent TGF beta 1: a mechanism for regulating pulmonary inflammation and fibrosis. *Cell* 96:319-328.
148. Scharffetter-Kochanek K, Lu H, Norman K, van Nood N, Munoz F, Grabbe S, McArthur M, Lorenzo I, Kaplan S, Ley K, Smith CW, Montgomery CA, Rich S, Beaudet AL (1998): Spontaneous skin ulceration and defective T cell function in CD18 null mice. *J Exp Med* 188:119-131.
149. Hodivala-Dilke KM, McHugh KP, Tsakiris DA, Rayburn H, Crowley D, Ullman-Cullere M, Ross FP, Collier BS, Teitelbaum S, Hynes RO (1999): Beta3-integrin-deficient mice are a model for Glanzmann thrombasthenia showing placental defects and reduced survival. *J Clin Invest* 103:229-238.

150. Du X, Ginsberg MH (1997): Integrin alpha IIb beta 3 and platelet function. *Thromb Haemost* 78:96-100.
151. Tronik-Le Roux D, Roullot V, Poujol C, Kortulewski T, Nurden P, Marguerie G (2000): Thrombasthenic mice generated by replacement of the integrin alpha(IIb) gene: demonstration that transcriptional activation of this megakaryocytic locus precedes lineage commitment. *Blood* 96:1399-1408.
152. McHugh KP, Hodivala-Dilke K, Zheng MH, Namba N, Lam J, Novack D, Feng X, Ross FP, Hynes RO, Teitelbaum SL (2000): Mice lacking beta3 integrins are osteosclerotic because of dysfunctional osteoclasts. *J Clin Invest* 105:433-440.
153. Reynolds LE, Wyder L, Lively JC, Taverna D, Robinson SD, Huang X, Sheppard D, Hynes RO, Hodivala-Dilke KM (2002): Enhanced pathological angiogenesis in mice lacking beta3 integrin or beta3 and beta5 integrins. *Nat Med* 8:27-34.
154. Brakebusch C, Grose R, Quondamatteo F, Ramirez A, Jorcano JL, Pirro A, Svensson M, Herken R, Sasaki T, Timpl R, Werner S, Fassler R (2000): Skin and hair follicle integrity is crucially dependent on beta 1 integrin expression on keratinocytes. *Embo J* 19:3990-4003.
155. Abraham S, Kogata N, Fassler R, Adams RH (2008): Integrin beta1 subunit controls mural cell adhesion, spreading, and blood vessel wall stability. *Circ Res* 102:562-570.
156. Durand C, Dzierzak E (2005): Embryonic beginnings of adult hematopoietic stem cells. *Haematologica* 90:100-108.
157. Iwasaki H, Akashi K (2007): Myeloid lineage commitment from the hematopoietic stem cell. *Immunity* 26:726-740.
158. Manz MG, Traver D, Miyamoto T, Weissman IL, Akashi K (2001): Dendritic cell potentials of early lymphoid and myeloid progenitors. *Blood* 97:3333-3341.
159. www.med.lu.se/hemato_linne/research_groups/stefan_karlsson
160. Potocnik AJ, Brakebusch C, Fassler R (2000): Fetal and adult hematopoietic stem cells require beta1 integrin function for colonizing fetal liver, spleen, and bone marrow. *Immunity* 12:653-663.
161. Papayannopoulou T (2000): Mechanisms of stem-/progenitor-cell mobilization: the anti-VLA-4 paradigm. *Semin Hematol* 37:11-18.
162. Kikuta T, Shimazaki C, Ashihara E, Sudo Y, Hirai H, Sumikuma T, Yamagata N, Inaba T, Fujita N, Kina T, Nakagawa M (2000): Mobilization of hematopoietic primitive and committed progenitor cells into blood in mice by anti-vascular adhesion molecule-1 antibody alone or in combination with granulocyte colony-stimulating factor. *Exp Hematol* 28:311-317.
163. Arroyo AG, Yang JT, Rayburn H, Hynes RO (1999): Alpha4 integrins regulate the proliferation/differentiation balance of multilineage hematopoietic progenitors in vivo. *Immunity* 11:555-566.
164. Levesque JP, Leavesley DI, Niutta S, Vadas M, Simmons PJ (1995): Cytokines increase human hemopoietic cell adhesiveness by activation of very late antigen (VLA)-4 and VLA-5 integrins. *J Exp Med* 181:1805-1815.
165. Katayama Y, Hidalgo A, Peired A, Frenette PS (2004): Integrin alpha4beta7 and its counterreceptor MAdCAM-1 contribute to hematopoietic progenitor recruitment into bone marrow following transplantation. *Blood* 104:2020-2026.

166. Grassinger J, Haylock DN, Storan MJ, Haines GO, Williams B, Whitty GA, Vinson AR, Be CL, Li S, Sorensen ES, Tam PP, Denhardt DT, Sheppard D, Choong PF, Nilsson SK (2009): Thrombin-cleaved osteopontin regulates hemopoietic stem and progenitor cell functions through interactions with alpha9beta1 and alpha4beta1 integrins. *Blood* 114:49-59.
167. Ross EA, Douglas MR, Wong SH, Ross EJ, Curnow SJ, Nash GB, Rainger E, Scheel-Toellner D, Lord JM, Salmon M, Buckley CD (2006): Interaction between integrin alpha9beta1 and vascular cell adhesion molecule-1 (VCAM-1) inhibits neutrophil apoptosis. *Blood* 107:1178-1183.
168. Moore MA, Metcalf D (1970): Ontogeny of the haemopoietic system: yolk sac origin of in vivo and in vitro colony forming cells in the developing mouse embryo. *Br J Haematol* 18:279-296.
169. Medvinsky AL, Samoylina NL, Muller AM, Dzierzak EA (1993): An early pre-liver intraembryonic source of CFU-S in the developing mouse. *Nature* 364:64-67.
170. Kumaravelu P, Hook L, Morrison AM, Ure J, Zhao S, Zuyev S, Ansell J, Medvinsky A (2002): Quantitative developmental anatomy of definitive haematopoietic stem cells/long-term repopulating units (HSC/RUs): role of the aorta-gonad-mesonephros (AGM) region and the yolk sac in colonisation of the mouse embryonic liver. *Development* 129:4891-4899.
171. Geminard C, de Gassart A, Vidal M (2002): Reticulocyte maturation: mitoptosis and exosome release. *Biocell* 26:205-215.
172. Erslev AJ (1995): Clinical manifestations and classification of erythrocyte disorders. In *Williams Hematology 5th ed* (Beutler E, Lichtman MA, Coller BS, Kipps TJ, eds), pp. 442-447; New York, McGraw-Hill
173. Eshghi S, Voegelzang MG, Hynes RO, Griffith LG, Lodish HF (2007): Alpha4beta1 integrin and erythropoietin mediate temporally distinct steps in erythropoiesis: integrins in red cell development. *J Cell Biol* 177:871-880.
174. Oldenborg PA, Zheleznyak A, Fang YF, Lagenaur CF, Gresham HD, Lindberg FP (2000): Role of CD47 as a marker of self on red blood cells. *Science* 288:2051-2054.
175. Brittain JE, Mlinar KJ, Anderson CS, Orringer EP, Parise LV (2001): Activation of sickle red blood cell adhesion via integrin-associated protein/CD47-induced signal transduction. *J Clin Invest* 107:1555-1562.
176. Dahl KN, Westhoff CM, Discher DE (2003): Fractional attachment of CD47 (IAP) to the erythrocyte cytoskeleton and visual colocalization with Rh protein complexes. *Blood* 101:1194-1199.
177. Delaunay J (1995): Genetic disorders of the red cell membranes. *FEBS Lett* 369:34-37.
178. McMullin MF (1999): The molecular basis of disorders of the red cell membrane. *J Clin Pathol* 52:245-248.
179. Kaushansky K (2006): Lineage-specific hematopoietic growth factors. *N Engl J Med* 354:2034-2045.
180. Youssefian T, Cramer EM (2000): Megakaryocyte dense granule components are sorted in multivesicular bodies. *Blood* 95:4004-4007.
181. Britannica Educational Publishing (2010): *Blood: Physiology and Circulation*. Human Body (Kara Rogers, ed), p. 52, The Rosen Publishing Group

182. Jin RC, Voetsch B, Loscalzo J (2005): Endogenous mechanisms of inhibition of platelet function. *Microcirculation* 12:247-258.
183. Bennett JS, Chan C, Vilaire G, Mousa SA, DeGrado WF (1997): Agonist-activated alpha v beta 3 on platelets and lymphocytes binds to the matrix protein osteopontin. *J Biol Chem* 272:8137-8140.
184. Nieswandt B, Brakebusch C, Bergmeier W, Schulte V, Bouvard D, Mokhtari-Nejad R, Lindhout T, Heemskerk JW, Zirngibl H, Fassler R (2001): Glycoprotein VI but not alpha 2 beta 1 integrin is essential for platelet interaction with collagen. *Embo J* 20:2120-2130.
185. Varga-Szabo D, Pleines I, Nieswandt B (2008): Cell adhesion mechanisms in platelets. *Arterioscler Thromb Vasc Biol* 28:403-412.
186. Bennett JS (2005): Structure and function of the platelet integrin alpha IIb beta 3. *J Clin Invest* 115:3363-3369.
187. Bennett JS, Berger BW, Billings PC (2009): The structure and function of platelet integrins. *J Thromb Haemost* 7 Suppl 1:200-205.
188. Savage B, Almus-Jacobs F, Ruggeri ZM (1998): Specific synergy of multiple substrate-receptor interactions in platelet thrombus formation under flow. *Cell* 94:657-666.
189. Lisman T, Weeterings C, de Groot PG (2005): Platelet aggregation: involvement of thrombin and fibrin(ogen). *Front Biosci* 10:2504-2517.
190. Encyclopaedia Britannica (2002): The New Encyclopædia Britannica: Macropædia: Knowledge in depth. Encyclopaedia Britannica.
191. Bokoch GM, Vlahos CJ, Wang Y, Knaus UG, Traynor-Kaplan AE (1996): Rac GTPase interacts specifically with phosphatidylinositol 3-kinase. *Biochem J* 315 (Pt 3):775-779.
192. Witko-Sarsat V, Rieu P, Descamps-Latscha B, Lesavre P, Halbwachs-Mecarelli L (2000): Neutrophils: molecules, functions and pathophysiological aspects. *Lab Invest* 80:617-653.
193. www.dent.ucla.edu/pic/members/neutrophils/neutrophils.html
194. Luster AD, Alon R, von Andrian UH (2005): Immune cell migration in inflammation: present and future therapeutic targets. *Nat Immunol* 6:1182-1190.
195. Berlin C, Bargatze RF, Campbell JJ, von Andrian UH, Szabo MC, Hasslen SR, Nelson RD, Berg EL, Erlandsen SL, Butcher EC (1995): alpha 4 integrins mediate lymphocyte attachment and rolling under physiologic flow. *Cell* 80:413-422.
196. Berlin-Rufenach C, Otto F, Mathies M, Westermann J, Owen MJ, Hamann A, Hogg N (1999): Lymphocyte migration in lymphocyte function-associated antigen (LFA)-1-deficient mice. *J Exp Med* 189:1467-1478.
197. Henderson RB, Hobbs JA, Mathies M, Hogg N (2003): Rapid recruitment of inflammatory monocytes is independent of neutrophil migration. *Blood* 102:328-335.
198. Henderson RB, Lim LH, Tessier PA, Gavins FN, Mathies M, Perretti M, Hogg N (2001): The use of lymphocyte function-associated antigen (LFA)-1-deficient mice to determine the role of LFA-1, Mac-1, and alpha 4 integrin in the inflammatory response of neutrophils. *J Exp Med* 194:219-226.
199. Phillipson M, Heit B, Colarusso P, Liu L, Ballantyne CM, Kubes P (2006): Intraluminal crawling of neutrophils to emigration sites: a molecularly distinct process from adhesion in the recruitment cascade. *J Exp Med* 203:2569-2575.

200. Carman CV, Sage PT, Sciuto TE, de la Fuente MA, Geha RS, Ochs HD, Dvorak HF, Dvorak AM, Springer TA (2007): Transcellular diapedesis is initiated by invasive podosomes. *Immunity* 26:784-797.
201. Vestweber D (2007): Adhesion and signaling molecules controlling the transmigration of leukocytes through endothelium. *Immunol Rev* 218:178-196.
202. Carman CV, Springer TA (2004): A transmigratory cup in leukocyte diapedesis both through individual vascular endothelial cells and between them. *J Cell Biol* 167:377-388.
203. Dangerfield J, Larbi KY, Huang MT, Dewar A, Nourshargh S (2002): PECAM-1 (CD31) homophilic interaction up-regulates alpha6beta1 on transmigrated neutrophils in vivo and plays a functional role in the ability of alpha6 integrins to mediate leukocyte migration through the perivascular basement membrane. *J Exp Med* 196:1201-1211.
204. Stefanidakis M, Koivunen E (2006): Cell-surface association between matrix metalloproteinases and integrins: role of the complexes in leukocyte migration and cancer progression. *Blood* 108:1441-1450.
205. Madri JA, Graesser D (2000): Cell migration in the immune system: the evolving inter-related roles of adhesion molecules and proteinases. *Dev Immunol* 7:103-116.
206. Kishimoto TK, Hollander N, Roberts TM, Anderson DC, Springer TA (1987): Heterogeneous mutations in the beta subunit common to the LFA-1, Mac-1, and p150,95 glycoproteins cause leukocyte adhesion deficiency. *Cell* 50:193-202.
207. Crowley CA, Curnutte JT, Rosin RE, Andre-Schwartz J, Gallin JI, Klempner M, Snyderman R, Southwick FS, Stossel TP, Babior BM (1980): An inherited abnormality of neutrophil adhesion. Its genetic transmission and its association with a missing protein. *N Engl J Med* 302:1163-1168.
208. Etzioni A, Frydman M, Pollack S, Avidor I, Phillips ML, Paulson JC, Gershoni-Baruch R (1992): Brief report: recurrent severe infections caused by a novel leukocyte adhesion deficiency. *N Engl J Med* 327:1789-1792.
209. Phillips ML, Schwartz BR, Etzioni A, Bayer R, Ochs HD, Paulson JC, Harlan JM (1995): Neutrophil adhesion in leukocyte adhesion deficiency syndrome type 2. *J Clin Invest* 96:2898-2906.
210. Etzioni A, Doerschuk CM, Harlan JM (1999): Of man and mouse: leukocyte and endothelial adhesion molecule deficiencies. *Blood* 94:3281-3288.
211. Lowe JB, Stoolman LM, Nair RP, Larsen RD, Berhend TL, Marks RM (1990): ELAM-1--dependent cell adhesion to vascular endothelium determined by a transfected human fucosyltransferase cDNA. *Cell* 63:475-484.
212. Marquardt T, Luhn K, Srikrishna G, Freeze HH, Harms E, Vestweber D (1999): Correction of leukocyte adhesion deficiency type II with oral fucose. *Blood* 94:3976-3985.
213. Luhn K, Wild MK, Eckhardt M, Gerardy-Schahn R, Vestweber D (2001): The gene defective in leukocyte adhesion deficiency II encodes a putative GDP-fucose transporter. *Nat Genet* 28:69-72.
214. Malinin NL, Zhang L, Choi J, Ciocea A, Razorenova O, Ma YQ, Podrez EA, Tosi M, Lennon DP, Caplan AI, Shurin SB, Plow EF, Byzova TV (2009): A point mutation in KINDLIN3 ablates activation of three integrin subfamilies in humans. *Nat Med* 15:313-318.

215. Svensson L, Howarth K, McDowall A, Patzak I, Evans R, Ussar S, Moser M, Metin A, Fried M, Tomlinson I, Hogg N (2009): Leukocyte adhesion deficiency-III is caused by mutations in *KINDLIN3* affecting integrin activation. *Nat Med* 15:306-312.
216. Zimmerman GA (2009): LAD syndromes: *FERMT3* kindles the signal. *Blood* 113:4485-4486.
217. Alon R, Etzioni A (2003): LAD-III, a novel group of leukocyte integrin activation deficiencies. *Trends Immunol* 24:561-566.
218. Kuijpers TW, Van Lier RA, Hamann D, de Boer M, Thung LY, Weening RS, Verhoeven AJ, Roos D (1997): Leukocyte adhesion deficiency type 1 (LAD-1)/variant. A novel immunodeficiency syndrome characterized by dysfunctional beta2 integrins. *J Clin Invest* 100:1725-1733.
219. McDowall A, Inwald D, Leitinger B, Jones A, Liesner R, Klein N, Hogg N (2003): A novel form of integrin dysfunction involving beta1, beta2, and beta3 integrins. *J Clin Invest* 111:51-60.
220. van Furth R, Cohn ZA (1968): The origin and kinetics of mononuclear phagocytes. *J Exp Med* 128(3):415-435
221. Geissmann F, Manz MG, Jung S, Sieweke MH, Merad M, Ley K Development of monocytes, macrophages, and dendritic cells. *Science* 327:656-661.
222. Springer TA (1990): Adhesion receptors of the immune system. *Nature* 346:425-434.
223. Beller DI, Springer TA, Schreiber RD (1982): Anti-Mac-1 selectively inhibits the mouse and human type three complement receptor. *J Exp Med* 156:1000-1009.
224. Caron E, Self AJ, Hall A (2000): The GTPase Rap1 controls functional activation of macrophage integrin alphaMbeta2 by LPS and other inflammatory mediators. *Curr Biol* 10:974-978.
225. Ortiz-Stern A, Rosales C (2003): Cross-talk between Fc receptors and integrins. *Immunol Lett* 90:137-143.
226. Suda T, Takahashi N, Martin TJ (1992): Modulation of osteoclast differentiation. *Endocr Rev* 13:66-80.
227. Benninghoff, A.; Drenckhahn, D. (2002). *Anatomie, Band I*
228. Vaananen HK, Zhao H, Mulari M, Halleen JM (2000): The cell biology of osteoclast function. *J Cell Sci* 113 (Pt 3):377-381.
229. Yasuda H, Shima N, Nakagawa N, Yamaguchi K, Kinosaki M, Mochizuki S, Tomoyasu A, Yano K, Goto M, Murakami A, Tsuda E, Morinaga T, Higashio K, Udagawa N, Takahashi N, Suda T (1998): Osteoclast differentiation factor is a ligand for osteoprotegerin/osteoclastogenesis-inhibitory factor and is identical to *TRANCE/RANKL*. *Proc Natl Acad Sci U S A* 95:3597-3602.
230. Yoshida H, Hayashi S, Kunisada T, Ogawa M, Nishikawa S, Okamura H, Sudo T, Shultz LD, Nishikawa S (1990): The murine mutation osteopetrosis is in the coding region of the macrophage colony stimulating factor gene. *Nature* 345:442-444.
231. Hsu H, Lacey DL, Dunstan CR, Solovyev I, Colombero A, Timms E, Tan HL, Elliott G, Kelley MJ, Sarosi I, Wang L, Xia XZ, Elliott R, Chiu L, Black T, Scully S, Capparelli C, Morony S, Shimamoto G, Bass MB, Boyle WJ (1999): Tumor necrosis factor receptor family member *RANK* mediates osteoclast differentiation and activation induced by osteoprotegerin ligand. *Proc Natl Acad Sci U S A* 96:3540-3545.

232. Lacey DL, Timms E, Tan HL, Kelley MJ, Dunstan CR, Burgess T, Elliott R, Colombero A, Elliott G, Scully S, Hsu H, Sullivan J, Hawkins N, Davy E, Capparelli C, Eli A, Qian YX, Kaufman S, Sarosi I, Shalhoub V, Senaldi G, Guo J, Delaney J, Boyle WJ (1998): Osteoprotegerin ligand is a cytokine that regulates osteoclast differentiation and activation. *Cell* 93:165-176.
233. Tolar J, Teitelbaum SL, Orchard PJ (2004): Osteopetrosis. *N Engl J Med* 351:2839-2849.
234. Boyce BF, Xing L (2007): Biology of RANK, RANKL, and osteoprotegerin. *Arthritis Res Ther* 9 Suppl 1:S1.
235. Saltel F, Destaing O, Bard F, Eichert D, Jurdic P (2004): Apatite-mediated actin dynamics in resorbing osteoclasts. *Mol Biol Cell* 15:5231-541.
236. Vaananen HK, Karhukorpi EK, Sundquist K, Wallmark B, Roininen I, Hentunen T, Tuukkanen J, Lakkakorpi P (1990): Evidence for the presence of a proton pump of the vacuolar H(+)-ATPase type in the ruffled borders of osteoclasts. *J Cell Biol* 111:1305-1311.
237. Teitelbaum SL (2006): Osteoclasts; culprits in inflammatory osteolysis. *Arthritis Res Ther* 8:201.
238. Salo J, Lehenkari P, Mulari M, Metsikko K, Vaananen HK (1997): Removal of osteoclast bone resorption products by transcytosis. *Science* 276:270-273.
239. Gogakos AI, Cheung MS, Bassett JHD, Williams GR (2009): Bone signaling pathways and treatment of osteoporosis. *Expert Review of Endocrinology & Metabolism*, Vol.4, No. 6, Pages 639-650
240. Destaing O, Saltel F, Geminard JC, Jurdic P, Bard F (2003): Podosomes display actin turnover and dynamic self-organization in osteoclasts expressing actin-green fluorescent protein. *Mol Biol Cell* 14:407-416.
241. Gimona M, Kaverina I, Resch GP, Vignat E, Burgstaller G (2003): Calponin repeats regulate actin filament stability and formation of podosomes in smooth muscle cells. *Mol Biol Cell* 14:2482-2491.
242. Burns S, Thrasher AJ, Blundell MP, Machesky L, Jones GE (2001): Configuration of human dendritic cell cytoskeleton by Rho GTPases, the WAS protein, and differentiation. *Blood* 98:1142-1149.
243. Chabadel A, Banon-Rodriguez I, Cluet D, Rudkin BB, Wehrle-Haller B, Genot E, Jurdic P, Anton IM, Saltel F (2007): CD44 and beta3 integrin organize two functionally distinct actin-based domains in osteoclasts. *Mol Biol Cell* 18:4899-4910.
244. Linder S, Nelson D, Weiss M, Aepfelbacher M (1999): Wiskott-Aldrich syndrome protein regulates podosomes in primary human macrophages. *Proc Natl Acad Sci U S A* 96:9648-9653.
245. Linder S, Higgs H, Hufner K, Schwarz K, Pannicke U, Aepfelbacher M (2000): The polarization defect of Wiskott-Aldrich syndrome macrophages is linked to dislocalization of the Arp2/3 complex. *J Immunol* 165:221-225.
246. Linder S, Hufner K, Wintergerst U, Aepfelbacher M (2000): Microtubule-dependent formation of podosomal adhesion structures in primary human macrophages. *J Cell Sci* 113 Pt 23:4165-4176.
247. Sanjay A, Houghton A, Neff L, DiDomenico E, Bardelay C, Antoine E, Levy J, Gailit J, Bowtell D, Horne WC, Baron R (2001): Cbl associates with Pyk2 and Src to regulate

- Src kinase activity, alpha(v)beta(3) integrin-mediated signaling, cell adhesion, and osteoclast motility. *J Cell Biol* 152:181-195.
248. Chellaiah M, Fitzgerald C, Alvarez U, Hruska K (1998): c-Src is required for stimulation of gelsolin-associated phosphatidylinositol 3-kinase. *J Biol Chem* 273:11908-11916.
249. Lakkakorpi PT, Nakamura I, Nagy RM, Parsons JT, Rodan GA, Duong LT (1999): Stable association of PYK2 and p130(Cas) in osteoclasts and their co-localization in the sealing zone. *J Biol Chem* 274:4900-4907.
250. Duong LT, Lakkakorpi PT, Nakamura I, Machwate M, Nagy RM, Rodan GA (1998): PYK2 in osteoclasts is an adhesion kinase, localized in the sealing zone, activated by ligation of alpha(v)beta3 integrin, and phosphorylated by src kinase. *J Clin Invest* 102:881-892.
251. Evans JG, Correia I, Krasavina O, Watson N, Matsudaira P (2003): Macrophage podosomes assemble at the leading lamella by growth and fragmentation. *J Cell Biol* 161:697-705.
252. Wang Y, Botvinick EL, Zhao Y, Berns MW, Usami S, Tsien RY, Chien S (2005): Visualizing the mechanical activation of Src. *Nature* 434:1040-1045.
253. Jurdic P, Saltel F, Chabadel A, Destaing O (2006): Podosome and sealing zone: specificity of the osteoclast model. *Eur J Cell Biol* 85:195-202.
254. Luxenburg C, Geblinger D, Klein E, Anderson K, Hanein D, Geiger B, Addadi L (2007): The architecture of the adhesive apparatus of cultured osteoclasts: from podosome formation to sealing zone assembly. *PLoS One* 2:e179.
255. Lane NE, Yao W, Nakamura MC, Humphrey MB, Kimmel D, Huang X, Sheppard D, Ross FP, Teitelbaum SL (2005): Mice lacking the integrin beta5 subunit have accelerated osteoclast maturation and increased activity in the estrogen-deficient state. *J Bone Miner Res* 20:58-66.
256. Helfrich MH, Nesbitt SA, Lakkakorpi PT, Barnes MJ, Bodary SC, Shankar G, Mason WT, Mendrick DL, Vaananen HK, Horton MA (1996): Beta 1 integrins and osteoclast function: involvement in collagen recognition and bone resorption. *Bone* 19:317-328.
257. Nesbitt S, Nesbit A, Helfrich M, Horton M (1993): Biochemical characterization of human osteoclast integrins. Osteoclasts express alpha v beta 3, alpha 2 beta 1, and alpha v beta 1 integrins. *J Biol Chem* 268:16737-16745.
258. Choi SJ, Han JH, Roodman GD (2001): ADAM8: a novel osteoclast stimulating factor. *J Bone Miner Res* 16:814-822.
259. Grant FD, Conlin PR, Brown EM (1990): Rate and concentration dependence of parathyroid hormone dynamics during stepwise changes in serum ionized calcium in normal humans. *J Clin Endocrinol Metab* 71:370-378.
260. Shapiro F (1993): Osteopetrosis. Current clinical considerations. *Clin Orthop Relat Res*:34-44.
261. Wiktor-Jedrzejczak W, Bartocci A, Ferrante AW, Jr., Ahmed-Ansari A, Sell KW, Pollard JW, Stanley ER (1990): Total absence of colony-stimulating factor 1 in the macrophage-deficient osteopetrotic (op/op) mouse. *Proc Natl Acad Sci U S A* 87:4828-4832.
262. Dai XM, Ryan GR, Hapel AJ, Dominguez MG, Russell RG, Kapp S, Sylvestre V, Stanley ER (2002): Targeted disruption of the mouse colony-stimulating factor 1 receptor gene results in osteopetrosis, mononuclear phagocyte deficiency, increased primitive progenitor cell frequencies, and reproductive defects. *Blood* 99:111-120.

263. Zhang DE, Hetherington CJ, Chen HM, Tenen DG (1994): The macrophage transcription factor PU.1 directs tissue-specific expression of the macrophage colony-stimulating factor receptor. *Mol Cell Biol* 14:373-381.
264. Simonet WS, Lacey DL, Dunstan CR, Kelley M, Chang MS, Luthy R, Nguyen HQ, Wooden S, Bennett L, Boone T, Shimamoto G, DeRose M, Elliott R, Colombero A, Tan HL, Trail G, Sullivan J, Davy E, Bucay N, Renshaw-Gegg L, Hughes TM, Hill D, Pattison W, Campbell P, Sander S, Van G, Tarpley J, Derby P, Lee R, Boyle WJ (1997): Osteoprotegerin: a novel secreted protein involved in the regulation of bone density. *Cell* 89:309-319.
265. Bucay N, Sarosi I, Dunstan CR, Morony S, Tarpley J, Capparelli C, Scully S, Tan HL, Xu W, Lacey DL, Boyle WJ, Simonet WS (1998): osteoprotegerin-deficient mice develop early onset osteoporosis and arterial calcification. *Genes Dev* 12:1260-1268.
266. Dougall WC, Glaccum M, Charrier K, Rohrbach K, Brasel K, De Smedt T, Daro E, Smith J, Tometsko ME, Maliszewski CR, Armstrong A, Shen V, Bain S, Cosman D, Anderson D, Morrissey PJ, Peschon JJ, Schuh J (1999): RANK is essential for osteoclast and lymph node development. *Genes Dev* 13:2412-2424.
267. Li J, Sarosi I, Yan XQ, Morony S, Capparelli C, Tan HL, McCabe S, Elliott R, Scully S, Van G, Kaufman S, Juan SC, Sun Y, Tarpley J, Martin L, Christensen K, McCabe J, Kostenuik P, Hsu H, Fletcher F, Dunstan CR, Lacey DL, Boyle WJ (2000): RANK is the intrinsic hematopoietic cell surface receptor that controls osteoclastogenesis and regulation of bone mass and calcium metabolism. *Proc Natl Acad Sci U S A* 97:1566-1571.
268. Grigoriadis AE, Wang ZQ, Cecchini MG, Hofstetter W, Felix R, Fleisch HA, Wagner EF (1994): c-Fos: a key regulator of osteoclast-macrophage lineage determination and bone remodeling. *Science* 266:443-448.
269. Iotsova V, Caamano J, Loy J, Yang Y, Lewin A, Bravo R (1997): Osteopetrosis in mice lacking NF-kappaB1 and NF-kappaB2. *Nat Med* 3:1285-1289.
270. Lomaga MA, Yeh WC, Sarosi I, Duncan GS, Furlonger C, Ho A, Morony S, Capparelli C, Van G, Kaufman S, van der Heiden A, Itie A, Wakeham A, Khoo W, Sasaki T, Cao Z, Penninger JM, Paige CJ, Lacey DL, Dunstan CR, Boyle WJ, Goeddel DV, Mak TW (1999): TRAF6 deficiency results in osteopetrosis and defective interleukin-1, CD40, and LPS signaling. *Genes Dev* 13:1015-1024.
271. Deng W, Stashenko P, Chen W, Liang Y, Shimizu K, Li YP (2001): Characterization of mouse *Atp6i* gene, the gene promoter, and the gene expression. *J Bone Miner Res* 16:1136-1146.
272. Scimeca JC, Franchi A, Trojani C, Parrinello H, Grosgeorge J, Robert C, Jaillon O, Poirier C, Gaudray P, Carle GF (2000): The gene encoding the mouse homologue of the human osteoclast-specific 116-kDa V-ATPase subunit bears a deletion in osteosclerotic (oc/oc) mutants. *Bone* 26:207-213.
273. Kornak U, Kasper D, Bosl MR, Kaiser E, Schweizer M, Schulz A, Friedrich W, Delling G, Jentsch TJ (2001): Loss of the ClC-7 chloride channel leads to osteopetrosis in mice and man. *Cell* 104:205-215.
274. Feng X, Novack DV, Faccio R, Ory DS, Aya K, Boyer MI, McHugh KP, Ross FP, Teitelbaum SL (2001): A Glanzmann's mutation in beta 3 integrin specifically impairs osteoclast function. *J Clin Invest* 107:1137-1144.
275. Rao H, Lu G, Kajiya H, Garcia-Palacios V, Kurihara N, Anderson J, Patrene K, Sheppard D, Blair HC, Windle JJ, Choi SJ, Roodman GD (2006): Alpha9beta1: a novel

- osteoclast integrin that regulates osteoclast formation and function. *J Bone Miner Res* 21:1657-1665.
276. Dossa T, Arabian A, Windle JJ, Dedhar S, Teitelbaum SL, Ross FP, Roodman GD, St-Arnaud R (2005): Osteoclast-specific inactivation of the integrin-linked kinase (ILK) inhibits bone resorption. *J Cell Biochem* 110:960-967.
277. Soriano P, Montgomery C, Geske R, Bradley A (1991): Targeted disruption of the c-src proto-oncogene leads to osteopetrosis in mice. *Cell* 64:693-702.
278. Boyce BF, Yoneda T, Lowe C, Soriano P, Mundy GR (1992): Requirement of pp60c-src expression for osteoclasts to form ruffled borders and resorb bone in mice. *J Clin Invest* 90:1622-1627.
279. Destaing O, Sanjay A, Itzstein C, Horne WC, Toomre D, De Camilli P, Baron R (2008): The tyrosine kinase activity of c-Src regulates actin dynamics and organization of podosomes in osteoclasts. *Mol Biol Cell* 19:394-404.
280. Schwartzberg PL, Xing L, Hoffmann O, Lowell CA, Garrett L, Boyce BF, Varmus HE (1997): Rescue of osteoclast function by transgenic expression of kinase-deficient Src in src^{-/-} mutant mice. *Genes Dev* 11:2835-2844.
281. Miyazaki T, Sanjay A, Neff L, Tanaka S, Horne WC, Baron R (2004): Src kinase activity is essential for osteoclast function. *J Biol Chem* 279:17660-17666.
282. Gil-Henn H, Destaing O, Sims NA, Aoki K, Alles N, Neff L, Sanjay A, Bruzzaniti A, De Camilli P, Baron R, Schlessinger J (2007): Defective microtubule-dependent podosome organization in osteoclasts leads to increased bone density in Pyk2^(-/-) mice. *J Cell Biol* 178:1053-1064.
283. Kaifu T, Nakahara J, Inui M, Mishima K, Momiyama T, Kaji M, Sugahara A, Koito H, Ujike-Asai A, Nakamura A, Kanazawa K, Tan-Takeuchi K, Iwasaki K, Yokoyama WM, Kudo A, Fujiwara M, Asou H, Takai T (2003): Osteopetrosis and thalamic hypomyelination with synaptic degeneration in DAP12-deficient mice. *J Clin Invest* 111:323-332.
284. Mocsai A, Humphrey MB, Van Ziffle JA, Hu Y, Burghardt A, Spusta SC, Majumdar S, Lanier LL, Lowell CA, Nakamura MC (2004): The immunomodulatory adapter proteins DAP12 and Fc receptor gamma-chain (FcRgamma) regulate development of functional osteoclasts through the Syk tyrosine kinase. *Proc Natl Acad Sci U S A* 101:6158-6163.
285. Koga T, Inui M, Inoue K, Kim S, Suematsu A, Kobayashi E, Iwata T, Ohnishi H, Matozaki T, Kodama T, Taniguchi T, Takayanagi H, Takai T (2004): Costimulatory signals mediated by the ITAM motif cooperate with RANKL for bone homeostasis. *Nature* 428:758-763.
286. Faccio R, Teitelbaum SL, Fujikawa K, Chappel J, Zallone A, Tybulewicz VL, Ross FP, Swat W (2005): Vav3 regulates osteoclast function and bone mass. *Nat Med* 11:284-290.
287. Saftig P, Hunziker E, Wehmeyer O, Jones S, Boyde A, Rommerskirch W, Moritz JD, Schu P, von Figura K (1998): Impaired osteoclastic bone resorption leads to osteopetrosis in cathepsin-K-deficient mice. *Proc Natl Acad Sci U S A* 95:13453-13458.
288. Hollberg K, Hultenby K, Hayman A, Cox T, Andersson G (2002): Osteoclasts from mice deficient in tartrate-resistant acid phosphatase have altered ruffled borders and disturbed intracellular vesicular transport. *Exp Cell Res* 279:227-238.
289. Duggan ME, Duong LT, Fisher JE, Hamill TG, Hoffman WF, Huff JR, Ihle NC, Leu CT, Nagy RM, Perkins JJ, Rodan SB, Wesolowski G, Whitman DB, Zartman AE, Rodan GA, Hartman GD (2000): Nonpeptide alpha(v)beta(3) antagonists. 1. Transformation of

- a potent, integrin-selective alpha(IIb)beta(3) antagonist into a potent alpha(v)beta(3) antagonist. *J Med Chem* 43:3736-3745.
290. Lark MW, Stroup GB, Dodds RA, Kapadia R, Hoffman SJ, Hwang SM, James IE, Lechowska B, Liang X, Rieman DJ, Salyers KL, Ward K, Smith BR, Miller WH, Huffman WF, Gowen M (2001): Antagonism of the osteoclast vitronectin receptor with an orally active nonpeptide inhibitor prevents cancellous bone loss in the ovariectomized rat. *J Bone Miner Res* 16:319-327.
291. Badger AM, Blake S, Kapadia R, Sarkar S, Levin J, Swift BA, Hoffman SJ, Stroup GB, Miller WH, Gowen M, Lark MW (2001): Disease-modifying activity of SB 273005, an orally active, nonpeptide alphavbeta3 (vitronectin receptor) antagonist, in rat adjuvant-induced arthritis. *Arthritis Rheum* 44:128-137.
292. Murphy MG, Cerchio K, Stoch SA, Gottesdiener K, Wu M, Recker R (2005): Effect of L-000845704, an alphaVbeta3 integrin antagonist, on markers of bone turnover and bone mineral density in postmenopausal osteoporotic women. *J Clin Endocrinol Metab* 90:2022-8202.



9. Acknowledgements

I would not have made it so far without the help of a lot of people and I would like to thank those, who made my theses possible:

I thank Prof. Dr. Reinhard Fässler for giving me the opportunity to be part of his outstanding lab and for being the first referee of my thesis. I want to express my sincere gratitude for all the support I got and the great working conditions I was offered during my time in his department.

Most thankful I am to PD Dr. Markus Moser for being my direct supervisor. All your ideas, all of our discussions, your patients and your tolerance were invaluable to me. You were a great teacher.

I want to thank Prof. Dr. Christian Wahl-Schott, who agreed to be the second referee of my thesis and Prof. Dr. Martin Biel, Prof. Dr. Dietmar Martin, PD Dr. Stefan Zahler and Prof. Dr. Karl-Peter Hopfner for being part of my thesis committee and for taking the time to review my work.

I would like to thank all my collaboration partners, namely Dr. Inaam Nakchbandi, Prof. Dr. Markus Sperandio, Dr. Marcus Krüger, Prof. Dr. Richard Hynes, Prof. Dr. Michael W. Hess, Prof. Dr. Kristian Pfaller and Prof. Dr. Dick Heinegard. My special thanks go to Prof. Dr. Pierre Jurdic and his lab at the ENS in Lyon, France, for teaching me how to culture osteoclasts and for excellent discussions and advices.

Thanks to all current and former members of the Fässler lab who shared with me the ups and downs of scientific life. Kathrin, Karin, Raphael, Conni, Michal, Alicja, Vaibhao, Arne, Frank, Anika, Sara, Hao-Ven, Uschi, Christa, Carmen, Armin, Klaus, Dr. Göhring: I will never forget what you have done for me, within and beside the lab. I also want to mention that Jens Päßler, Mia Kleber and their team are the best animal care takers I can think of. Thanks a lot for all your help.

Besides all these people, most thankful I am to my parents and my brother. You never left me alone, especially in the last year of my thesis, when my life got really complicated. Thank you for all the love and support I got and the trust you put in me. Finally, Stephan, I have to thank you, as it was often not easy to handle me in the past six month. You light up my life.



10. Curriculum Vitae

PERSONAL INFORMATION

Name Sarah Marianne Schmidt
Address Hatzfelder Weg 25
81476 München, Germany
Date of Birth 01.03.1983
Place of Birth Lauingen, Germany
Marital status single
Nationality German

EDUCATION AND SCIENTIFIC EXPERIENCE

12/2007 – present **Max Planck Institute of Biochemistry, Martinsried, Germany**
Department of Molecular Medicine, Prof. Dr. Reinhard Fässler
PhD student with PD Dr. Markus Moser

04/2007 – 11/2007 **Max Planck Institute of Biochemistry, Martinsried, Germany**
Department of Molecular Medicine, Prof. Dr. Reinhard Fässler
Diploma thesis with PD Dr. Markus Moser (Functional characterization
of Kindlin-3 in cells of the haematopoietic system)

10/2002 – 11/2007 **Eberhardt-Karls-University, Tübingen**
Diploma studies in biochemistry
Major subjects: biochemistry, virology, pharmaceutical chemistry
Final grade: 1.2, Dipl. biochem.

09/1993 - 06/2002 **Johann-Michael-Sailer-Gymnasium, Dillingen a. d. Donau**
Secondary school
Allgemeine Hochschulreife (general degree for university entrance)
Final grade: 1.1

09/1989 – 08/1993 **Angelina-Egger-Grundschule Dillingen a. d. Donau**
Primary school



11. Supplements

In the following, publications I to III are reprinted. On the enclosed CD the supplementary tables for paper I and the supplementary videos for paper II can be found.

PAPER I

SILAC Mouse for Quantitative Proteomics Uncovers Kindlin-3 as an Essential Factor for Red Blood Cell Function

Marcus Krüger,^{1,3} Markus Moser,^{2,3} Siegfried Ussar,² Ingo Thievensen,² Christian A. Luber,¹ Francesca Forner,¹ Sarah Schmidt,² Sara Zanivan,¹ Reinhard Fässler,^{2,*} and Matthias Mann^{1,*}

¹Department of Proteomics and Signal Transduction

²Department of Molecular Medicine

Max-Planck-Institute for Biochemistry, 82152 Martinsried, Germany

³These authors contributed equally to this work

*Correspondence: faessler@biochem.mpg.de (R.F.), mmann@biochem.mpg.de (M.M.)

DOI 10.1016/j.cell.2008.05.033

SUMMARY

Stable isotope labeling by amino acids in cell culture (SILAC) has become a versatile tool for quantitative, mass spectrometry (MS)-based proteomics. Here, we completely label mice with a diet containing either the natural or the ¹³C₆-substituted version of lysine. Mice were labeled over four generations with the heavy diet, and development, growth, and behavior were not affected. MS analysis of incorporation levels allowed for the determination of incorporation rates of proteins from blood cells and organs. The F2 generation was completely labeled in all organs tested. SILAC analysis from various organs lacking expression of β1 integrin, β-Parvin, or the integrin tail-binding protein Kindlin-3 confirmed their absence and disclosed a structural defect of the red blood cell membrane skeleton in Kindlin-3-deficient erythrocytes. The SILAC-mouse approach is a versatile tool by which to quantitatively compare proteomes from knockout mice and thereby determine protein functions under complex in vivo conditions.

INTRODUCTION

The administration of radioactive or stable isotope tracers to animals is a well established technique by which to investigate the rate of protein synthesis and protein degradation. (Wolfe and Chinkes, 2005). This technology has been used for many decades (Schoenheimer and Rittenberg, 1935). The infusion of stable isotopes (¹³C or ¹⁵N) as tracers combined with measurements of ¹³CO₂ or ¹⁵N in urinary urea or ammonia is a broadly used technique by which to explore the amino acid flux in metabolic pathways (Bier, 1997; Dietz et al., 1982). Extensive incorporation of ¹³C or ¹⁵N stable isotopes does not result in discernable health effects of the treated animals (Doherty and Beynon, 2006; Gregg et al., 1973).

Mass spectrometry (MS) is not inherently quantitative, and relative protein expression changes are instead most accurately measured by comparison of the natural form of a peptide with its stable isotope analog (Ong and Mann, 2005). In recent years, ¹⁵N labeling has been applied to microorganisms such as yeast (Oda et al., 1999; Pratt et al., 2002), *Caenorhabditis elegans*, and *Drosophila* (Krijgsveld et al., 2003). Even a rat has been partially (Wu et al., 2004) or completely ¹⁵N labeled (McClatchy et al., 2007). In addition, nonsaturated labeling of a chicken, by using the essential amino acid valine, allows for the MS-based analysis of protein turnover rates in vivo (Doherty et al., 2005).

Our laboratory has previously described stable isotope labeling by amino acids in cell culture (SILAC) (Mann, 2006; Ong et al., 2002), which has unique advantages for quantitative and functional proteomics because of its inherent accuracy of quantitation and the ease of interpretation of MS results (Blagoev et al., 2004; Kratchmarova et al., 2005). In a SILAC experiment, two cell populations are generated: one in a medium that contains the natural amino acid (i.e., ¹²C₆-lysine), and the other in a medium that contains the heavy isotope-substituted version (i.e., ¹³C₆-lysine). This allows for direct comparison of protein expression levels by mixing the nonlabeled “light” and the labeled “heavy” cell populations (Cox and Mann, 2007). Each peptide appears as a pair in MS analysis with a difference in mass of 6 Da, and the relative peak intensities reflect the abundance ratios. To date, SILAC labeling has been limited to cell culture or microorganisms. To extend this powerful technique to higher organisms, Oda and coworkers have SILAC labeled the Neuro 2A cell line to serve as an internal standard for quantitation of a subset of peptides of the mouse brain proteome (Ishihama et al., 2005).

In the present paper, we report the development of a mouse SILAC diet that leads to complete labeling of the F2 generation. We used in vivo SILAC quantitation to analyze newly synthesized proteins from plasma and tissue samples in vivo. Furthermore, we validated our in vivo quantitation system by comparing the proteomes from platelets, heart, and erythrocytes from β1 integrin-, β-Parvin-, and Kindlin-3-deficient mice, respectively.

Integrins are heterodimeric transmembrane proteins, consist of α and β subunits, are ubiquitously expressed, and perform

cell-cell and cell-matrix adhesion functions. Association of the corresponding α and β subunits is required for their stability and transport to the plasma membrane, as single subunits are not stable and are rapidly degraded. Integrin-mediated cell adhesion triggers intracellular signaling pathways (outside-in signaling) that control migration, proliferation, survival, and differentiation of cells. Prior to ligand binding, integrins require an energy-dependent activation step, which is triggered within the cell (inside-out signaling) and is characterized by a profound conformational change in both integrin subunits. Although the mechanism(s) underlying integrin activation are far from understood, it is believed that the binding of the FERM-domain-containing adaptor proteins talin and Kindlin to the integrin β cytoplasmic domains represents the last step in the activation pathway (Calderwood, 2004; Moser et al., 2008).

Upon activation and ligand binding, integrins recruit and assemble a multiprotein complex at the site of cell adhesion that fulfills two major tasks: it connects the extracellular matrix with the actin cytoskeleton, and it alters the fluxes of many intracellular signaling pathways. A preformed complex consisting of the three proteins, ILK, PINCH, and Parvin, represents an important component of the integrin adhesion complex (Legate et al., 2006). Parvins comprise a family of three proteins, α -, β - and γ -Parvin, that directly bind to ILK, F-actin, and other actin-associated proteins, thereby linking the adhesion complex to the actin cytoskeleton and controlling actin dynamics.

Kindlins have recently been identified within the integrin-mediated cell adhesion complex and represent an additional family of ILK-binding proteins (Montanez et al., 2007). They consist of three members (Kindlin-1–3) and are named after the gene mutated in Kindler syndrome, an autosomal recessive skin blister disease in humans. Kindlin-3 expression is restricted to hematopoietic cells, and the highest levels are in megakaryocytes (Ussar et al., 2006). Inactivation of the Kindlin-3 gene in mice results in severe anemia, which is thought to be due to a bleeding defect caused by impaired activation of platelet integrins, defects in platelet aggregation, and thrombus formation (Moser et al., 2008).

To screen for potential defects in other cellular compartments of the hematopoietic system in Kindlin-3-deficient mice, we compared their proteome with those from control mice. During the course of these studies, we discovered a deficit of structural proteins in the plasma membrane of Kindlin-3-deficient erythrocytes, which contributes to the severe anemia seen in Kindlin-3-deficient mice.

RESULTS

A Heavy SILAC Diet Has No Influence on Weight Gain and Fertility

We prepared a SILAC diet by mixing $^{13}\text{C}_6$ -lysine or $^{12}\text{C}_6$ -lysine into a customized lysine-free mouse diet to a final concentration of 1% (Figure 1A) according to standard mouse nutritional requirements (Benevenga et al., 1995). The amino acid content was subsequently checked by hydrolysis and cation exchange chromatography (Figure S1 available online). We first tested whether the diet permits normal weight gain by feeding mice with a regular diet or the SILAC diet (with $^{12}\text{C}_6$ -lysine or

$^{13}\text{C}_6$ -lysine). During an observation period of 4 weeks, all animals showed the same food consumption and a similar increase in body weight of about 17% (Figures S2A and S2B), normal fertility, and motor activity irrespective of the diet consumed. Furthermore, we SILAC labeled mice over four generations (see below), indicating that the labeling is compatible with normal development and physiology. Thus, we conclude that SILAC labeling with a $^{13}\text{C}_6$ -substituted essential amino acid diet does not lead to obvious discernable health effects in mice (Figure 1B).

SILAC Incorporation Rates Differ in Blood, Liver, and Gut Epithelium

To track $^{13}\text{C}_6$ -lysine incorporation into the proteome over time, we sampled blood each week for 4 weeks. Serum proteins were separated on 1D gels in triplicate, in-gel digested, and analyzed by high-resolution MS. The average relative standard deviation of all quantified proteins was ~20% (Figure 1C), an accuracy similar to what was seen in previous SILAC quantitation experiments (Blagoev et al., 2004; Ong et al., 2003).

As an example of different incorporation levels, SILAC peptide pairs of three serum proteins and one red blood cell protein are shown in Figure 1C. For serum albumin, we observed a SILAC ratio of 1:3.2, indicating that at least 74% of the protein had been newly synthesized during the first week of feeding. Because proteins can be synthesized from dietary amino acids as well as from amino acids derived by protein catabolism, this value is a lower limit for the true turnover (Beynon and Pratt, 2005). After 4 weeks, the three serum proteins were labeled to 90%. In contrast, hemoglobin was only labeled to 57% after 4 weeks (Figure 1C), due to the 60-day half-life of mouse erythrocytes (Berlin et al., 1959). Additional profiles of blood proteins are listed in Table S1.

Next, we measured the labeling efficiencies of a number of organs after 4 weeks of feeding with the SILAC diet. Proteins from heart showed an average protein ratio of 1:4.4 (Figure 2A; Table S2), much lower than the serum proteins. Furthermore, the distribution of SILAC ratios was relatively broad, reflecting the different incorporation rates of individual cell types and the “contamination” of serum proteins in nonperfused samples. For example, serum albumin has a similarly high incorporation rate in blood (ratio 9) and heart (ratio 10) (Figures 1C and 2A). In contrast to heart tissue, in which most cells are quiescent, the intestinal epithelium regenerates within a few days (Radtke and Clevers, 2005). Disaggregating the epithelium from the digestive tube resulted in a more homogeneous cell pool consisting of only a few cell types. As a consequence, we observed a high SILAC ratio of $1:9.1 \pm 2.1$ reflecting a labeling efficiency of more than 90% (Figure 2B), which is fully consistent with the high proliferation rate of this tissue. For example, villin-1, a marker for epithelial cells from the digestive system, showed a SILAC ratio of 1:10.

Liver has a number of different physiological roles, including carrying out metabolic functions and producing major blood proteins. Accordingly, we observed a wide distribution of SILAC-incorporation ratios among liver proteins. Hepatocytes are the predominant liver cell type, and they are very rich in mitochondria. To demonstrate that in vivo SILAC ratios can be measured with subcellular resolution, we isolated mitochondria from liver

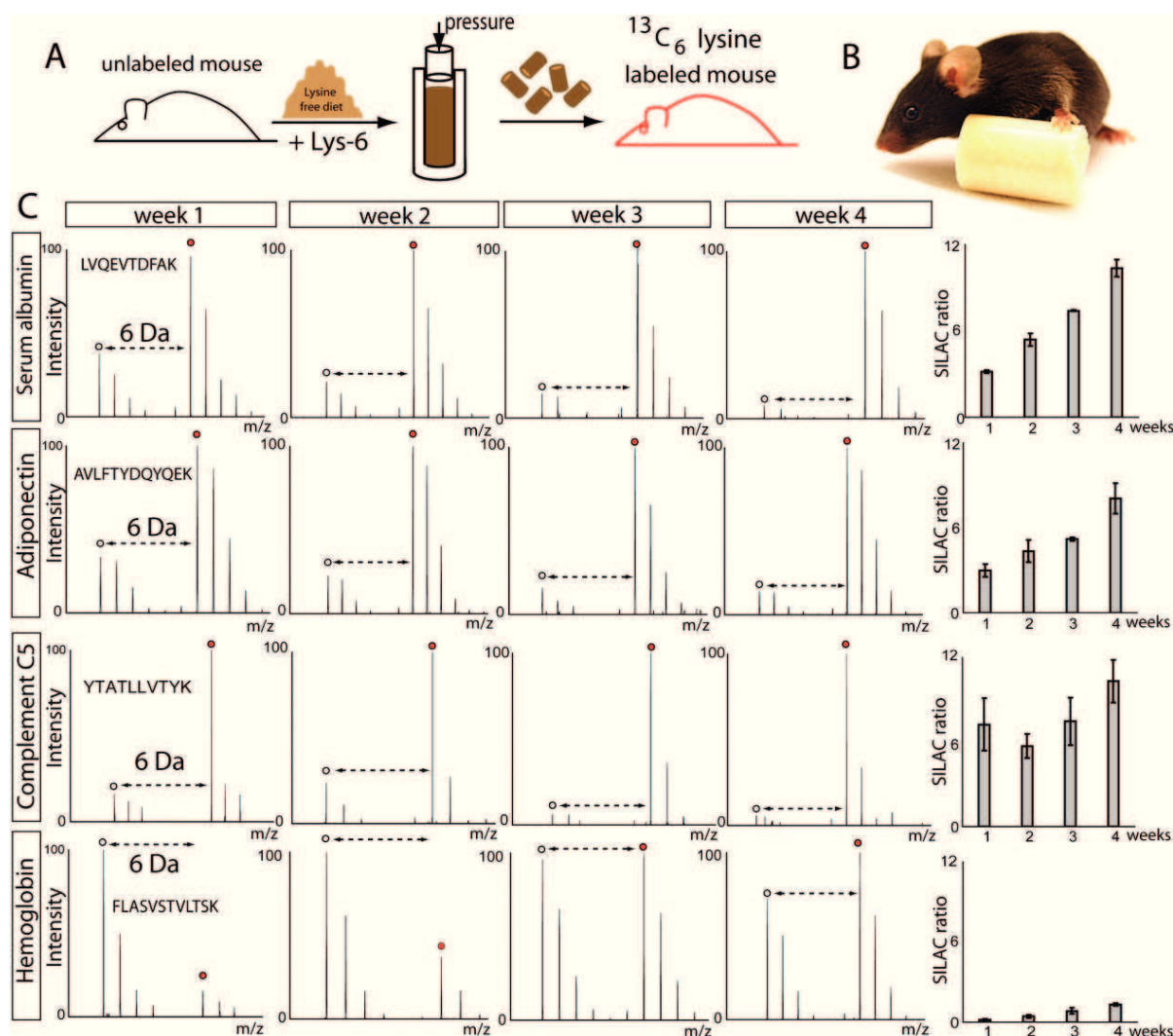


Figure 1. SILAC Labeling and Incorporation Rates of Blood Proteins

(A) Mice are SILAC labeled by being fed a pelleted, lysine-free diet supplemented with normal or heavy lysine.

(B) Mice on a SILAC diet cannot be visually distinguished from mice with a normal, commercial diet.

(C) Mass spectra showing SILAC pairs of a representative peptide for four blood proteins. The right-hand side shows lysine-6 incorporation over the course of 4 weeks as an average measurement of triplicates.

cells (Forner et al., 2006) and compared their labeling ratios to whole-cell lysates from the same sample (Figure 2C, black bars). Interestingly, proteins from mitochondria showed an average SILAC ratio of $1:8.6 \pm 2.4$. This shows that the incorporation rates of an organelle are more narrowly distributed and distinguishable from that of a whole tissue.

We next investigated several cell types of the hematopoietic system. Platelets are cell fragments that are constantly released by megakaryocytes into the blood stream. They have a half-life of ~7–9 days. We isolated platelets from a SILAC mouse after 4 weeks of labeling and measured incorporation levels of 86% from 241 quantified proteins (Figure 2D). In contrast, serum albumin, which was also measured within the platelet sample due to serum contamination, has a much higher incorporation level

compared to platelet proteins. Analysis of the red blood cell proteome revealed a significantly lower $^{13}\text{C}_6$ -lysine incorporation of 75% (Figure 2E). Thus, consideration of SILAC-incorporation rates could aid in the determination of the origin of the same proteins from different cellular pools via their different dynamic incorporation rates.

To combine SILAC-mouse analysis with cell sorting to obtain an accurately defined cell population, we separated CD45R-positive B lymphocytes from spleen by fluorescence-activated cell sorting (FACS) (Figures 2F and S3). An in-solution protein digest was performed from lysates of 1×10^6 spleen cells (Table S2F). The distribution of measured ratios was $1:5.4 \pm 1.3$, demonstrating that FACS-sorted populations of interest can readily be investigated in the SILAC mouse.

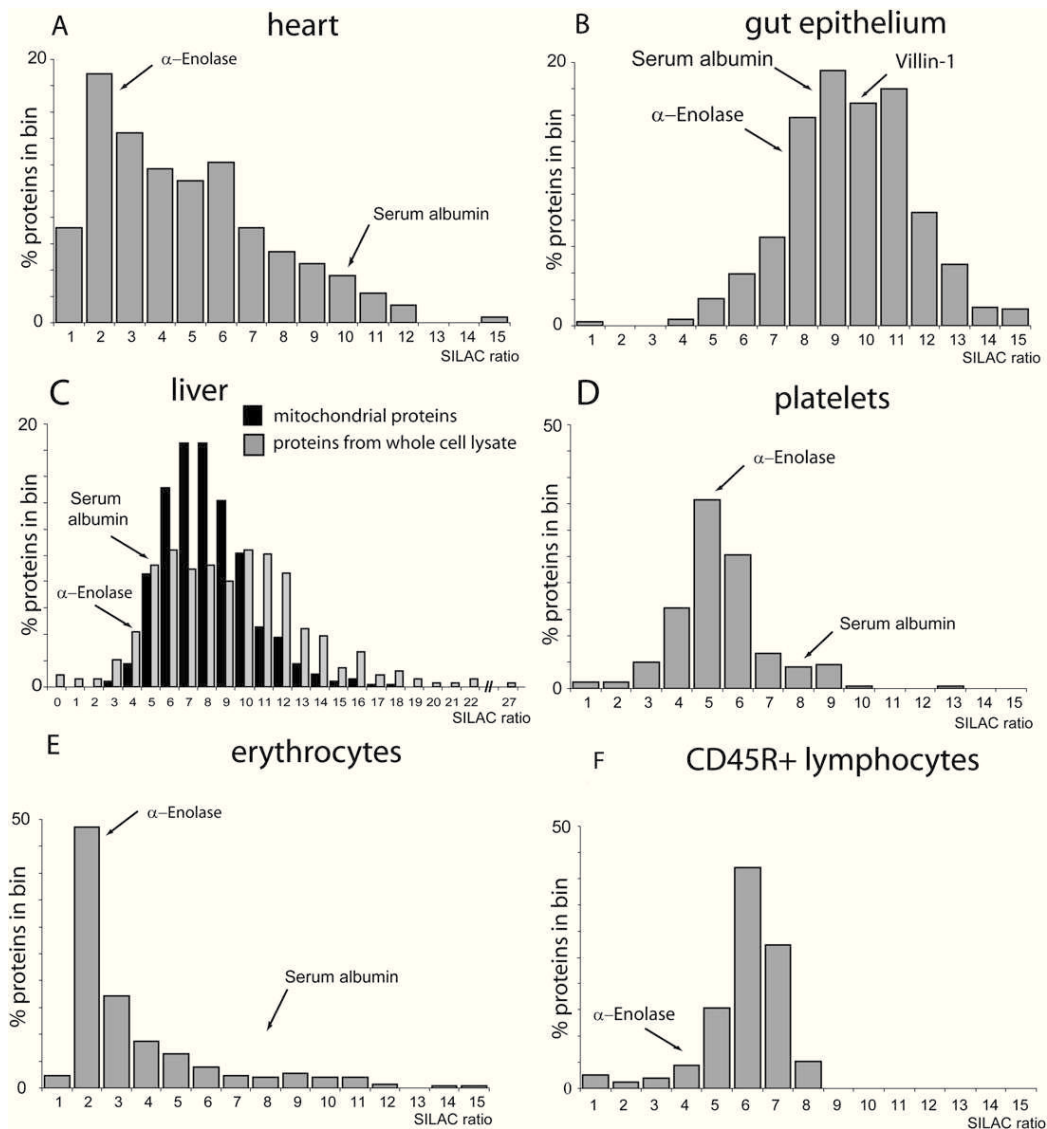


Figure 2. SILAC Label Incorporation into Different Cell Types and Tissues after 4 Weeks

(A–F) The panels show the relative number of proteins with the specified ratios for each proteome investigated. (A) Heart tissue. (B) Gut epithelium. (C) Incorporation into whole liver (gray bars) is compared with incorporation into liver mitochondria (black bars). (D) Platelets. (E) Erythrocytes. (F) CD45R-positive B lymphocytes from spleen.

Taken together, our results indicate that feeding mice with a SILAC diet is a suitable approach to label proteins *in vivo* and to follow their metabolic incorporation in any organ.

Complete SILAC-Based Labeling of F2 Mice

Although the label efficiency was relatively high in many tissues, we found that extending the labeling time did not lead to complete labeling. This is likely due to the recycling of internal amino acid sources (Doherty et al., 2005). Since labeling rates above 95% are required to perform comparative and quantitative proteomics by MS, we started feeding our mice over several generations with the heavy diet. Importantly, the consumption of the heavy diet did not affect litter size (Figure S2). The F1–F4 off-

spring developed normally, gained weight within the normal weight-gain chart (Figure S2), and showed normal mating behavior. Furthermore, newborn animals of the F1 generation were almost completely labeled, reaching ~93% in blood, brain, and liver (Figures 3 and S4). To obtain fully labeled animals to serve as internal standards and to investigate if SILAC labeling could be performed for many generations, we bred F2, F3, and F4 mice. These mice contained virtually no unlabeled peptides (Figures 3B, 3C, and 5A; Table S3).

Proteome of β 1 Integrin-Deficient Platelets

For validation of our *in vivo* quantitative proteomics approach, we analyzed and compared protein lysates from β 1 integrin-deficient

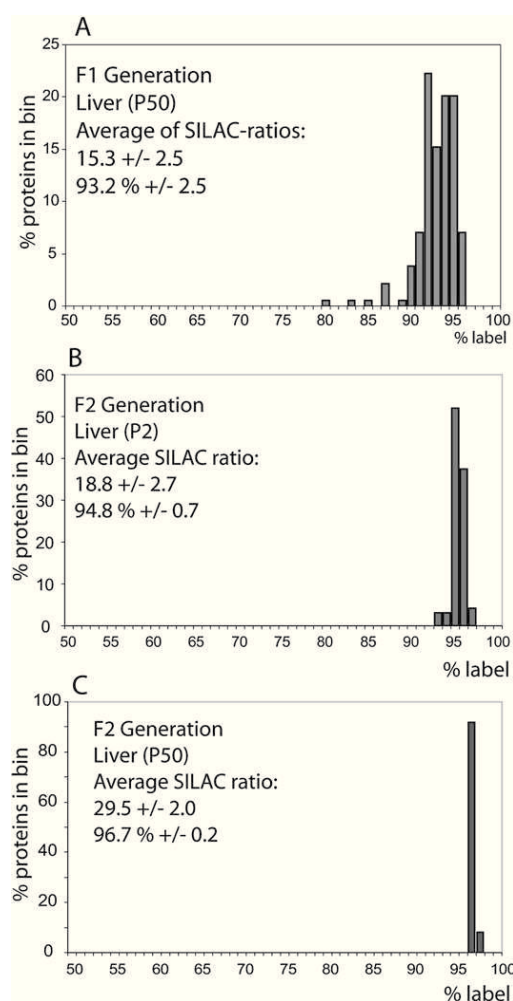


Figure 3. Complete Labeling of the F2 Generation

(A) Label efficiency of the liver of a 2-day-old mouse of the F1 generation. (B and C) Histograms of liver proteins with the specified percent incorporation at (B) P2 and at (C) P50 of the F2 generation. The averages of the SILAC ratios and the corresponding percent of the SILAC labeling are displayed in the histogram. The analysis encompasses ~100 proteins.

and control platelets (Nieswandt et al., 2001). We generated $\beta 1$ integrin-deficient platelets by intercrossing $\beta 1$ floxed mice ($\beta 1^{fl/fl}$) with a transgenic mouse expressing an Mx1 promoter-driven, interferon-inducible Cre (Mx1-Cre) (Brakebusch et al., 2000; Kuhn et al., 1995). We treated $\beta 1^{fl/fl}$; Mx1-Cre mice with synthetic double-stranded RNA (polyinosinic-polycytidylic acid, pl-pC), which triggers endogenous interferon production and subsequent Mx1-Cre activity. This leads to deletion of the $\beta 1$ integrin gene in all hematopoietic cells, including megakaryocytes. To monitor the knockout efficiency of $\beta 1$ integrin, we compared platelets from labeled wild-type animals with platelet populations from three groups of mice: (1) nonlabeled wild-type platelets; (2) platelets from nonlabeled, non-pl-pC-induced $\beta 1^{fl/fl}$; Mx1-Cre mice; and (3) platelets from nonlabeled, pl-pC-induced $\beta 1^{fl/fl}$; Mx1-Cre mice (Figure 4). All mice were backcrossed on a C57BL/6 background to reduce genetic variability.

We quantified ~645 proteins in these platelets, and, as expected, protein ratios of labeled and nonlabeled wild-type platelets were tightly distributed, with an overall ratio of 1:1. The quantitative MS analysis revealed complete loss of $\beta 1$ integrin in platelets from pl-pC-induced $\beta 1^{fl/fl}$; Mx1-Cre mice (Figure 4F). The proteins with the next highest ratios were the dimerization partners of the $\beta 1$ integrin subunit, strikingly confirming the sensitivity and reliability of our SILAC-mouse labeling system (Figure 4I). In a boxplot analysis, $\beta 1$, $\alpha 2$, and $\alpha 6$ integrins were all more than ten interquartile ranges away from the median (Figure S5A; Table S4). The complete loss of both α subunits can be explained by the formation of a stable integrin heterodimer during the synthesis and transport of the complexed integrin subunits to the plasma membrane. Without the correct β integrin subunit, the α subunit is rapidly degraded (Hynes, 2002). In contrast, the loss of $\beta 1$ integrin has no impact on the expression of other integrins, such as the major platelet integrin $\alpha IIb\beta 3$.

In addition, several other proteins in $\beta 1$ integrin-deficient platelets were outliers in the boxplot (Figure S5A; Table S4). However, a second independent experiment did not verify these proteins as being significantly downregulated. (Figure S5C). In contrast, the $\beta 1$ integrin dimerization partners $\alpha 2$ and $\alpha 6$ integrins were again strongly reduced (Figure S5).

Interestingly, the analysis of platelets from noninduced $\beta 1^{fl/fl}$; Mx1-Cre mice also revealed a slight downregulation of the $\beta 1$, $\alpha 2$, and $\alpha 6$ integrin levels compared to labeled wild-type platelets (Figure 4J). This effect is due to the natural, endogenous α/β interferon production in the bone marrow causing a low Mx1 promoter activity (Kuhn et al., 1995). The detection of this “leak” impressively underscores the sensitivity of our quantitative proteomics approach.

β -Parvin Deficiency in Heart Is Compensated by α -Parvin Induction

We next wanted to confirm the applicability of our *in vivo* SILAC approach to analyze the proteomes from knockout mice in a solid organ. To this end, we compared the proteomes from hearts of β -Parvin-deficient mice with those of control littermates. As a heavy standard, we used heart lysates from 2-week-old mice of the F4 generation, which showed an overall 97.7% incorporation of ^{13}C -lysine (Figure 5A). To test our quantitation system, we mixed “heavy” and “light” protein lysates from wild-type hearts in ratios of 1:1, 1:2, and 1:4. As shown in (Figure 5B), mixing of protein lysates from different heart samples gave rise to SILAC ratios that accurately reflected the lysate mixture.

β -Parvin represents the dominant Parvin isoform of the heart, since α -Parvin is only weakly present and γ -Parvin is absent from heart tissue. β -Parvin-deficient mice were generated by homologous recombination of a targeting vector in embryonic stem (ES) cells, which lacks exons 2 and 3 of the β -Parvin gene (I.T. and R.F., unpublished data). β -Parvin-deficient mice were viable and fertile and did not show any overt phenotype, indicating that β -Parvin is not essential for mouse development and organ formation. Mass spectrometric measurements of whole protein lysates from β -Parvin-deficient and control hearts of 2-week-old animals showed a complete absence of β -Parvin in knockout animals (Figures 5C and 5D). Out of 1205 proteins, only 4 proteins showed a two-fold decrease in their abundance compared to

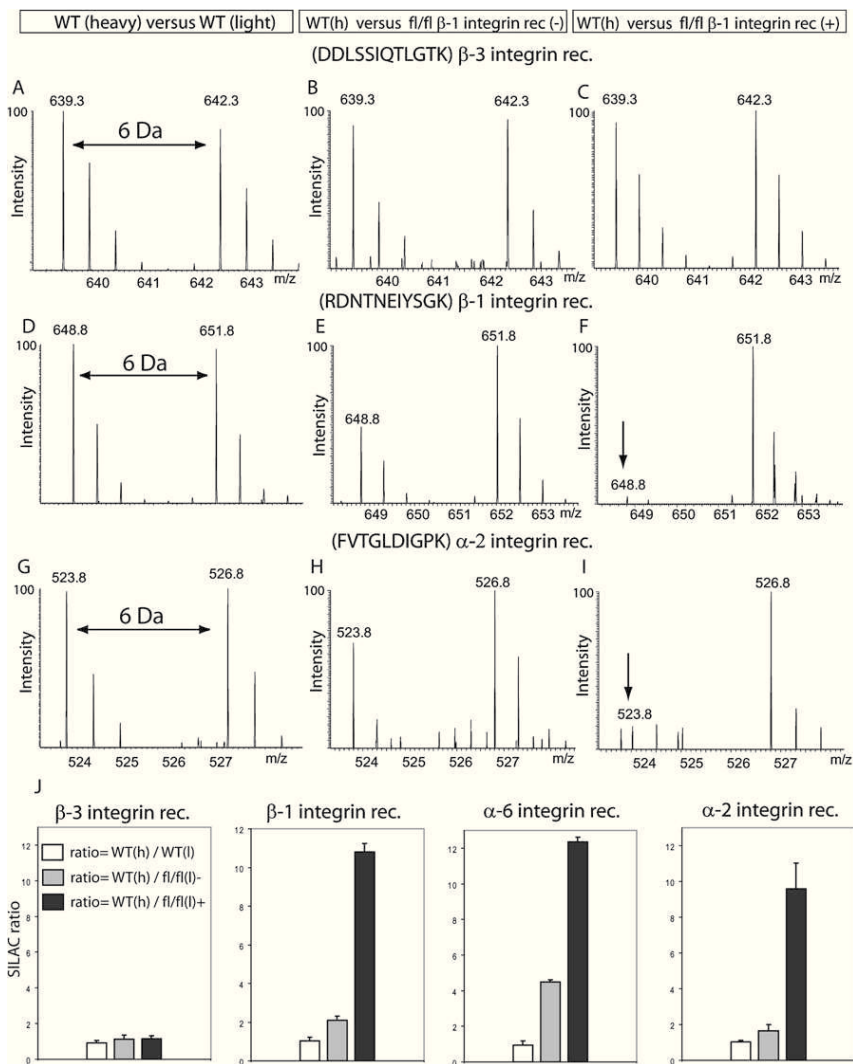


Figure 4. Analysis of $\beta 1$ Integrin Knockout Platelets

(A–J) (A, D, and G) Platelets from SILAC-labeled wild-type mice were mixed with platelets from a nonlabeled wild-type control mouse. Comparison of the wild-type SILAC mouse with (B, E, and H) noninduced $\beta 1^{fl/fl}$; Mx1-Cre mice and with (C, F, and I) pl-pC-induced $\beta 1^{fl/fl}$; Mx1-Cre mice. The slight decrease of $\beta 1$ integrin shown in (E) is due to Cre activity induced by low endogenous interferon expression. The arrows in (F) and (I) label the reduced peak intensity of $\beta 1$ and $\alpha 2$ integrin, respectively. (J) Summary of quantified SILAC ratios for $\beta 3$, $\beta 1$, $\alpha 2$, and $\alpha 6$ integrin subunits. White bars represent the ratio between the labeled wild-type WT(h) animal and the nonlabeled wild-type animal, gray bars represent the SILAC ratio of WT(h) and noninduced $\beta 1^{fl/fl}$, and black bars represent the SILAC ratio between WT(h) and induced $\beta 1^{fl/fl}$; Mx1-Cre. The error bars show the variability of the measured ratios.

paired integrin trafficking in the absence of Kindlin-3 (Figure S6B).

We have previously reported that Kindlin-3 (also known as “unc-related protein 2”) is present in red blood cells (Pasini et al., 2006). This was confirmed by different SILAC-incorporation levels in platelets (incorporation rate of 1:6.0) compared to erythrocytes (incorporation rate of 1:2.1), measured after the initial 4-week labeling period (Figures 2, S7A, and S7B). Furthermore, Kindlin-3 gene activity in Ter119-positive Kindlin-3-heterozygous erythroblasts was further corroborated by measuring Kindlin-3 promoter-driven β -galactosidase reporter gene activity with FACS (Figure S7C).

wild-type hearts (Table S5). Interestingly, lack of β -Parvin had no dramatic consequence on the level of ILK and PINCH-1, which are the two other components of the ILK/Pinch/Parvin complex. The two-fold increase of α -Parvin in β -Parvin-deficient hearts suggests that the absence of an obvious phenotype is due to compensatory upregulation of α -Parvin (Figure 5C).

Kindlin-3 Deficiency Disrupts the Red Blood Cell Membrane Skeleton

Kindlin-3-deficient mice die at birth and suffer from severe bleeding, anemia, and pale skin color (Figures 7A and 7B; Moser et al., 2008). To further validate the power of in vivo SILAC and to obtain novel insights into Kindlin-3 function, we performed quantitative proteomics of platelets and erythrocytes from Kindlin-3^{-/-} mice. Platelet analysis identified Kindlin-3 as the protein with the highest fold change of more than 1200 platelet proteins (Figure S6A; Table S6). Interestingly, the levels of integrin α IIb and $\beta 3$ subunits were normal, suggesting that the reduced surface levels found by FACS (Moser et al., 2008) were due to an im-

To investigate whether loss of Kindlin-3 affects erythroid cells, we determined and quantitatively compared the proteomes from wild-type, Kindlin-3^{+/-}, and Kindlin-3^{-/-} erythrocytes (Figure 6; Table S7). MS confirmed a 50% reduction of Kindlin-3 in heterozygous and a complete absence of Kindlin-3 in Kindlin-3^{-/-} erythrocytes (Figure 6A). Out of 881 proteins identified in all 3 proteomes, more than 50 were two-fold increased in Kindlin-3^{-/-} erythrocytes, and only a few revealed a more than two-fold reduction. Interestingly, a large proportion of the upregulated proteins was annotated to be nuclear (Table S7).

Blood smears from Kindlin-3^{-/-} embryos and P3 animals showed a strong reduction of cells when compared to wild-type controls and, in concordance with this proteomic finding, many more nucleated erythroblasts (Figures 7B and 7C). In addition, the size and shape of Kindlin-3^{-/-} erythrocytes were markedly irregular.

Scanning electron microscopy showed abnormally shaped erythrocytes with striking membrane invaginations and protuberances (Figure 7D). Red blood cell membrane abnormalities

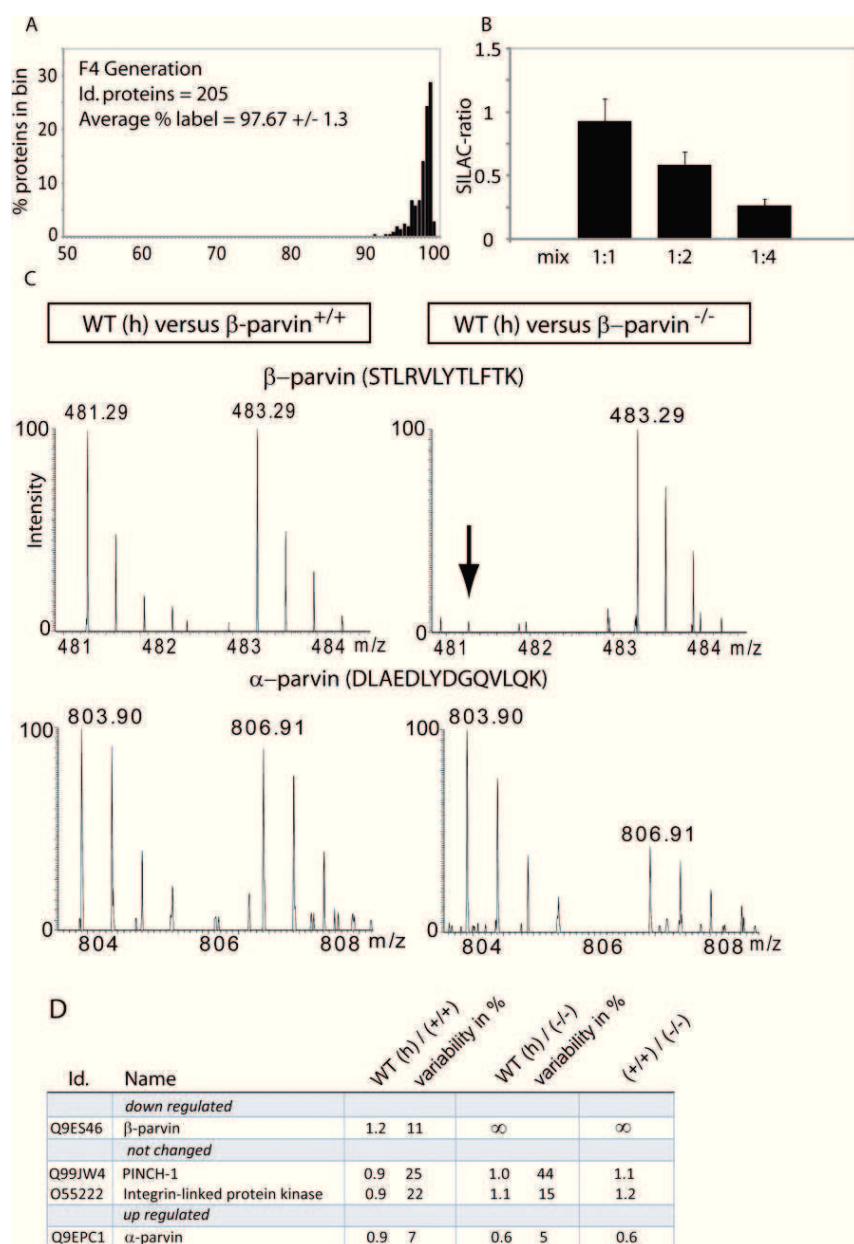


Figure 5. Analysis of Heart Tissue from β -Parvin Knockout Mice

(A) $^{13}\text{C}_6$ -Lysine incorporation of heart tissue from mice of the F4 generation shows a label efficiency of 97.7%.

(B) Heart tissue from labeled and nonlabeled animals was mixed 1:1, 1:2, and 1:4. The measured SILAC ratios after in-solution digestion were 0.93 ± 0.17 for the 1:1 mix, 0.58 ± 0.10 for the 1:2 mix, and 0.26 ± 0.05 for the 1:4 mix. Approximately 300 SILAC protein ratios were used for the quantification.

(C) Heart tissue from SILAC-labeled wild-type mice was mixed with nonlabeled β -Parvin (+/+) and β -Parvin (-/-) hearts. The arrow indicates the complete absence of β -Parvin.

(D) SILAC ratios of selected proteins.

and Kindlin-3^{-/-} mice and compared them to ghosts from SILAC-labeled control animals (Figure 7E). Quantitative SILAC-based analysis revealed an almost complete absence of ankyrin-1, band 4.1, adducin-2, and dematin (Figure 7F, right rows; Table S8), whereas other membrane-skeleton proteins, like α/β spectrin and band 3, were not changed.

Together, these findings show that Kindlin-3 is required for the assembly of a subset of proteins within the red blood cell membrane skeleton. Furthermore, the proteomic, morphological, and functional data provide a clear explanation for the anemia that leads to postnatal lethality.

DISCUSSION

Thus far, quantitative gene expression comparisons in higher organisms have been restricted to RNA analyses by gene chip approaches. These methods have many advantages: for example, ready accessibility and the fact that, in principle, almost all genes can be analyzed on one

chip. However, because of posttranscriptional regulation as well as regulated protein degradation, these data do not necessarily predict changes in protein levels within cells or tissues. Furthermore, there are specific cell populations, such as the platelets and erythrocytes investigated here, that are devoid of mRNA and are therefore out of reach for these techniques.

Here, we show that SILAC, a versatile and successful method for quantitative proteomics in cell culture-based systems or microorganisms, can be extended to mammalian model systems. Mice can be SILAC labeled without any obvious effect on growth, behavior, or fertility. SILAC food preparation is straightforward and not particularly expensive when considering other resources required for the generation and maintenance of

are often caused by mutations within membrane-skeleton proteins, and the absence of key components can have drastic consequences on the stability of the red cell membrane (Delaunay, 1995). To obtain an explanation for the structural defects, we quantitatively compared the membrane-skeleton proteins from total erythrocytes by using SILAC-based MS. The levels of the most prominent skeleton proteins (e.g., α/β spectrin, ankyrin, band 3, band 4.1, band 4.2, and actin) did not significantly differ between wild-type and Kindlin-3^{-/-} mice.

Next, we determined whether these proteins have formed a stable meshwork that is connected with the erythrocyte membrane. To address this question, we isolated the erythrocyte membranes (so called red blood cell "ghosts") from wild-type

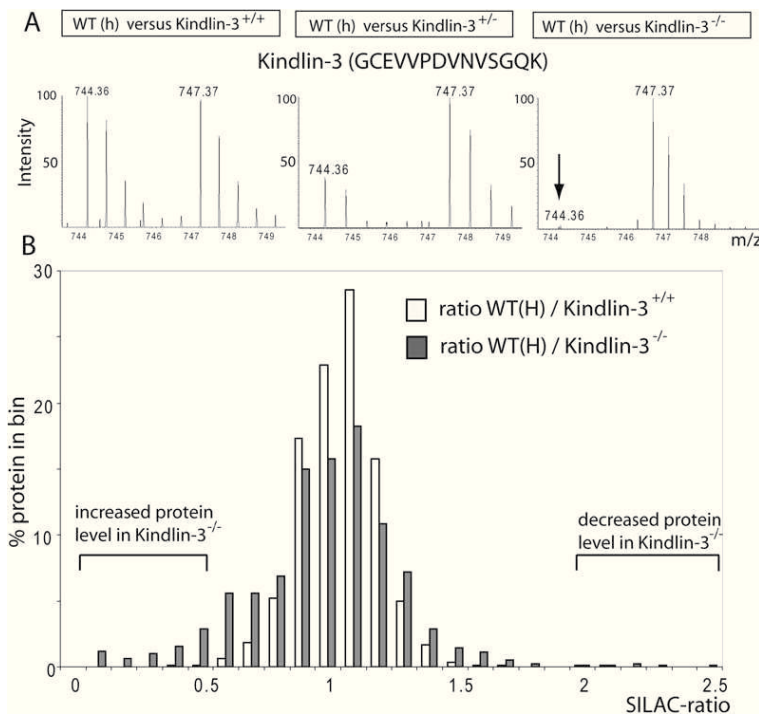


Figure 6. Quantitative Proteomics of Erythrocytes from Kindlin-3^{-/-} Mice

(A) Mass spectra of a Kindlin-3 peptide SILAC pair in Kindlin-3^{+/+}, Kindlin-3^{+/-}, and Kindlin-3^{-/-} erythrocytes.

(B) Histogram of SILAC ratios of wild-type (white bars) and Kindlin-3^{-/-} (gray bars) erythrocytes. The measured ratios were grouped into ratio bins, and the y axis shows the relative number of detected ratios per bin.

knockout animals. We chose ¹³C₆-lysine labeling, as lysine is not converted into other amino acids. This makes endoprotease Lys-C the preferred choice as the proteolytic enzyme. Another interesting enzyme for SILAC mice is Lys-N, which has recently been described as an efficient enzyme for proteomics and de novo peptide sequencing (Taouatas et al., 2008). Organs derived from SILAC mice can serve as standards for a large number of subsequent experiments, in which wild-type and knockout mice are compared. Importantly, cell types such as intestinal epithelium that are difficult to study ex vivo can be analyzed by the in vivo SILAC approach. Moreover, the SILAC mouse can serve as a reference model at any biological scale, from the whole organ through specific cell types down to intracellular compartments or single proteins of interest. As an example, we used SILAC mice to successfully study the mitochondrial proteome, which can be extended to investigations in relevant organs from metabolic or neurodegenerative disease models. In studies in which a large number of mice are required—such as in toxicology studies—labeled organ tissue could be stored and used as an internal standard for each measurement. A labeled SILAC-mouse liver, for example, yields sufficient internal standard for more than 1000 measurements. Although not shown here, phosphopeptides can also be enriched from SILAC mice and can serve as a standard for functional and time-resolved phosphoproteomics (Olsen et al., 2006).

We analyzed the proteomes of cells from three independent knockout mice. In all analyses, the complete absence of the targeted genes was immediately revealed by the SILAC technique. Furthermore, heterozygous Kindlin-3 animals present the expected two-fold reduction from wild-type levels, emphasizing the quantitative nature of our proteomic technology. This may be particularly useful in quantifying knockdown efficiencies in

transgenic RNAi mice. The sensitivity of the SILAC-based quantitation system became remarkably obvious by an observation from the β 1 integrin inactivation in platelets. Deletion of the β 1 integrin gene in hematopoietic cells is achieved by the induction of the Mx1-Cre transgene through the injection of pl-pC into β 1 integrin floxed animals. Even without induction of Cre, the low expression levels of naturally expressed α/β interferon activated the Mx1 promoter and triggered β 1 integrin deletion in a few cells. Even this slight difference in total β 1 integrin expression proved sufficient for detection by the SILAC method.

Our proteomic data on platelets of β 1 integrin mice showed that, although integrins control a number of different signaling pathways, the lack of the

β 1 integrin has no consequences on the levels of other proteins in platelets, apart from its dimerization partners α 2 and α 6 integrins. This may be due to the fact that, in resting platelets, integrins are inactive and signaling into the cell is only induced upon stimulation via molecules like thrombin or collagen (Ruggeri, 2002). Further studies with the SILAC-mouse system could focus on activation of signaling cascades during platelet aggregation by using phosphoproteomics.

To test the SILAC-based analysis in a solid organ system, we compared the proteomes from heart of β -Parvin-deficient mice with control littermates. The complexity of a tissue, formed by different cell types, poses no limitation for the quantitative analysis by MS. The interpretation of results, however, is more challenging because changes in protein levels may result from non-cell-autonomous defects caused, for example, by altered cell-cell communication rather than cell-autonomous defects.

To study the molecular cause of the anemia observed in Kindlin-3 mutants, we analyzed the consequences of this deletion on the proteome of platelets and erythrocytes. Recently, we characterized Kindlin-3 as an essential factor for the activation of platelet integrins (Moser et al., 2008). Kindlin-3 directly binds to the cytoplasmic tails of both β 1 and β 3 integrin subunits. Its expression is restricted to cells of the hematopoietic system (Ussar et al., 2006). Our SILAC-based analysis of Kindlin-3-deficient erythrocytes revealed an increased amount of nuclear proteins, prompting us to investigate consequences of the knockout on this cell type. Consistent with the proteomic results, we found an increased number of nucleated erythroblasts in blood smears. Furthermore, Kindlin-3-deficient erythrocytes are irregular in size and shape. The structural defects of the red blood cell membrane skeleton suggested an additional function of Kindlin-3. With the help of the SILAC method, we quantitatively

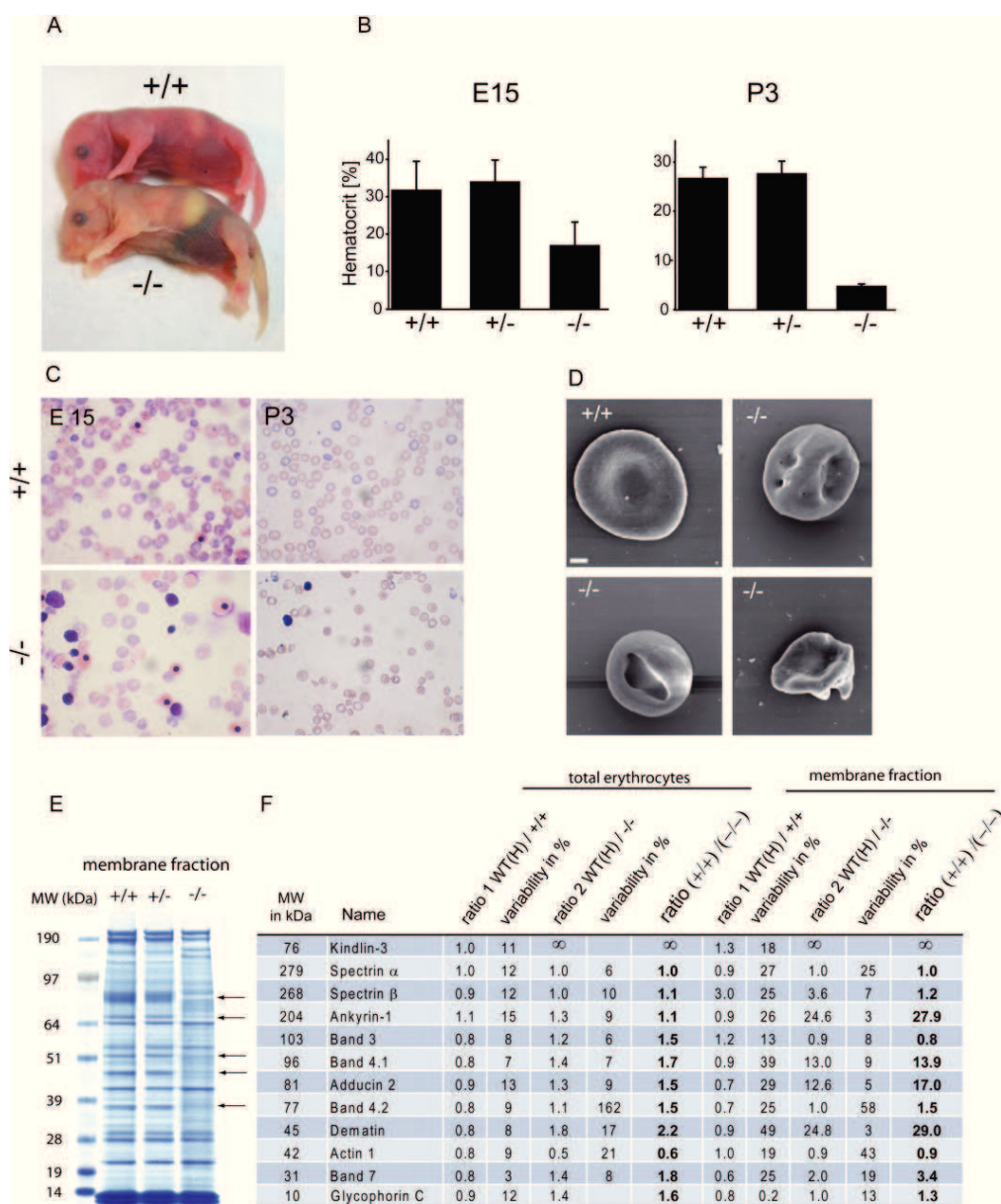


Figure 7. Kindlin-3-Deficient Erythrocytes Show Disrupted Membrane Skeletons

(A) Kindlin-3 knockout mice are anemic.

(B) Decreased hematocrit in Kindlin-3^{-/-} mutants at embryonic day 15 and P3.

(C) Blood smears from E15 embryos and P3 wild-type and Kindlin-3^{-/-} mice reveal fewer erythrocytes and an increased number of nucleated erythroblasts.

(D) Scanning electron microscopy of wild-type and Kindlin-3^{-/-} erythrocytes. The scale bar represents 1 μ m.

(E) "Ghost" lysates from wild-type, heterozygous, and Kindlin-3^{-/-} mice were stained by Coomassie blue after SDS-PAGE. The arrows indicate the absence of proteins within the membrane-skeleton fraction of Kindlin-3^{-/-} erythrocytes.

(F) SILAC-ratio comparison of total erythrocytes (left rows) and the membrane fraction (right row).

compared the membrane-skeleton proteins of control and Kindlin-3-deficient erythrocytes and revealed a critical role of Kindlin-3 in the formation or stabilization of this structure. The inner surface of the red blood cell membrane is laminated by a protein network that is linked to transmembrane proteins. In humans and mice, mutations in genes encoding ankyrin, band 3, spec-

trin, and protein 4.1 or protein 4.2 cause hereditary spherocytosis or poikilocytosis, often accompanied with hemolytic anemias (Delaunay, 1995; Peters et al., 1998; Rybicki et al., 1995; Shi et al., 1999; Southgate et al., 1996). The dramatic reduction of ankyrin-1, protein 4.1, and dematin in membrane preparations from Kindlin-3-deficient erythrocytes explains the severe

malformations. Thus, loss of Kindlin-3 affects erythropoiesis by disrupting the assembly of structural components within the red blood cell membrane skeleton.

In summary, a direct combination of the SILAC technology for quantitative proteomics with the large number of powerful mouse models generated by the community is now possible. We have demonstrated here how proteomics can be combined with several of the powerful technologies already used in this endeavor. We are confident that this technology will help to elucidate disease processes and guide novel intervention strategies.

Data Availability

Data used for quantitation accompany this article online.

EXPERIMENTAL PROCEDURES

Materials and Reagents

$^{13}\text{C}_6$ -Lysine (98 atom % ^{13}C) was purchased from Silantes, Martinsried, Germany. Chemicals for the “in-solution” and “in-gel” digests were purchased from Sigma-Aldrich, and LysC was obtained from WAKO. Wild-type mice were obtained from an in-house C57Bl/6 colony.

Knockout Mice

Transgenic mice expressing the Cre recombinase under the control of the Mx1 promoter (Kuhn et al., 1995) were mated with mice carrying a floxed $\beta 1$ integrin gene (Brakebusch et al., 2000). To ensure extensive downregulation of the $\beta 1$ integrin on platelets, pl-pC (250 μg per mouse) (Amersham) was injected intraperitoneally three times in a 2-day interval.

Kindlin-3-deficient mice were generated as described by Moser et al. (2008). A detailed description of the β -Parvin gene inactivation will be published elsewhere (I.T. and R.F., unpublished data).

Food Preparation, Weight Gain, and Food Consumption

A customized lysine-free mouse diet (Harlan-Teklad, TD.99386) was combined with the heavy $^{13}\text{C}_6$ -lysine and the natural isotope L-lysine (Sigma) to a final concentration of 1%. To obtain a homogenous distribution of the amino acid, the powder was vigorously mixed with a blender for 5 min. For the preparation of food pellets, ~ 10 g of the mixture was filled into an in-house-manufactured cylinder with an inner diameter of 1.5 cm and a length of 10 cm. Food was compressed with an exactly fitting pestle for 1 min. Pellets were taken out and dried overnight at room temperature. After drying, the pellets were cut into smaller pieces.

The lysine content was checked as described (Moore et al., 1958). Although the hydrolysis with subsequent chromatography does not allow for the exact determination of the amino acid contents, the supplemented lysine amount was comparable to that in the customized diet containing the natural lysine isotope.

For testing weight gain and food consumption, one group ($n = 3$ females) was fed with a regular mouse diet, one group ($n = 3$ females) was fed with the customized lysine-free diet supplemented with natural lysine (Sigma), and one animal was fed with the diet containing the heavy isotope for lysine. All animals were fed ad libitum and had access to water.

Food consumption was measured daily for 10 days during breeding and weaning periods (Figure S2). The label percentage was calculated as the mean of the heavy-labeled peptide signal divided by the sum of the light and heavy signals.

Sample Preparation

Blood Samples

Mice were anesthetized with isofluran, and 20 μl blood was taken from the retro-orbital plexus. Blood samples were incubated with heparin (20 U/ml), and, after centrifugation, the supernatant was frozen in liquid nitrogen and stored at -80°C .

Tissue Harvest

After sacrificing animals by cervical dislocation, tissues were dissected, washed in phosphate-buffered saline (PBS [pH 7.4]), and frozen in liquid nitrogen. For protein isolation, tissues were homogenized in a buffer containing 1% NP-40, 0.1% sodium deoxycholate, 150 mM NaCl, 1 mM EDTA, 50 mM Tris (pH 7.5), and protease inhibitors (Complete tablets, Roche). The lysates were centrifuged at $14,000 \times g$ to pellet cellular debris. A Bradford assay was performed to determine protein concentrations of the supernatants.

Mitochondria Isolation

Liver tissue was quickly washed in water, then washed three times in 250 mM sucrose, 10 mM Tris-HCl, 0.1 mM EGTA (pH 7.4) supplemented with protease inhibitors (Roche). Crude mitochondria were isolated as described previously (Forner et al., 2006) and were purified on a 30% Percoll density centrifugation gradient.

Platelets were isolated by differential centrifugation steps as described by Moebius et al. (2005).

Epithelial Cell Isolation from Gut

Small intestine was cut open and washed with PBS. The small intestine was transferred to dissociation buffer (130 mM NaCl, 10 mM EDTA, 10 mM HEPES [pH 7.4], 10% FCS, and 1 mM DTT) and was incubated for 45 min on a rotor at 37°C . The rest of the intestine was removed, and the epithelial clumps were collected by centrifugation at 800 rpm for 5 min and washed in PBS.

B Cell Isolation

For B cell isolation, spleen was cut into small fragments and digested with collagenase and DNase, followed by the addition of EDTA. Subsequently, cells were incubated with anti-CD45R, anti-CD3, and anti-CD49b (BD PharMingen). B cells were selected as cells that stained positive for CD45R (B220) (Coffman, 1982) and negative for both anti-CD3 and anti-CD49b and were then sorted by using a FACS Aria system (Becton Dickinson).

Mass Spectrometry

For protein separation, samples were loaded on a NuPAGE 4%–12% Bis-Tris gel (Invitrogen). After staining of the gel with the Colloidal Blue Staining Kit (Invitrogen), evenly sized gel pieces were excised from the gel and processed for enhanced liquid chromatography-mass spectrometry (GeLC-MS).

For blood analysis, Coomassie-stained gel lanes were cut into eight pieces. To determine incorporation ratios, we analyzed three gel pieces per lane from heart, gut epithelia, liver, red blood cell, and platelet samples.

The gel pieces were subjected to in-gel reduction and alkylation, followed by LysC digestion as previously described (Andersen et al., 2005; Shevchenko et al., 1996). Finally, peptides were extracted twice by adding an equal volume of 30% acetonitrile/0.3% trifluoroacetic acid (TFA) in water to digest the mixture, followed by a final extraction with 100% acetonitrile. Extracts were evaporated in a speedvac to remove acetonitrile and were subsequently acidified with 0.5% TFA. Samples were desalted and concentrated with StageTips and were resuspended in 5 μl of 0.5% acetic acid/1% TFA (Rappsilber et al., 2003). In-solution digestion of proteins was performed as described by Ong and Mann (2006).

Reverse-phase nano-LC-MS/MS was performed by using an Agilent 1100/1200 nanoflow LC system (Agilent Technologies) with a cooled, thermostated 96-well autosampler. The LC system was coupled to a 7-Tesla LTQ-FT or LTQ Orbitrap instrument (Thermo Fisher Scientific) equipped with a nano-electrospray source (Proxeon). Chromatographic separation of peptides was performed in a 10 cm long 8 μm tip opening/75 μm inner diameter capillary needle (Proxeon). The column was custom made with methanol slurry of reverse-phase ReproSil-Pur C18-AQ 3 μm resin (Dr. Maisch, GmbH). The LysC-digested peptide mixtures were autosampled at a flow rate of 0.5 $\mu\text{l}/\text{min}$ and then eluted with a linear gradient at a flow rate of 0.25 $\mu\text{l}/\text{min}$. The mass spectrometers were operated in the data-dependent mode to automatically measure MS and MS/MS. LTQ-FT full scan MS spectra (from m/z 300 to m/z 1600) were acquired with a resolution of $R = 100,000$ at m/z 400 (after accumulation to a target value of 3,000,000 in the linear ion trap). The five most intense ions were sequentially isolated and fragmented in the linear ion trap by using collisionally induced dissociation at a target value of 10,000 (Olsen et al., 2004).

Raw data files were converted to Mascot generic format files with in-house software (Raw2MSM), and Mascot (version 2.0) was used for a database search and protein identification. The following search

parameters were used in all MASCOT searches: LysC digest; no missed cleavage; carbamidomethylation of cysteine set as a fixed modification; and oxidation of methionines and L-lysine-6 allowed as variable modifications. The maximum allowed mass deviation for MS and MS/MS scans was 10 ppm and 0.5 Da, respectively. Only proteins that had at least two peptides with ion scores >20 were considered for identification and quantitation. MSQuant (Schulze and Mann, 2004) was used to verify and quantify the resulting SILAC-peptide pairs. All proteomic results were deposited in the publicly accessible MAPU database (Zhang et al., 2007). A target decoy database approach was used to identify false-positive peptides and to set threshold criteria such that <1% false positives were included in the peptide list (Tables S1 and S2, statistics sheet). After mass recalibration with MSQuant, the average absolute mass error of all peptides was better than 3 ppm.

Samples from all mouse mutants were analyzed by the in-house-developed software MaxQuant (Cox and Mann, 2007; Graumann et al., 2008). Briefly, MaxQuant performs a peak list, SILAC- and XIC-based quantitation, false-positive rates (Gingras et al., 2007), and peptide identification based on Mascot search results.

All data were searched against the International Protein Index sequence database (mouse IPI, version 3.24) (Kersey et al., 2004). Fold-change for ghost proteins was determined from the gel slice corresponding to the expected migration of the full-length protein.

Blood Cell Analyses

Hematocrit was measured from peripheral blood with a hematology analyzer (Nihon Kohden).

For "ghost" preparation, erythrocytes were washed twice in 0.9% NaCl, 10 mM sodium phosphate buffer (pH 7.0) before hypotonic lysis were performed in 0.25% NaCl, 10 mM sodium phosphate buffer (pH 7.0). Lysis was performed in several rounds in hypotonic buffer until the pellet became white.

Flow Cytometry

Flow cytometric lacZ staining of hematopoietic cells was performed on Ter119-positive bone marrow cells that have been incubated with the fluorescent β -galactosidase substrate FDG (fluorescein di- β -D-galactopyranoside) (Sigma) as described (Montanez et al., 2007). Flow cytometry was carried out on a Becton Dickinson FACSCalibur.

SUPPLEMENTAL DATA

Supplemental Data include seven figures and eight tables for protein identification and quantification and are available with this article online at <http://www.cell.com/cgi/content/full/134/2/353/DC1/>.

ACKNOWLEDGMENTS

We thank other members of the department for proteomics and signal transduction and the Department of Molecular Medicine for sharing insights. Meredith O'Keeffe provided critical help in FACS sorting. We thank Gerhard Waner for imaging erythrocytes by scanning electron microscopy. This work was supported by a long-term European Molecular Biology Organization fellowship to M.K., by the 6th and 7th framework program of the European Union, by the Austrian Science Foundation (SFB021), and by the Max Planck Society.

Received: February 18, 2008

Revised: April 29, 2008

Accepted: May 20, 2008

Published: July 24, 2008

REFERENCES

Andersen, J.S., Lam, Y.W., Leung, A.K., Ong, S.E., Lyon, C.E., Lamond, A.I., and Mann, M. (2005). Nucleolar proteome dynamics. *Nature* 433, 77–83.

Benevenga, N.J., Calvert, C., Eckhart, C.D., Fahey, G.C., Greger, J.L., Keen, C.L., Knapka, J.J., Magalhaes, H., and Oftedal, O.T. (1995). Nutrient require-

ments of the mouse. In *Nutrient Requirements of Laboratory Animals*, J. Overton, ed. (Washington, D.C.: National Academy Press), pp. 192.

Berlin, N.I., Waldmann, T.A., and Weissman, S.M. (1959). Life span of red blood cell. *Physiol. Rev.* 39, 577–616.

Beynon, R.J., and Pratt, J.M. (2005). Metabolic labeling of proteins for proteomics. *Mol. Cell. Proteomics* 4, 857–872.

Bier, D.M. (1997). Stable isotopes in biosciences, their measurement and models for amino acid metabolism. *Eur. J. Pediatr.* 156 (Suppl 1), S2–S8.

Blagoev, B., Ong, S.E., Kratchmarova, I., and Mann, M. (2004). Temporal analysis of phosphotyrosine-dependent signaling networks by quantitative proteomics. *Nat. Biotechnol.* 22, 1139–1145.

Brakebusch, C., Grose, R., Quondamatteo, F., Ramirez, A., Jorcano, J.L., Pirro, A., Svensson, M., Herken, R., Sasaki, T., Timpl, R., et al. (2000). Skin and hair follicle integrity is crucially dependent on β 1 integrin expression on keratinocytes. *EMBO J.* 19, 3990–4003.

Calderwood, D.A. (2004). Integrin activation. *J. Cell Sci.* 117, 657–666.

Coffman, R.L. (1982). Surface antigen expression and immunoglobulin gene rearrangement during mouse pre-B cell development. *Immunol. Rev.* 69, 5–23.

Cox, J., and Mann, M. (2007). Is proteomics the new genomics? *Cell* 130, 395–398.

Delaunay, J. (1995). Genetic disorders of the red cell membranes. *FEBS Lett.* 369, 34–37.

Dietz, W.H., Jr., Wolfe, M.H., and Wolfe, R.R. (1982). A method for the rapid determination of protein turnover. *Metabolism* 31, 749–754.

Doherty, M.K., and Beynon, R.J. (2006). Protein turnover on the scale of the proteome. *Expert Rev. Proteomics* 3, 97–110.

Doherty, M.K., Whitehead, C., McCormack, H., Gaskell, S.J., and Beynon, R.J. (2005). Proteome dynamics in complex organisms: using stable isotopes to monitor individual protein turnover rates. *Proteomics* 5, 522–533.

Forner, F., Foster, L.J., Campanaro, S., Valle, G., and Mann, M. (2006). Quantitative proteomic comparison of rat mitochondria from muscle, heart, and liver. *Mol. Cell. Proteomics* 5, 608–619.

Gingras, A.C., Gstaiger, M., Raught, B., and Aebersold, R. (2007). Analysis of protein complexes using mass spectrometry. *Nat. Rev. Mol. Cell Biol.* 8, 645–654.

Graumann, J., Hubner, N.C., Kim, J.B., Ko, K., Moser, M., Kumar, C., Cox, J., Schoeler, H., and Mann, M. (2008). SILAC-labeling and proteome quantification of mouse embryonic stem cells to a depth of 5111 proteins. *Mol. Cell. Proteomics* 7, 672–683. Published online November 28, 2007. 10.1074/mcp.M700460-MCP200.

Gregg, C.T., Hutson, J.Y., Prine, J.R., Ott, D.G., and Furchner, J.E. (1973). Substantial replacement of mammalian body carbon with carbon-13. *Life Sci.* 13, 775–782.

Hynes, R.O. (2002). Integrins: bidirectional, allosteric signaling machines. *Cell* 110, 673–687.

Ishihama, Y., Sato, T., Tabata, T., Miyamoto, N., Sagane, K., Nagasu, T., and Oda, Y. (2005). Quantitative mouse brain proteomics using culture-derived isotope tags as internal standards. *Nat. Biotechnol.* 23, 617–621.

Kersey, P.J., Duarte, J., Williams, A., Karavidopoulou, Y., Birney, E., and Apweiler, R. (2004). The International Protein Index: an integrated database for proteomics experiments. *Proteomics* 4, 1985–1988.

Kratchmarova, I., Blagoev, B., Haack-Sorensen, M., Kassem, M., and Mann, M. (2005). Mechanism of divergent growth factor effects in mesenchymal stem cell differentiation. *Science* 308, 1472–1477.

Krijgsveld, J., Ketting, R.F., Mahmoudi, T., Johansen, J., Artal-Sanz, M., Verrijzer, C.P., Plasterk, R.H., and Heck, A.J. (2003). Metabolic labeling of *C. elegans* and *D. melanogaster* for quantitative proteomics. *Nat. Biotechnol.* 21, 927–931.

Kuhn, R., Schwenk, F., Aguet, M., and Rajewsky, K. (1995). Inducible gene targeting in mice. *Science* 269, 1427–1429.

Legate, K.R., Montanez, E., Kudlacek, O., and Fassler, R. (2006). ILK, PINCH and parvin: the tIPP of integrin signalling. *Nat. Rev. Mol. Cell Biol.* 7, 20–31.

- Mann, M. (2006). Functional and quantitative proteomics using SILAC. *Nat. Rev. Mol. Cell Biol.* 7, 952–958.
- McClatchy, D.B., Dong, M.Q., Wu, C.C., Venable, J.D., and Yates, J.R., 3rd. (2007). ^{15}N metabolic labeling of mammalian tissue with slow protein turnover. *J. Proteome Res.* 6, 2005–2010.
- Moebius, J., Zahedi, R.P., Lewandrowski, U., Berger, C., Walter, U., and Sickmann, A. (2005). The human platelet membrane proteome reveals several new potential membrane proteins. *Mol. Cell. Proteomics* 4, 1754–1761.
- Montanez, E., Piwko-Czuchra, A., Bauer, M., Li, S., Yurchenco, P., and Fassler, R. (2007). Analysis of integrin functions in peri-implantation embryos, hematopoietic system, and skin. *Methods Enzymol.* 426, 239–289.
- Moore, S., Spackman, D.H., and Stein, W.H. (1958). Automatic recording apparatus for use in the chromatography of amino acids. *Fed. Proc.* 17, 1107–1115.
- Moser, M., Nieswandt, B., Ussar, S., Pozgajova, M., and Fassler, R. (2008). Kindlin-3 is essential for integrin activation and platelet aggregation. *Nat. Med.* 14, 325–330. Published online February 17, 2008. 10.1038/nm1722.
- Nieswandt, B., Brakebusch, C., Bergmeier, W., Schulte, V., Bouvard, D., Mokhtari-Nejad, R., Lindhout, T., Heemskerk, J.W., Zirngibl, H., and Fassler, R. (2001). Glycoprotein VI but not $\alpha 2\beta 1$ integrin is essential for platelet interaction with collagen. *EMBO J.* 20, 2120–2130.
- Oda, Y., Huang, K., Cross, F.R., Cowburn, D., and Chait, B.T. (1999). Accurate quantitation of protein expression and site-specific phosphorylation. *Proc. Natl. Acad. Sci. USA* 96, 6591–6596.
- Olsen, J.V., Ong, S.E., and Mann, M. (2004). Trypsin cleaves exclusively C-terminal to arginine and lysine residues. *Mol. Cell. Proteomics* 3, 608–614.
- Olsen, J.V., Blagoev, B., Gnadt, F., Macek, B., Kumar, C., Mortensen, P., and Mann, M. (2006). Global, in vivo, and site-specific phosphorylation dynamics in signaling networks. *Cell* 127, 635–648.
- Ong, S.E., and Mann, M. (2005). Mass spectrometry-based proteomics turns quantitative. *Nat. Chem. Biol.* 1, 252–262.
- Ong, S.E., and Mann, M. (2006). A practical recipe for stable isotope labeling by amino acids in cell culture (SILAC). *Nat. Protoc.* 1, 2650–2660.
- Ong, S.E., Blagoev, B., Kratchmarova, I., Kristensen, D.B., Steen, H., Pandey, A., and Mann, M. (2002). Stable isotope labeling by amino acids in cell culture, SILAC, as a simple and accurate approach to expression proteomics. *Mol. Cell. Proteomics* 1, 376–386.
- Ong, S.E., Kratchmarova, I., and Mann, M. (2003). Properties of ^{13}C -substituted arginine in stable isotope labeling by amino acids in cell culture (SILAC). *J. Proteome Res.* 2, 173–181.
- Pasini, E.M., Kirkegaard, M., Mortensen, P., Lutz, H.U., Thomas, A.W., and Mann, M. (2006). In-depth analysis of the membrane and cytosolic proteome of red blood cells. *Blood* 108, 791–801.
- Peters, L.L., Weier, H.U., Walensky, L.D., Snyder, S.H., Parra, M., Mohandas, N., and Conboy, J.G. (1998). Four paralogous protein 4.1 genes map to distinct chromosomes in mouse and human. *Genomics* 54, 348–350.
- Pratt, J.M., Robertson, D.H., Gaskell, S.J., Riba-Garcia, I., Hubbard, S.J., Sidhu, K., Oliver, S.G., Butler, P., Hayes, A., Petty, J., et al. (2002). Stable isotope labelling in vivo as an aid to protein identification in peptide mass fingerprinting. *Proteomics* 2, 157–163.
- Radtke, F., and Clevers, H. (2005). Self-renewal and cancer of the gut: two sides of a coin. *Science* 307, 1904–1909.
- Rappsilber, J., Ishihama, Y., and Mann, M. (2003). Stop and go extraction tips for matrix-assisted laser desorption/ionization, nanoelectrospray, and LC/MS sample pretreatment in proteomics. *Anal. Chem.* 75, 663–670.
- Ruggeri, Z.M. (2002). Platelets in atherothrombosis. *Nat. Med.* 8, 1227–1234.
- Rybicki, A.C., Musto, S., and Schwartz, R.S. (1995). Decreased content of protein 4.2 in ankyrin-deficient normoblastosis (nb/nb) mouse red blood cells: evidence for ankyrin enhancement of protein 4.2 membrane binding. *Blood* 86, 3583–3589.
- Schoenheimer, R., and Rittenberg, D. (1935). Deuterium as an indicator in the study of intermediary metabolism. *Science* 82, 156–157.
- Schulze, W.X., and Mann, M. (2004). A novel proteomic screen for peptide-protein interactions. *J. Biol. Chem.* 279, 10756–10764.
- Shevchenko, A., Wilm, M., Vorm, O., and Mann, M. (1996). Mass spectrometric sequencing of proteins silver-stained polyacrylamide gels. *Anal. Chem.* 68, 850–858.
- Shi, Z.T., Afzal, V., Collier, B., Patel, D., Chasis, J.A., Parra, M., Lee, G., Paszty, C., Stevens, M., Walensky, L., et al. (1999). Protein 4.1R-deficient mice are viable but have erythroid membrane skeleton abnormalities. *J. Clin. Invest.* 103, 331–340.
- Southgate, C.D., Chishti, A.H., Mitchell, B., Yi, S.J., and Palek, J. (1996). Targeted disruption of the murine erythroid band 3 gene results in spherocytosis and severe haemolytic anaemia despite a normal membrane skeleton. *Nat. Genet.* 14, 227–230.
- Taouatas, N., Drugan, M.M., Heck, A.J., and Mohammed, S. (2008). Straight-forward ladder sequencing of peptides using a Lys-N metalloendopeptidase. *Nat. Methods* 5, 405–407. Published online April 20, 2008. 10.1038/nmeth.1204.
- Ussar, S., Wang, H.V., Linder, S., Fassler, R., and Moser, M. (2006). The Kindlins: subcellular localization and expression during murine development. *Exp. Cell Res.* 312, 3142–3151.
- Wolfe, R.R., and Chinkes, D.L. (2005). *Isotope tracers in metabolic research* (New Jersey: Wiley-LISS).
- Wu, C.C., MacCoss, M.J., Howell, K.E., Matthews, D.E., and Yates, J.R., 3rd. (2004). Metabolic labeling of mammalian organisms with stable isotopes for quantitative proteomic analysis. *Anal. Chem.* 76, 4951–4959.
- Zhang, Y., Zhang, Y., Adachi, J., Olsen, J.V., Shi, R., de Souza, G., Pasini, E., Foster, L.J., Macek, B., Zougman, A., et al. (2007). MAPU: Max-Planck Unified database of organellar, cellular, tissue and body fluid proteomes. *Nucleic Acids Res.* 35, D771–D779.

Cell, Volume 134

Supplemental Data

SILAC Mouse for Quantitative Proteomics

Uncovers Kindlin-3 as an Essential Factor

for Red Blood Cell Function

Marcus Krueger, Markus Moser, Siegfried Ussar, Ingo Thievensen, Christian A. Luber, Francesca Forner, Sarah Schmidt, Sara Zanivan, Reinhard Fässler, and Matthias Mann

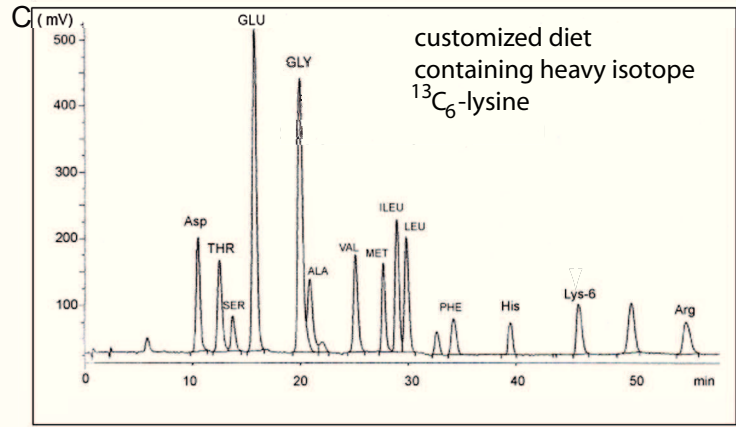
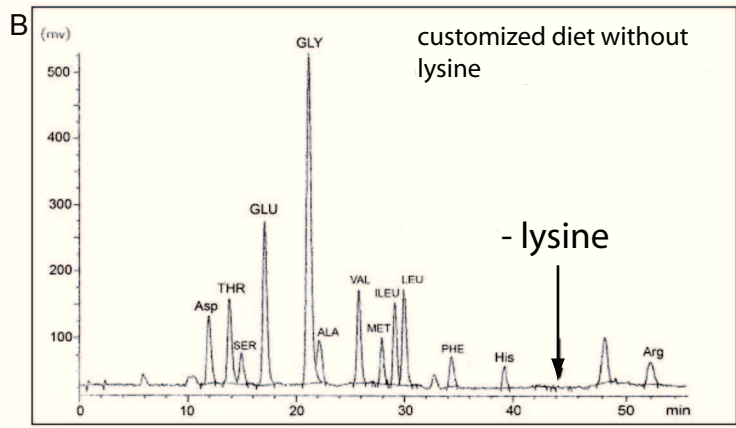
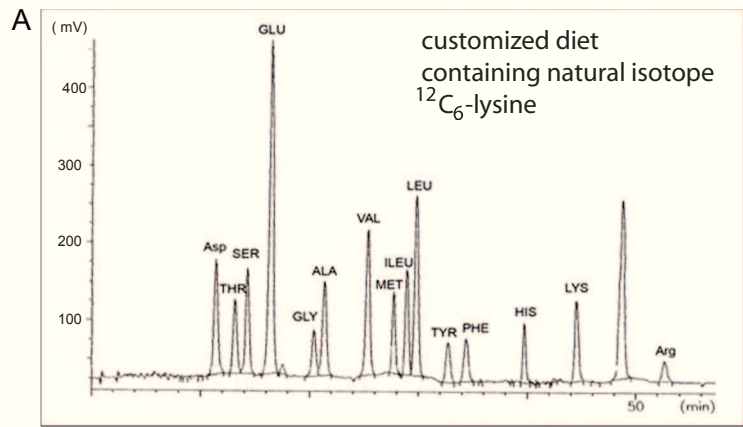


Figure S2

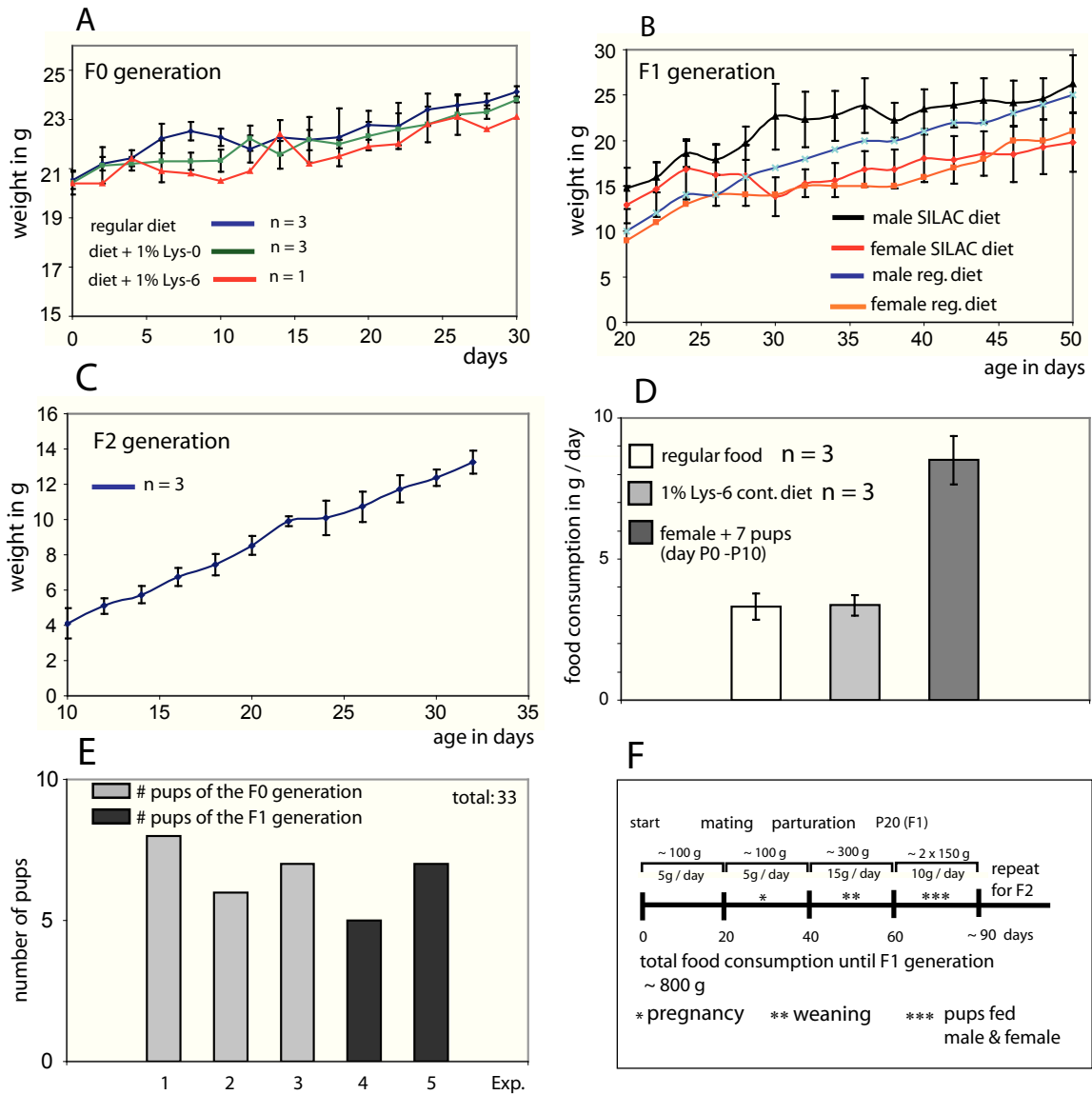


Figure S3

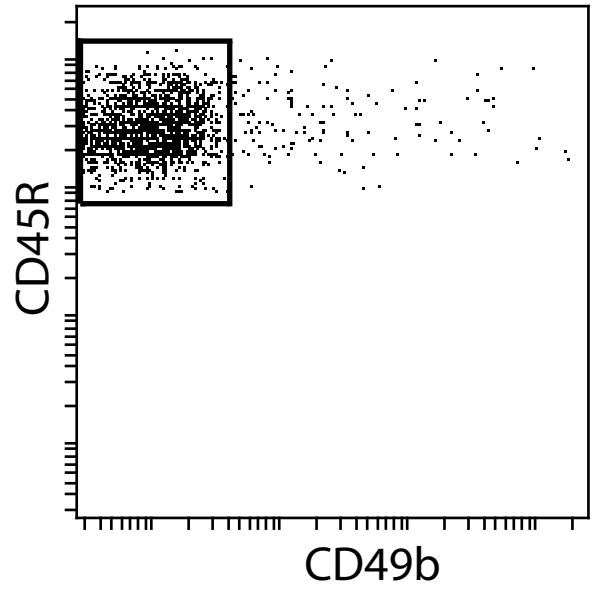
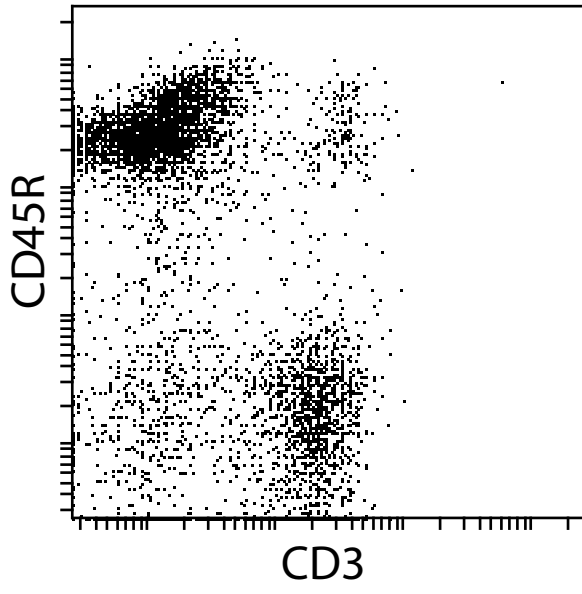


Figure S4

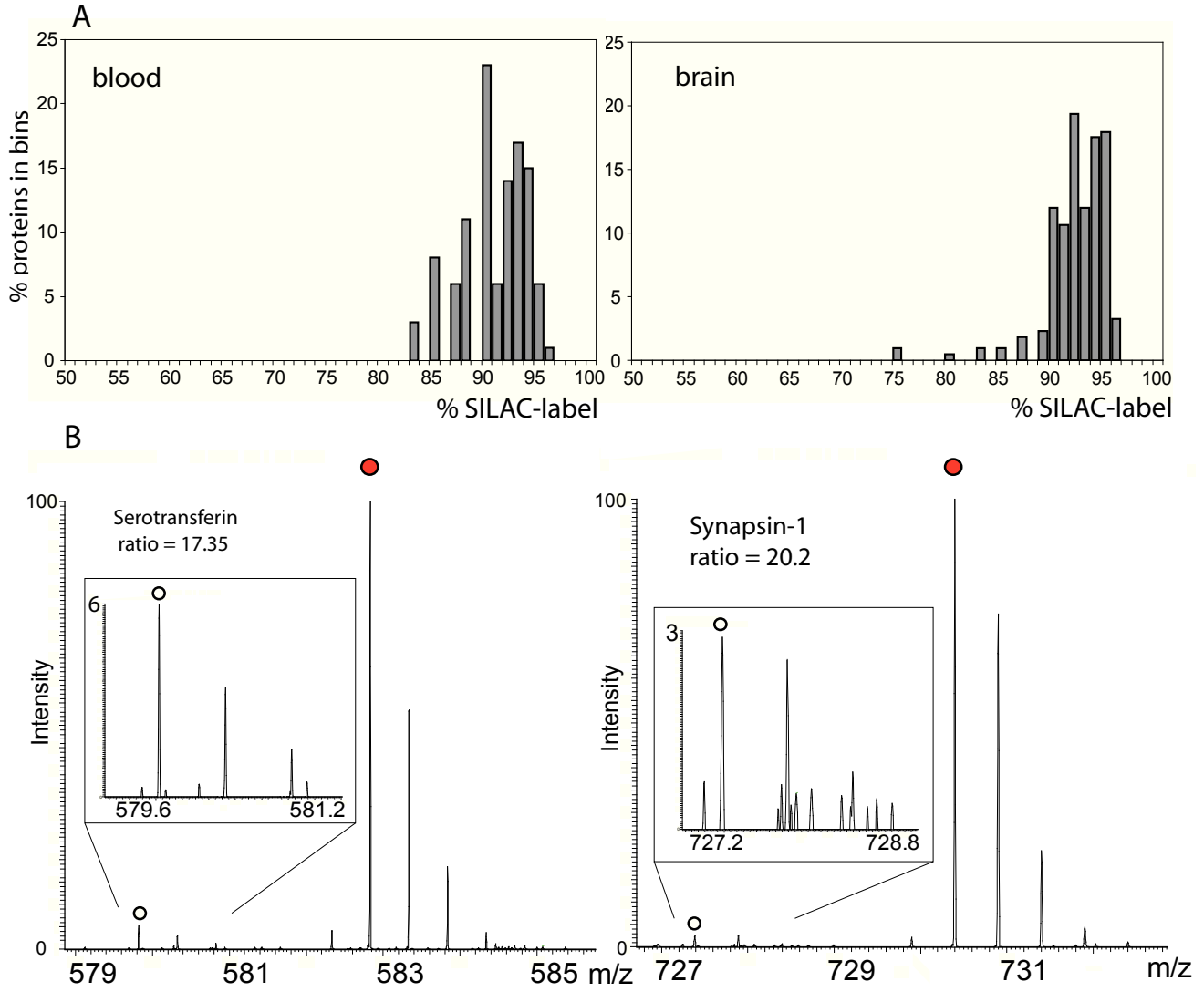


Figure S5

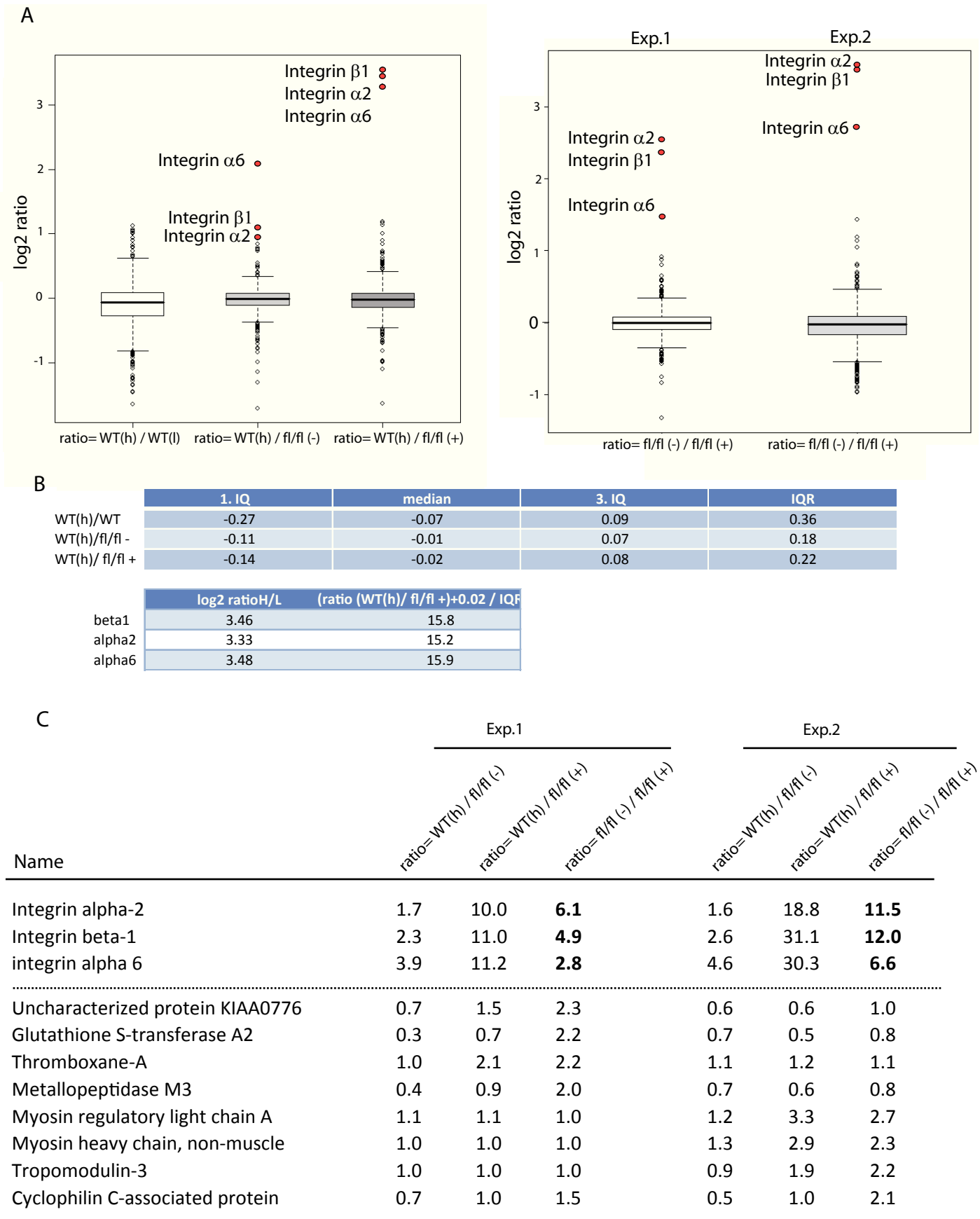
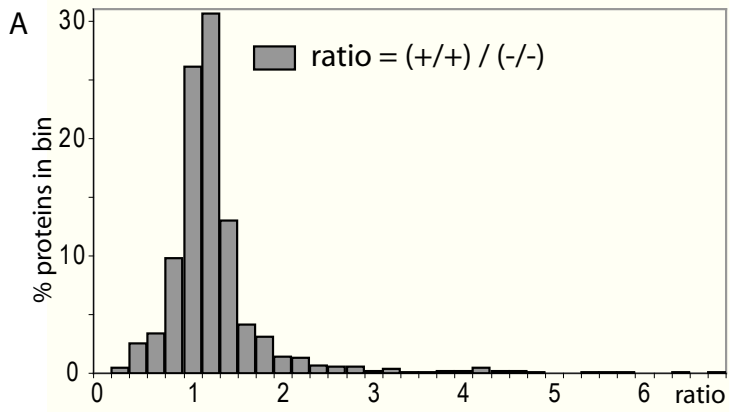


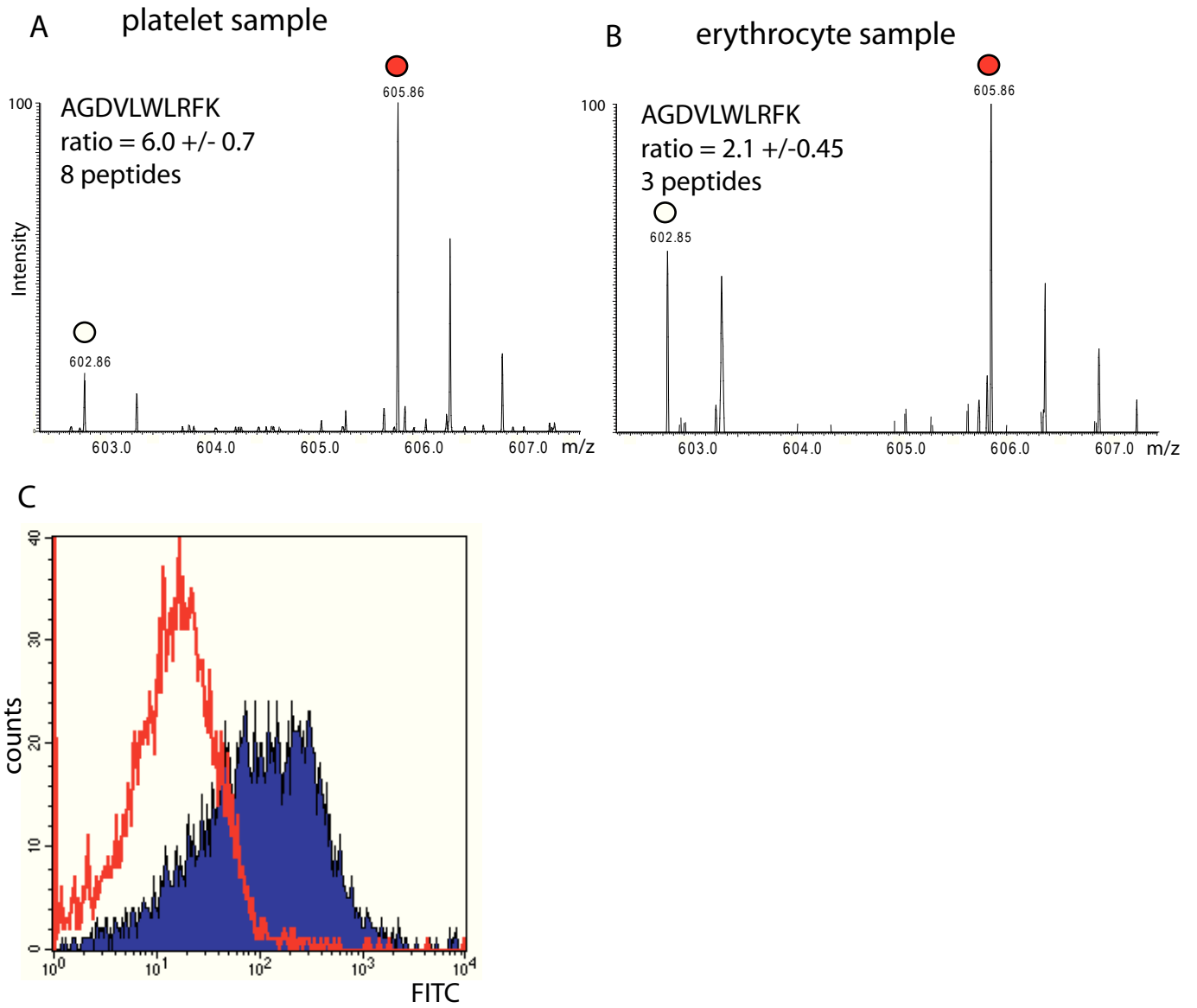
Figure S6

**B****FACS****SILAC**

Glycoprotein	Wild-type	Kindlin-3 -/-	Glycoprotein	WT(H)	WT(H)	WT(L)
				WT(L)	Kindlin-3-/(L)	Kindlin-3-/(L)
α IIb β 3	786.0 \pm 34.1	588.5 \pm 44.7	Integrin beta-3	0.9	0.9	1.1
α 2 β 1	50.0 \pm 0.8	30.0 \pm 1.1	Integrin alpha-IIb	0.9	1.0	1.1
α 5 β 1	26.7 \pm 1.2	15.7 \pm 2.0	Integrin alpha-2	1.0	1.1	1.1
GPIba	410.8 \pm 99.3	469.8 \pm 122.1	Integrin beta-1	1.0	1.7	1.7
GPV	259.1 \pm 32.1	232.0 \pm 13.4	Integrin alpha-5	1.3	4.2	3.3
GPIX	348.5 \pm 7.8	425.0 \pm 31.6	Integrin beta-1	1.0	1.7	1.7
GPVI	24.8 \pm 2.1	16.5 \pm 0.4	Platelet glycoprotein Ib-alpha	1.4	1.4	1.0
CD9	1567 \pm 63.3	1002.3 \pm 58.0	Platelet glycoprotein V	0.9	1.1	1.2
			n.d.			
			n.d.			
			CD9	1.2	1.6	1.3

Figure S7

Kindlin-3



PAPER II

Kindlin-3 is required for β_2 integrin-mediated leukocyte adhesion to endothelial cells

Markus Moser¹, Martina Bauer¹, Stephan Schmid², Raphael Ruppert¹, Sarah Schmidt¹, Michael Sixt¹, Hao-Ven Wang¹, Markus Sperandio² & Reinhard Fässler¹

Integrin activation is essential for the function of all blood cells, including platelets and leukocytes¹. The blood cell-specific FERM domain protein Kindlin-3 is required for the activation of the β_1 and β_3 integrins on platelets². Impaired activation of β_1 , β_2 and β_3 integrins on platelets and leukocytes is the hallmark of a rare autosomal recessive leukocyte adhesion deficiency syndrome in humans called LAD-III, characterized by severe bleeding and impaired adhesion of leukocytes to inflamed endothelia³. Here we show that Kindlin-3 also binds the β_2 integrin cytoplasmic domain and is essential for neutrophil binding and spreading on β_2 integrin-dependent ligands such as intercellular adhesion molecule-1 and the complement C3 activation product iC3b. Moreover, loss of Kindlin-3 expression abolished firm adhesion and arrest of neutrophils on activated endothelial cells *in vitro* and *in vivo*, whereas selectin-mediated rolling was unaffected. Thus, Kindlin-3 is essential to activate the β_1 , β_2 and β_3 integrin classes, and loss of Kindlin-3 function is sufficient to cause a LAD-III-like phenotype in mice.

Leukocyte adhesion to vessel walls and subsequent transmigration into tissues is mediated through a sequential adhesion cascade, which allows blood cells to overcome the high shear forces within blood vessels. The cascade is initiated by transient selectin-carbohydrate interactions, which trigger leukocyte rolling on the surface of activated endothelial cells. Rolling leukocytes sense immobilized chemokines, and chemokine receptor signaling induces activation of β_2 integrins. Activated β_2 integrins mediate firm binding to counter-receptors on the endothelial cell followed by transmigration of leukocytes through the endothelial layer⁴. The central role of integrins and selectins in this multistep process is impressively highlighted by leukocyte adhesion deficiency (LAD) syndromes in man, which can be caused either by mutations in the gene encoding β_2 integrin (LAD-I)⁵ or by impaired glycosylation of selectin ligands (LAD-II)^{6–8}.

In recent years, several groups have identified individuals suffering from a novel form of LAD syndrome that has been termed LAD-III or LAD-I variant. LAD-III is inherited in an autosomal recessive manner and is characterized by a complete inability to induce activation of β_1 ,

β_2 and β_3 integrins in hematopoietic cells, resulting in severe bleeding due to impaired platelet aggregation and recurrent infections due to abrogated leukocyte adhesion to activated endothelial cells³. Activation of leukocyte integrins can be triggered by various receptor signaling pathways, including chemokine receptors. These signals have been proposed to induce the binding of talin to integrin β_1 , β_2 and β_3 cytoplasmic domains, resulting in a shift of integrins from a low-affinity to a high-affinity state for ligands (integrin activation)⁹. As talin is ubiquitously expressed, and talin ablation leads to early embryonic lethality in mice¹⁰, it is highly unlikely that mutations in the gene encoding talin cause LAD-III. One group of researchers found a mutation in a splice acceptor site of the *CALDAGGEF1* (official symbol *RASGRP2*) gene and loss of *CALDAGGEF1* messenger RNA in two subjects with LAD-III (ref. 11). Notably, mice lacking *CALDAG-GEF1* also suffer from defects in platelet and leukocyte integrin function¹². Moreover, *CALDAG-GEF1* functions as a guanine exchange factor for the small GTPase Rap1, which, in turn, activates leukocyte and platelet integrins downstream of multiple receptors including receptors for chemokines¹¹. However, other individuals with LAD-III lack mutations in the *CALDAGGEF1* gene (see Svensson *et al.*¹³ and Malinin *et al.*¹⁴ in this issue) and show normal Rap1 activity in platelets and leukocytes^{15,16}, suggesting that mutations in another gene cause this disease.

We recently showed that the FERM domain-containing, integrin β tail-binding protein Kindlin-3 (encoded by the *Fermt3* gene, called *Kindlin3* here) is required to activate β_1 and β_3 integrins in platelets². Kindlin-3 belongs to a unique family (Kindlin-1, Kindlin-2 and Kindlin-3) of focal adhesion proteins. Kindlin-1 is expressed in epithelial cells, and mutations in the gene encoding Kindlin-1 cause a skin-blistering disease in man called Kindler syndrome¹⁷. Kindlin-2 is widely expressed, and gene ablation in mice results in peri-implantation lethality due to severely compromised function of β_1 and β_3 integrins¹⁸. Kindlin-3 is exclusively expressed in hematopoietic cells¹⁹, and mice lacking *Kindlin3* (*Kindlin3*^{-/-} mice) suffer from fatal anemia, which is caused by severe bleeding and erythrocytopenia^{2,20}. *Kindlin3*^{-/-} mice also show markedly reduced size and cellularity of spleen and thymus and lack detectable mesenteric lymph nodes (Supplementary Fig. 1 online).

¹Department of Molecular Medicine, Max Planck Institute of Biochemistry, Am Klopferspitz 18, 82152 Martinsried, Germany. ²Walter Brendel Center for Experimental Medicine, Ludwig-Maximilians-Universität, Marchioninistrasse 15, 81377 Munich, Germany. Correspondence should be addressed to R.F. (faessler@biochem.mpg.de).

Received 23 September 2008; accepted 5 January 2009; Published online 22 February 2009; doi:10.1038/nm.1921

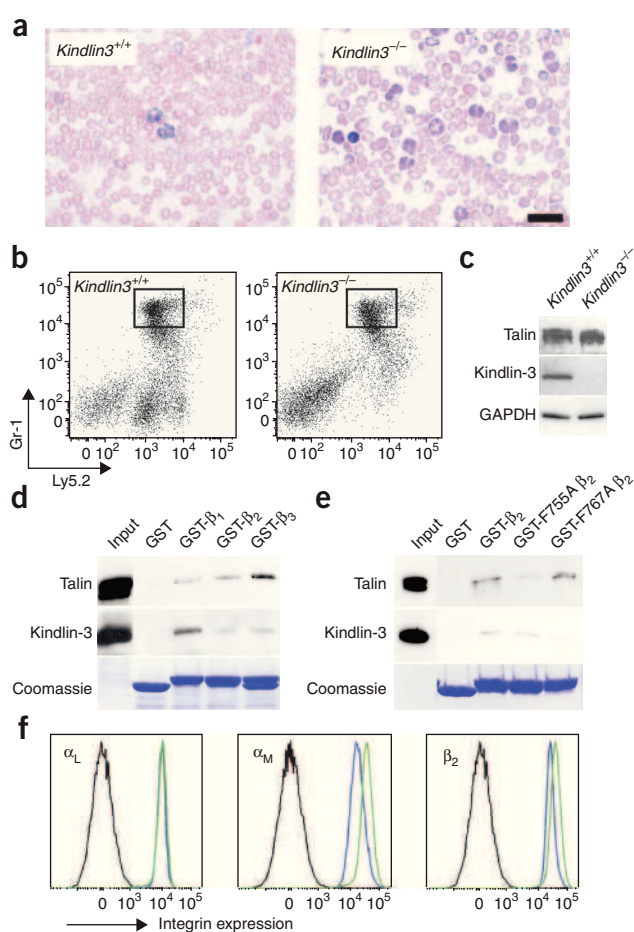


Figure 1 Characterization of PMNs in *Kindlin3*^{-/-} chimeric mice. (a) Peripheral blood smears from control and *Kindlin3*^{-/-} chimeras. Scale bar, 20 μ m. (b) FACS profile of bone marrow-derived cells from control and *Kindlin3*^{-/-} chimeras stained for Gr-1-FITC and CD45.2 (Ly5.2)-allophycocyanin. PMNs from the boxed area were sorted and used for all *in vitro* experiments. (c) Western blot analysis of sorted PMNs from *Kindlin3*^{+/+} and *Kindlin3*^{-/-} chimeras showing talin and Kindlin-3 expression. Glyceraldehyde 3-phosphate dehydrogenase (GAPDH) was used as a loading control. (d,e) GST fusions to β_1 , β_2 and β_3 (d) and β_2 , F755A β_2 and F767A β_2 (e) integrin cytoplasmic domains were incubated with platelet cell lysates and used in pull-down assays to assess the binding of these integrin domains to talin and Kindlin-3. (f) Surface expression of α_L , α_M and β_2 integrins on PMNs from control and *Kindlin3*^{-/-} chimeras (black lines show isotype controls; blue lines show *Kindlin3*^{+/+}; green lines show *Kindlin3*^{-/-}).

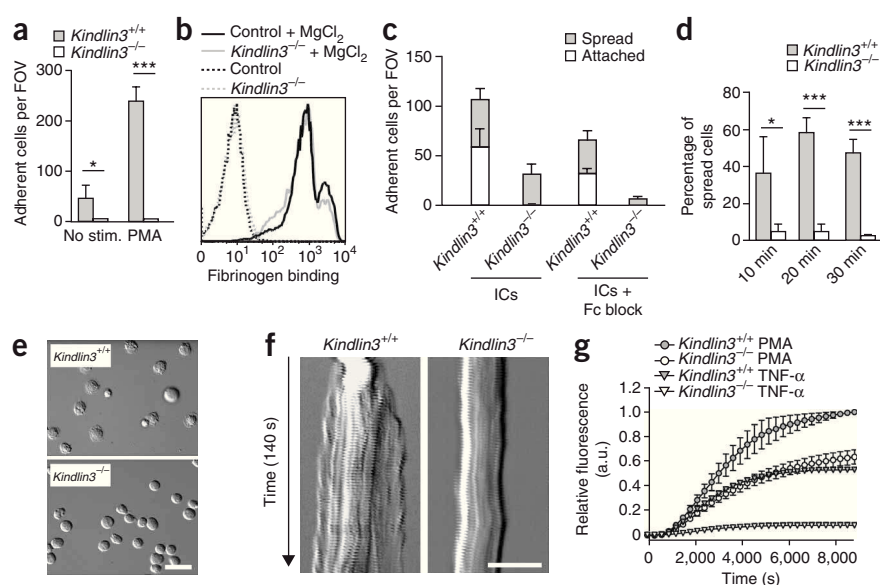
(F755A or F767A) and performed pull-down experiments. Kindlin-3 still bound to the F755A β_2 integrin tail mutant but was unable to interact with the F767A β_2 integrin tail mutant (Fig. 1e), indicating that the binding occurs at the distal NXXF motif and is spatially conserved among all integrin tails tested so far. FACS analysis revealed normal amounts of α_L and slightly increased amounts of α_M and β_2 integrin subunits on *Kindlin3*^{-/-} PMNs (Fig. 1f). Furthermore, the expression of other surface receptors such as CD43, CD44 and P-selectin glycoprotein ligand-1 was also not altered in the absence of Kindlin-3 expression (Supplementary Fig. 3 online). Together these data indicate that the absence of Kindlin-3 expression permits the formation and maturation of PMNs. Similar to the granulocytosis observed in individuals with LAD-I, LAD-II and LAD-III as well as in β_2 integrin-deficient mice²¹, there is granulocytosis in *Kindlin3*^{-/-} chimeric mice, presumably due to a compensatory response to impaired granulocyte number or function in tissues or both.

Next we tested whether β_2 integrins can be activated in the absence of Kindlin-3 by seeding *Kindlin3*^{-/-} PMNs on glass surfaces coated with intercellular adhesion molecule-1 (ICAM-1), the endothelial counter-receptor for the leukocyte integrins $\alpha_L\beta_2$ and $\alpha_M\beta_2$ that are crucial for tight adhesion and arrest of rolling PMNs on activated endothelium. Untreated PMNs did not show substantial adhesion and spreading (Fig. 2a), indicating that they were not activated during their isolation. In the presence of phorbol-12-myristate-13-acetate (PMA), a diacylglycerol analog triggering intracellular signaling events leading to activation of integrins ('inside-out' signaling), PMNs from *Kindlin3*^{+/+} chimeras rapidly adhered and spread on ICAM-1. In contrast, adhesion and spreading of *Kindlin3*^{-/-} PMNs on ICAM-1 was completely absent (Fig. 2a). To test whether the defect in β_2 integrin activation in *Kindlin3*^{-/-} PMNs is due specifically to a defect in 'inside-out' signaling, we used MnCl₂ to induce β_2 integrin activation. We incubated PMNs in suspension with fluorescently labeled fibrinogen, a ligand for the $\alpha_M\beta_2$ and $\alpha_V\beta_3$ integrins, and measured the extent of fibrinogen binding by FACS. Notably, *Kindlin3*^{+/+} and *Kindlin3*^{-/-} PMNs bound comparable amounts of fibrinogen (Fig. 2b). Together, these findings indicate that Kindlin-3 is a key player in the intracellular signaling cascade leading to β_2 integrin activation.

To corroborate the dependence of β_2 integrin activation on Kindlin-3, we measured PMN adhesion and spreading on immobilized immune complexes, which is triggered by Fc γ receptor-mediated inside-out activation of $\alpha_M\beta_2$ integrin and binding to the activated complement component iC3b²². Whereas control PMNs adhered strongly to immune complexes and approximately half of the adherent PMNs spread, Kindlin-3-deficient PMNs adhered weakly to immune complexes and did not spread (Fig. 2c,d). The adhesion of mutant PMNs to immune complexes occurred in an Fc γ receptor-dependent

To test whether Kindlin-3 deficiency leads to defective leukocyte adhesion and function, we generated fetal liver cell chimeras from wild-type (*Kindlin3*^{+/+}) and *Kindlin3*^{-/-} embryos to circumvent post-natal lethality of *Kindlin3*^{-/-} mice² and analyzed their polymorphonuclear granulocytes (PMNs) *in vitro* and *in vivo*. Peripheral blood smears 5 weeks after the fetal liver cell transfer indicated that the number of PMNs was markedly increased in *Kindlin3*^{-/-} chimeras (Fig. 1a). This was confirmed by determining the absolute counts of PMNs in peripheral blood, which reached $3,500 \pm 1,000$ cells per μ l (mean \pm s.d.; $n = 9$) in *Kindlin3*^{+/+} and $31,200 \pm 27,000$ cells per μ l ($n = 9$) in *Kindlin3*^{-/-} fetal liver cell chimeras (counts of other blood cell types are shown in Supplementary Table 1 online). Despite the severe granulocytosis, the size and nuclear morphology of PMNs from peripheral blood or bone marrow as well as the expression of surface markers such as Gr-1 were similar in *Kindlin3*^{+/+} and *Kindlin3*^{-/-} chimeras (Fig. 1a,b). Western blot analysis confirmed loss of Kindlin-3 expression in bone marrow-derived *Kindlin3*^{-/-} PMNs, whereas talin amounts were normal (Fig. 1c). Pull-down experiments with recombinant β_1 , β_2 and β_3 integrin cytoplasmic tails incubated with platelet lysates showed a clear Kindlin-3 interaction with the β_2 integrin cytoplasmic tail, although this binding was weaker compared with binding of Kindlin-3 to β_1 or β_3 integrin cytoplasmic domains (Fig. 1d). The cytoplasmic domain of β_1 and β_3 integrins contains two NXXY (where X is any amino acid) motifs, whereas the β_2 integrin tail contains two NXXF motifs (Supplementary Fig. 2 online). To test whether Kindlin-3 shares a similar spatial binding property on the integrin β_2 tail as on β_1 and β_3 integrin tails, we substituted each phenylalanine residue in these motifs individually with an alanine

Figure 2 Functional properties of *Kindlin3*^{-/-} PMNs. (a) Adhesion of neutrophils to coated ICAM-1. Control and *Kindlin3*^{-/-} PMNs were treated with or without PMA (*n* = 4, each assay was performed in triplicate). FOV, field of view. (b) Fibrinogen binding of control and *Kindlin3*^{-/-} PMNs, as analyzed by flow cytometry. Cells were incubated with either EDTA as a negative control or with MnCl₂. (c) Adhesion of PMNs on immune complexes. *Kindlin3*^{+/+} and *Kindlin3*^{-/-} PMNs were plated on immune complexes (IC) in the absence or presence of antibody to Fcγ receptor (Fc block) (*n* = 3, each assay was performed in triplicate). (d) Spreading of PMNs on immune complexes. *Kindlin3*^{+/+} and *Kindlin3*^{-/-} PMNs were stimulated with TNF-α before plating. Spreading was analyzed 10, 20 and 30 min after plating (*n* = 4). In a and d, graphs show means ± s.d.; Student's *t* test was used for comparing different datasets. (*, *P* < 0.05; **, *P* < 0.01; ***, *P* < 0.001). (e) Differential interference contrast microscopy of *Kindlin3*^{+/+} and *Kindlin3*^{-/-} PMNs 20 min after plating on immune complexes. Scale bar, 25 μm. (f) Kymographs of a *Kindlin3*^{+/+} or a *Kindlin3*^{-/-} PMN plated on immune complexes and imaged with differential interference contrast microscopy. Scale bar, 10 μm. (g) Oxidative burst after β₂ integrin-mediated activation of PMNs. Sorted PMNs from *Kindlin3*^{+/+} and *Kindlin3*^{-/-} chimeras were stimulated with either TNF-α or PMA and then the production of free ROIs was measured. Data are means ± s.d. of three independent experiments, each conducted in triplicate. a.u., arbitrary units.



manner, as Fcγ receptor blockage abolished *Kindlin3*^{-/-} PMN cell adhesion (Fig. 2c). Quantification of cell morphology after plating revealed that around 60% of *Kindlin3*^{+/+} PMNs became flattened on immobilized immune complexes, whereas no significant spreading was observed with *Kindlin3*^{-/-} PMNs (Fig. 2d). For closer inspection, we followed PMNs contacting the immune complex-coated surfaces with time-lapse video microscopy using differential interference contrast optics. Upon surface contact, *Kindlin3*^{+/+} PMNs spread within a time frame of less than 1 min and subsequently remained flattened and stationary with a ruffling periphery (Fig. 2e and Supplementary Video 1 online). In sharp contrast, *Kindlin3*^{-/-} PMNs showed severely impaired spreading, despite active surface dynamics with peripheral ruffling and occasional small lamellae that extended onto the surface (Fig. 2e and Supplementary Video 1). To characterize spreading behavior, we quantified the plasma membrane extension rates of spreading PMNs by kymography. Spreading control PMNs rapidly increased their diameters within 60 s after contacting the surface, whereas the diameter of *Kindlin3*^{-/-} PMNs remained unchanged (Fig. 2f).

The spreading of preactivated PMNs on adhesive surfaces triggers a β₂ integrin-dependent degranulation and a respiratory burst that can be measured as free reactive oxygen intermediates (ROIs). Therefore, we seeded PMNs pretreated with tumor necrosis factor-α (TNF-α) on immune complexes and quantified the kinetics of ROI release. In line with findings from PMNs derived from β₂ integrin-deficient mice²³ and subjects with LAD-I (ref. 24), *Kindlin3*^{-/-} PMNs were completely unresponsive, whereas *Kindlin3*^{+/+} cells showed a burst of ROI (Fig. 2g). PMA treatment partially bypasses the adhesion dependency of the reaction²⁴. Accordingly, under PMA stimulation *Kindlin3*^{-/-} PMNs showed a considerable rescue of ROI production, indicating a constitutive capability to undergo respiratory burst and confirming the normal differentiation state of these cells (Fig. 2g).

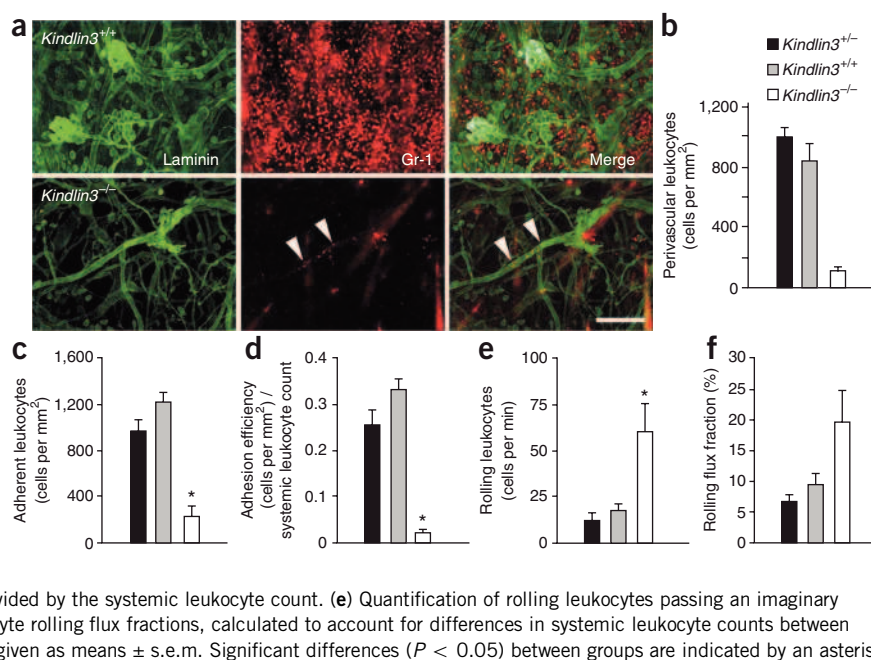
To explore the consequences of abolished β₂ integrin activation in *Kindlin3*^{-/-} chimeras, we studied leukocyte extravasation into the perivascular tissue *in vivo*. Initially, we applied phorbol esters (croton oil) to the ears of the mice and examined infiltration of PMNs into

perivascular tissue 4 h later by determining PMN distribution in relation to the vascular basement membrane. In *Kindlin3*^{+/+} chimeric mice, many Gr-1-positive cells transmigrated into the interstitium, where they became evenly distributed (Fig. 3a). In contrast, in *Kindlin3*^{-/-} chimeric mice, Gr-1-positive cells were completely absent from the perivascular tissue, but were visible within the vasculature (Fig. 3a). We next investigated rolling, adhesion and extravasation of PMNs from nonchimeric *Kindlin3*^{+/+} mice (as a control) and from *Kindlin3*^{+/+} and *Kindlin3*^{-/-} chimeric mice in TNF-α-stimulated cremaster muscle venules. In line with the croton oil experiment, Giemsa staining of treated cremaster tissues revealed a strong and widespread influx of *Kindlin3*^{+/+} or *Kindlin3*^{+/+} PMNs into the interstitium 3 hours after TNF-α application, whereas extravasation of *Kindlin3*^{-/-} PMNs was markedly reduced (Fig. 3b). Together these findings indicate that *Kindlin3*^{-/-} chimeric mice suffer from a considerable PMN extravasation deficiency as in individuals with LAD-I, LAD-II or LAD-III.

To determine which step in the extravasation cascade is affected by the absence of Kindlin-3, we analyzed leukocyte rolling and adhesion in TNF-α-stimulated cremaster muscle venules of nonchimeric *Kindlin3*^{+/+} mice and *Kindlin3*^{+/+} and *Kindlin3*^{-/-} chimeric mice by intravital microscopy. Microvascular parameters such as vessel diameter, blood flow velocity and wall shear rate were similar among all three types of mice (Supplementary Table 2 online), despite a significant elevation of PMN counts in the peripheral blood of *Kindlin3*^{-/-} chimeric mice (*P* < 0.05). In line with previous observations²⁵ and as shown here, TNF-α treatment markedly lowered systemic leukocyte counts in *Kindlin3*^{+/+} mice and in *Kindlin3*^{+/+} chimeric mice (Supplementary Table 2). TNF-α-treatment in *Kindlin3*^{-/-} chimeric mice also decreased systemic leukocyte counts, but these counts were significantly higher than in *Kindlin3*^{+/+} mice or *Kindlin3*^{+/+} chimeric mice (Supplementary Table 2, *P* < 0.05).

In TNF-α-stimulated cremaster muscle venules of *Kindlin3*^{-/-} chimeric mice, the number of adherent leukocytes was significantly reduced (220 ± 100 cells per mm²) when compared to *Kindlin3*^{+/+} mice or *Kindlin3*^{+/+} chimeric mice (980 ± 90 cells per mm² and

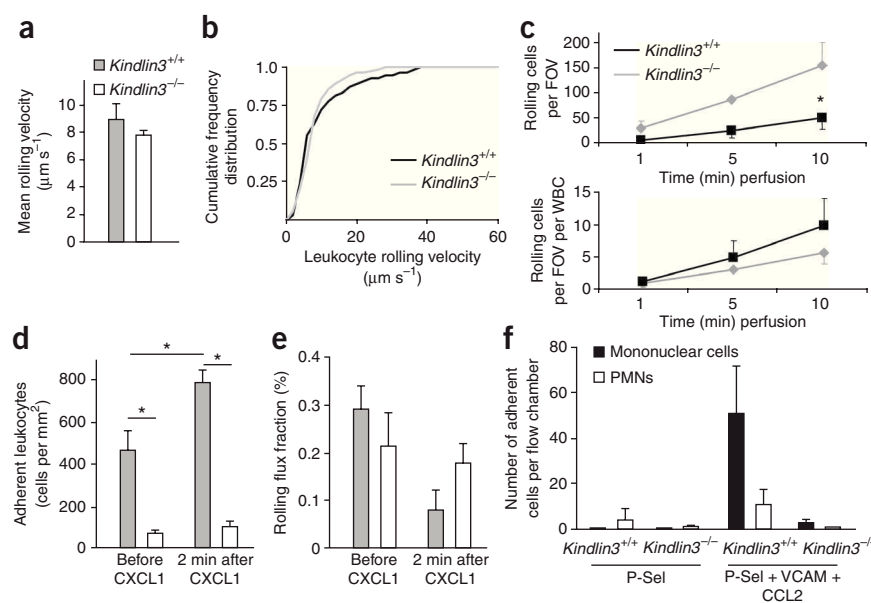
Figure 3 Abrogated leukocyte adhesion and extravasation in *Kindlin3*^{-/-} chimeras. (a) Sections of phorbol ester-treated ears from *Kindlin3*^{+/+} and *Kindlin3*^{-/-} chimeric mice, stained with a pan-laminin antibody (green) to visualize endothelial basement membranes and Gr-1 (red) to visualize neutrophils. Arrowheads indicate Gr-1-positive cells within blood vessels of *Kindlin3*^{-/-} chimeras. Scale bar, 200 μ m. (b) Quantification of perivascular leukocytes in whole-mount Giemsa staining of TNF- α -stimulated cremaster muscles from non-chimeric *Kindlin3*^{+/-} mice (15 venules in four mice), *Kindlin3*^{+/+} (15 venules in four mice) and *Kindlin3*^{-/-} (21 venules in four mice) chimeras 3 h after cytokine application. Data are means \pm s.e.m. (c) Leukocyte adhesion in TNF- α -stimulated cremaster muscle venules assessed in 13 cremaster muscle venules of four *Kindlin3*^{+/-} mice, 19 venules of six *Kindlin3*^{+/+} chimeric mice and 13 cremaster muscle venules of four *Kindlin3*^{-/-} chimeric mice. (d) Leukocyte adhesion efficiency, given as the number of adherent leukocytes per mm² vascular surface area divided by the systemic leukocyte count. (e) Quantification of rolling leukocytes passing an imaginary perpendicular line over the vessel in 1 min. (f) Leukocyte rolling flux fractions, calculated to account for differences in systemic leukocyte counts between *Kindlin3*^{+/+} mice and *Kindlin3*^{-/-} mice. All values are given as means \pm s.e.m. Significant differences ($P < 0.05$) between groups are indicated by an asterisk.



1,220 \pm 80 cells per mm², respectively, $P < 0.05$ versus *Kindlin3*^{-/-} chimeric mice), indicating that Kindlin-3 is crucial for leukocyte adhesion *in vivo* (Fig. 3c). Because leukocyte adhesion is greatly influenced by the number of available circulating leukocytes, we also calculated leukocyte adhesion efficiency, which is defined by the ratio of adherent leukocytes to circulating leukocytes. Owing to the high systemic leukocyte count in *Kindlin3*^{-/-} chimeras, the adhesion efficiency was dramatically reduced in *Kindlin3*^{-/-} chimeric mice (0.02 \pm 0.01) when compared to *Kindlin3*^{+/-} mice or *Kindlin3*^{+/+} chimeric mice (0.25 \pm 0.033 and 0.35 \pm 0.03, respectively, $P < 0.05$ versus *Kindlin3*^{-/-} chimeric mice; Fig. 3d).

Next, we analyzed leukocyte rolling in TNF- α -stimulated cremaster muscle venules, which depends on P-selectin and E-selectin in this model²⁵. We observed a significant increase in the number of rolling leukocytes in *Kindlin3*^{-/-} chimeric mice (60 \pm 16 cells per min) as compared to *Kindlin3*^{+/-} mice or *Kindlin3*^{+/+} chimeric mice (12 \pm 4 cells per min and 18 \pm 3 cells per min, respectively, $P < 0.05$ versus *Kindlin3*^{-/-} mice; Fig. 3e and Supplementary Videos 2 and 3 online). However, after correcting leukocyte rolling for differences in the total number of systemic leukocytes (rolling flux fraction), we did not observe any significant difference in rolling between *Kindlin3*^{+/+} and *Kindlin3*^{-/-} chimeric mice (Fig. 3f). We also analyzed mean leukocyte

Figure 4 Leukocyte rolling and adhesion under *in vivo* and *in vitro* conditions. (a,b) Mean leukocyte rolling velocity (a) and the cumulative frequency distribution (b) of leukocyte rolling velocities from analysis of TNF- α -stimulated postcapillary venules of cremaster muscles from *Kindlin3*^{+/+} ($n = 54$ venules from four mice) and *Kindlin3*^{-/-} ($n = 111$ venules from four mice) chimeric mice. (c) Top, quantification of leukocyte rolling in an *ex vivo* flow chamber system (P-selectin-coated microglass capillaries) perfused with whole blood from *Kindlin3*^{+/+} ($n = 5$ chambers from four mice) and *Kindlin3*^{-/-} ($n = 3$ chambers from four mice) chimeric mice. Bottom, the number of rolling leukocytes was corrected for differences in systemic leukocyte counts between *Kindlin3*^{+/+} and *Kindlin3*^{-/-} chimeric mice. WBC, white blood cell. (d,e) Assessment of leukocyte adhesion (d) and leukocyte rolling (e) in unstimulated cremaster muscle venules of *Kindlin3*^{+/+} ($n = 4$) and *Kindlin3*^{-/-} ($n = 3$) chimeric mice before and 2 min after injection of the arrest chemokine CXCL1. (f) β 1 integrin-dependent adhesion of leukocytes from *Kindlin3*^{+/+} ($n = 3$) and *Kindlin3*^{-/-} chimeric mice ($n = 3$) *ex vivo*. Flow chambers were coated with P-selectin only or a mixture of P-selectin, VCAM-1 and CCL2, connected to the carotid artery, perfused with whole blood for 10 min, and the number of adherent PMNs and mononuclear cells was counted. For each condition, chambers in at least three mice were used. All data are shown as means \pm s.e.m.; significant differences ($P < 0.05$) are indicated by asterisk.



rolling velocities and cumulative frequency distribution of leukocyte rolling velocities and found that they were similar in *Kindlin3*^{+/+} and *Kindlin3*^{-/-} chimeric mice, suggesting that selectin-mediated rolling is not disturbed in the absence of Kindlin-3 (Fig. 4a,b). This was further confirmed in an *ex vivo* flow chamber assay²⁶, where leukocyte rolling on immobilized recombinant mouse (rm) P-selectin was indistinguishable between leukocytes from *Kindlin3*^{+/+} and *Kindlin3*^{-/-} chimeric mice after correction for differences in systemic leukocyte counts (Fig. 4c). To further confirm the *in vivo* leukocyte adhesion defect of *Kindlin3*^{-/-} chimeric mice, we blocked leukocyte rolling in TNF- α -stimulated cremaster muscle venules by systemic injection of blocking antibodies against P- and E-selectin during intravital microscopic observation. The blocking antibodies abruptly abolished leukocyte rolling in *Kindlin3*^{+/+} mice and in *Kindlin3*^{+/+} and *Kindlin3*^{-/-} chimeric mice as previously described for wild-type mice²⁷. Five minutes after antibody injection, a substantial number of adherent leukocytes were still present in *Kindlin3*^{+/+} mice and in *Kindlin3*^{+/+} chimeric mice (940 \pm 80 cells per mm² and 1,070 \pm 90 cells per mm², respectively, data not shown), whereas only a few adherent leukocytes were observed in *Kindlin3*^{-/-} chimeric mice (230 \pm 50 cells per mm², data not shown; **Supplementary Videos 4 and 5** online). Taken together, these data indicate that Kindlin-3 is not required for leukocyte rolling on inflamed endothelium but is essential for their firm adhesion.

To investigate whether Kindlin-3 is also required for chemokine-induced leukocyte arrest *in vivo*, we systemically injected the neutrophil arrest-inducing chemokine CXCL1 (also known as keratinocyte-derived chemokine, KC)²⁵ into *Kindlin3*^{+/+} and *Kindlin3*^{-/-} chimeric mice and observed leukocyte adhesion and rolling. CXCL1 injection into *Kindlin3*^{+/+} mice triggered a significant increase in the number of adherent leukocytes in postcapillary venules of the exteriorized cremaster muscle, which was accompanied by a marked drop in the number of rolling leukocytes (Fig. 4d,e and **Supplementary Video 6** online). In contrast, injection of CXCL1 into *Kindlin3*^{-/-} chimeric mice did not change leukocyte adhesion and rolling (Fig. 4d,e and **Supplementary Video 7** online), showing that chemokine-triggered leukocyte arrest is also almost completely absent in *Kindlin3*^{-/-} mice.

Finally, we addressed the role of Kindlin-3 in β_1 integrin-mediated leukocyte adhesion with an autoperfused flow chamber assay²⁶. Chambers were coated with a mixture of rmP-selectin, rm vascular cell adhesion molecule-1 (VCAM-1) and rmCCL2 or with rmP-selectin only and connected to the carotid artery of *Kindlin3*^{+/+} or *Kindlin3*^{-/-} chimeric mice. Leukocyte adhesion was assessed 10 min after the start of perfusion with whole blood. In *Kindlin3*^{+/+} chimeric mice, mononuclear cells adhered preferably to the surface coated with all three proteins compared to the surface coated with rmP-selectin only, for which adhered cells were almost completely absent (Fig. 4f). In contrast, in *Kindlin3*^{-/-} chimeric mice, leukocytes failed to adhere to the surface coated with all three proteins (Fig. 4f), suggesting that Kindlin-3 is crucial for β_1 integrin- and β_2 integrin-dependent adhesion.

Our study demonstrates that Kindlin-3 is essential for the activation of β_2 integrins in PMNs. Consequently, lack of Kindlin-3 expression prevents adhesion and spreading of PMNs on β_2 integrin ligands such as ICAM-1 and iC3b and results in a severe leukocyte adhesion deficiency *in vivo*. The mechanism underlying Kindlin-3-mediated activation β_2 integrin is similar to that underlying its activation of the β_1 and β_3 integrins, as Kindlin-3 is capable of binding the distal NXXF motif of the β_2 integrin cytoplasmic domain, albeit with a lower efficiency than its binding to this motif in the β_1 and β_3 integrins.

The defects seen in *Kindlin3*^{-/-} mice—a severe leukocyte adhesion deficiency and fatal bleeding—bear a striking similarity to the

symptoms observed in individuals with LAD-III. Furthermore, the gene defect causing LAD-III has been mapped to chromosome 11 in humans, where the *Kindlin3* gene is located. *Kindlin3* is thus a prime candidate to be mutated in LAD-III. However, a recent study identified a mutation in the *CALDAGGEF1* gene, which encodes a RAP-1 guanine exchange factor, to cause LAD-III (ref. 11). Notably, Svensson *et al.*¹³ report in this issue that subjects with LAD-III who have mutations in *CALDAGGEF1* also carry nonsense mutations in their *Kindlin3* gene. Furthermore, reexpression of a *Kindlin3* cDNA fully rescued the adhesion and spreading defect in leukocytes from these subjects. In contrast, reexpression of *CALDAGGEF1* did not rescue these defects. It will be useful now to clarify whether mutations in different genes such as *CALDAGGEF1* and *Kindlin3* can indeed give rise to the same LAD-III syndrome and how and where they function in the signaling pathway that leads to β_2 integrin activation. Studies with mouse mutants suggest that deficiencies of either protein can lead to a LAD-like phenotype^{2,12}, although CALDAG-GEF1-deficient mice seem to have slightly milder defects than those lacking Kindlin-3. The reason for this difference could be that Kindlin-3 controls both inside-out and 'outside-in' signaling of integrins², whereas CALDAG-GEF1 has a role only in Rap-mediated inside-out integrin activation¹¹.

METHODS

Generation of fetal liver cell chimeras. We recently generated *Kindlin3*-deficient mice². We obtained fetal liver cells from embryonic day 15 *Kindlin3*^{+/+} or *Kindlin3*^{-/-} embryos by pushing liver tissue through a cell strainer (Falcon). We injected 4 \times 10⁶ cells into the tail vein of lethally irradiated (10 Gy) recipient C57BL/6 mice (Charles River Laboratories). Four to five weeks after transfer, we either isolated PMNs from the bone marrow or used the mice for intravital microscopy. All mouse experiments were performed with approval by the District Government of Upper Bavaria.

Intravital microscopy. We injected rmTNF- α (R&D Systems) intrascrotally at a dose of 500 ng per mouse in a volume of 0.3 ml sterile saline. Two hours later, we anesthetized the mice as previously described²⁵ and placed them onto a heating pad to maintain body temperature at 37 °C. After intubation and carotid artery cannulation for blood sampling and application of antibodies and chemokines, we surgically prepared the cremaster muscle for intravital microscopy as previously described²⁸. Briefly, after opening the scrotum, we exteriorized the cremaster muscle and spread it over a cover glass. We gently moved the epididymis and testis aside to get microscopic access to the cremaster muscle microcirculation and its postcapillary venules. We performed intravital microscopy on an upright microscope (Olympus BX51) with a saline immersion objective (40 \times and 0.8 numerical aperture). We recorded experiments via CCD camera (model CF8/1, Kappa) on a Panasonic S-VHS recorder. We also made recordings with a digital camera (LaVision Biotech) and stored them on a computer with Inspector software package (LaVision Biotech). We then used the digital recordings offline to generate movie clips with ImageJ software (US National Institutes of Health). During the experiment, we obtained systemic blood samples (10 μ l into 90 μ l Türk's solution, Merck) to assess systemic white blood cell counts. In some experiments, we stimulated the postcapillary venules of the exteriorized cremaster muscle by systemic injection of keratinocyte-derived chemokine (CXCL1, 600 ng per mouse, Natutec) and assessed leukocyte rolling and adhesion before and 2 min after injection of CXCL1 as previously described²⁵.

Data analysis of intravital experiments. We measured vessel diameter and vessel segment length of postcapillary venules with a digital image processing system²⁹. We obtained centerline red blood cell velocities in microvessels of the cremaster muscle by a dual photodiode and a digital on-line cross-correlation program (Circusoft Instrumentation), and we converted them offline to mean blood flow velocities as previously described²⁸. We assessed wall shear rates as previously reported³⁰. We defined rolling flux as the number of rolling cells per min. We defined rolling PMN flux fraction as the percentage of rolling PMNs in all PMNs passing the same vessel in 1 min²⁸. We considered PMNs that did not

move for more than 30 s to be adherent. We assessed the number of adherent leukocytes as the number of adherent cells per mm² vessel surface area²⁵.

Whole-mount histology. To assess extravasated leukocytes in TNF- α -stimulated cremaster muscles, we prepared whole mounts of cremaster muscles as previously described²⁵. Briefly, while the cremaster muscle was still mounted on the stage for intravital microscopy, we fixed the tissue with 4% paraformaldehyde in 0.1 M phosphate buffer (pH 7.4). We removed the cremaster muscle and mounted it flat on a superfrost glass slide (Menzel), air-dried it for 5–10 min and fixed it in 4% paraformaldehyde in 0.1 M phosphate buffer (pH 7.4) for 24 h at 4 °C. After fixation, we washed the tissue three times in 0.1 M phosphate buffer with 5% ethanol, stained it with Giemsa (Sigma) at 20 °C for 5 min and developed it in 0.01% acetic acid for contrast. We washed the developed slides in water, 75% ethanol, 95% ethanol, 100% ethanol and fresh xylene and then mounted them in mounting medium (AGAR Scientific). We assessed the number of extravasated leukocytes in Giemsa-stained cremaster muscles with a Zeiss upright microscope and a 100 \times and 1.3 numerical aperture oil immersion objective (Zeiss).

Ex vivo flow chamber assay. We used an autoperfused flow chamber assay as previously described²⁶. Briefly, we used rectangular microglass capillaries (VitroCom) as flow chambers. We coated the flow chambers with rmP-selectin (20 μ g ml⁻¹, R&D Systems), rmCCL2 (3 μ g ml⁻¹, Natutec) and rmVCAM-1 (15 μ g ml⁻¹, R&D Systems). We blocked nonspecific binding by incubating the flow chambers with 10% casein (Sigma) for 2 h at 20 °C. After blocking, we rinsed the flow chambers with normal saline and connected them to the mouse carotid artery via polyethylene tubing. We fixed the flow chamber itself under an upright fluorescence microscope (BX51 WI, Olympus) with a saline immersion objective (20 \times and 0.95 numerical aperture, Olympus). We observed rolling of leukocytes within the flow chamber for 10 min and recorded their rolling via a charge-coupled device camera system (CF8HS; Kappa) on a Panasonic S-VHS recorder. We assessed leukocyte adhesion after a 10-min perfusion by counting adherent mononuclear cells and neutrophils in a 10-mm flow chamber segment; the adherent cells were stained by gentle flushing of the chamber with Türk's stain (Merck).

Statistical analyses. We performed statistical analyses with the GraphPad Prism software (version 5.00, GraphPad). Data are presented as means \pm s.d. or means \pm s.e.m. We used unpaired Student's *t* tests or one-way analysis of variance followed by a multiple pairwise comparison test (Dunn's test) as appropriate to compare datasets. Asterisks indicate significant differences (*, *P* < 0.05, **, *P* < 0.01 and ***, *P* < 0.005).

Additional methods. Detailed methodology is described in the **Supplementary Methods** online.

Note: Supplementary information is available on the Nature Medicine website.

ACKNOWLEDGMENTS

We thank the members of the Fässler lab for discussions, R. Zent for careful reading of the manuscript, K. Kessenbrock for help with the oxidative burst experiment, T. Lämmermann for help with the skin inflammation assay and S. Dietzel for help with generating the movie clips. The work was funded by the Deutsche Forschungsgemeinschaft and the Max Planck Society.

AUTHOR CONTRIBUTIONS

M.M., M.S. and R.F. designed and supervised research, analyzed data and wrote the paper. M.M., M.B., S. Schmid, R.R., S. Schmidt, M. Sixt, H.-V.W. and M. Sperandio performed experiments. All authors discussed the results and commented on the manuscript.

Published online at <http://www.nature.com/naturemedicine/>

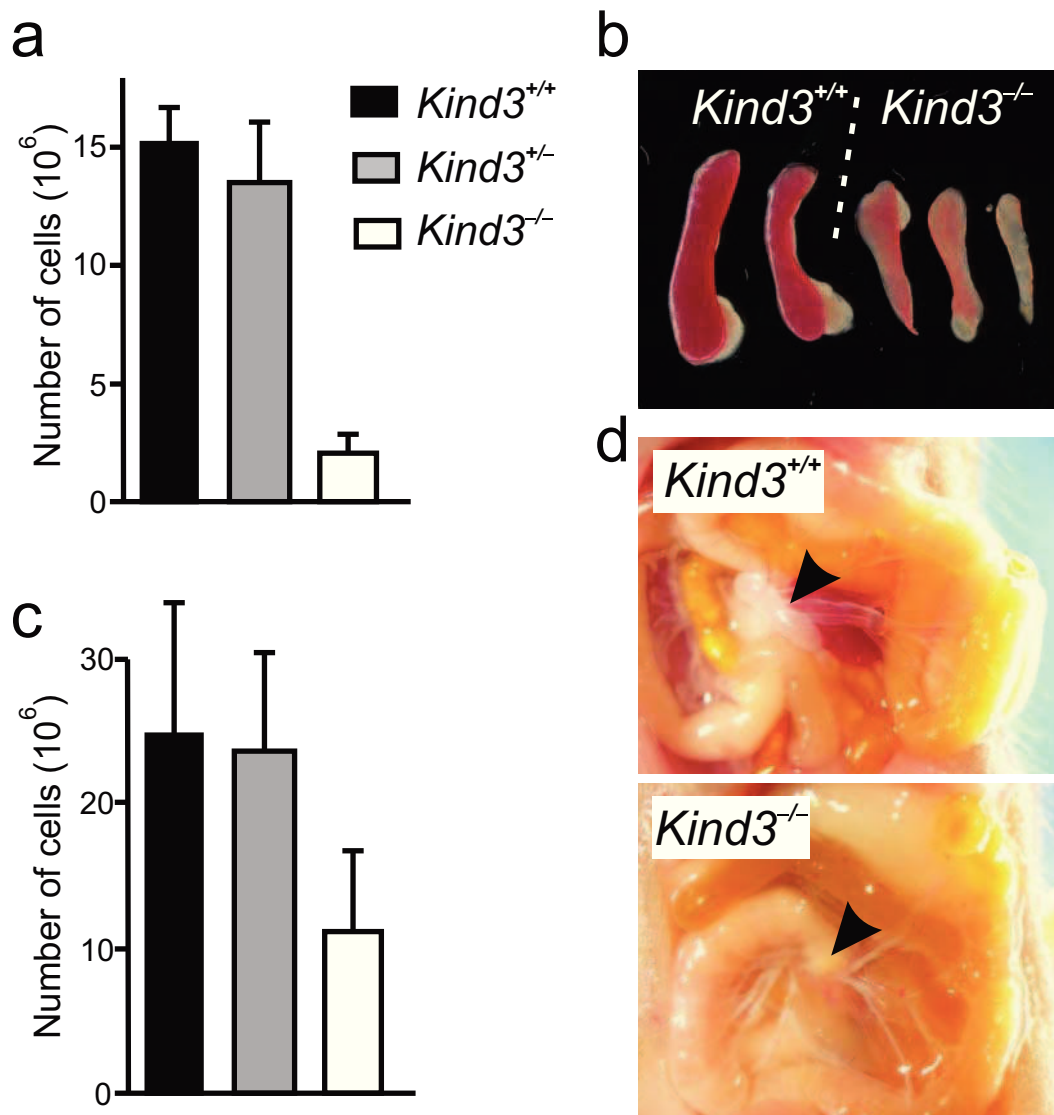
Reprints and permissions information is available online at <http://npg.nature.com/reprintsandpermissions/>

1. Hynes, R.O. Integrins: bidirectional, allosteric signaling machines. *Cell* **110**, 673–687 (2002).

2. Moser, M., Nieswandt, B., Ussar, S., Pozgajova, M. & Fassler, R. Kindlin-3 is essential for integrin activation and platelet aggregation. *Nat. Med.* **14**, 325–330 (2008).
3. Alon, R. & Etzioni, A. LAD-III, a novel group of leukocyte integrin activation deficiencies. *Trends Immunol.* **24**, 561–566 (2003).
4. Ley, K., Laudanna, C., Cybulsky, M.I. & Nourshargh, S. Getting to the site of inflammation: the leukocyte adhesion cascade updated. *Nat. Rev. Immunol.* **7**, 678–689 (2007).
5. Anderson, D.C. & Springer, T.A. Leukocyte adhesion deficiency: an inherited defect in the Mac-1, LFA-1, and p150,95 glycoproteins. *Annu. Rev. Med.* **38**, 175–194 (1987).
6. Karsan, A. *et al.* Leukocyte adhesion deficiency type II is a generalized defect of *de novo* GDP-fucose biosynthesis. Endothelial cell fucosylation is not required for neutrophil rolling on human nonlymphoid endothelium. *J. Clin. Invest.* **101**, 2438–2445 (1998).
7. Lubke, T. *et al.* Complementation cloning identifies CDG-IIc, a new type of congenital disorders of glycosylation, as a GDP-fucose transporter deficiency. *Nat. Genet.* **28**, 73–76 (2001).
8. Luhn, K., Wild, M.K., Eckhardt, M., Gerardy-Schahn, R. & Vestweber, D. The gene defective in leukocyte adhesion deficiency II encodes a putative GDP-fucose transporter. *Nat. Genet.* **28**, 69–72 (2001).
9. Sampath, R., Gallagher, P.J. & Pavalko, F.M. Cytoskeletal interactions with the leukocyte integrin beta2 cytoplasmic tail. Activation-dependent regulation of associations with talin and alpha-actinin. *J. Biol. Chem.* **273**, 33588–33594 (1998).
10. Monkley, S.J. *et al.* Disruption of the talin gene arrests mouse development at the gastrulation stage. *Dev. Dyn.* **219**, 560–574 (2000).
11. Pasvolksky, R. *et al.* A LAD-III syndrome is associated with defective expression of the Rap-1 activator CalDAG-GEFI in lymphocytes, neutrophils, and platelets. *J. Exp. Med.* **204**, 1571–1582 (2007).
12. Bergmeier, W. *et al.* Mice lacking the signaling molecule CalDAG-GEFI represent a model for leukocyte adhesion deficiency type III. *J. Clin. Invest.* **117**, 1699–1707 (2007).
13. Svensson, L. *et al.* Leukocyte adhesion deficiency-III is caused by mutations in *KINDLIN3* affecting integrin activation. *Nat. Med.* advance online publication doi:10.1038/nm.1931 (22 February 2009).
14. Malinin, N.L. *et al.* A point mutation in *KINDLIN3* ablates activation of three integrin subfamilies in humans. *Nat. Med.* advance online publication doi:10.1038/nm.1917 (22 February 2009).
15. Kuijpers, T.W. *et al.* Natural history and early diagnosis of LAD-1/variant syndrome. *Blood* **109**, 3529–3537 (2007).
16. Kuijpers, T.W. *et al.* Leukocyte adhesion deficiency type 1 (LAD-1)/variant. A novel immunodeficiency syndrome characterized by dysfunctional β_2 integrins. *J. Clin. Invest.* **100**, 1725–1733 (1997).
17. Jobard, F. *et al.* Identification of mutations in a new gene encoding a FERM family protein with a pleckstrin homology domain in Kindler syndrome. *Hum. Mol. Genet.* **12**, 925–935 (2003).
18. Montanez, E. *et al.* Analysis of integrin functions in peri-implantation embryos, hematopoietic system, and skin. *Methods Enzymol.* **426**, 239–289 (2007).
19. Ussar, S., Wang, H.V., Linder, S., Fassler, R. & Moser, M. The Kindlins: subcellular localization and expression during murine development. *Exp. Cell Res.* **312**, 3142–3151 (2006).
20. Kruger, M. *et al.* SILAC mouse for quantitative proteomics uncovers kindlin-3 as an essential factor for red blood cell function. *Cell* **134**, 353–364 (2008).
21. Scharffetter-Kochanek, K. *et al.* Spontaneous skin ulceration and defective T cell function in CD18 null mice. *J. Exp. Med.* **188**, 119–131 (1998).
22. Jones, S.L., Knaus, U.G., Bokoch, G.M. & Brown, E.J. Two signaling mechanisms for activation of $\alpha_M \beta_2$ avidity in polymorphonuclear neutrophils. *J. Biol. Chem.* **273**, 10556–10566 (1998).
23. Mocsai, A., Zhou, M., Meng, F., Tybulewicz, V.L. & Lowell, C.A. Syk is required for integrin signaling in neutrophils. *Immunity* **16**, 547–558 (2002).
24. Nathan, C. *et al.* Cytokine-induced respiratory burst of human neutrophils: dependence on extracellular matrix proteins and CD11/CD18 integrins. *J. Cell Biol.* **109**, 1341–1349 (1989).
25. Frommhold, D. *et al.* Sialyltransferase ST3Gal-IV controls CXCR2-mediated firm leukocyte arrest during inflammation. *J. Exp. Med.* **205**, 1435–1446 (2008).
26. Smith, M.L., Sperandio, M., Galkina, E.V. & Ley, K. Autoperfused mouse flow chamber reveals synergistic neutrophil accumulation through P-selectin and E-selectin. *J. Leukoc. Biol.* **76**, 985–993 (2004).
27. Sperandio, M. *et al.* Severe impairment of leukocyte rolling in venules of core 2 glucosaminyltransferase-deficient mice. *Blood* **97**, 3812–3819 (2001).
28. Sperandio, M., Pickard, J., Unnikrishnan, S., Acton, S.T. & Ley, K. Analysis of leukocyte rolling *in vivo* and *in vitro*. *Methods Enzymol.* **416**, 346–371 (2006).
29. Pries, A.R. A versatile video image analysis system for microcirculatory research. *Int. J. Microcirc. Clin. Exp.* **7**, 327–345 (1988).
30. Long, D.S., Smith, M.L., Pries, A.R., Ley, K. & Damiano, E.R. Microviscometry reveals reduced blood viscosity and altered shear rate and shear stress profiles in microvessels after hemodilution. *Proc. Natl. Acad. Sci. USA* **101**, 10060–10065 (2004).

Kindlin-3 is required for $\beta 2$ integrin-mediated leukocyte adhesion to endothelial cells.

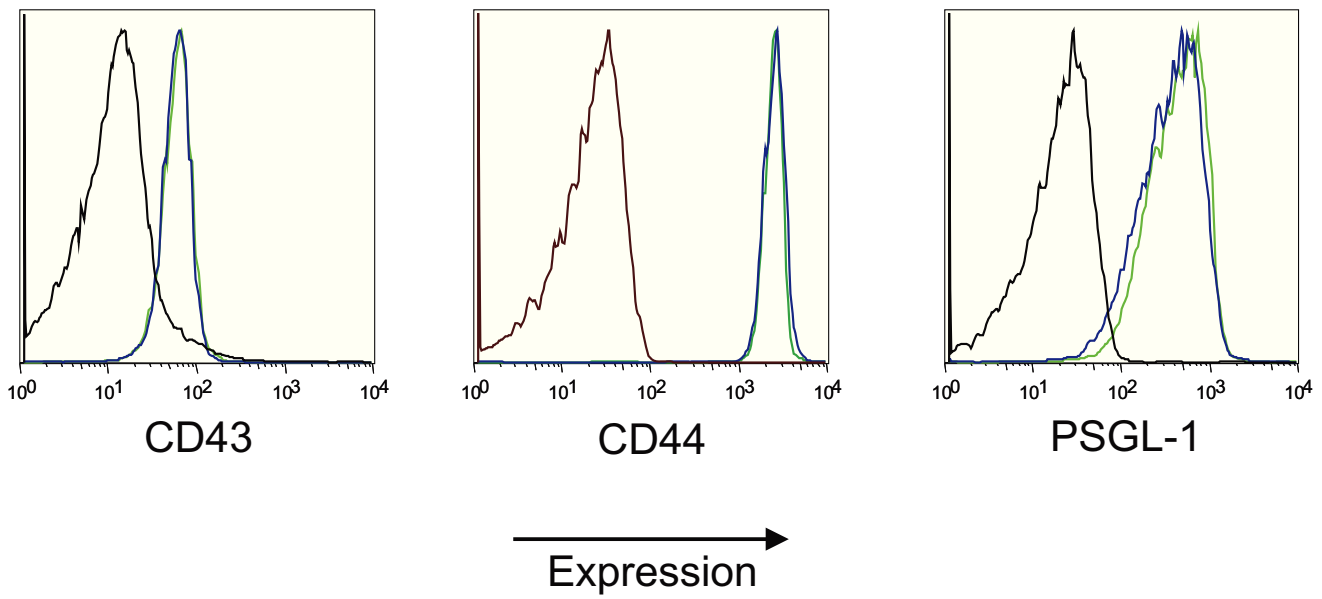
Markus Moser, Martina Bauer, Stephan Schmid, Raphael Ruppert, Sarah Schmidt, Michael Sixt, Hao-Ven Wang, Markus Sperandio, Reinhard Fässler



Supplementary Figure 1: Development of secondary lymphoid tissues is also affected in $Kind3^{-/-}$ mice. Reduced cellularity of spleen (a) and thymus (c) in $Kind3^{-/-}$ newborn mice compared to wild-type or heterozygous animals. (b) shows the reduced size of spleens from two days old $Kind3^{-/-}$ mice compared to $Kind3^{+/+}$ controls. (d) Lack of mesenteric lymph nodes in $Kind3^{-/-}$ mice.

β 1A KLLMIIHDRREFAKFEKEKMNAKWDTGENPIYKSAVTTVVNPKYEGK
 β 1D KLLMIIHDRREFAKFEKEKMNAKWDTQENPIYKSPINNFKNPNYGRKAGL
 β 2 KALIHLSDLREYRRFEKEKLSQWNND NPLFKSATTTVMNPKFAES
 β 3 KLLITIHDRKEFAKFEERARAKWDTANNPLYKEATSTFTNITYRGT

Supplementary figure 2: Sequence comparison of the cytoplasmic domains of β 1A, β 1D, β 2 and β 3 integrins. The two NxxY/F motifs of each integrin tail are highlighted. Please note that β 2 integrins contain a Phenylalanine (F) instead of an Tyrosine (Y).



Supplementary figure 3: Surface expression of CD43, CD44 and PSGL-1. Surface expression levels of CD43, CD44 and PSGL-1 on PMNs from *Kind3*^{+/+} (blue line) and *Kind3*^{-/-} (green line) chimeras. The black lines show isotype controls.

Supplementary Table 1. Peripheral blood counts of *Kind*^{+/+} and *Kind3*^{-/-} fetal liver cell chimeras. Data are presented as mean ± SEM. The number of mice is shown in parenthesis.

**P*<0.05 vs. *Kind*^{+/+} according to Student *t* test.

	<i>Kind</i> ^{+/+}	<i>Kind3</i> ^{-/-}
Neutrophils (x10 ³ /μl)	3,5 ± 0,3 (9)	31,2 ± 8,9* (9)
Lymphocytes (x10 ³ /μl)	9,6 ± 1,6 (9)	5,0 ± 1,1* (8)
Monocytes (x10 ³ /μl)	0,60 ± 0,05 (8)	1,35 ± 0,3* (9)
Eosinophiles (x10 ³ /μl)	0,54 ± 0,09 (8)	1,12 ± 0,42 (9)
Basophils (x10 ³ /μl)	0,20 ± 0,04 (9)	0,11 ± 0,05 (8)
Red blood cells (x10 ⁶ /μl)	11,0 ± 0,4 (9)	4,3 ± 0,6* (9)
Hemoglobin (g/dl)	14,0 ± 0,4 (9)	8,1 ± 0,9* (9)

Supplementary Table 2. Hemodynamic and microvascular parameters in TNF- α -stimulated cremaster muscle venules of constitutive *Kind3*^{+/-} mice (control), *Kind3*^{+/+} and *Kind3*^{-/-} fetal liver cell chimeras. Vessel diameter, centerline velocity, and wall shear rate are presented as mean \pm SEM of all investigated venules.

	Mice	Venules	Diameter	Centerline velocity	Wall shear rate	Systemic leukocyte counts
	(N)	(N)	(μm)	($\mu\text{m/s}$)	(s^{-1})	(cells/ μl)
control	4	13	27 \pm 3	1.800 \pm 270	1.600 \pm 240	4.100 \pm 800
<i>Kind3</i> ^{+/+}	6	19	30 \pm 1	2.100 \pm 150	1.800 \pm 170	3.700 \pm 300
<i>Kind3</i> ^{-/-}	4	14	31 \pm 2	1.500 \pm 230	1.300 \pm 180	12.900 \pm 3.500
			n.s.	n.s	n.s	* p<0.05

Supplementary Methods

Peripheral blood cell counts. Mice were bled from the retroorbital sinus into EDTA-coated tubes. Blood cell counts were determined using a Hemavet 950 analyzer (Drew Scientific Inc., Oxford, CT). Blood smears were prepared with Pappenheim-stain .

Western blot analysis. Protein lysates from FACS sorted leukocytes were subjected to a 5-15% gradient SDS-PAGE. After blotting, PVDF membranes were probed with anti-Kindlin-3¹, anti-Talin (Sigma) and anti-GAPDH (Chemicon) antibodies.

GST fusion protein pull-down assays. The β 1A, β 2, β 2F755A, β 2F767A, and β 3 integrin cytoplasmic domains were expressed as GST-fusion proteins in BL21 cells upon 1mM IPTG induction. Bacteria were washed and lysed in buffer A (150 mM NaCl, 1 mM EDTA, 30 mM Tris, pH 7,4) containing 100 μ g ml⁻¹ lysozyme for 15 min on ice, followed by sonication. After dialysis against buffer B (100 mM NaCl, 50 mM Tris pH 7.5, 1% NP-40, 10% glycerol, 2 mM MgCl₂) GST-fusion proteins were bound to glutathione-Sepharose beads (Novagen), eluted in 50 mM Tris, pH 8, 20 mM glutathione and dialysed against buffer C (20 mM Tris pH 7.5, 20% glycerol, 100 mM KCl, 0.2 mM EDTA, 2 mM DTT, 10 mM β -glycerophosphate).

For GST-pull-down experiments, GST-fusion proteins were bound to glutathione-Sepharose beads for 1h at RT in buffer A. Fresh platelet lysates were incubated with GST or GST-integrin cytoplasmic-domain fusion proteins for 4 h or overnight at 4°C. The glutathione-Sepharose beads were washed 4 times with buffer A containing 0,15% Triton X-100 and 10 mM EDTA. Bound proteins were eluted from the beads by boiling in SDS sample buffer following separation by a SDS-PAGE and Western blotting.

Antibodies. The E-selectin blocking mAb 9A9 (rat anti-mouse IgG1, 30 μ g per mouse) specifically blocks E-selectin dependent rolling *in vivo*² and was a gift from Dr. B. Wolitzky (Mitocor, San Diego, CA). The P-selectin mAb RB40.34 (rat anti-mouse IgG1, 30 μ g per mouse) blocks P-selectin-dependent leukocyte rolling *in vivo*² and was a gift from Dr. D. Vestweber (Max-Planck-Institute for Molecular Biomedicine, Münster, Germany).

Adhesion to ICAM-1, fibrinogen and immune complexes. 16-well glass chamber slides (NUNC) were coated with $2,5 \mu\text{g ml}^{-1}$ recombinant human intercellular adhesion molecule-1 (ICAM-1, R&D Systems) in coating buffer (150 mM NaCl, 20 mM Tris-HCl, 2 mM MgCl_2 , pH 9,0) over night at 4°C . Custom made glass bottom dishes were coated with immune complexes as follows; 5 mg ml^{-1} ovalbumin (Sigma, A5503) in PBS was incubated over night at 4°C . After washing three times with PBS, $25 \mu\text{g ml}^{-1}$ rabbit anti-chicken ovalbumin antiserum (Sigma) was added for one hour at room temperature and the dishes were washed three times with PBS. PMNs were isolated by flushing the bone marrow of *Kind3*^{+/+} or *Kind3*^{-/-} chimeric mice that were transplanted 4 to 5 weeks earlier as described³. Bone marrow cells were stained with Gr-1 fluorescein isothiocyanate (FITC) (clone RB6-8C5) and CD45.2 allophycocyanine (APC) (clone 104) monoclonal antibodies (both eBioscience) and double positive cells were purified using fluorescence activated cell sorting (FACS Aria, BD Biosciences). PMNs were either left untreated or stimulated with Phorbol-12-Myristate-13-Acetate (PMA, 33 ng ml^{-1} , Calbiochem) during the adhesion assay. After blocking the slides for 1 hour at room temperature with 10% bovine serum albumine (BSA) in phosphate buffered saline (PBS), 5×10^4 cells per well in cell culture medium (RPMI 1640, 10% FCS, 25 mM HEPES; all from GIBCO) were added and the slides were incubated for 30 min in a tissue culture incubator. To block Fc γ -receptor mediated adhesion on immune complexes incubation was performed in the presence of anti-Fc γ III/II receptor antibody (BD Biosciences - Pharmingen). Subsequently the slots were detached, slides were washed twice in PBS and fixed in 2,5% glutaraldehyde in PBS for 2 hours on ice. All conditions were performed in triplicates. After fixation the number of adherent cells was determined by acquisition of phase contrast pictures from each well and quantified using the integrated morphometry analysis module of MetaMorph software (Molecular Devices).

To test adhesion to fibrinogen, FACS sorted bone marrow derived PMNs were incubated with PBS containing 10 mM HEPES, $150 \mu\text{g ml}^{-1}$ Alexa 546-labelled fibrinogen (Invitrogen) and either 2 mM EDTA or 3 mM MnCl_2 for 30 min at room temperature. Cells were washed once in the same buffer without fibrinogen, taken up in 200 μl buffer and measured immediately by flow cytometry. Dead cells were excluded from the analysis by staining with propidium-iodide ($2,5 \mu\text{g ml}^{-1}$, Sigma).

Cell spreading and oxidative burst on immune complexes. Immune complexes were prepared as described above. PMNs were stimulated 15 min before and during the assay with 10 ng ml^{-1}

TNF- α in cell culture medium. 5×10^4 cells per dish were added and movies with a 10 sec frame rate acquired with an Axiovert 40 C inverted microscope (Zeiss) equipped with a LD A-Plan 20x/0,30 objective (Zeiss), a custom-built climate chamber, PAL cameras (Prosilica) and custom made software (SVS Vistek). Spread cells were counted manually. Differential interference contrast movies were acquired with a Zeiss Axiovert 200M microscope equipped with a Pln Apo 40x/0,95 objective (Zeiss) and a Coolsnap HQ2 camera (Roper scientific) automated by Metamorph software (Molecular Devices).

To test PMN activation by immune complexes *in vitro*, immobilized immune complexes were prepared by coating 96-well tissue culture plates as above. FACS sorted bone marrow derived PMNs were resuspended at a density of 2×10^6 cells per ml in phenol red-free RPMI medium 1640 (Invitrogen) containing 10% FCS (Invitrogen), 25 mM HEPES (Invitrogen) and 5 μ M dihydrorhodamine 6G (Invitrogen). Cells were either stimulated with 10 ng ml⁻¹ mouse TNF- α (Roche) and added to immobilized immune complexes or activated with 33 ng ml⁻¹ PMA (Calbiochem) and added to uncoated wells as positive control. TNF- α -stimulated PMNs plated on OVA-coated wells served as negative control. Each condition was measured in triplicates. The increase in fluorescence was measured over time at 37°C with a FLUOstar OPTIMA (BMG Labtech) fluorometer. For each time point, the mean fluorescence read on negative control coating was subtracted from the mean fluorescence induced by immune complex-coating or PMA stimulation. To compare independent experiments, oxidative burst responses were normalized to the maximum production of reactive oxygen species by WT neutrophils.

Skin inflammation model. Croton oil (Sigma-Aldrich) was diluted to 1% in acetone, and this dilution was topically applied to the ventral and the dorsal sides (20 μ l each) of the ears of *Kind3*^{+/+} and *Kind3*^{-/-} chimeric mice. After 4 h, mice were sacrificed and the earflaps were split into two halves by carefully separating the dorsal and ventral skin. For histological analysis, dorsal and ventral halves of ears were subjected to whole-mount immunostaining. After fixation in paraformaldehyde, ear halves were blocked in with 1% BSA (PAA Laboratories) in PBS for 1h at room temperature, probed with biotin-labeled anti-Gr-1 (RB6-8C5; BD Biosciences-Pharmingen) to identify PMNs and anti-pan-laminin (L9393; Sigma-Aldrich) to visualize the endothelial basement membrane, diluted in 1% BSA in PBS overnight at 4°C (with shaking), and washed with 1% BSA in PBS. Antibodies were detected with a repeated cycle of staining with anti-rabbit Alexa Fluor 488 (Invitrogen) and anti-rat Cy3 (Dianova) before tissue was embedded

in evanol and representative images taken with a Zeiss Axio Imager equipped with an ApoTome (Zeiss).

Supplementary references

1. Ussar, S., Wang, H.V., Linder, S., Fassler, R. & Moser, M. The Kindlins: subcellular localization and expression during murine development. *Exp Cell Res* **312**, 3142-3151 (2006).
2. Sperandio, M., *et al.* Severe impairment of leukocyte rolling in venules of core 2 glucosaminyltransferase-deficient mice. *Blood* **97**, 3812-3819 (2001).
3. Montanez, E., *et al.* Analysis of integrin functions in peri-implantation embryos, hematopoietic system, and skin. *Methods Enzymol* **426**, 239-289 (2007).

Supplementary Video 1

Cell spreading on immobilized immune complexes. Spreading of *Kindlin3*^{+/+} and *Kindlin3*^{-/-} PMNs was observed by differential interference contrast microscopy.

Supplementary Video 2

Leukocyte rolling and adhesion in control fetal liver cell chimeras. Intravital transillumination microscopy was used to visualize leukocyte rolling and adhesion in TNF- α -stimulated cremaster muscle venules of *Kindlin3*^{+/+} chimeric mice. Note the abundance of leukocytes firmly adherent on the inflamed endothelium and the rather low number of rolling leukocytes.

Supplementary Video 3

Leukocyte rolling and adhesion in *Kindlin3*^{-/-} fetal liver cell chimeras. Leukocyte rolling and adhesion in TNF- α -stimulated cremaster muscle venules of *Kindlin3*^{-/-} mice was observed by intravital microscopy. Due to the severe adhesion defect in *Kindlin3*^{-/-} mice, leukocyte adhesion is rare while many rolling leukocytes are seen.

Supplementary Video 4

Leukocyte adhesion in *Kindlin3*^{+/+} fetal liver cell chimeras after blocking leukocyte rolling. Leukocyte adhesion was recorded in TNF- α -stimulated cremaster muscle venules of *Kindlin3*^{+/+} chimeric mice five minutes after injection of anti-E-selectin blocking mAb 9A9 and anti-P-selectin blocking mAb RB40.34. Leukocyte rolling is completely absent, while a significant number of leukocytes is still firmly adherent on the inflamed endothelium.

Supplementary Video 5

Leukocyte adhesion in *Kindlin3*^{-/-} fetal liver cell chimeras after blocking leukocyte rolling. Five minutes after systemic injection of anti-E-selectin blocking mAb 9A9 and anti-P-selectin blocking mAb RB40.34 into *Kindlin3*^{-/-} chimeric mice, leukocyte rolling was completely blocked in TNF- α -stimulated cremaster muscle venules. In contrast to *Kindlin3*^{+/+} chimeric mice, leukocyte adhesion is almost completely absent in *Kindlin3*^{-/-} chimeras illustrating the crucial role of Kindlin-3 for firm leukocyte adhesion.

Supplementary Video 6

Chemokine-induced leukocyte arrest in *Kindlin3*^{+/+} fetal liver cell chimeras following systemic injection of CXCL1. Leukocyte adhesion and rolling was recorded before, during, and after injection of 600 ng CXCL1. Application of CXCL1 (indicated by the appearance of a white square) into *Kindlin3*^{+/+} mice led to a significant increase in leukocyte adhesion accompanied by a dramatic drop in leukocyte rolling.

Supplementary Video 7

Chemokine-induced leukocyte arrest in *Kindlin3*^{-/-} fetal liver cell chimeras following systemic injection of CXCL1. In contrast to *Kindlin3*^{+/+} mice, leukocyte adhesion and rolling in *Kindlin3*^{-/-} mice were similar before, during (indicated by the white square), and after injection of 600 ng CXCL1 demonstrating that Kindlin-3 is essential in mediating chemokine-triggered firm leukocyte arrest *in vivo*.

PAPER III

Kindlin-3–mediated signaling from multiple integrin classes is required for osteoclast-mediated bone resorption

Sarah Schmidt,¹ Inaam Nakchbandi,^{1,2} Raphael Ruppert,¹ Nina Kawelke,^{1,2} Michael W. Hess,³ Kristian Pfaller,³ Pierre Jurdic,⁴ Reinhard Fässler,¹ and Markus Moser¹

¹Max Planck Institute of Biochemistry, D-82152 Martinsried, Germany

²University of Heidelberg, D-69120 Heidelberg, Germany

³Innsbruck Medical University, Division of Histology and Embryology, A-6020 Innsbruck, Austria

⁴University of Lyon, Ecole Normale Supérieure de Lyon, 69364 Lyon, France

The blood cell-specific kindlin-3 protein is required to activate leukocyte and platelet integrins. In line with this function, mutations in the *KINDLIN-3* gene in man cause immunodeficiency and severe bleeding. Some patients also suffer from osteopetrosis, but the underlying mechanism leading to abnormal bone turnover is unknown. Here we show that kindlin-3–deficient mice develop severe osteopetrosis because of profound adhesion and spreading defects in bone-resorbing osteoclasts. Mechanistically, loss of kindlin-3 impairs the activation of

$\beta 1$, $\beta 2$, and $\beta 3$ integrin classes expressed on osteoclasts, which in turn abrogates the formation of podosomes and sealing zones required for bone resorption. In agreement with these findings, genetic ablation of all integrin classes abolishes the development of podosomes, mimicking kindlin-3 deficiency. Although loss of single integrin classes gives rise to podosomes, their resorptive activity is impaired. These findings show that osteoclasts require their entire integrin repertoire to be regulated by kindlin-3 to orchestrate bone homeostasis.

Introduction

Integrins are α/β heterodimeric cell surface receptors that bind extracellular matrix proteins and cell counter receptors. A hallmark of integrins is their ability to reversibly shift between different affinity states for their ligands. The shift from an inactive to an active conformation is triggered by the direct binding of talin and kindlin to the cytoplasmic domains of $\beta 1$, $\beta 2$, and $\beta 3$ integrins, and is called integrin inside-out signaling (Moser et al., 2009b). Active integrins recruit and assemble large multimolecular complexes at their short cytoplasmic domains controlling several cellular processes such as organization of the cytoskeleton, migration, proliferation, differentiation, and apoptosis (integrin outside-in signaling; Legate et al., 2009).

Correspondence to Markus Moser: moser@biochem.mpg.de

Abbreviations used in this paper: AP, alkaline phosphatase; FAK, focal adhesion kinase; GAPDH, glyceraldehyde 3-phosphate dehydrogenase; LAD, leukocyte adhesion deficiency; M-CSF, macrophage-colony stimulating factor; MMP, matrix metalloproteinase; ON, overnight; OPG, osteoprotegerin; pQCT, peripheral quantitative computer tomography; PTH, parathyroid hormone; RANKL, receptor activator of nuclear factor κB ligand; TRAP, tartrate-resistant acid phosphatase; WASp, Wiskott-Aldrich syndrome protein.

Kindlins are a family of evolutionary conserved, intracellular FERM (4.1, ezrin, radixin, moesin) domain-containing proteins that are recruited to integrin adhesion sites (Moser et al., 2009b). Mammals have three members, called kindlin-1, -2, and -3. In contrast to the widely expressed kindlin-1 and -2, kindlin-3 expression is restricted to hematopoietic cells (Weinstein et al., 2003; Ussar et al., 2006). The importance of kindlin-3 for integrin activation in vivo was first described in kindlin-3–deficient mice, which suffer from bleeding and leukocyte adhesion defects (Moser et al., 2008, 2009a). Further cellular and molecular analyses of mouse and human blood cells revealed that kindlin-3 is required for activation of $\alpha IIb\beta 3$ on platelets and $\beta 2$ integrins on leukocytes (Moser et al., 2009b). Based on these findings, several groups identified mutations in the human kindlin-3 gene in patients with leukocyte adhesion deficiency (LAD) type III syndrome, which

© 2011 Schmidt et al. This article is distributed under the terms of an Attribution-Noncommercial-Share Alike-No Mirror Sites license for the first six months after the publication date (see <http://www.rupress.org/terms>). After six months it is available under a Creative Commons License (Attribution-Noncommercial-Share Alike 3.0 Unported license, as described at <http://creativecommons.org/licenses/by-nc-sa/3.0/>).

Supplemental Material can be found at:
<http://jcb.rupress.org/content/suppl/2011/02/28/jcb.201007141.DC1.html>

is characterized by recurrent bacterial and fungal infections and severe bleeding (Kuijpers et al., 2009; Malinin et al., 2009; Moser et al., 2009a; Svensson et al., 2009). In addition to the severe platelet and leukocyte dysfunction, increased bone mass was observed in several LAD-III patients (Kilic and Etzioni, 2009; McDowall et al., 2010; Sabnis et al., 2010). It was recently proposed that the osteopetrosis is caused by increased osteogenic potential of mesenchymal stem cells (Malinin et al., 2009).

Bone remodeling depends on a tight interplay of osteoblasts that form bone and osteoclasts that resorb bone. Osteoblasts are derived from mesenchymal stem cells and cluster their integrins in adhesion sites termed focal adhesions (FAs). Osteoclasts are large, multinucleated cells that derive from the monocyte lineage and arrange their integrins in adhesion structures called podosomes. Podosomes contain a dotlike core of actin filaments, which is perpendicularly oriented to the plasma membrane and surrounded by a ringlike arrangement of adhesion, adaptor, and signaling molecules such as integrins, paxillin, vinculin, talin, protein kinases, and actin-associated molecules (Linder and Kopp, 2005). Podosomes are found in all cells of the monocytic cell lineage (macrophages, dendritic cells, etc.), smooth muscle cells, endothelial cells, src-transformed fibroblasts, and certain epithelial cells (Linder and Aepfelbacher, 2003). Bone-resorbing osteoclasts arrange their podosomes by interconnecting the actin cytoskeleton into densely packed rings called sealing zones. They delineate the active sites of bone resorption and form a pocket, into which protons and bone-resorbing proteases are secreted (Luxenburg et al., 2007). Sealing zones are attached to the bone matrix via $\alpha v \beta 3$ integrin. Although mature osteoclasts express integrins of the $\beta 1$, $\beta 2$, and αv families, it is believed that $\alpha v \beta 3$ integrins are the major adhesion proteins in osteoclast biology. This observation is largely based on the matrix degradation defects observed in Glanzmann patients or mice carrying null mutations in the $\beta 3$ integrin gene. The reduced resorptive activity was thought to be caused by loss of $\alpha v \beta 3$ -mediated signaling that regulates cell polarity and cytoskeletal reorganization (McHugh et al., 2000; Faccio et al., 2003a). It cannot be excluded, however, that $\beta 1$ and/or $\beta 2$ integrins also play a role in osteoclast-mediated bone resorption in vivo (Helfrich et al., 1996; Rao et al., 2006).

Increased bone mineralization has been proposed to be the cause for the osteopetrosis in LAD-III patients (Malinin et al., 2009). It remains unclear, however, whether loss of kindlin-3 is indeed responsible for the increased bone mass and whether this bone abnormality is caused by an osteoblast and/or osteoclast dysfunction. In this paper, we find that kindlin-3-deficient mice develop a severe osteopetrotic phenotype caused by osteoclast dysfunctions. We show that kindlin-3-deficient osteoclasts fail to activate all their integrin classes, which in turn leads to their inability to spread and reorganize the actin cytoskeleton, as well as a failure to form podosomes and sealing zones and to degrade bone matrix. Our results indicate that all integrin classes are required for osteoclast-mediated bone resorption.

Results

Kindlin-3-deficient mice develop severe osteopetrosis

Kindlin-3-deficient (kindlin-3^{-/-}) mice die a few days after birth because of a severe anemia caused by massive bleeding and erythrocyte defects (Krüger et al., 2008; Moser et al., 2008). To analyze whether kindlin-3 affects bone development, we performed histology and peripheral quantitative computer tomography (pQCT) on long bones from kindlin-3^{-/-} mice. At postnatal day 4 (P4), kindlin-3^{-/-} bones showed a significant increase in trabecular bone accompanied by a marked decrease in bone marrow (Fig. 1 A). Van Kossa staining showed increased calcified bone (Fig. 1 B). pQCT analysis confirmed a significant increase in bone mineral density (BMD; Fig. 1 C). Bone surface as determined by static histomorphometry was markedly increased in the absence of kindlin-3 (Fig. 1 D).

To define the onset of the osteopetrosis, we compared the histology of control and mutant long bones from different developmental stages. At embryonic day 14 (E14), long bones from kindlin-3^{-/-} embryos showed normal primary ossification centers surrounded by a normal coat of membranous bone (Fig. S1 A). At E16, kindlin-3^{-/-} bones displayed increased ossification, and at birth, the bone mass further increased at the expense of the bone marrow cavity (Fig. S1 A). Alkaline phosphatase (AP) staining of osteoblasts and tartrate-resistant acid phosphatase (TRAP)-positive osteoclasts did not significantly differ between control and mutant bones at E14, E16, and P1 (Fig. S1, A and B).

Loss of kindlin-3 leads to severe osteoclast dysfunction

It has been proposed that a dysfunction of osteoblasts is responsible for increased bone density in LAD-III patients (Malinin et al., 2009). To test whether this is also the case in kindlin-3^{-/-} mice, we performed histomorphometric analysis, which showed normal osteoblast numbers per unit of bone surface in kindlin-3^{-/-} bones (Fig. S2 A). Calvaria-derived osteoblasts isolated from wild-type and kindlin-3^{-/-} pups revealed comparable levels of gene expression for osteoblastic markers such as AP, osteocalcin, and collagen I as well as normal AP activity (Fig. S2, B, D, and E). Furthermore, the generation of mineralized bone nodules in vitro was similar in osteoblasts from both genotypes (Fig. S2, F–H). Finally, and in line with the normal biological activity of kindlin-3^{-/-} osteoblasts, wild-type osteoblasts expressed kindlin-2 but neither kindlin-3 nor kindlin-1 (Fig. S2 C).

To determine whether osteoclasts are defective, we performed TRAP staining and histomorphometric measurements of P4 kindlin-3^{-/-} bones, which revealed that the number of TRAP-positive osteoclasts per bone surface was significantly increased by more than threefold (Fig. 1, E and F). Despite the elevated number of osteoclasts, the surface covered by osteoclasts was significantly decreased in kindlin-3^{-/-} bones (Fig. 1 G). Consistent with the failure to erode bone, Ca²⁺ levels in the serum of kindlin-3^{-/-} mice were significantly decreased (Fig. 1 H), and parathyroid hormone (PTH) levels were increased (Fig. 1 I). Indeed, cultured osteoclasts differentiated from wild-type blood

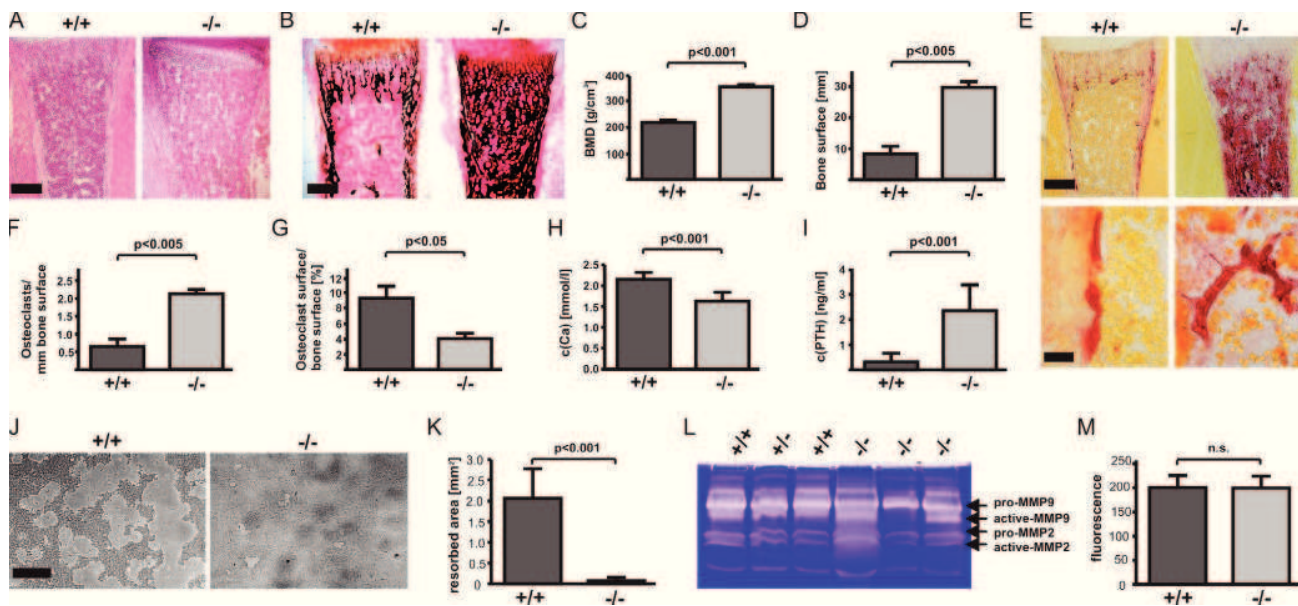


Figure 1. Kindlin-3^{-/-} mice develop severe osteopetrosis. (A and B) Histology of tibiae of P4 wild-type and kindlin-3^{-/-} mice stained with hematoxylin and eosin (A) and van Kossa (B). (C and D) Quantitative peripheral computer tomography measurements determining bone mineral density (C) and histomorphometric analysis to determine bone surface from bones of P4 wild-type and kindlin-3^{-/-} mice (D); *n* = 3. (E) Histology of tibiae of P4 wild-type and kindlin-3^{-/-} mice stained for TRAP activity. (F and G) Histomorphometric analyses determining the number of osteoclasts (F) and surface covered by osteoclasts (G) of wild-type and kindlin-3^{-/-} mice; *n* = 3. (H) Ca²⁺ levels in serum of P4 wild-type and kindlin-3^{-/-} mice; *n* = 8. (I) PTH levels in plasma of P3 wild-type and kindlin-3^{-/-} mice; *n* = 10. (J and K) Resorption pits (J) and their quantification (K) of wild-type and kindlin-3^{-/-} osteoclasts cultured on calcium apatite coated slides; *n* = 7. (L) Zymography of cell culture supernatants from primary wild-type and kindlin-3^{-/-} osteoclasts. (M) Cathepsin K activity from lysates of primary wild-type and kindlin-3^{-/-} osteoclasts. Data are presented as mean ± SD (error bars). P-values indicate significant differences from wild-type (Student's *t* test). n.s., not significant. Bars: (A and B) 250 μm; (E, top) 250 μm; (E, bottom) 25 μm; (J) 100 μm.

precursors expressed high levels of kindlin-3 but neither kindlin-1 nor -2 (Fig. 2 B and Fig. S2 C).

These data suggest that kindlin-3^{-/-} osteoclasts are functionally impaired. To address this finding, we tested the resorptive activity of kindlin-3^{-/-} osteoclasts by seeding them on an artificial calcified matrix (osteologic slides) as well as dentin discs. Although wild-type osteoclasts resorbed large areas of mineralized matrix, kindlin-3^{-/-} osteoclasts were incapable of doing so (Fig. 1 J and not depicted). Morphometric image analysis of the resorbed areas revealed that resorption by kindlin-3^{-/-} osteoclasts was >20-fold lower than wild-type cells (Fig. 1 K). The profound resorption defects were not accompanied by diminished secretion of proteolytic enzymes, as secretion of matrix metalloproteinase 2 (MMP2) and -9 and cathepsin K activities were indistinguishable between control and kindlin-3^{-/-} osteoclasts (Fig. 1, L and M).

Altogether, these findings indicate that osteopetrosis in kindlin-3^{-/-} mice is caused by a dysfunction of osteoclasts rather than osteoblasts.

Kindlin-3 is not required for osteoclast differentiation

Osteoclasts originate from monocytic precursors in response to the actions of macrophage-colony stimulating factor (M-CSF) and receptor activator of nuclear factor κB ligand (RANKL; Teitelbaum and Ross, 2003). Although the serum levels of M-CSF were similar (unpublished data), circulating levels of RANKL were increased eightfold in kindlin-3^{-/-} mice (Fig. 2 A). Serum concentrations of

osteoprotegerin (OPG), an inhibitor of RANKL, were similar between wild-type and kindlin-3^{-/-} mice. Treatment of kindlin-3^{-/-} osteoclasts with RANKL *in vitro* induced a strong and sustained p38 and JNK phosphorylation that was comparable to wild-type osteoclasts (Fig. S3). The high levels of RANKL in the serum and the normal response to RANKL by kindlin-3^{-/-} osteoclasts provides a plausible explanation for the increased osteoclastogenesis in kindlin-3^{-/-} bones.

M-CSF and RANKL treatment induced the expression of osteoclastogenic markers such as cathepsin K, MMP9, and calcitonin receptor in wild-type and kindlin-3^{-/-} fetal liver cells (Fig. 2 B). Even though induction of marker gene expression was slightly delayed in kindlin-3^{-/-} cells, they nevertheless reached wild-type levels 6 d after cytokine treatment (Fig. 2 B). It should be noted that the expression of kindlin-3 remained stable throughout the differentiation period, and that kindlin-1 and -2 were expressed in neither wild-type nor kindlin-3^{-/-} cells upon cytokine treatment (Fig. 2 C).

Finally, we determined the number of nuclei in the osteoclasts as a marker for pre-osteoclast fusion and differentiation. Notably, *in vitro* generated kindlin-3^{-/-} osteoclasts showed a lower tendency to form larger (>20 nuclei) polykaryons (Fig. 2 D), presumably because of decreased adhesion and cell spreading; however, a significant shift toward more multinucleated osteoclasts was detected in bone sections from kindlin-3^{-/-} mice (Fig. 2 E). This discrepancy can be explained by the increased number of osteoclast precursors triggered by the elevated RANKL levels in kindlin-3^{-/-} mice.

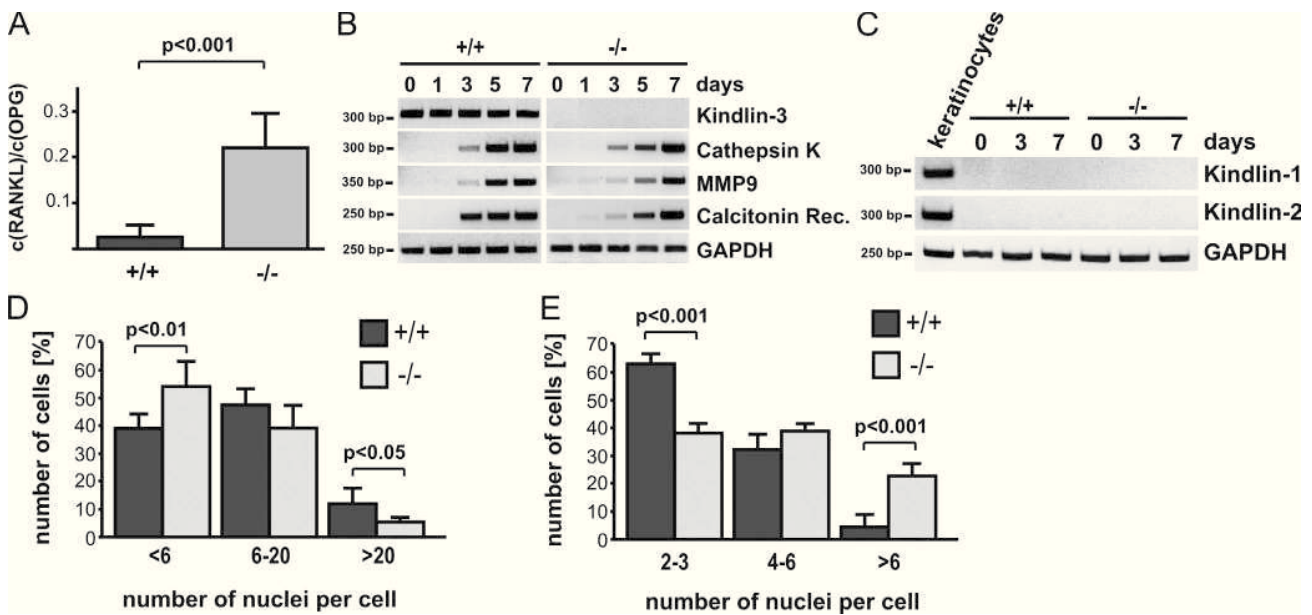


Figure 2. **Differentiation of kindlin-3^{-/-} osteoclasts.** (A) RANKL/OPG ratio in plasma of P3 wild-type and kindlin-3^{-/-} mice; $n = 11$. (B) RT-PCR of osteoclastogenic markers upon M-CSF and RANKL treatment of wild-type and kindlin-3^{-/-} fetal liver cells. (C) RT-PCR of kindlin-1 and -2 expression during in vitro osteoclast differentiation. RNA from keratinocytes served as positive control. (D) Number of nuclei per osteoclast 5 d after induction of differentiation; 1,004 cells of each genotype obtained from five independent experiments were analyzed. (E) Osteoclast nuclear numbers determined from histological sections of P4 tibiae. 63 and 252 osteoclasts from wild-type and kindlin-3^{-/-} bone sections were analyzed, respectively. Data are presented as mean \pm SD (error bars). P-values indicate significant differences from wild-type (Student's *t* test).

Altogether, these data suggest that although osteoclast differentiation is slightly delayed in the absence of kindlin-3 in vitro, it occurs efficiently in kindlin-3^{-/-} mice.

Kindlin-3 promotes osteoclast adhesion by regulating integrin activation

Kindlin-3 is required for the activation of integrins and integrin-mediated adhesion (Moser et al., 2008, 2009a). To evaluate osteoclast adhesion, we seeded wild-type and kindlin-3^{-/-} osteoclasts on osteopontin, a natural ligand for osteoclasts. Although wild-type osteoclasts adhered readily to osteopontin, kindlin-3^{-/-} osteoclasts showed significantly reduced adhesion (Fig. 3 A). Interestingly, kindlin-3^{-/-} osteoclasts adhered to both glass and cell culture plastic, particularly when cultured over several days. Because the transmembrane proteoglycan CD44 has also been shown to support osteoclast adhesion to osteopontin, fibronectin, collagen, and laminin (Goodison et al., 1999; Ponta et al., 2003), we hypothesized that CD44 might mediate the remaining osteoclast adhesion in the absence of kindlin-3. To test this hypothesis, we incubated pre-osteoclasts with a blocking anti-CD44 antibody and observed that the adhesion of kindlin-3^{-/-} cells to fibronectin was further reduced, which indeed indicates that CD44 contributes to osteoclast adhesion (Fig. S4, A and B).

To determine integrin expression, we measured their levels on macrophages, as the large size and strong adhesive properties of mature osteoclasts prevented their analysis by flow cytometry. Indeed, kindlin-3^{-/-} macrophages express ~76% and 63% of β 1 and β 3 integrins, respectively, when compared with wild-type macrophages. The expression of α v β 5, which

decreases during osteoclast maturation, and α 4 β 1, α 5 β 1, and α L β 2 were similar in wild-type and kindlin-3^{-/-} cells; however, α M β 2 was reduced to ~80% in kindlin-3^{-/-} cells. (Fig. 3 B and Fig. S4 C). Next, we addressed the affinity states of integrins by determining the binding of the 9EG7 antibody, which recognizes activated mouse β 1 integrins, and the binding of a fluorescently labeled FN fragment (FNIII7-10), which is bound by active α v (α v β 3 and α v β 5) and α 5 β 1 integrins. Resting kindlin-3^{-/-} macrophages failed to bind 9EG7 and showed considerably reduced FNIII7-10 binding, whereas MnCl₂ treatment, which can bypass inside-out-mediated integrin activation, markedly increased 9EG7 and FNIII7-10 binding (Fig. 3, C and D). Furthermore, adhesion to ICAM-1, a ligand for β 2 integrins, was strongly diminished in kindlin-3^{-/-} macrophages compared with control cells (Fig. 3 E). Manganese treatment only partially rescued the adhesion defect of kindlin-3^{-/-} cells, which suggests that kindlin-3 also operates in integrin outside-in signaling.

Collectively, these data indicate that loss of kindlin-3 results in a severe adhesion defect caused by impaired activation and outside-in signaling of β 1, β 2, and α v integrins.

Osteoclasts require kindlin-3 for integrin and growth factor signaling

Biochemical signaling events triggered by integrins and growth factor receptors control osteoclast adhesion, spreading, fusion, and differentiation (Ross and Teitelbaum, 2005). Wild-type osteoclasts generated from fetal liver cells differentiated into well-spread, multinucleated osteoclasts within 4–6 d of culture (Fig. 4 A). In contrast, kindlin-3^{-/-} fetal liver cells, which also

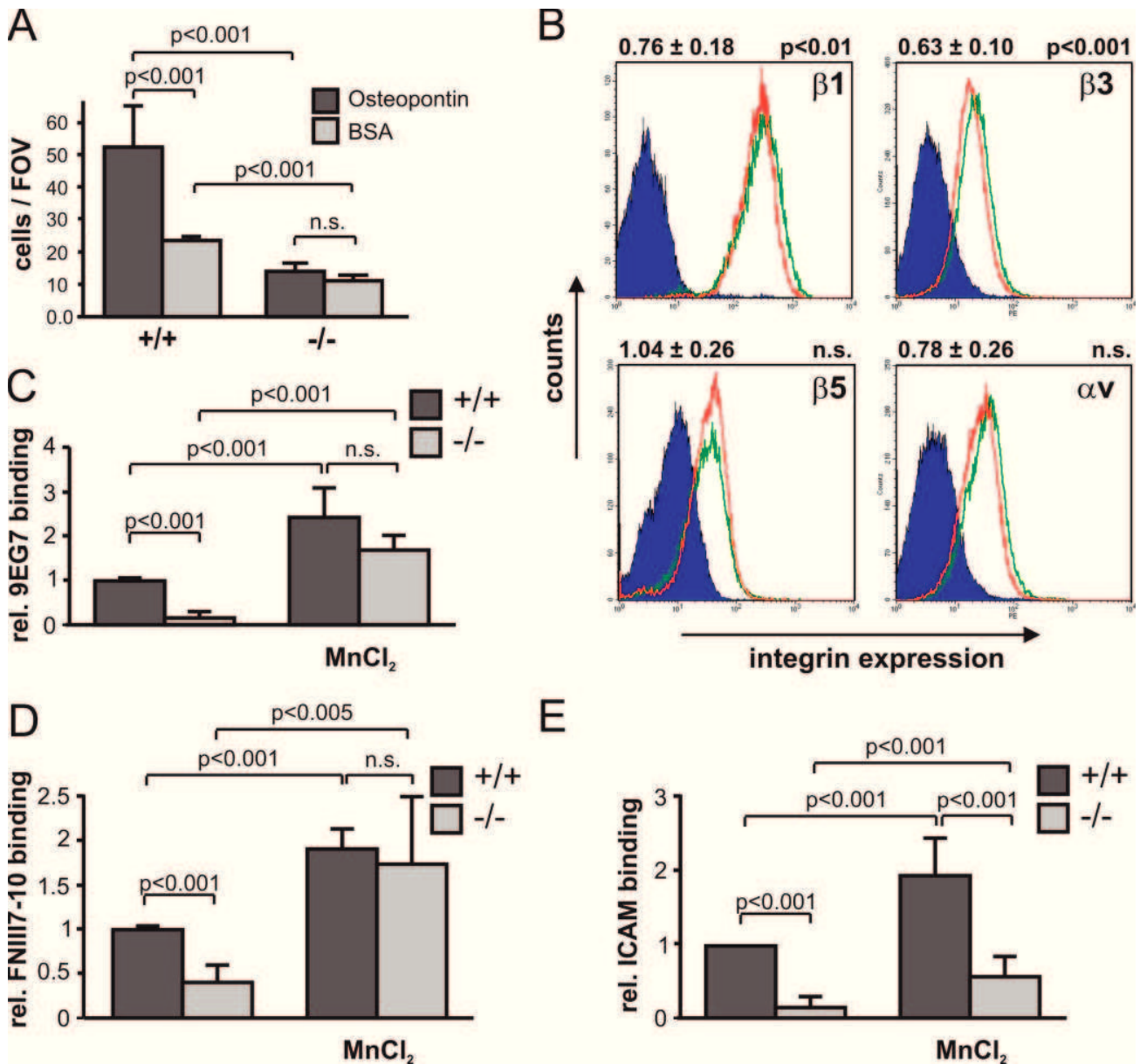


Figure 3. Integrin defects in kindlin-3^{-/-} osteoclasts. (A) Adhesion of primary wild-type and kindlin-3^{-/-} osteoclasts to osteopontin. Number of adherent cells per field of view (FOV) is shown. (B) Surface expression of β1, β3, β5, and αV integrins on wild-type (green) and kindlin-3^{-/-} (red) macrophages. Isotype control staining is shown in dark blue. Numbers above graphs indicate integrin expression on kindlin-3^{-/-} cells (mean ± SD) relative to wild-type cells (n = 6). (C) 9EG7 binding on wild-type and kindlin-3^{-/-} macrophages in the presence or absence of 2 mM MnCl₂. (D) Binding of Alexa Fluor 647-labeled FNIII7-10 by wild-type and kindlin-3^{-/-} macrophages in the presence or absence of 3 mM MnCl₂. Data show mean ± SD of four independent experiments and were subtracted by background binding of the isotype and EDTA control, respectively. (E) Wild-type and kindlin-3^{-/-} macrophages plated on ICAM-1 in the presence or absence of 1 mM MnCl₂. P-values indicate significant differences from wild-type (Student's *t* test).

produced multinucleated TRAP-positive cells, failed to spread (Fig. 4 A). Phalloidin staining showed an actin belt beneath the plasma membrane of control osteoclasts, whereas kindlin-3^{-/-} osteoclasts displayed randomly distributed actin patches in their cytoplasm (Fig. 4 B). Mn²⁺-mediated activation of integrins was unable to improve the spreading defect, suggesting that kindlin-3 is also required for integrin outside-in signaling, which is central in organizing the osteoclast cytoskeleton (unpublished data). Retroviral expression of EGFP-kindlin-3 into kindlin-3^{-/-} fetal liver cells rescued the formation of well-spread

osteoclasts. Notably, expression of integrin-binding mutant EGFP-kindlin-3 (EGFP-kindlin-3-QA; Moser et al., 2008) did not rescue osteoclast spreading, whereas fusion significantly improved compared with cells infected with a control virus (Fig. S5, A and B).

Next, we analyzed whether integrin-mediated adhesion signaling can still occur in the absence of kindlin-3. Adhesion on vitronectin triggered phosphorylation of c-Src and focal adhesion kinase (FAK) in wild-type pre-osteoclasts, but induced only a weak phosphorylation in kindlin-3^{-/-} pre-osteoclasts

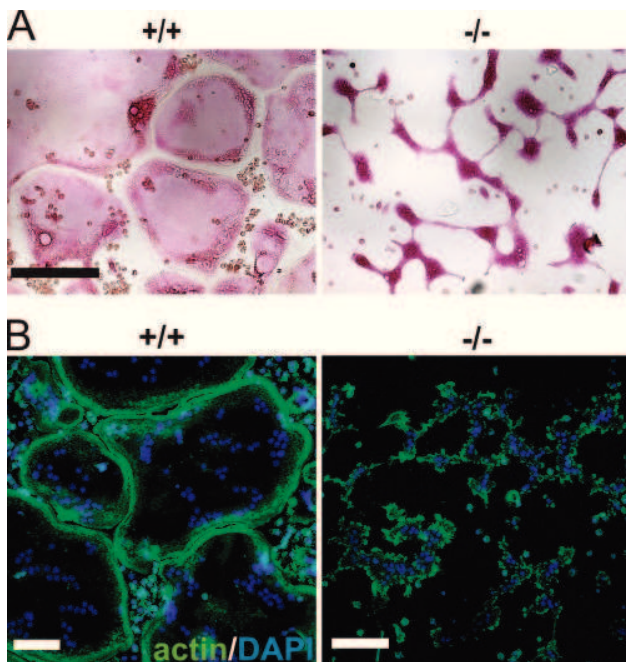


Figure 4. **Defective spreading of kindlin-3^{-/-} osteoclasts.** (A) Wild-type and kindlin-3^{-/-} osteoclasts grown on glass coverslips and stained for TRAP. (B) F-actin (stained with phalloidin, green) and nuclei (DAPI, blue) in wild-type and kindlin-3^{-/-} osteoclasts. Bars, 100 μ m.

(Fig. 5 A), further corroborating the finding that integrin-mediated signaling is severely compromised in the absence of kindlin-3. This weak activation is either triggered by integrin-independent signaling processes or by some residual integrin activity that exists even in the absence of kindlin-3.

A previous study demonstrated that loss of α v β 3 integrin function in osteoclasts can be compensated by high concentrations of M-CSF (Faccio et al., 2003b). To test whether kindlin-3 loss can also be overcome by high levels of cytokines, we treated wild-type and mutant fetal liver cells with RANKL and different concentrations of M-CSF. Wild-type fetal liver cells differentiated within 4 d into large, multinucleated osteoclasts when cultured at low M-CSF levels (20 ng/ml), whereas kindlin-3^{-/-} fetal liver cells rarely fused into polykaryons. High levels of M-CSF (100 ng/ml) rescued polykaryon formation but not the spreading defect of kindlin-3^{-/-} cells (Fig. 5 B). Moreover, although low levels of M-CSF failed to induce normal phosphorylation of Erk, Akt, and Syk in kindlin-3^{-/-} osteoclasts, high levels were able to induce normal phosphorylation of these signaling proteins (Fig. 5 C), which suggests normal differentiation of kindlin-3^{-/-} osteoclasts in the presence of high M-CSF levels.

Altogether, these findings show that kindlin-3 recruitment to integrins is required for their activation, actin reorganization, and cell spreading, as well as amplification of growth factor signaling in osteoclasts.

Kindlin-3 is required for the formation and arrangement of podosomes

Osteoclast adhesion is mediated by the formation of specialized adhesion structures called podosomes when they are cultured

on glass or bone matrix. Wild-type pre-osteoclasts were able to form typical podosomes consisting of a central actin core surrounded by a ring of adhesion molecules including α v β 3 and β 1 integrins, vinculin, paxillin, and talin (Fig. 6, A, C, and D; and not depicted). Kindlin-3^{-/-} cells formed small, actin core-like structures surrounded by a diffuse actin cloud. Vinculin, talin, and paxillin colocalized with the actin cloud, whereas α v and β 1 integrins were diffusely distributed throughout the plasma membrane (Fig. 6, A, C, and D; and not depicted). Fluorescence intensity profiling through actin-core units revealed that actin cores alternate with vinculin rings in wild-type podosomes, whereas this alternating pattern of actin and vinculin staining was lost in kindlin-3^{-/-} cells (Fig. 6 B). Approximately half (59.9% \pm 11.1%) of the actin dots from kindlin-3^{-/-} cells were depleted of vinculin and considered to be podosome structures even though a discrete vinculin ring was rarely observed. Re-expression of GFP-kindlin-3 into kindlin-3^{-/-} pre-osteoclasts restored the size of the F-actin dots and the ringlike distribution of vinculin around the F-actin cores (Fig. S5 C). On the contrary, the integrin-binding mutant EGFP-kindlin-3-QA did not rescue podosome formation in kindlin-3^{-/-} pre-osteoclasts and showed a diffuse distribution throughout the cell membrane when expressed in control pre-osteoclasts (Fig. S5 C). The percentage of cells that form normal podosomes was similar in EGFP-kindlin-3-expressing control and kindlin-3^{-/-} cells, whereas re-expression of the EGFP-kindlin-3-QA resulted in significantly fewer podosome-forming cells (Fig. S5 D). Re-expression of the integrin-binding mutant kindlin-3 did just partially improve the diffuse vinculin and F-actin localization in kindlin-3^{-/-} cells (Fig. S5 C). In line with the normal podosome formation in EGFP-kindlin-3-expressing kindlin-3^{-/-} cells, α v integrins colocalized with vinculin to podosome rings, whereas α v integrins were diffusely distributed in the membrane of kindlin-3^{-/-} cells expressing an EGFP-kindlin-3-QA construct (Fig. S5 E). Finally, the resorptive activity of kindlin-3^{-/-} osteoclasts expressing an EGFP-kindlin-3-QA was five times less compared with kindlin-3-deficient osteoclasts expressing wild-type EGFP-kindlin-3 (Fig. S5 F).

High-resolution scanning electron microscopy confirmed that kindlin-3^{-/-} osteoclasts were able to form small actin patches, which were surrounded by a loose network of radial actin fibers (Fig. 7 A). In sharp contrast, control osteoclasts formed large actin cores within podosome clusters, which were extensively interconnected by thick actin bundles (Fig. 7 A). Despite their smaller size, the actin cores of kindlin-3^{-/-} cells colocalized with cortactin, Arp2/3, and Wiskott-Aldrich syndrome protein (WASp), which are known core components of podosomes (Linder and Aepfelbacher, 2003), indicating that podosomal actin core formation occurs in the absence of kindlin-3 and activated integrins (Fig. 7, B–D).

Mature osteoclasts arrange their podosomes into different higher ordered structures. On glass, they form a ring at the periphery of the cell called the podosomal belt (Fig. 8 A); whereas on mineralized matrices, they form several smaller ringlike adhesion structures called sealing zones (Fig. 8 B; Jurdic et al., 2006). Kindlin-3^{-/-} osteoclasts were not able to form podosomal rings on glass surfaces or on sealing zones

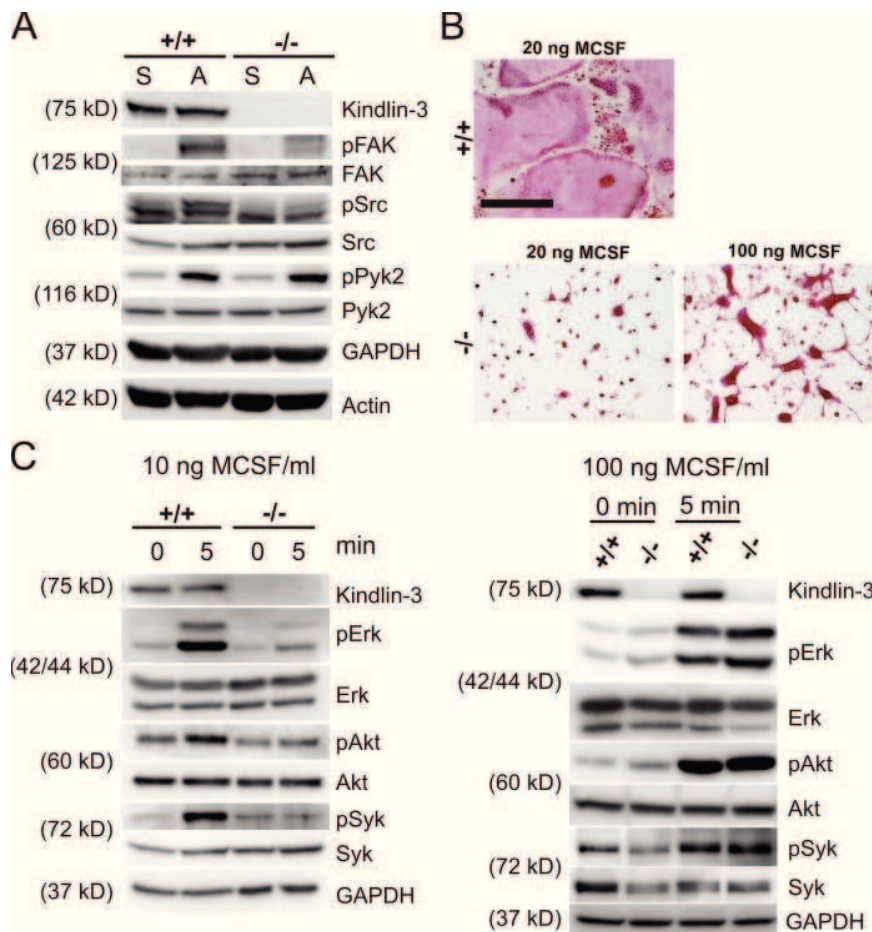


Figure 5. Impaired adhesion and M-CSF signaling in kindlin-3^{-/-} pre-osteoclasts. (A) Wild-type and kindlin-3^{-/-} pre-osteoclasts either maintained in suspension (S) or replated on vitronectin (A). Western blotting for kindlin-3, p-FAK, FAK, p-src, Src, p-Pyk2, and Pyk2. GAPDH and actin served as loading controls. (B) TRAP staining of wild-type and kindlin-3^{-/-} osteoclasts treated with 40 ng/ml RANKL together with either 20 ng/ml or 100 ng/ml M-CSF. Bar, 250 μ m. (C) Starved wild-type and kindlin-3^{-/-} osteoclasts treated with either 10 ng/ml or 100 ng/ml M-CSF. Western blotting for activated Erk and Akt. Activated Syk was determined by immunoprecipitation followed by immunoblotting with anti-phosphotyrosine (4G10) antibody.

on bone matrices. F-actin and vinculin often colocalized in patches and were usually localized to the cell periphery (Fig. 8, A and B). The formation of podosomal belts and sealing zones requires an intact microtubule network (Destaing et al., 2003, 2005). We therefore analyzed microtubule organization and acetylation by immunofluorescence microscopy and Western blot analysis. Both the total and acetylated microtubule pools were similar between kindlin-3^{-/-} and wild-type osteoclasts (Fig. 8, C and D). Furthermore, phosphorylation and the total amount of Pyk2, which is required for microtubule stability and acetylation in osteoclasts (Gil-Henn et al., 2007), were not altered in kindlin-3^{-/-} cells (Fig. 5 A), an observation that was also made in β 3 integrin-deficient osteoclasts (Faccio et al., 2003a).

These data indicate that kindlin-3 is not required for initial actin core formation. However, actin core maturation and interconnection, podosome formation, and their subsequent assembly into belts and sealing zones depend on kindlin-3.

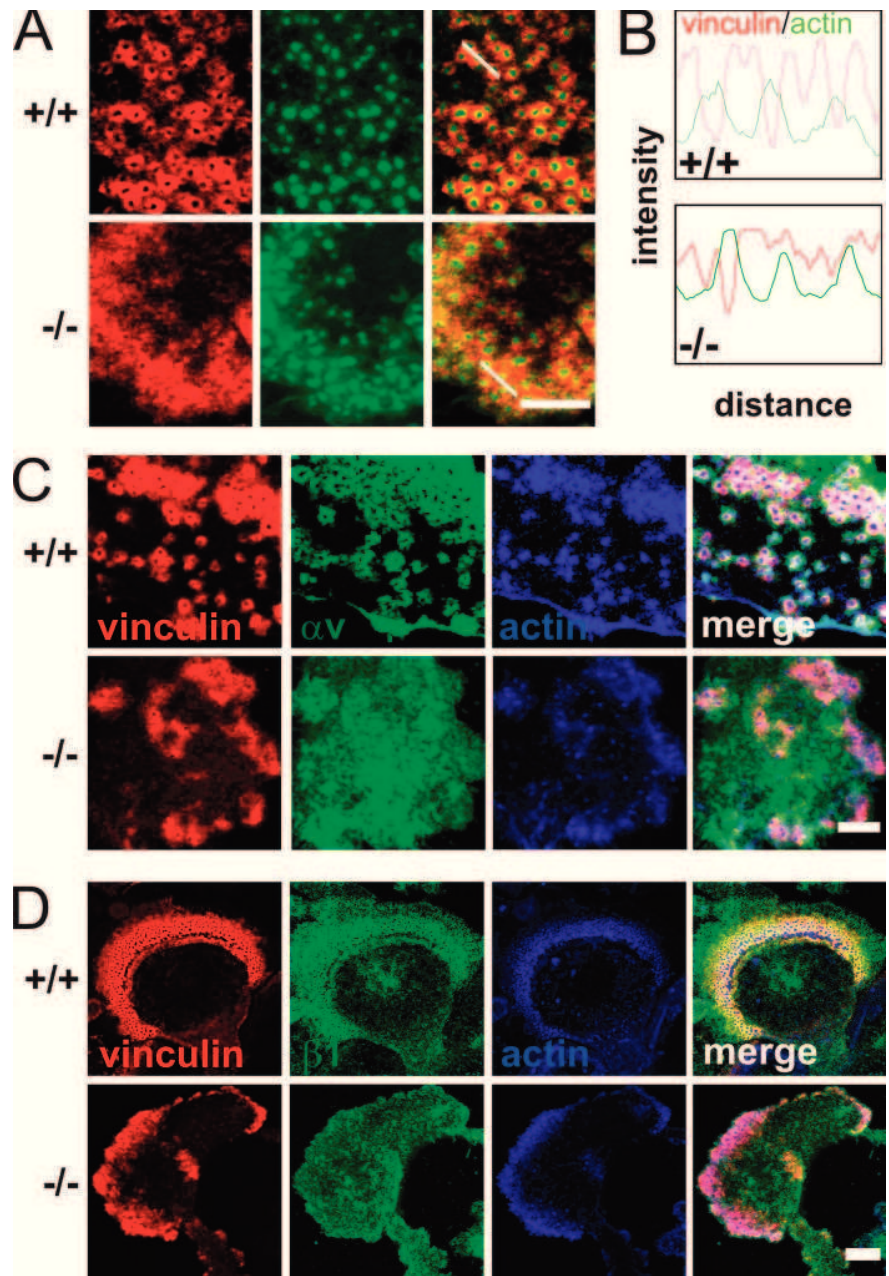
β 1, β 2, and α v integrin classes are required for normal osteoclast function

α v β 3 integrin is considered the major functional integrin on osteoclasts. In contrast to the severe osteopetrotic phenotype of kindlin-3-deficient mice, however, loss of α v β 3 leads to a mild and protracted osteopetrosis in mice and humans. This discrepancy

led us to hypothesize that additional integrins contribute to the kindlin-3^{-/-} osteoclast defect. To test this, we established osteoclast cultures from mice lacking the β 1, β 2, or α v integrin genes, respectively, and from mice lacking a combination of two or all three integrin genes. In addition, we generated osteoclasts from β 3 integrin-deficient mice to test whether other α v integrins in addition to α v β 3 play a significant role in osteoclast biology. Bone marrow cells with a single or α v/ β 1 or β 1/ β 2 double integrin-null mutation differentiated into multinucleated, spread, and TRAP-positive osteoclasts. Osteoclasts lacking both α v and β 2 integrins formed polykaryons but were less efficient in spreading and localizing their nuclei to the cell periphery (Fig. 9 A). Bone marrow cells lacking β 1/ β 2/ α v integrins were only able to form a few mono- and binucleated cells with TRAP activity, which suggests that loss of all integrin classes severely impairs osteoclastogenesis in vitro (Fig. 9 A). Notably, although these cells did not spread, they weakly adhered on glass.

Individual podosomes, podosome clusters, and podosome belts of β 1, β 2, and β 1/ β 2 double integrin-null cells were indistinguishable from wild-type cells. α v- and β 3-deficient cells showed smaller podosome clusters with irregular distributed podosome units (Fig. 9 B). Deletion of α v together with β 1 or β 2 integrins abolished cluster formation completely, and typical podosomes with a discrete vinculin ring were rarely

Figure 6. Impaired podosome formation in kindlin-3^{-/-} osteoclasts. (A) Vinculin (red) and F-actin staining (phalloidin, green) of pre-osteoclasts plated on glass coverslips and observed by confocal microscopy. (B) Fluorescence intensity profile through three actin-core units (indicated by the white lines in A) of wild-type and kindlin-3^{-/-} pre-osteoclasts. (C and D) vinculin (red) and F-actin staining (phalloidin, blue) together with α v integrin (green; C) or β 1 integrin (green; D). Bars (A and C) 5 μ m; (D) 10 μ m.



observed (Fig. 9 B). Similar to loss of kindlin-3, cells lacking β 1/ β 2/ α v integrins formed small actin dots lacking an adhesion ring (Figs. 9 B and 6 A). In agreement with these observations, we found that the diameter of the actin core was significantly smaller (\sim 650 nm) in podosomes from kindlin-3^{-/-}, β 1/ β 2/ α v triple-null, and α v/ β 1 and α v/ β 2 double-null pre-osteoclasts when compared with wild-type cells (\sim 800 nm) or cells with a single integrin or a double β 1/ β 2 integrin gene ablation (Fig. 9 C). Podosome belts of α v-deficient cells often failed to surround the entire cell and were significantly thinner than belts from β 3-deficient cells, which showed a belt size that was intermediate between control and α v-deficient osteoclasts (Fig. 9, D and E). α v/ β 1 as well as α v/ β 2 integrin-deficient osteoclasts showed even thinner

actin belts, which contained fewer and irregularly localized actin dots (Fig. 9, D and E).

Finally, we differentiated bone marrow-derived cells on a calcified matrix and evaluated their sealing zones and their capability to resorb matrix. The absence of a single integrin or the simultaneous loss of β 1 and β 2 still allowed sealing zone formation (Fig. 10 A), whereas the absence of α v together with either β 1 or β 2 integrins abolished the formation of a distinct ring (Fig. 10 A). The resorptive activity of α v/ β 1- and α v/ β 2-deficient osteoclasts was reduced to 30% of the wild-type level. Despite the presence of sealing zones in single integrin-null osteoclasts, their resorptive activity was diminished by 50%, indicating that each individual integrin family member contributes to functional sealing zone formation and bone degradation (Fig. 10 B).

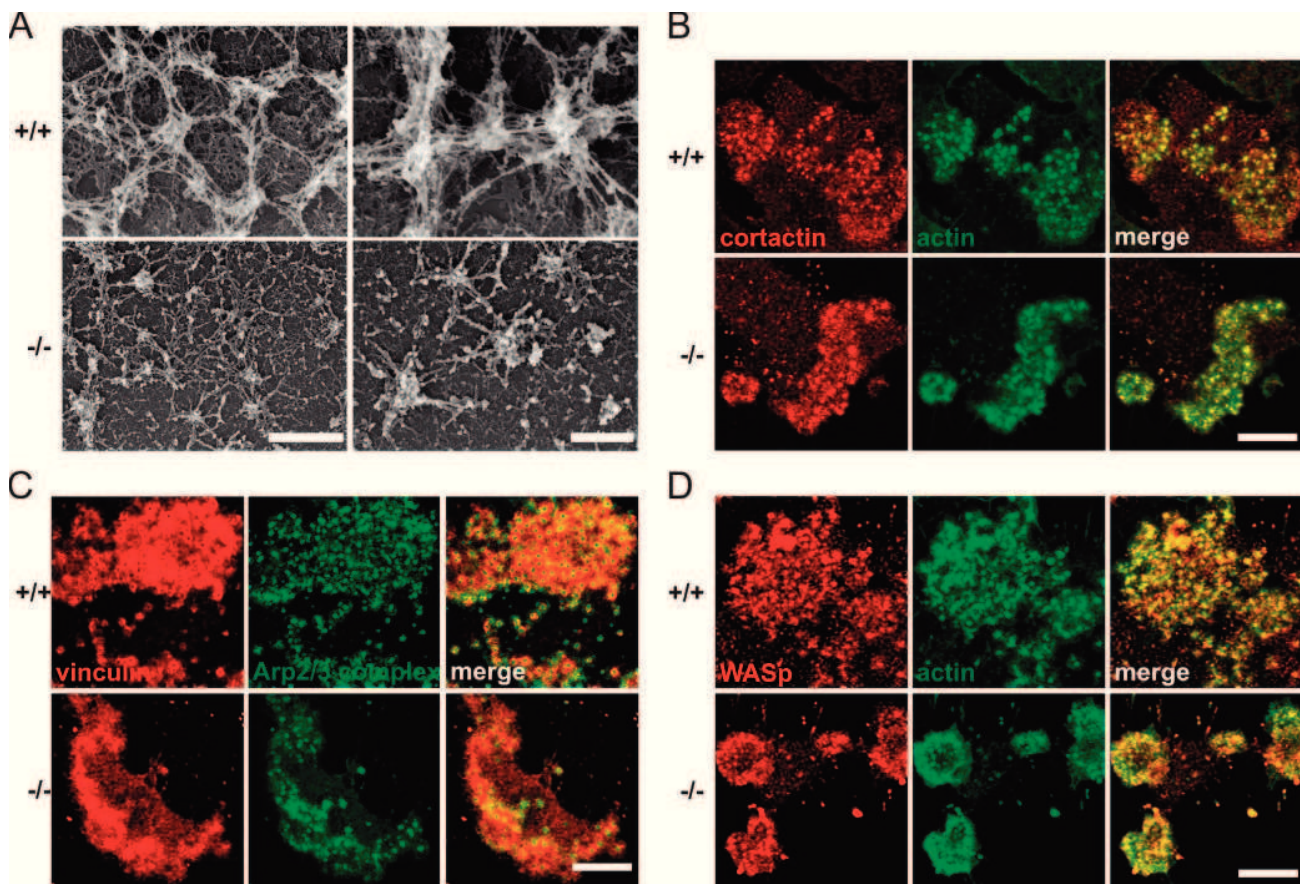


Figure 7. **Podosomal actin core formation is not abolished in kindlin-3^{-/-} cells.** (A) Scanning electron microscopy of basal membrane preparations of wild-type and kindlin-3^{-/-} osteoclasts. (B–D) Colocalization of cortactin (red) and F-actin (phalloidin, green; B), F-actin (red) and Arp2/3 (green; C), and WASp (red) and F-actin (green; D) in podosome clusters of wild-type and kindlin-3^{-/-} pre-osteoclasts analyzed by confocal microscopy. Bars: (A, left) 1 μ m; (A, right) 500 nm; (B–D) 10 μ m.

Discussion

Several LAD-III patients have displayed increased bone mineral density (Kilic and Etzioni, 2009; Malinin et al., 2009; McDowall et al., 2010; Sabnis et al., 2010), which points to the possibility that kindlin-3 plays a role in bone homeostasis. In search for an explanation of this observation, Malinin et al. (2009) reported that mesenchymal stem cells isolated from LAD-III patients produced significantly higher amounts of cartilage and bone in transplantation experiments, and concluded that the increased bone mass was caused by increased matrix deposition by hyperactive osteoblasts. Although kindlin-3 is highly and exclusively expressed in hematopoietic cells, osteoblasts express kindlin-2 but lack kindlin-3 expression, which suggests that the increased bone mass in LAD-III patients either developed independently of kindlin-3 or was caused by a dysfunction of a cell type other than osteoblasts. In this paper, we tested this hypothesis by analyzing bone formation in mice lacking kindlin-3.

Kindlin-3^{-/-} mice develop a severe osteopetrosis that is already apparent at birth. When we first analyzed the osteoblasts of kindlin-3-deficient mice *in vivo* and *in vitro*, we found that they appeared normal in terms of their numbers, morphological appearance, localization to the bone, expression of marker genes, and matrix production. The only abnormality we could

detect was a significantly elevated RANKL/OPG ratio in the serum of kindlin-3^{-/-} mice. RANKL secretion by osteoblasts is triggered in response to PTH, which is released by the parathyroid gland when serum Ca²⁺ levels decrease because of diminished bone resorption (Grant et al., 1990; Suda et al., 1999). An immediate consequence of high RANKL levels is enhanced differentiation of osteoclasts, which derive from the monocytic lineage and express high levels of kindlin-3. Indeed, we found reduced levels of Ca²⁺ and markedly increased levels of PTH in the blood of kindlin-3^{-/-} mice. Consistent with the high circulating RANKL levels, we found a dramatic increase in the number of multinucleated osteoclasts in bones of kindlin-3^{-/-} mice. These osteoclasts, however, completely failed to degrade bone matrix *in vitro*. In search for a mechanistic explanation for the dysfunction of kindlin-3^{-/-} osteoclasts, we identified several cellular defects that could be ascribed to kindlin-3's principal task to activate several classes of integrins and subsequently mediate their outside-in signaling properties.

Our findings show that differentiation of kindlin-3^{-/-} osteoclasts is slightly delayed and that fusion into multinucleated polykaryons is less efficient under *in vitro* conditions. However, the number of large polykaryons is significantly higher in kindlin-3^{-/-} bones. This is most likely caused by increased RANKL-induced osteoclastogenesis that compensates

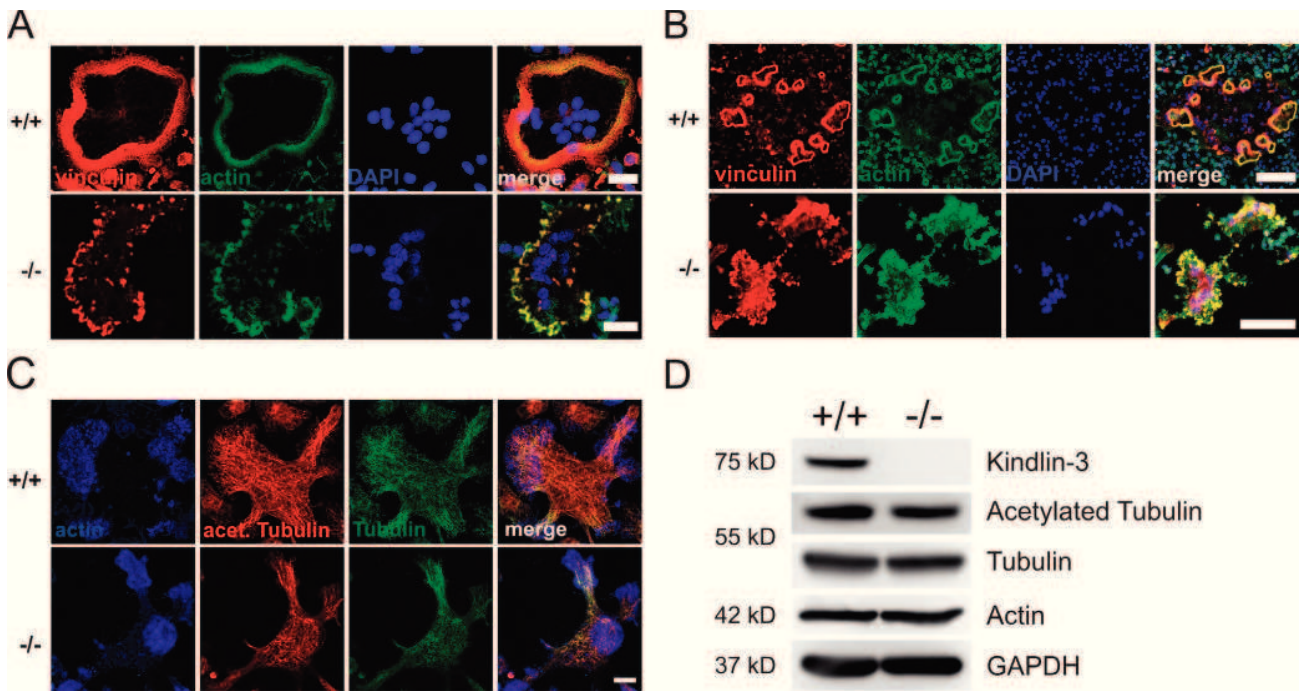


Figure 8. **Abnormal F-actin distribution but normal microtubule organization and acetylation in kindlin-3^{-/-} osteoclasts.** (A) Vinculin (red) and F-actin staining (phalloidin, green) of wild-type and kindlin-3^{-/-} osteoclasts plated on glass coverslips. (B) Vinculin (red) and F-actin staining (phalloidin, green) of wild-type and kindlin-3^{-/-} osteoclasts plated on mineral surface of osteologic slides. DAPI (blue) shows nuclei (A and B). (C) Wild-type and kindlin-3^{-/-} osteoclasts were labeled with phalloidin (blue), anti-acetylated tubulin (green), and anti-tubulin antibodies. (D) Cell lysates from wild-type and kindlin-3^{-/-} osteoclasts were immunoblotted with antibodies against kindlin-3, acetylated tubulin, and tubulin. Antibodies against actin and GAPDH were used as loading controls. Bars: (A) 25 μ m; (B) 100 μ m; (C) 10 μ m.

the fusion defects in vivo. Although TRAP-positive, multinucleated kindlin-3^{-/-} osteoclasts are present at very high numbers in kindlin-3^{-/-} mice, their shape and ability to adhere to bone surfaces is severely impaired. Similarly, adhesion to and binding of several extracellular matrix proteins and to ICAM-1 is also almost completely abrogated. We have previously shown that kindlin-3 interaction with β 1 and β 3 tails is required to activate

platelet integrins and that binding to β 2 tails is required to activate leukocyte integrins (Moser et al., 2008, 2009a). Our findings here demonstrate that this essential function of kindlin-3 is also conserved in osteoclasts. Osteoclasts require kindlin-3 to mediate β 1 and α v integrin binding to fibronectin and osteopontin and β 2 integrin binding to ICAM-1. This suggests that α v β 3 integrins, considered the most important integrin class

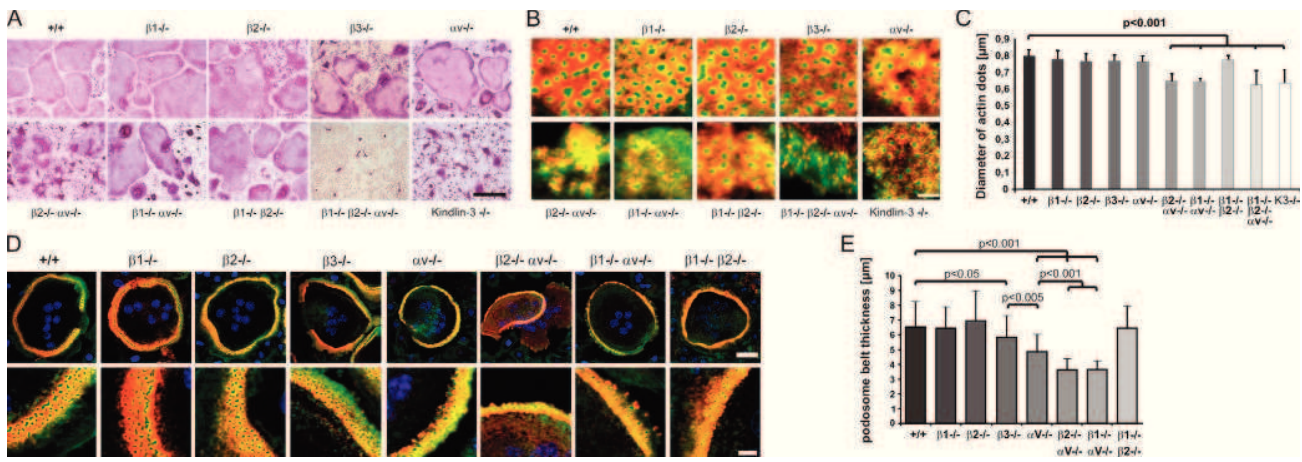


Figure 9. **Podosomes and actin belts in integrin-deficient osteoclasts.** (A) Wild-type and single, double, and triple integrin-deficient osteoclasts stained for TRAP. (B) Vinculin (red) and F-actin staining (phalloidin, green) of wild-type and integrin-deficient pre-osteoclasts plated on glass. (C) Diameters of actin dots in pre-osteoclasts with indicated genotypes measured using MetaMorph software; $n = 6/5/5/8/9/6/6/6/8/9$ different cells from each genotype taken to measure the actin core size. (D) Vinculin (red) and F-actin staining (phalloidin, green) of wild-type and integrin-deficient osteoclasts plated on glass. DAPI (blue) shows nuclei. (E) Diameter of podosomal belts of wild-type and integrin-deficient osteoclasts plated on glass. Data are presented as mean \pm SD (error bars). P-values indicate significant differences from wild-type (Student's *t* test). Bars: (A) 100 μ m; (B) 2 μ m; (D, top) 25 μ m; (D, bottom) 5 μ m.

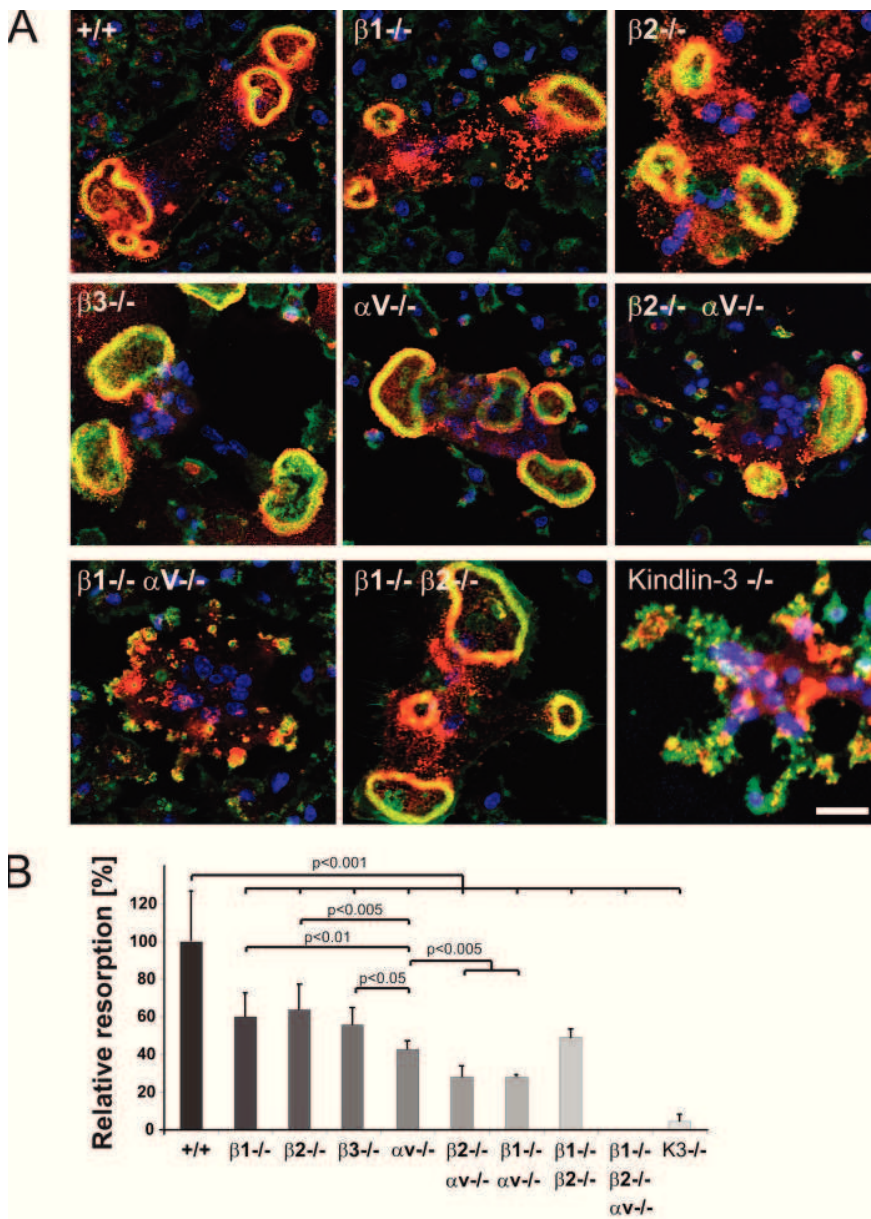


Figure 10. Sealing zones of integrin-deficient osteoclasts. (A) Vinculin (red) and F-actin staining (phalloidin, green) of wild-type and integrin-deficient osteoclasts plated on a mineral surface. DAPI staining (blue) shows nuclei. Bar, 25 μm. (B) Resorption activity of wild-type and integrin-deficient osteoclasts plated on calcium apatite-coated slides quantified with MetaMorph. Number of analyzed slides per genotype: n = 26/6/6/6/6/3/3/3/8. Data are presented as mean ± SD (error bars). P-values indicate significant differences from wild-type (Student's *t* test).

of osteoclasts, are just one of several integrin players during osteoclast-mediated bone resorption. This finding was corroborated by a series of genetic experiments in which we ablated several integrin genes either individually or in combination in osteoclasts. The experiments revealed an already strongly reduced resorptive activity of osteoclasts when the β1, β2, or αV integrin genes were individually ablated, and a further functional decline when two integrin classes were absent from osteoclasts. The finding that αV-deficient osteoclasts show a significantly more pronounced defect in matrix degradation compared with β3-deficient osteoclasts corroborates our hypothesis that other integrins beside αVβ3 also play an important role in osteoclast function. The ablation of all three integrin classes does not permit osteoclast development in vitro. This made it impossible to test their resorptive activity. In light of the severe defects in osteoclasts lacking two classes of integrins, it is fair

to assume that loss of all three integrin classes leads to a further impairment. These findings provide an explanation for the much more severe osteopetrotic phenotype of kindlin-3^{-/-} mice compared with β3 integrin mutants. Interestingly, in contrast to the failure of osteoclast differentiation in the absence of β1, β2, and αV integrins, kindlin-3 deficiency does not impair osteoclast differentiation both in vivo and in vitro. The reason for this observation is not clear. Because kindlins and talins shift the equilibrium of integrins toward their activation state, it is possible that certain processes such as cell fusion can proceed with just a few activated integrins and thus do not require the kindlin-3-mediated equilibrium shift, whereas other processes such as adhesion and podosome formation require a larger number of activated integrins. These questions can be addressed with osteoclasts of engineered mice carrying hypomorphic alleles for β1, β2, and αV integrins. If true, very low levels of integrins

should allow cell fusion but not bone resorption to proceed. An alternative scenario could be that cells that are plated for several days in the presence of serum and integrin ligands can activate integrins from outside and trigger integrin signaling even without efficient inside-out signaling. This is obviously not possible in the absence of all integrin classes.

Loss of kindlin-3 expression or a triple knockout of the $\beta 1$, $\beta 2$, and αv integrin genes is also accompanied by impaired podosome formation. Podosomes consist of an integrin ring and a central actin core. Interestingly, small actin cores containing core proteins such as cortactin, Arp2/3, and WASp form in kindlin-3-deficient osteoclasts. Similarly, $\beta 1/\beta 2/\alpha v$ -integrin deficient macrophages also form actin cores with a reduced diameter, indicating that the induction of actin polymerization occurs independently of integrin action, whereas their maturation requires an integrin signaling program. This observation is in agreement with previous studies showing that actin core formation and osteoclast adhesion to the substratum can also be mediated by the transmembrane proteoglycan CD44 in an integrin-independent manner (Chabadel et al., 2007). Actin cores lacking an adhesion ring are also found in c-src-deficient osteoclasts, which suggests that c-src activity is central for their maturation and acts as an upstream signaling molecule required for the assembly of integrins and cytoplasmic adhesion proteins (Destaing et al., 2008; Saltel et al., 2008).

Treatment of kindlin-3^{-/-} osteoclasts with Mn²⁺ significantly improved integrin-mediated adhesion but restored neither the defective F-actin reorganization nor podosome organization and assembly. This finding is in agreement with several reports demonstrating that kindlins mediate both inside-out as well as outside-in integrin signaling (Larjava et al., 2008; Moser et al., 2009b; Plow et al., 2009). Moreover, this interesting observation also indicates that integrin arrangement around F-actin cores cannot be accomplished solely by an active integrin; kindlin-3 and/or kindlin-3-associated proteins are required in addition. Another consequence of the abrogated integrin outside-in signaling in kindlin-3^{-/-} osteoclasts includes diminished FAK and Syk activation upon adhesion to extracellular matrix and impaired Erk and Akt phosphorylation that is seen only upon treatment with low concentrations of M-CSF, whereas high M-CSF levels are associated with normal Erk and Akt phosphorylation, indicating that integrin outside-in signals represent an amplifier of M-CSF-induced c-Fms signaling.

This study shows for the first time that osteoclast-mediated bone resorption depends on multiple integrin classes, which are under control of kindlin-3. Further work will be required to elucidate the individual contributions of each integrin subclass during podosome maturation and assembly, and whether certain signaling pathways that control the organization of the cytoskeleton and the formation of sealing zones are directed by specific integrins in osteoclasts.

Materials and methods

Reagents

Recombinant murine M-CSF and receptor activator of NF- κ B ligand (RANKL) were obtained from R&D Systems and PeproTech, respectively. Osteopontin was purified from bovine plasma (provided by D. Heinegård, University of Lund, Lund, Sweden; Franzén and Heinegård, 1985).

Mice

Kindlin-3^{-/-} and integrin $\beta 3$ ^{-/-} mice have been described previously (Hodivala-Dilke et al., 1999; Moser et al., 2008). Multiple integrins were deleted by intercrossing mice carrying conditional null mutations in the αv ($\alpha v^{\text{flox/flox}}$) and $\beta 1$ ($\beta 1^{\text{flox/flox}}$) genes (Potocnik et al., 2000), a constitutive null mutation in the $\beta 2$ ($\beta 2^{-/-}$) gene (Scharffetter-Kochanek et al., 1998), and the Mx1Cre transgene (Kühn et al., 1995). All mice were from a mixed 129/SvJxC57BL/6 background. Cre expression in the hematopoietic system was induced by a single intraperitoneal injection of 250 mg polyI/C (GE Healthcare). 7 d after polyI/C treatment, bone marrow cells were isolated and checked for integrin surface expression via FACS. All animals were kept under specific pathogen-free conditions at the animal facility of the Max Planck Institute of Biochemistry.

Antibodies

The following antibodies were used for immunostaining of cells: mouse anti- α -tubulin antibody, mouse anti-talin, mouse anti-cortactin, rabbit anti-actin, and mouse anti-acetylated tubulin (all from Sigma-Aldrich); rat anti-tubulin, rat anti-integrin $\beta 1$, and rat anti-integrin αv (all from Millipore); mouse anti-p-Tyrosine (clone pY99) and mouse anti-WASp (both from Santa Cruz Biotechnology, Inc.); rabbit anti-p16 subunit of Arp2/3 complex (Abcam); and FITC and Cy3-labeled secondary antibodies (Jackson ImmunoResearch Laboratories, Inc.). Phalloidin dyes were obtained from Invitrogen.

The following antibodies were used for flow cytometry: hamster IgG anti-integrin $\beta 1$, isotype control hamster IgG, and isotype control mouse IgG1 (all from Biologend); rat IgG2a anti-integrin $\beta 2$, rat IgG2a anti-integrin $\beta 7$, rat IgG2a anti-integrin $\alpha 4$, rat IgG2a anti-integrin $\alpha 5$, rat IgG2a anti-integrin αL , rat IgG1 anti-integrin αv , isotype control rat IgG1, isotype control rat IgG2a, and rat anti-integrin $\beta 1$ clone 9EG7 (all from BD); and hamster IgG anti-integrin $\beta 3$, mouse IgG1 anti-integrin $\beta 5$, and rat IgG2b anti-integrin αM , isotype control rat IgG2b (all from eBioscience).

The following antibodies were used for Western blotting: mouse anti-glyceraldehyde 3-phosphate dehydrogenase (anti-GAPDH; Merck); rabbit anti-actin and mouse anti-talin (both from Sigma-Aldrich); rabbit anti-JNK, rabbit anti-pJNK Thr183/Tyr185, rabbit anti-p38, rabbit anti-p38 Thr180/Tyr182, rabbit anti-pSrc Tyr418, rabbit anti-Pyk2, rabbit anti-pPyk2 Tyr402, rabbit anti-P42/44 MAPK, rabbit anti-pP42/44 MAPK Thr202/Tyr204, rabbit anti-Akt, and rabbit anti-pAkt Ser473 (all from Cell Signaling Technology); rabbit anti-FAK and rat anti-tubulin (both from Millipore); rabbit anti-pFAK Tyr397 and rabbit anti-src (both from Invitrogen); and mouse anti-Syk (Abcam).

Histology

Long bones were dissected, freed from soft tissue, and either embedded in plastic (Osteo-Bed Bone Embedding kit, Polysciences Inc.) or decalcified in 10% EDTA/PBS and embedded in paraffin. Paraffin sections were stained with hematoxylin and eosin and for TRAP activity using a commercial kit (Sigma-Aldrich). AP and van Kossa staining were performed according to standard protocols. The number of nuclei in osteoclasts was determined in plastic embedded bone sections from three different 4-d-old animals.

Pictures were taken by bright field microscopy with a microscope (Axioskop; Carl Zeiss, Inc.) equipped with a camera (DC500; Leica), 10x NA 0.3, 20x NA 0.50, and 40x NQ 0.75 objectives, and IM50 software. Pictures were edited with Photoshop (Adobe).

Measurement of RANKL, OPG, and PTH concentrations

Blood was collected from P2-P5 mice after decapitation using a microvette (CB 300 LH; Sarstedt); samples were then centrifuged for 3 min at 7,000 g and the plasma was harvested. The concentrations of RANKL and OPG were determined with ELISA kits from R&D Systems, and the intact PTH concentration was determined with an ELISA kit from Immotopics International.

Osteoclast culture

Osteoclasts were differentiated in vitro either from fetal liver cells or from bone marrow. E14.5 wild-type and kindlin-3^{-/-} fetal liver cells were obtained by pushing the fetal liver through a 70- μ m cell strainer (BD). The cells were kept in α -MEM supplemented with 20 ng/ml M-CSF overnight (ON). Nonadherent cells were collected after 24 h. Leukocytes were isolated from the interface after centrifugation at 1,000 g for 20 min in leukocyte separation medium (Laboratoires Eurobio), then washed with α -MEM medium and seeded at a concentration of 2,000 cells/mm² in osteoclast differentiation medium (α -MEM containing 10% heat inactivated FCS, 100 U/ml penicillin, and 100 μ g/ml streptomycin with 50 ng/ml M-CSF and 40 ng/ml RANKL). Cells were cultured at 37°C in 5% CO₂ for 5–8 d, and medium was changed every second day. Staining for TRAP

activity was performed after 5 d in culture. Pictures were taken with a microscope (Axioskop) using a 20x NA 0.50 objective (see Histology).

For pre-osteoclast generation, 5×10^6 interface cells were plated on a 10-cm dish and cultured in osteoclast differentiation medium for 2 d. Cells were washed with PBS and lifted with 10 mM EDTA in PBS. Adherent cells that were treated with osteoclast differentiation medium for at least 2 d but had yet not fused into polykaryons were defined as pre-osteoclasts.

Isolation and functional assays with primary osteoblasts

Mouse calvarial osteoblasts were isolated from newborn mice as described previously (Wu et al., 1992). 8×10^4 primary osteoblasts were cultured in α -MEM in a 12-well plate until confluence. Osteoblastogenic medium (α -MEM, 10% FCS, 5 mM β -glycerophosphate, and 10 mg/ml ascorbic acid) was added to induce osteoblast differentiation. Osteoblast identity was confirmed at day 4 of differentiation by RT-PCR for AP, osteocalcin, and collagen I expression.

AP staining was performed on osteoblasts fixed in 4% PFA for 15 min and stained with DIG III solution (0.4% nitro-blue tetrazolium chloride [NBT]/5-bromo-4-chloro-3'-indolylphosphate p-toluidine salt [BCIP], 0.4 M Tris-HCl, pH 9.5, 0.4 M NaCl, and 0.2 M $MgCl_2$). To determine AP activity, osteoblasts from 12-well plates were collected in 500 μ l lysis buffer (10 mM Tris-HCl, pH 7.5, 0.5 mM $MgCl_2$, 0.1% Triton X-100, and 1x protease inhibitors) and homogenized by sonication for 20 s followed by centrifugation. 50 μ l of the supernatant was mixed with 50 μ l of 10 mM p-nitrophenylphosphate (Sigma-Aldrich) in 0.1 M glycine, 1 mM $MgCl_2$, and 1 mM $ZnCl_2$, pH 10.4, and incubated for 30 min at 37°C. 50 μ l 1 M NaOH was added to stop the reaction, and absorption at 405 nm was measured. Assays were performed in triplicate and the AP activity was normalized to the initial protein content.

Alizarin red S (ARS) staining and quantification of in vitro mineralization of osteoblasts was performed at day 21 after induction of osteoblast differentiation as described previously (Gregory et al., 2004). In brief, cells were fixed in 4% PFA for 15 min at RT, washed twice with ddH_2O , and incubated with 2% ARS, pH 4.2 (adjusted with NH_4OH) for 20 min while shaking. Cells were washed five times with ddH_2O for 5 min each and pictured. Bound ARS was dissolved in 10% acetic acid for 30 min at RT. The cell layer was scraped from the plate, transferred to a reaction tube, and vigorously shaken for 30 s. The suspension was overlaid with mineral oil, heated to exactly 85°C for 10 min, and kept on ice for 5 min. After centrifugation at 20,000 g for 15 min, two equivalents of 10% NH_4OH were added to five equivalents of ARS solution to get a pH of 4.1–4.5. This solution was measured at 405 nm in triplicate.

Pictures were obtained using a stereomicroscope (MZ FLIII; Leica) equipped with a Plan-Apochromat 1.0x objective, a ProgRes C14 camera, and Photoshop (Adobe) software.

RT-PCR

RT-PCR was used to examine the expression levels of osteoclast and osteoblast marker genes. Osteoclasts were obtained as described; cells at time point day 0 were taken immediately after performing the gradient centrifugation, cells at time point day 1 were cultured for 24 h in differentiation medium containing RANKL and M-CSF, and so on.

Total RNA was isolated using an RNeasy kit (QIAGEN). cDNA was obtained using the SuperScriptTM III Reverse transcription kit (Invitrogen). The following primers were used: calcitonin receptor 1b forward, 5'-TTTACC-GACGAGCAACGCCTACGC-3', and reverse, 5'-CATGTAGGACTCG-GCCTCGTGGG-3'; cathepsin K forward, 5'-GCTATATGACCACTGCTTTC-CAATACG-3', and reverse, 5'-ACTGCATGGTTCACATTATCACGGTC-3'; GAPDH forward, 5'-TCGTGGATCTGACGTGCCGCCTG-3', and reverse, 5'-CACACCCTGTTGCTGTAGCCGT-3'; collagen forward, 5'-AAGAG-GCGAGAGAGGTTCC-3', and reverse, 5'-ATCACCAGGTTACCTTTCG-3'; kindlin-3 forward, 5'-AGCTGTCTCTGCTGCGTGCTC-3', and reverse, 5'-ATACCTTGCTGCATGAGGCAC-3'; MMP9 forward, 5'-CGAGTGGAC-GCGACCGTAGTTGG-3', and reverse, 5'-CAGGCTTAGAGCCACGACCAT-ACAG-3'; kindlin-1 forward, 5'-CTACACCTCTTTGACTTG-3', and reverse, 5'-AGGGATGTCAGTTATGTC-3'; kindlin-2 forward, 5'-GTACCGAAGTAG-ACTGCAAGG-3', and reverse, 5'-CATACGGCATATCAAGTAGGC-3'; AP forward, 5'-CCITTTGGCTCTCTCCAAG-3', and reverse, 5'-CTGGCCTTCT-CATCCAGTTC-3'; and osteocalcin forward, 5'-AAGCAGGAGGGCAATA-AGGT-3', and reverse, 5'-AGTGTCTGTGACATCCATAC-3'.

Adhesion assays

12-mm glass slides were coated for 6 h at RT with 5 μ g/ml bovine osteopontin in PBS or with 3% BSA. The adhesion assay was performed with osteoclasts, which were directly isolated from long bones as described previously (Flores et al., 1992; Ek-Rylander et al., 1994). In brief, all four

legs of newborn wild-type and kindlin-3^{-/-} mice were minced and rotated for 1 h at 37°C in α -MEM containing 10% FCS. Afterward, the freed cells were seeded onto the coated-glass slides for 1 h and the slides were carefully washed with medium to remove nonadherent cells. The adherent cells were allowed to spread ON and were then TRAP-stained.

Macrophage adhesion on ICAM-1 was performed as described previously (Chavakis et al., 2008). In brief, 96-well plates were coated with 4 μ g/ml recombinant human ICAM-1 (R&D Systems) in coating buffer (150 mM NaCl, 20 mM Tris-HCl, and 2 mM $MgCl_2$, pH 9) ON at 4°C, blocked with 3% BSA in PBS for 1 h at RT, then incubated with 50,000 macrophages for 30 min in a tissue culture incubator in the presence or absence of 1 mM $MnCl_2$. Each condition was assayed in quadruplet. After washing with PBS containing 1% BSA, adherent cells were fixed in 4% PFA for 10 min and stained with 5 mg/ml crystal violet in 2% ethanol for 30 min. After washing, the remaining dye was dissolved in 2% SDS. Staining intensity was measured in an ELISA plate reader at 550 nm.

Resorption assay

Osteoclasts isolated from bones of P2–P4 wild-type and kindlin-3^{-/-} mice or in vitro differentiated from fetal liver cells or bone marrow were plated in osteoclast differentiation medium on osteologic slides (BD) for 1 wk. To quantify matrix resorption, cells were removed from the slides by treating them with 1% Triton X-100 and mechanical agitation, pictures were obtained with a microscope (Axioskop; 20x NA 0.50 objective, see Histology), and the resorbed area was measured using MetaMorph software. Alternatively, cells were cultured on dentin discs (Immunodiagnostic Systems) and resorption pits were visualized by staining with 1% toluidine blue in 0.5% sodium tetraborate for 3 min.

Immunofluorescence

Cells were plated on 12-mm coverslips coated with FCS for 1 h at 37°C, fixed with 4% PFA in PBS for 10 min or with 4% PFA for 1 min followed by a methanol fixation for 10 min at -20°C, and permeabilized with 0.25% Triton X-100 in PBS for 20 min. Blocking was performed for 1 h with 3% BSA in PBS. Cells were then incubated with the primary antibody in blocking solution for 3 h at RT or at 4°C ON. F-actin was visualized with Alexa Fluor 488–Phalloidin or Alexa Fluor 647–Phalloidin. Cells were imaged at RT with a SP2 confocal microscope (DMIRE2; Leica) using Leica Confocal Software (version 2.5 Build 1227) with 40x NA 1.25 and 100x NA 1.40 oil objective lenses. Single channels were imaged sequentially. All pictures were processed with Photoshop (Adobe).

Actin core size was measured in the actin channel by using MetaMorph software from at least six cells of each genotype. 50 actin dots were measured from each individual cell. The podosome belt size was obtained by measuring the thickness of the vinculin ring of at least 20 belts from osteoclasts that were differentiated in three or more independent preparations. Actin cores from at least 10 different pre-osteoclasts were analyzed. From each cell, 25 actin cores were analyzed.

Retroviral infections

EGFP-kindlin-3 and EGFP-kindlin-3-QA constructs (Moser et al., 2008) were amplified and directionally cloned using the EcoRI and BamHI sites of the pCLMFG retroviral vector (Naviaux et al., 1996). Vesicular stomatitis virus G–pseudotyped retroviral vectors were produced by transient transfection of 293T (human embryonic kidney) cells. Viral particles were concentrated from cell culture supernatant as described previously (Pfeifer et al., 2000) and used for infection of fetal liver cells. Fetal liver cells were prepared for differentiation into osteoclasts as described. Cells were cultured in medium containing 10 ng/ml M-CSF and 40 ng/ml RANKL for 5 d, and were used for TRAP and immunofluorescence staining and matrix degradation assays, or were lysed for Western blotting.

Gelatin zymography

Osteoclasts were isolated from bones of P2–P4 wild-type and kindlin-3^{-/-} mice, plated in osteoclast differentiation medium in a single 24 well for about 1 wk, and washed and incubated with serum-free α -MEM for 24 h. The conditioned medium was harvested, concentrated in Centricon filter units (10 kD cut-off; Millipore), mixed with nonreducing SDS sample buffer, and run on an SDS gel with a 4% stacking gel and a 12% running gel containing 0.2% gelatin. Gels were incubated twice for 15 min at RT in 0.2% Triton X-100 in ddH_2O and then for several days at 37°C in MMP reaction buffer (50 mM Tris-HCl, pH 7.5, 0.2 M NaCl, 5 mM $CaCl_2$, and 0.02% NaN_3). The bands of gelatinolytic activity were revealed after staining with Coomassie blue.

Cathepsin K activity measurement

Functional cathepsin K concentration was measured in protein lysates of cultured osteoclasts using a Cathepsin K Activity Assay kit (BioVision, Inc.). The assay was performed according to the manufacturer's instructions using 50 µg protein lysate per measurement.

Bone mineral density and histomorphometric measurements

pQCT of the distal femur was performed with XCT Research SA* (StraTec Medizintechnik). Bone density was measured exactly in the middle of the bone length using peel mode 2 with the threshold set at 100. Calcein labeling was performed as follows: 50 µl of 5 mg/ml calcein (Sigma-Aldrich) in 0.9% NaCl and 50 mM NaHCO₃ was injected at P0 and exactly 24 h later intraperitoneally. Mice were sacrificed 15 h after the second injection and long bones were dissected, fixed in 70% ethanol, and embedded in polymethylmethacrylate. 3-µm sections of the distal femur were deplasticized and stained for Masson-Goldner by hematoxylin (Gill II; Carl Roth), acid fuchsin-ponceau xylydine, and phosphomolybdic acid-orange G for visualizing cells, and osteoid and light green for visualizing mineralized matrix. Cancellous bone was examined in the 1-mm band below the growth plate, whereas primary cancellous bone was examined in the first 200 µm and secondary cancellous bone in the remaining 800 µm. Data presented were combined for both types. Histomorphometric analysis was performed according to the standards set forth by the American Society for Bone and Mineral Research (Parfitt et al., 1987). The following parameters were examined: osteoid surface (OS), bone surface (BS), osteoblast number (Ob.N), osteoclast number (Oc.N), and osteoclast surface (Oc.S). Measurements were performed by a person blinded to the genotype of the mice.

Flow cytometry

Fetal liver cell-derived macrophages and pre-osteoclasts were incubated with Fc receptor-blocking antibody (Millipore) and then with the appropriate fluorophore-conjugated monoclonal antibodies for 30 min on ice. Analysis was performed with a FACSCalibur (BD). β1 integrin activation was induced with 2 mM Mn²⁺ and analyzed with the 9EG7 antibody and a fluorophore-conjugated anti-rat antibody. 9EG7 binding was normalized to β1 integrin surface levels.

FNIII7-10 binding assay

Human FNIII7-10 fragment was subcloned into pET15b plasmid (Invitrogen), expressed in bacteria, and subsequently labeled with Alexa Fluor 647 carboxylic acid via a succinimidyl ester (Invitrogen) as described previously (Czuchra et al., 2006). To assess ligand-binding properties, fetal liver-derived macrophages were harvested and incubated with Alexa Fluor 647-coupled FNIII7-10 fragment in TBS in the presence or absence of 10 mM EDTA or 2 mM MnCl₂, respectively, and then subjected to flow cytometry analysis. Mean fluorescence of EDTA-treated cells was considered unspecific signal and was subtracted from all values.

Blocking of CD44-mediated adhesion

Osteoclast precursors were lifted using 10 mM EDTA in PBS and were first incubated for 15 min with an Fc receptor-blocking antibody followed by a 15 min incubation with either an anti-CD44-blocking antibody (BD) or rat IgG2b (eBioscience) before seeding on a fibronectin-coated surface. After adhesion for 30 min, cells were carefully rinsed with PBS and fixed with 4% PFA. Pictures were obtained using a microscope (Axiovert 40C; Carl Zeiss, Inc.) with a camera (Prosilica), a 10x objective lens, and FireWire Recorder software.

RANKL- and M-CSF-signaling

Mature osteoclasts were serum starved in α-MEM for 3–4 h and treated with either recombinant M-CSF (100 ng/ml or 10 ng/ml) or recombinant RANKL (100 ng/ml) for the times indicated. Cells were washed in cold PBS, lysed on ice with modified RIPA lysis buffer (50 mM Tris-HCl, pH7.3, 150 mM NaCl, 2 mM EDTA, 1% Triton X-100, 0.5% sodium deoxycholate, 1x protease inhibitor mixture [Roche], and 1x phosphatase inhibitor cocktail 1+2 [Sigma-Aldrich]) and incubated on ice for 10 min. Cell lysates were cleared by centrifugation at 14,000 rpm for 10 min at 4°C, and 40 µg of total lysates was subjected to 10% SDS-PAGE, transferred onto polyvinylidene fluoride membranes, blocked for 1 h in 5% BSA in TBS-T for detecting phosphorylated proteins or in 5% skim milk in TBS-T for detecting other proteins, then incubated with primary antibodies at 4°C ON followed by probing with HRP-labeled secondary antibodies (Jackson ImmunoResearch Laboratories).

For detection of Syk phosphorylation, 500 µg of lysate was used for immunoprecipitation. Lysate was incubated with 3 µg of primary antibody

ON at 4°C on a rotator, then protein G-Sepharose beads (Sigma-Aldrich) were added to the lysates, incubated for 3 h at 4°C on a rotator, washed three times in lysis buffer, and boiled in 3x SDS sample buffer for 5 min. After centrifugation, proteins were separated by 10% SDS-PAGE, Western blotted, and probed using an HRP-labelled 4G10 antibody (Millipore).

Electron microscopy

Primary osteoclasts were cultured on glass coverslips and then "unroofed" as described previously (Heuser, 2000; Luxenburg et al., 2007). In brief, cells were exposed to hypotonic buffer (20% PHEM, 6 mM Pipes, 5 mM Hepes, 0.4 mM Mg₂SO₄, and 2 mM EGTA) and broken by brief sonication for 2 s. The resulting ventral membrane preparations were fixed with 2.5% (vol/vol) glutaraldehyde in 0.1 M phosphate buffer (pH 7.4, 1 h at RT), postfixated with 1% (wt/vol) aqueous OsO₄, dehydrated, critical-point dried, and sputter-coated with 10 nm Au-Pd. Samples were viewed at 5 kV with a scanning electron microscope (DSM 982-Gemini; Carl Zeiss, Inc.).

Statistical analysis

A Student's *t* test was used to analyze histomorphometric data, osteoblast data, ELISA assays, β1 integrin activation, osteoclast fusion, belt thickness, resorption, and adhesion. *P* < 0.05 was considered to be statistically significant. All graphs include standard deviation error bars.

Online supplemental material

Fig. S1 shows histological sections of control and kindlin-3^{-/-} long bones from different developmental stages indicating progressive ossification in kindlin-3^{-/-} mice. Fig. S2 shows normal biological activity of kindlin-3^{-/-} osteoblasts. Fig. S3 shows normal p38 and JNK phosphorylation of kindlin-3^{-/-} osteoclasts upon RANKL treatment in vitro. Fig. S4 shows that CD44 contributes to the residual adhesion of kindlin-3^{-/-} pre-osteoclasts and integrin surface expression levels on control and kindlin-3^{-/-} macrophages. Fig. S5 shows that retroviral-expressed EGFP-kindlin-3 rescues cell spreading, podosome formation, and matrix degradation in kindlin-3^{-/-} osteoclasts, whereas expression of an integrin-binding mutant EGFP-kindlin-3 construct fails to do so.

We thank the Fässler laboratory members for discussion and Kyle Legate for critically reading the manuscript, Hildegard Reiter for performing the retroviral infections, Dick Heinegard for osteopontin, Angelika Flörl (Innsbruck Medical University, Austria) for excellent technical assistance with the electron microscopy work, and Chantal Domenget (University of Lyon, France) for support with osteoclast culture. We also thank Shahin Begum and Richard Hynes (Massachusetts Institute of Technology, Cambridge, MA) for isolating and providing bones from β3 integrin-deficient mice.

The work was supported by seventh framework program of the European Union and the Max Planck Society. The authors declare that they have no competing financial interests.

Submitted: 26 July 2010

Accepted: 2 February 2011

References

- Chabadel, A., I. Bañon-Rodríguez, D. Cluet, B.B. Rudkin, B. Wehrle-Haller, E. Genot, P. Jurdic, I.M. Anton, and F. Saltel. 2007. CD44 and beta3 integrin organize two functionally distinct actin-based domains in osteoclasts. *Mol. Biol. Cell.* 18:4899–4910. doi:10.1091/mbc.E07-04-0378
- Chavakis, E., G. Carmona, C. Urbich, S. Göttig, R. Henschler, J.M. Penninger, A.M. Zeiher, T. Chavakis, and S. Dimmeler. 2008. Phosphatidylinositol-3-kinase-gamma is integral to homing functions of progenitor cells. *Circ. Res.* 102:942–949. doi:10.1161/CIRCRESAHA.107.164376
- Czuchra, A., H. Meyer, K.R. Legate, C. Brakebusch, and R. Fässler. 2006. Genetic analysis of beta1 integrin "activation motifs" in mice. *J. Cell Biol.* 174:889–899. doi:10.1083/jcb.200604060
- Destaing, O., F. Saltel, J.C. Géminard, P. Jurdic, and F. Bard. 2003. Podosomes display actin turnover and dynamic self-organization in osteoclasts expressing actin-green fluorescent protein. *Mol. Biol. Cell.* 14:407–416. doi:10.1091/mbc.E02-07-0389
- Destaing, O., F. Saltel, B. Gilquin, A. Chabadel, S. Khochbin, S. Ory, and P. Jurdic. 2005. A novel Rho-mDia2-HDAC6 pathway controls podosome patterning through microtubule acetylation in osteoclasts. *J. Cell Sci.* 118:2901–2911. doi:10.1242/jcs.02425
- Destaing, O., A. Sanjay, C. Itzstein, W.C. Horne, D. Toomre, P. De Camilli, and R. Baron. 2008. The tyrosine kinase activity of c-Src regulates actin dynamics and organization of podosomes in osteoclasts. *Mol. Biol. Cell.* 19:394–404. doi:10.1091/mbc.E07-03-0227

- Ek-Rylander, B., M. Flores, M. Wendel, D. Heinegård, and G. Andersson. 1994. Dephosphorylation of osteopontin and bone sialoprotein by osteoclastic tartrate-resistant acid phosphatase. Modulation of osteoclast adhesion in vitro. *J. Biol. Chem.* 269:14853–14856.
- Faccio, R., D.V. Novack, A. Zallone, F.P. Ross, and S.L. Teitelbaum. 2003a. Dynamic changes in the osteoclast cytoskeleton in response to growth factors and cell attachment are controlled by beta3 integrin. *J. Cell Biol.* 162:499–509. doi:10.1083/jcb.200212082
- Faccio, R., S. Takeshita, A. Zallone, F.P. Ross, and S.L. Teitelbaum. 2003b. c-Fms and the alphavbeta3 integrin collaborate during osteoclast differentiation. *J. Clin. Invest.* 111:749–758.
- Flores, M.E., M. Norgård, D. Heinegård, F.P. Reinholt, and G. Andersson. 1992. RGD-directed attachment of isolated rat osteoclasts to osteopontin, bone sialoprotein, and fibronectin. *Exp. Cell Res.* 201:526–530. doi:10.1016/0014-4827(92)90305-R
- Franzén, A., and D. Heinegård. 1985. Isolation and characterization of two sialoproteins present only in bone calcified matrix. *Biochem. J.* 232:715–724.
- Gil-Henn, H., O. Destaing, N.A. Sims, K. Aoki, N. Alles, L. Neff, A. Sanjay, A. Bruzzaniti, P. De Camilli, R. Baron, and J. Schlessinger. 2007. Defective microtubule-dependent podosome organization in osteoclasts leads to increased bone density in *Pyk2(-/-)* mice. *J. Cell Biol.* 178:1053–1064. doi:10.1083/jcb.200701148
- Goodison, S., V. Urquidí, and D. Tarin. 1999. CD44 cell adhesion molecules. *MP. Mol. Pathol.* 52:189–196. doi:10.1136/mp.52.4.189
- Grant, F.D., P.R. Conlin, and E.M. Brown. 1990. Rate and concentration dependence of parathyroid hormone dynamics during stepwise changes in serum ionized calcium in normal humans. *J. Clin. Endocrinol. Metab.* 71:370–378. doi:10.1210/jcem-71-2-370
- Gregory, C.A., W.G. Gunn, A. Peister, and D.J. Prockop. 2004. An Alizarin red-based assay of mineralization by adherent cells in culture: comparison with cetylpyridinium chloride extraction. *Anal. Biochem.* 329:77–84. doi:10.1016/j.ab.2004.02.002
- Helfrich, M.H., S.A. Nesbitt, P.T. Lakkakorpi, M.J. Barnes, S.C. Bodary, G. Shankar, W.T. Mason, D.L. Mendrick, H.K. Väänänen, and M.A. Horton. 1996. Beta 1 integrins and osteoclast function: involvement in collagen recognition and bone resorption. *Bone.* 19:317–328. doi:10.1016/S8756-3282(96)00223-2
- Heuser, J. 2000. The production of ‘cell cortices’ for light and electron microscopy. *Traffic.* 1:545–552. doi:10.1034/j.1600-0854.2000.010704.x
- Hodivala-Dilke, K.M., K.P. McHugh, D.A. Tsakiris, H. Rayburn, D. Crowley, M. Ullman-Culleré, F.P. Ross, B.S. Collier, S. Teitelbaum, and R.O. Hynes. 1999. Beta3-integrin-deficient mice are a model for Glanzmann thrombasthenia showing placental defects and reduced survival. *J. Clin. Invest.* 103:229–238. doi:10.1172/JCI5487
- Jurdic, P., F. Saltel, A. Chabadel, and O. Destaing. 2006. Podosome and sealing zone: specificity of the osteoclast model. *Eur. J. Cell Biol.* 85:195–202. doi:10.1016/j.ejcb.2005.09.008
- Kilic, S.S., and A. Etzioni. 2009. The clinical spectrum of leukocyte adhesion deficiency (LAD) III due to defective CalDAG-GEF1. *J. Clin. Immunol.* 29:117–122. doi:10.1007/s10875-008-9226-z
- Krüger, M., M. Moser, S. Ussar, I. Thievensen, C.A. Lubner, F. Forner, S. Schmidt, S. Zanivan, R. Fässler, and M. Mann. 2008. SILAC mouse for quantitative proteomics uncovers kindlin-3 as an essential factor for red blood cell function. *Cell.* 134:353–364. doi:10.1016/j.cell.2008.05.033
- Kühn, R., F. Schwenk, M. Aguet, and K. Rajewsky. 1995. Inducible gene targeting in mice. *Science.* 269:1427–1429. doi:10.1126/science.7660125
- Kuijpers, T.W., E. van de Vijver, M.A. Weterman, M. de Boer, A.T. Tool, T.K. van den Berg, M. Moser, M.E. Jakobs, K. Seeger, O. Sanal, et al. 2009. LAD-1/variant syndrome is caused by mutations in FERMT3. *Blood.* 113:4740–4746. doi:10.1182/blood-2008-10-182154
- Larjava, H., E.F. Plow, and C. Wu. 2008. Kindlins: essential regulators of integrin signalling and cell-matrix adhesion. *EMBO Rep.* 9:1203–1208. doi:10.1038/embor.2008.202
- Legate, K.R., S.A. Wickström, and R. Fässler. 2009. Genetic and cell biological analysis of integrin outside-in signaling. *Genes Dev.* 23:397–418. doi:10.1101/gad.1758709
- Linder, S., and M. Aepfelbacher. 2003. Podosomes: adhesion hot-spots of invasive cells. *Trends Cell Biol.* 13:376–385. doi:10.1016/S0962-8924(03)00128-4
- Linder, S., and P. Kopp. 2005. Podosomes at a glance. *J. Cell Sci.* 118:2079–2082. doi:10.1242/jcs.02390
- Luxenburg, C., D. Geblinger, E. Klein, K. Anderson, D. Hanein, B. Geiger, and L. Addadi. 2007. The architecture of the adhesive apparatus of cultured osteoclasts: from podosome formation to sealing zone assembly. *PLoS ONE.* 2:e1179. doi:10.1371/journal.pone.0000179
- Malinin, N.L., L. Zhang, J. Choi, A. Ciocea, O. Razorenova, Y.Q. Ma, E.A. Podrez, M. Tosi, D.P. Lennon, A.I. Caplan, et al. 2009. A point mutation in KINDLIN3 ablates activation of three integrin subfamilies in humans. *Nat. Med.* 15:313–318. doi:10.1038/nm.1917
- McDowall, A., L. Svensson, P. Stanley, I. Patzak, P. Chakravarty, K. Howarth, H. Sabnis, M. Briones, and N. Hogg. 2010. Two mutations in the KINDLIN3 gene of a new leukocyte adhesion deficiency III patient reveal distinct effects on leukocyte function in vitro. *Blood.* 115:4834–4842. doi:10.1182/blood-2009-08-238709
- McHugh, K.P., K. Hodivala-Dilke, M.H. Zheng, N. Namba, J. Lam, D. Novack, X. Feng, F.P. Ross, R.O. Hynes, and S.L. Teitelbaum. 2000. Mice lacking beta3 integrins are osteosclerotic because of dysfunctional osteoclasts. *J. Clin. Invest.* 105:433–440. doi:10.1172/JCI8905
- Moser, M., B. Nieswandt, S. Ussar, M. Pozgajova, and R. Fässler. 2008. Kindlin-3 is essential for integrin activation and platelet aggregation. *Nat. Med.* 14:325–330. doi:10.1038/nm1722
- Moser, M., M. Bauer, S. Schmid, R. Ruppert, S. Schmidt, M. Sixt, H.V. Wang, M. Sperandio, and R. Fässler. 2009a. Kindlin-3 is required for beta2 integrin-mediated leukocyte adhesion to endothelial cells. *Nat. Med.* 15:300–305. doi:10.1038/nm.1921
- Moser, M., K.R. Legate, R. Zent, and R. Fässler. 2009b. The tail of integrins, talin, and kindlins. *Science.* 324:895–899. doi:10.1126/science.1163865
- Naviaux, R.K., E. Costanzi, M. Haas, and I.M. Verma. 1996. The pCL vector system: rapid production of helper-free, high-titer, recombinant retroviruses. *J. Virol.* 70:5701–5705.
- Parfitt, A.M., M.K. Drezner, F.H. Glorieux, J.A. Kanis, H. Malluche, P.J. Meunier, S.M. Ott, and R.R. Recker. 1987. Bone histomorphometry: standardization of nomenclature, symbols, and units. *J. Bone Miner. Res.* 2:595–610. doi:10.1002/jbmr.5650020617
- Pfeifer, A., T. Kessler, S. Silletti, D.A. Cheresh, and I.M. Verma. 2000. Suppression of angiogenesis by lentiviral delivery of PEX, a noncatalytic fragment of matrix metalloproteinase 2. *Proc. Natl. Acad. Sci. USA.* 97:12227–12232. doi:10.1073/pnas.220399597
- Plow, E.F., J. Qin, and T. Byzova. 2009. Kindling the flame of integrin activation and function with kindlins. *Curr. Opin. Hematol.* 16:323–328. doi:10.1097/MOH.0b013e32832ea389
- Ponta, H., L. Sherman, and P.A. Herrlich. 2003. CD44: from adhesion molecules to signalling regulators. *Nat. Rev. Mol. Cell Biol.* 4:33–45. doi:10.1038/nrm1004
- Potocnik, A.J., C. Brakebusch, and R. Fässler. 2000. Fetal and adult hematopoietic stem cells require beta1 integrin function for colonizing fetal liver, spleen, and bone marrow. *Immunity.* 12:653–663. doi:10.1016/S1074-7613(00)80216-2
- Rao, H., G. Lu, H. Kajiyama, V. Garcia-Palacios, N. Kurihara, J. Anderson, K. Patrene, D. Sheppard, H.C. Blair, J.J. Windle, et al. 2006. Alpha9beta1: a novel osteoclast integrin that regulates osteoclast formation and function. *J. Bone Miner. Res.* 21:1657–1665. doi:10.1359/jbmr.060718
- Ross, F.P., and S.L. Teitelbaum. 2005. alphavbeta3 and macrophage colony-stimulating factor: partners in osteoclast biology. *Immunol. Rev.* 208:88–105. doi:10.1111/j.0105-2896.2005.00331.x
- Sabnis, H., A. Kirpalani, J. Horan, A. McDowall, L. Svensson, A. Cooley, T. Merck, S. Jobe, N. Hogg, and M. Briones. 2010. Leukocyte adhesion deficiency-III in an African-American patient. *Pediatr. Blood Cancer.* 55:180–182.
- Saltel, F., A. Chabadel, E. Bonnelye, and P. Jurdic. 2008. Actin cytoskeletal organization in osteoclasts: a model to decipher transmigration and matrix degradation. *Eur. J. Cell Biol.* 87:459–468. doi:10.1016/j.ejcb.2008.01.001
- Scharffetter-Kochanek, K., H. Lu, K. Norman, N. van Nood, F. Munoz, S. Grabbe, M. McArthur, I. Lorenzo, S. Kaplan, K. Ley, et al. 1998. Spontaneous skin ulceration and defective T cell function in CD18 null mice. *J. Exp. Med.* 188:119–131. doi:10.1084/jem.188.1.119
- Suda, T., N. Takahashi, N. Udagawa, E. Jimi, M.T. Gillespie, and T.J. Martin. 1999. Modulation of osteoclast differentiation and function by the new members of the tumor necrosis factor receptor and ligand families. *Endocr. Rev.* 20:345–357. doi:10.1210/er.20.3.345
- Svensson, L., K. Howarth, A. McDowall, I. Patzak, R. Evans, S. Ussar, M. Moser, A. Metin, M. Fried, I. Tomlinson, and N. Hogg. 2009. Leukocyte adhesion deficiency-III is caused by mutations in KINDLIN3 affecting integrin activation. *Nat. Med.* 15:306–312. doi:10.1038/nm.1931
- Teitelbaum, S.L., and F.P. Ross. 2003. Genetic regulation of osteoclast development and function. *Nat. Rev. Genet.* 4:638–649. doi:10.1038/nrg1122
- Ussar, S., H.V. Wang, S. Linder, R. Fässler, and M. Moser. 2006. The Kindlins: subcellular localization and expression during murine development. *Exp. Cell Res.* 312:3142–3151. doi:10.1016/j.yexcr.2006.06.030
- Weinstein, E.J., M. Bourner, R. Head, H. Zakeri, C. Bauer, and R. Mazzarella. 2003. URP1: a member of a novel family of PH and FERM domain-containing membrane-associated proteins is significantly over-expressed in lung and colon carcinomas. *Biochim. Biophys. Acta.* 1637:207–216.
- Wu, H., R. Fässler, A. Schnieke, D. Barker, K.H. Lee, V. Chapman, U. Francke, and R. Jaenisch. 1992. An X-linked human collagen transgene escapes X inactivation in a subset of cells. *Development.* 116:687–695.

Supplemental material

JCB

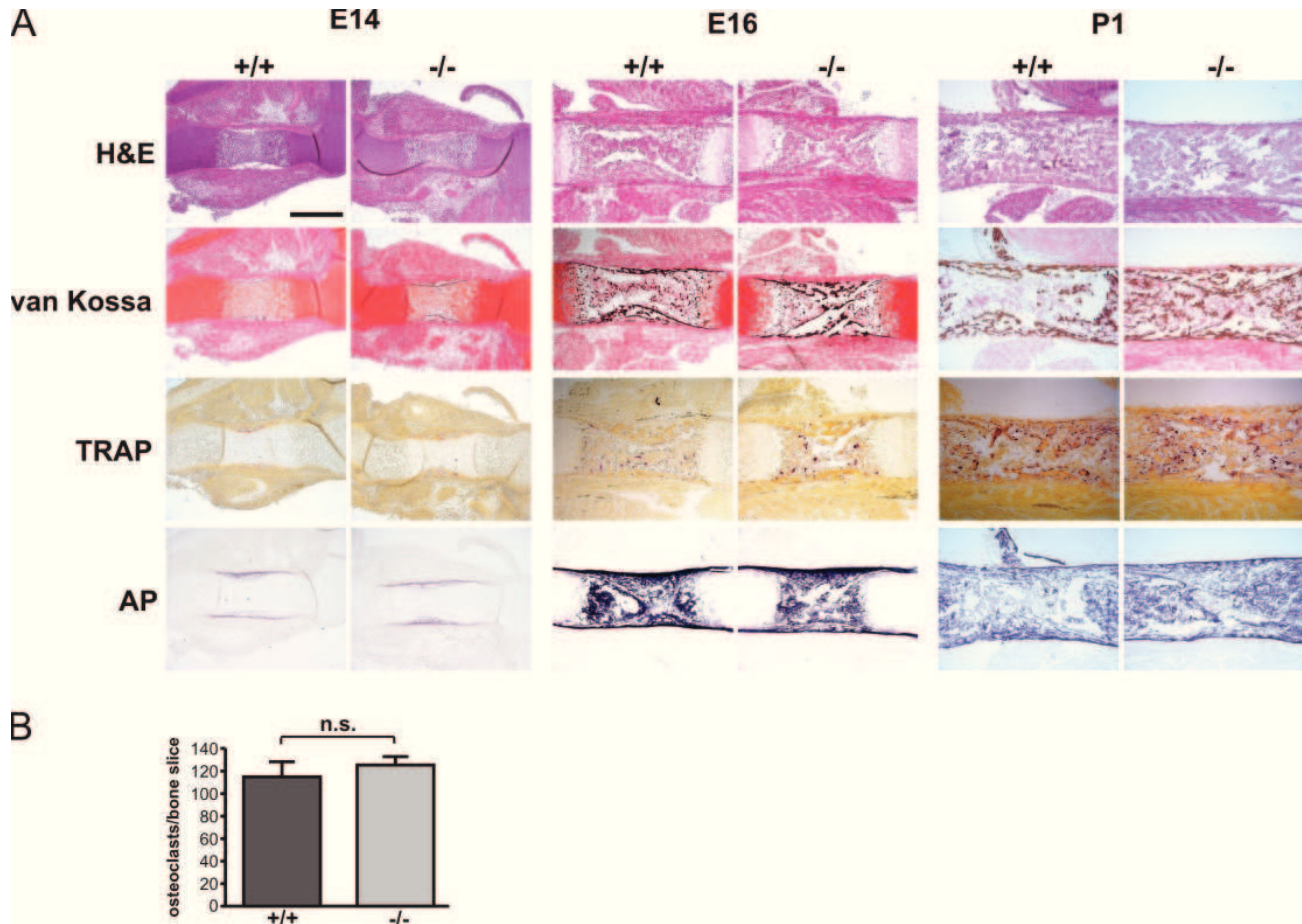
Schmidt et al., <http://www.jcb.org/cgi/content/full/jcb.201007141/DC1>

Figure S1. **Fetal development of osteopetrosis.** (A) Histology of femora from wild-type and kindlin-3^{-/-} embryos at E14, E16, and P1. Consecutive sections stained with hematoxylin and eosin (H&E), van Kossa, TRAP, and AP activity. Bar, 200 μ m. (B) Number of TRAP-positive osteoclasts in histological sections from wild-type and kindlin-3^{-/-} femora at P1. n.s., not significant.

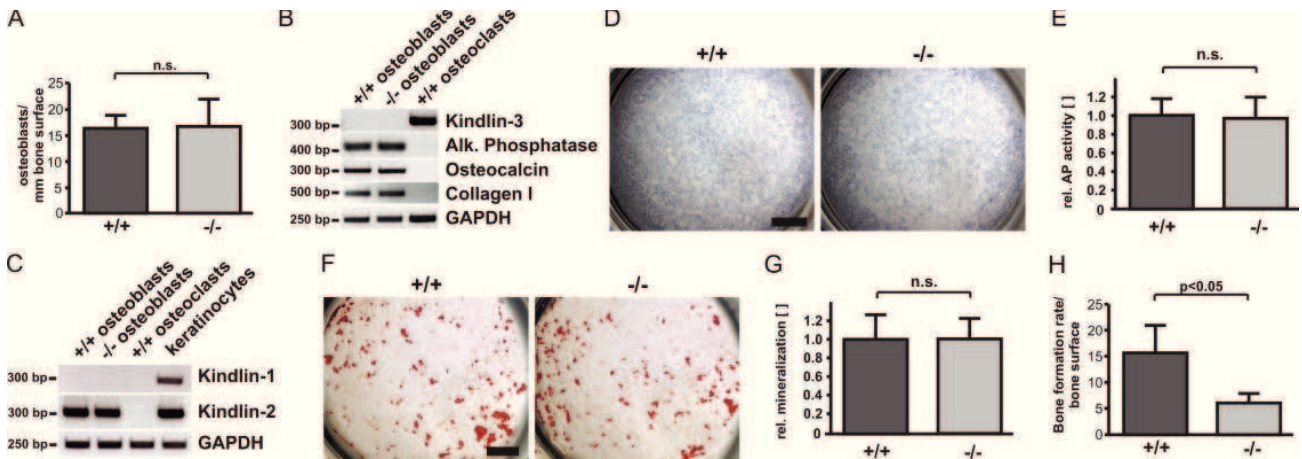


Figure S2. **Osteoblasts are normal in kindlin-3^{-/-} mice.** (A) Histomorphometric measurement of osteoblast number per bone surface in tibiae of P2 wild-type and kindlin-3^{-/-} mice; *n* = 4. (B) RT-PCR of osteoblast markers and kindlin-3 in primary wild-type and kindlin-3^{-/-} osteoblasts and wild-type osteoclasts. (C) RT-PCR of kindlin-1 and -2 in wild-type and kindlin-3^{-/-} osteoblasts and control osteoclasts. RNA from keratinocytes was used as a control. (D) Primary calvarial osteoblasts from wild-type and kindlin-3^{-/-} newborn mice stained for AP. Bar, 3 mm. (E) Relative AP activity in lysates from primary wild-type and kindlin-3^{-/-} osteoblasts was measured photometrically at 405 nm; *n* = 10/4. (F) Bone nodule formation by cultured wild-type and kindlin-3^{-/-} osteoblasts visualized by Alizarin red S staining. Bar, 3 mm. (G) Quantification of mineralization after Alizarin red S dye extraction and photometric measurement at 405 nm; *n* = 6/4. (H) Bone formation rate corrected to bone surface measured by histomorphometry; *n* = 4. Data are presented as mean ± SD (error bars).

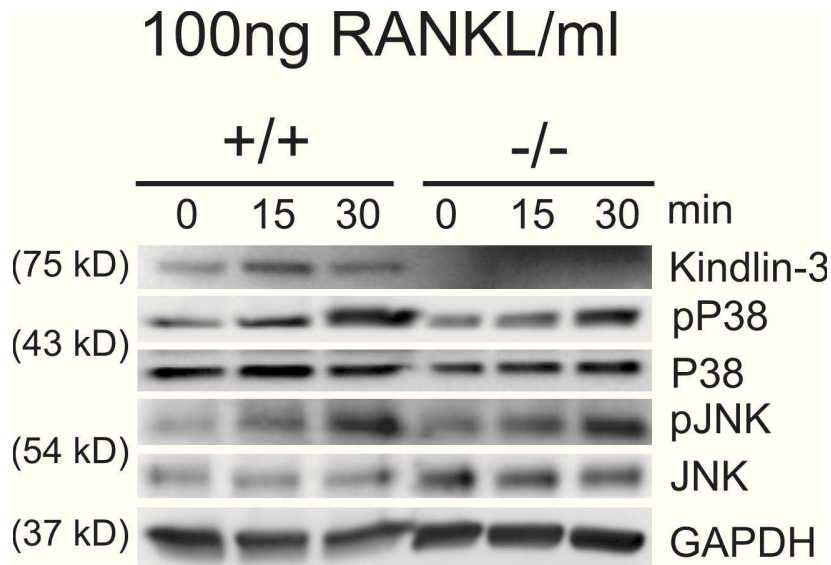


Figure S3. **Normal RANKL signaling in kindlin-3^{-/-} osteoclasts.** Starved wild-type and kindlin-3^{-/-} osteoclasts treated with 100 ng/ml RANKL for the indicated time periods. Western blot analyses for p-p38 and p-JNK are shown.

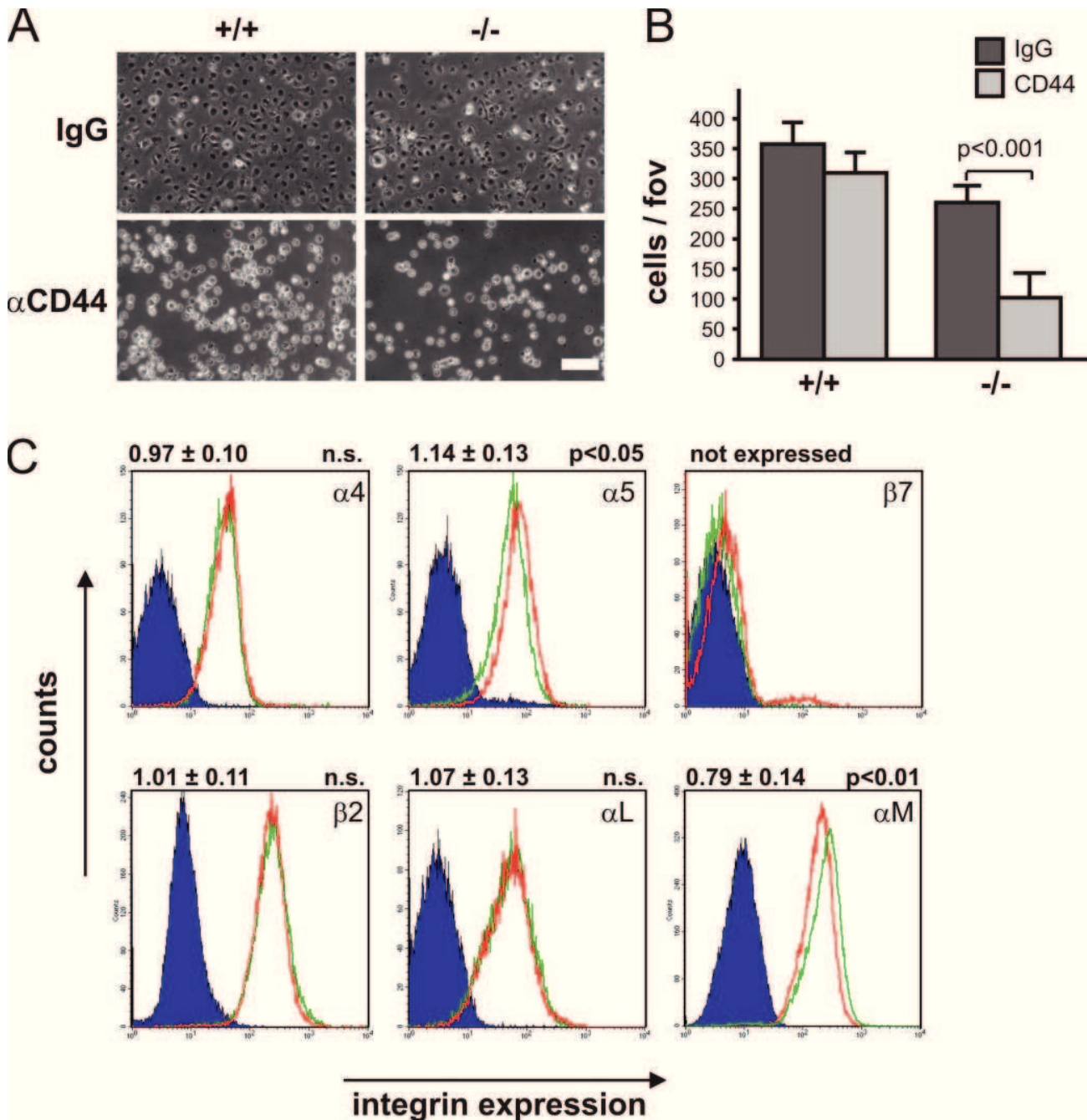


Figure S4. **CD44-mediated adhesion of kindlin-3^{-/-} pre-osteoclasts and integrin expression levels on kindlin-3^{-/-} macrophages.** (A and B) Wild-type and kindlin-3^{-/-} pre-osteoclasts were treated with either an isotype control or an α-CD44 antibody and plated on fibronectin. Cells were imaged (A) and quantified (B) after gentle washing and fixation; n = 4. Bar, 100 μm. (C) α4, α5, αL, αM, β2, and β7 integrin surface expression of wild-type (green) and kindlin-3^{-/-} (red) macrophages. Isotype control staining is shown in dark blue. Data are presented as mean ± SD (error bars). P-values indicate significant differences from wild-type (Student's *t* test).

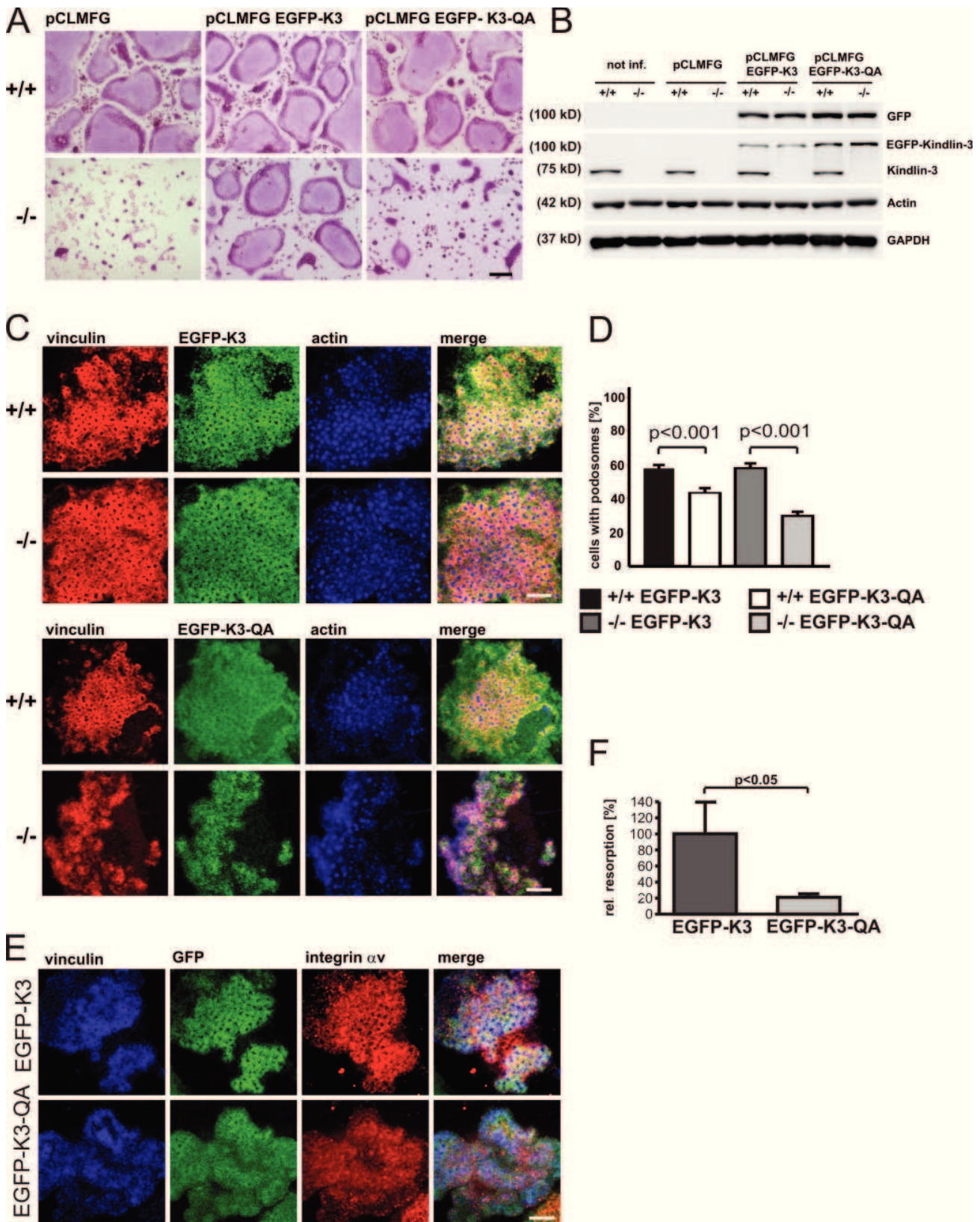


Figure S5. **Re-expression of wild-type and an integrin-binding mutant kindlin-3 in kindlin-3^{-/-} osteoclasts.** (A) TRAP staining of wild-type and kindlin-3^{-/-} osteoclasts transduced with either control virus (pCLMFG), or viruses expressing EGFP-kindlin-3 or an integrin-binding mutant EGFP-kindlin-3-QA. Bar, 100 μ m. (B) Western blotting for GFP and kindlin-3 indicates relative expression levels of endogenous and retroviral-induced wild-type and mutant kindlin-3 expression in osteoclasts. GAPDH and actin served as loading controls. (C) Vinculin (red) and F-actin staining (phalloidin, blue) of wild-type and kindlin-3^{-/-} osteoclasts transduced with an EGFP-kindlin-3 or an EGFP-kindlin-3 binding mutant EGFP-kindlin-3-QA (green). Bar, 5 μ m. (D) The percentage of infected fetal liver cells that formed podosomes was quantified in four independent experiments. (E) Vinculin (blue) and integrin α v (red) staining of kindlin-3^{-/-} osteoclasts transduced with viruses expressing EGFP-kindlin-3 or mutant EGFP-kindlin-3-QA (green). Bar, 5 μ m. (F) Resorption activity of kindlin-3^{-/-} osteoclasts transduced with an EGFP-kindlin-3 or mutant EGFP-kindlin-3-QA-expressing virus on calcium apatite-coated slides quantified with MetaMorph; $n = 3$. Data are presented as mean \pm SD (error bars). P-values indicate significant differences from wild-type (Student's t test).